

Probability of damage of masonry structures due to external ground vibrations

P.C.C. Potuijt

Probability of damage of masonry structures due to external ground vibrations

By

Pieter Cornelis Carel Potuijt

in partial fulfilment of the requirements for the degree of

Master of Science

in Civil Engineering

for the track Structural Engineering

and the specialisation Structural Mechanics

at the Delft University of Technology,

to be defended publicly on Wednesday June 5, 2019 at 11:30

Student number:	4167457	
Date	05/06/2019	
Supervisor:	Prof. dr. ir. J.G. Rots	<i>TU Delft</i>
Thesis committee:	Prof. dr. ir. J.G. Rots	<i>TU Delft</i>
	Dr. ir. P.C.J. Hoogenboom	<i>TU Delft</i>
	Ir. S. Pasterkamp	<i>TU Delft</i>
	Ir. P.A. Korswagen	<i>TU Delft</i>
	Dr. Ing. H. Netzel	<i>CRUX Engineering BV</i>

This thesis is confidential and cannot be made public until June 5th, 2019.

An electronic version of this thesis is available at <http://repository.tudelft.nl/>.

ABSTRACT

The SBR richtlijn A states threshold values for the vibration speeds causing a 1% probability of failure of masonry structures. These threshold values are very useful for structural designers, because during the construction of new structures or the demolition of existing structures, it is important to know if these structural vibrations can lead to damage to surrounding structures. However, for vibration speeds that exceed those threshold values, it is difficult to calculate the probability of failure of those structures. During this thesis, a procedure is proposed as a guideline to calculate probabilities of failure for masonry façades for vibration speeds higher than these threshold values.

Many factors influence the probability of failure for masonry structures, like soil properties, masonry properties, initial damage, initial loads or the type and frequency of structural vibrations. Also, it is important to know what should be considered damage. All these factors are implemented in this procedure. The proposed procedure is set up using two different models: a structural model, where the loads and façade dimensions and properties are implemented, and a probabilistic model, where the structural results are implemented, as well as stochastic parameters for some properties. This model leads to a probability of failure.

For the structural model, the software package SCIA Engineer has been used in this project. The structural model ensures that after drafting the façade, implementing the masonry properties, and applying the initial loads and the vibration speed and frequency, the maximum tensile stress for this frequency can be calculated. The tensile stress is the property that will determine if the structure fails, since the tensile stress of masonry is generally low. This tensile stress should then be implemented in the probabilistic model, which also takes the dispersion of the tensile strength and Young's Modulus into account. A Monte Carlo simulation is performed, which results in the probability of failure of the specific façade for a specific vibration speed and frequency.

This thesis' main focus was the linear-elastic procedure, where no soil-structure interaction was involved. Since masonry does not behave linearly after the first cracks initiate, some assumptions have been made to enable the calculation to be executed in a linear-elastic way, e.g. that failure occurs if the tensile strength is exceeded over a length of 210 mm. Also, in reality, soil-structure interaction will occur and will produce different structural results and following this, different probabilities of failure. Therefore, this study is able to provide a satisfactory statement regarding the probability of failure for masonry structures, but is not able to substantiate this statement completely.

In this thesis, the proposed procedure has also been executed on three different masonry facades in the city of Delft. The procedure is described extensively using these facades to provide a clear example how the reader can implement this procedure in their own projects. Also, because of the execution of this procedure on these façades, comparisons could be made, so the difference in probabilities of failure between façades, but also between different kinds of soil and vibration frequencies could be investigated.

The results show that the proposed procedure gives an adequate approximation for the probability of failure for masonry structures loaded by construction induced vibrations. Also, the results have been compared to a nonlinear case. This comparison shows that the assumptions that had to be made to approach this problem in a linear-elastic way were sometimes too conservative, but some assumptions were also a little too bold. Also, it is demonstrated that soil-masonry stresses have quite some influence on the structural results and therefore on the probability of failure, but more research regarding this topic is necessary to form a substantiated statement regarding the stresses at the soil-masonry interface.

Summarized, for this thesis, an assessment has been computed to determine the probabilities of failure for masonry structures using linear-elastic calculations. By following this procedure, one will be able to gather a good approximation of the probability of failure. However more research has to be conducted to ensure the soundness of this procedure.

ACKNOWLEDGEMENTS

First of all, during the persuasion of my bachelor's and master's degree at the faculty of Civil Engineering and Geosciences, my exchange program in Japan and internships, my teachers, colleagues and peers have taught me a great set of skills in subjects like engineering, collaboration and reflection. I'd like to thank everyone who helped me along this road and I would like to thank some people in particular.

I would like to express my gratitude to the members of my thesis committee. I would like to thank professor Jan Rots for the supervision of my thesis and for your useful questions during progress meetings which would always make me reflect on the choices I made during this thesis. Also, I would like to thank my supervisors Pierre Hoogenboom and Sander Pasterkamp for your adequate and fast feedback on my report and my questions and the discussions we could have regarding my research topic. I would like to thank Holger Netzel of CRUX Engineering B.V. for the meetings we had where we could discuss my progress and for your input regarding the practical aspect of my product. I would like to thank Paul Korswagen for the final phase of the project where you helped me with my presentation and my final report.

Moreover, I would like to express my gratitude for my colleagues at CRUX Engineering B.V., especially those who worked alongside me in Delft. Besides helping me with my thesis, it was pleasant to work with such nice colleagues who gave me a perfect environment to perform my research and write my thesis.

I would like to thank my friends for their everlasting support. There were some difficult times during this thesis and you helped me through those by our conversations and by providing me with the required distraction. You made it possible for me to put things into perspective and this improved my self-awareness a lot.

Lastly, I would like to express my gratitude for my family, especially my parents. I would like to thank you for your unconditional support and your belief in me during my studies, for providing me with the best conditions for self-development and putting my happiness above everything else. I would like to thank my brother, my sisters and my brother-in-law. I'm very grateful for our special bond, where we are there for each other as both family members and friends. I would also like to thank my niece for always being able to put a smile on my face.

Pieter Potuijt, The Hague, May 26th

TABLE OF CONTENTS

Abstract.....	III
Acknowledgements.....	V
Indices	X
List of Tables.....	XII
List of Figures	XIII
1. Introduction	1
1.1 Research topic.....	1
1.2 Problem statement	1
1.3 Reading guide.....	1
2. Goals and procedures	2
2.1 Research questions	2
2.2 Research procedure	2
2.2.1. Literature study.....	2
2.2.2 Experiments	2
2.2.3 Results and comparisons.....	3
3. Literature study.....	4
3.1 Geodynamics.....	4
3.1.1 General vibrations	4
3.1.2 Wave propagation	7
3.1.3 Dynamic properties soil.....	11
3.2 Masonry	14
3.2.1 Introduction.....	14
3.2.2 Properties of masonry	16
3.2.3 Failure modes	21
3.3 Finite Element Method and crack models	23
3.3.1 Introduction.....	23
3.3.2 Preprocessing	25
3.3.3 Analysis.....	27
3.3.4 Post-processing.....	27
3.3.5 Discrete vs smeared cracking	28
3.4 Probabilistics	28
3.4.1 Reliability	28
3.4.2 Reliability methods	30
3.4.3 Possible reliability methods regarding the project.....	31
3.5 Software possibilities	32

3.5.1	Finite element analysis	32
3.5.2	Probabilistic design	33
4.	Computational experiments	34
4.1	Choice of boundaries, definitions, software, loads, procedures	34
4.1.1	Boundaries.....	34
4.1.2	Definitions	35
4.1.3	Choice of software.....	36
4.1.4	Loads.....	36
4.1.5	Calculation procedure	39
4.2	Choice of models.....	41
4.2.1	Oude Delft 81	42
4.2.2	Bieslandsekade 22	44
4.2.3	Van Tijenstraat 8.....	46
4.3	Proposed procedure	48
4.4	Failure criterion.....	52
5.	Comparison TNO report.....	60
5.1	Step 1: Structural analysis.....	60
5.1.1	Structural parameters	60
5.1.2	Structural results	62
5.1.3	Conclusion	66
5.2	Step 2: Probabilistic methods	66
5.2.1	Monte Carlo or FORM.....	67
5.2.2	Proposed procedure and TNO method	71
6.	Modeling and results.....	78
6.1	Outline	78
6.2	Model.....	78
6.3	Loads	81
6.3.1	Initial loads	81
6.3.2	Vibration loads.....	81
6.4	Maximum tensile stress and relation with Young's Modulus	83
6.4.1	Maximum tensile stress.....	83
6.4.2	Relation tensile stress – Young's Modulus	84
6.5	Step 1: Initial Loads	85
6.5.1	Oude Delft	85
6.5.2	Van Tijenstraat.....	86
6.5.3	Bieslandsekade	87
6.6	Initial load and vibration load, no soil-structure interaction	88

6.6.1	Elaborated examples	89
6.6.2	Results	93
7.	Comparison studies.....	98
7.1	Constraints	98
7.2	Stresses at the soil-masonry interface	104
7.3	Nonlinear material parameters	108
8.	Conclusion and recommendation	114
	Appendices	- 1 -
	Appendix A: Elaboration of the model.....	- 2 -
	A.1 Example spring-columns	- 2 -
	A.2 Vibration loads	- 4 -
	A.3 Example curve-fit	- 5 -
	A.4 Example Matlab script	- 6 -
	Appendix B: Results test façade	- 8 -
	Results Oude Delft	- 8 -
	Results Van Tijenstraat.....	- 12 -
	Results Bieslandsekade	- 16 -
	References	- 20 -

INDICES

$A; A_m$	Amplitude	[mm]
A_p	Pile cross-section area	[m ²]
α	Damping variable soil	[-]
α	Angle	[°]
c	Propagation velocity	[m/s]
c_p	Wave propagation speed in pile	[m/s]
c_s	Shear wave velocity of the soil at the pile/soil interface	[m/s]
γ_{mob}	Mobile load factor	[-]
E	Young's Modulus	[N/mm ²]
f	Frequency	[Hz]
f_t	Tensile strength	[N/mm ²]
G	Shear modulus	[Pa]
G_{max}	Maximum shear modulus	[Pa]
n	Principal stress	[N/mm ²]
ν	Poisson's ratio	[-]
PI	Plasticity index	[-]
Q_{mob}	Mobile load	[kN/m ²]
Q_{sw}	Self-weight	[kN/m ²]
q_{tot}	Total load	[kN/m]
R_s	Dynamic soil resistance along the pile shaft	[kN]
r	Radius	[m]
ρ	Material density	[kg/m ³]
ρ_{soil}	Soil density	[kg/m ³]
S_p	Contact area between shaft and soil	[m ²]
s	Span	[m]
σ	Stress	[N/mm ²]
T	Period	[s]

v	Wave propagation velocity	[m/s]
v'	Particle velocity	[m/s]
v_p	P-Wave velocity	[m/s]
v_p	Particle velocity of the pile	[m/s]
v_s	Shear wave velocity	[m/s]
ϕ	Phase difference	[s]
z	Vertical displacement	[mm]
Z_p	Pile impedance	[Pa*s/m]
z_s	Soil impedance for shear waves	[kNs/m ³]
ω	Circular frequency	[rad/s]

LIST OF TABLES

Table 1 – Symbols of velocity and angles of waves, modified after Woods (1997)	10
Table 2 – α -value of different soils, modified after Woods (1997).....	11
Table 3 – Velocities of body waves in different soil types (Head & Jardine, 1992).....	12
Table 4 – Summary of properties regarding wave propagation, modified after Head & Jardine (1992)	12
Table 5 – Characteristics that influence compressive strength (Hendry, Sinha, & Davies, 1997).....	16
Table 6 – Finite element characteristics	25
Table 7 – Reliability levels	30
Table 8 – Reliability index to chance of failure	31
Table 9 – Comparison FEM-software	33
Table 10 – Wave lengths for various propagation velocities and frequencies	34
Table 11 – Masonry properties	35
Table 12 – Initial loads	37
Table 13 – Stochastic parameters	50
Table 14 – Average tensile stresses for a 210 mm section	57
Table 15 – Average tensile stresses for a 100 mm section	57
Table 16 – Properties model TNO report	60
Table 17 – Stochastic properties for good quality masonry	66
Table 18 – Stochastic properties for bad quality masonry.....	67
Table 19 – Stochastic properties for monumental masonry.....	67
Table 20 – Sample sizes.....	68
Table 21 – Stochastic parameters TNO report (Waarts, 1997)	71
Table 22 – Stochastic parameters	72
Table 23 – Stress values for the bottom right corner of the opening.....	74
Table 24 – Initial loads	81
Table 25 – Phase differences	82
Table 26 – Displacements per frequency.....	82
Table 27 – Oude Delft stochastic parameters	84
Table 28 – Maximum initial stresses Oude Delft.....	85
Table 29 – Maximum initial stresses Van Tijenstraat.....	86
Table 30 – Maximum initial stresses Van Tijenstraat.....	87
Table 31 – Principal stresses top left corner door	90
Table 32 – Initial stresses top left corner door	90
Table 33 – Maximum stresses 10 Hz, sandy soil, 12 mm/s vibration speed	101
Table 34 – Maximum tensile stress in node K42 for different constraining situations.....	101
Table 35 – Maximum stresses 10 Hz, clay soil, 12 mm/s vibration speed	102
Table 36 – Maximum stresses 5 Hz, sandy soil, 12 mm/s vibration speed	102
Table 37 – Maximum stresses 5 Hz, clay soil, 12 mm/s vibration speed	102
Table 38 – Maximum stresses 20 Hz, sandy soil, 12 mm/s vibration speed	102
Table 39 – Maximum stresses 20 Hz, clay soil, 12 mm/s vibration speed	102
Table 40 – Maximum stresses 10 Hz, sandy soil, 12 mm/s vibration speed, Bieslandsekade	102
Table 41 – Maximum stresses 5 Hz, sandy soil, 12 mm/s vibration speed, Bieslandsekade	103
Table 42 – Principal tensile stresses for nodes with highest stresses.....	105
Table 43 – Maximum tensile stresses for different Young’s Moduli.....	- 5 -

LIST OF FIGURES

Figure 1 – Project flowchart	3
Figure 2 – Harmonic motion	5
Figure 3 – Block style periodic motion (Vrouwenvelder)	5
Figure 4 – Random earthquake vibration (Vrouwenvelder)	6
Figure 5 – Transient motion	6
Figure 6 – P-waves (Braile, 2007)	8
Figure 7 – S-waves (Braile, 2007)	8
Figure 8 – R-waves (Braile, 2007)	9
Figure 9 – Love waves (Braile, 2007)	9
Figure 10 – Reflected and refracted rays from incident P, SV and SH waves, modified after Deckner (2013)	9
Figure 11 – Relationship between shear modulus, shear strain and plasticity index Deckner (2013)	11
Figure 12 – Stretcher bond, modified after Gerrits (2008)	15
Figure 13 – English bond, modified after Gerrits (2008)	15
Figure 14 – Raking stretcher bond, modified after Gerrits (2008)	15
Figure 15 – Flemish bond, modified after Gerrits (2008)	15
Figure 16 – Brickwork strength vs brick strength (Hendry et al., 1997)	17
Figure 17 – Stress-strain curve for masonry loaded in compression (Hendry et al., 1997)	18
Figure 18 – Relationship between the bond tension and the moisture content of the bricks (Hendry et al., 1997)	19
Figure 19 – Relationship between shear strength and precompression. (Hendry et al., 1997)	20
Figure 20 – Vertical tension (Schipper, 2017)	21
Figure 21 – Horizontal tension (Schipper, 2017)	21
Figure 22 – Shear (Schipper, 2017)	22
Figure 23 – Diagonal crack in a church in Quebec City , Canada (EERI, 1988)	22
Figure 24 – Vertical compression (Schipper, 2017)	22
Figure 25 – Horizontal compression (Schipper, 2017)	22
Figure 26 – Bending (Schipper, 2017)	23
Figure 27 – Body with forces and boundary conditions, modified after Qi (2006)	24
Figure 28 – Input and output, modified after Qi (2006)	24
Figure 29 – Plane stress element (Hendriks & Rots, 2015)	25
Figure 30 – Meshes. Top left is the original structure, the others show meshes with different element sizes. ..	26
Figure 31 – Stress contour for a simple distributed load	27
Figure 32 – Displacements for a simple distributed load	27
Figure 33 – Failure Probability	30
Figure 34 – Vibration in time	37
Figure 35 – Displacement in time	38
Figure 36 – Displacement in space (from 0 to 10 m) for t=0	38
Figure 37 – Displacement in space (from 0 to 10 m) for t=0.04	39
Figure 38 – Oude Delft 81	42
Figure 39 – Geometry Oude Delft 81	43
Figure 40 – Bieslandsekade 22	44
Figure 41 – Geometry Bieslandsekade 22	45
Figure 42 – Van Tijenstraat 8	46
Figure 43 – Geometry Van Tijenstraat 8	47
Figure 44 – Structure	48
Figure 45 – Flowchart of the procedure	51

Figure 46 – Structure used for comparison with nonlinear material parameters	52
Figure 47 – Stress contour 100 mm mesh.....	53
Figure 48 – Stress contour zoomed in at bottom right corner of the window	53
Figure 49 – Structure used for comparison with nonlinear material parameters	54
Figure 50 – Probability of failure for various mesh sizes	54
Figure 51 – Probability of failure for a 12 mm/s vibration speed	55
Figure 52 – Length of the fracture zone vs mesh size	55
Figure 53 – 210 mm section, 100 mm mesh size	56
Figure 54 – 210 mm section, 80 mm mesh size	56
Figure 55 – 210 mm section, 50 mm mesh size	56
Figure 56 – 210 mm section, 40 mm mesh size	56
Figure 57 – Stress contour 100 mm mesh.....	58
Figure 58 – Stress contour zoomed in at bottom right corner of the window	58
Figure 59 – Stress contour 216 mm mesh.....	59
Figure 60 – Compared methods.....	59
Figure 61 – Translation sinusoidal loads to trapezoidal load	61
Figure 62 – Mesh.....	61
Figure 63 – TNO report x-stresses. Opening on left side	62
Figure 64 – SCIA results x-stresses. Opening on left side.....	62
Figure 65 – TNO report y-stresses. Opening on left side.	63
Figure 66 – SCIA results y-stresses. Opening on left side.....	63
Figure 67 – TNO report x-stresses. Opening in the middle	64
Figure 68 – SCIA results x-stresses. Opening in the middle	64
Figure 69 – TNO report y-stresses. Opening in the middle.....	65
Figure 70 – SCIA results y-stresses. Opening in the middle	65
Figure 71 – Matlab script for bad quality masonry	68
Figure 72 – Probability of failure of bad state masonry.....	69
Figure 73 – Probability of failure of good state masonry.....	70
Figure 74 – Probability of failure of monumental masonry	70
Figure 75 – Results according to the TNO report, modified after Waarts (1997)	71
Figure 76 – Envelop structural tensile stresses	72
Figure 77 – Zoomed in corner at moment of failure (mesh size: 100 mm)	73
Figure 78 – Stress contour around opening for a vibration speed of 12 mm/s	73
Figure 79 – Tensile stress versus Young’s Modulus	74
Figure 80 – Curve-fit for $E < 3600 \text{ N/mm}^2$	75
Figure 81 – Curve-fit for $E > 3600 \text{ N/mm}^2$	75
Figure 82 – Probabilty of failure for a 10 Hz vibration in a sandy soil.....	76
Figure 83 – Comparison TNO report and proposed procedure	77
Figure 84 – Flowchart of the calculation.....	77
Figure 85 – Oude Delft dimensions.....	79
Figure 86 – SCIA model Oude Delft	80
Figure 87 – Floor and roof loads	81
Figure 88 – Self-weight masonry.....	81
Figure 89 – Loads for 3 Hz.....	82
Figure 90 – Dynamic load function for 3 Hz, for spring-column 6	83
Figure 91 – Exceedance over a length of 210 mm. Top left window, bottom left corner	84
Figure 92 – Relationship maximum tensile stress-Young’s Modulus Oude Delft	84
Figure 93 – Stresses due to initial loads Oude Delft	85
Figure 94 – Stresses due to initial loads Van Tijenstraat.....	86
Figure 95 – Stresses due to initial loads Van Tijenstraat.....	87

Figure 96 – Contour plot Oude Delft 10 Hz, sandy soil, 12 mm/s vibration speed	89
Figure 97 – Top left corner door	89
Figure 98 – Matlab script for Monte Carlo simulation	91
Figure 99 – Probability of failure vs vibration speed Oude Delft, 10 Hz, sandy soil.....	91
Figure 100 – Contour plot Van Tijenstraat 10 Hz, sandy soil, 12 mm/s vibration speed	92
Figure 101 – Contour plot Bieslandsekade 10 Hz, sandy soil, 12 mm/s vibration speed	93
Figure 102 – Results Oude Delft.....	94
Figure 103 – Results Oude Delft, all cases.....	94
Figure 104 – 10 Hz sand	95
Figure 105 – 4 Hz sand	95
Figure 106 – Comparison TNO report Waarts.....	96
Figure 107 – Example structure	98
Figure 108 – Contour plot 10 Hz, sandy soil, constrained.....	99
Figure 109 – Zoomed in at top left corner door, 10 Hz, sandy soil, constrained	99
Figure 110 – Contour plot 10 Hz, sandy soil, single unconstrained	99
Figure 111 – Zoomed in at top left corner door, 10 Hz, sandy soil, single unconstrained	100
Figure 112 – Contour plot 10 Hz, sandy soil, double unconstrained	100
Figure 113 – Zoomed in at top left corner door, 10 Hz, sandy soil, double unconstrained	100
Figure 114 – Probability of failure for different constraint configurations.....	101
Figure 115 – Example structure	104
Figure 116 – Line spring support.....	105
Figure 117 – Contour plot 10 Hz, sandy soil, 12 mm/s, without spring support.....	105
Figure 118 – Contour plot 10 Hz, sandy soil, 12 mm/s, with spring support	106
Figure 119 – Reaction forces at t=0,17 s	106
Figure 120 – Reaction Forces at t=0,37 s	107
Figure 121 – Structure used for comparison with nonlinear material parameters	108
Figure 122 – Contour plot sand 10 Hz (0.26 mm displacement amplitude)	109
Figure 123 – Zoomed in at bottom right corner window, sand 10 Hz (0.26 mm displacement amplitude)	109
Figure 124 – Zoomed in at bottom right corner window, reduced Young’s Modulus, sand 10 Hz (0.26 mm displacement amplitude)	110
Figure 125 – Zoomed in at bottom right corner window, reduced Young’s Modulus, sand 10 Hz (0.26 mm displacement amplitude)	110
Figure 126 – Zoomed in at bottom right corner window, reduced Young’s Modulus, sand 10 Hz (0.355 mm displacement amplitude)	111
Figure 127 – Zoomed in at bottom right corner window, reduced Young’s Modulus, sand 10 Hz (0.476 mm displacement amplitude)	111
Figure 128 – Contour plot sand 10 Hz (0.476 mm displacement amplitude)	112
Figure 129 – Zoomed in at bottom right corner window, sand 10 Hz (0.476 mm displacement amplitude)	112
Figure 130 – Loads on spring-columns.....	- 2 -
Figure 131 – Resulting displacements.....	- 2 -
Figure 132 – Results $k=10^{18}$ N/m.....	- 3 -
Figure 133 – Results $k=10^{10}$ N/m.....	- 3 -
Figure 134 – Dynamic load function	- 4 -
Figure 135 – Maximum tensile stresses – Young’s Modulus scatter	- 5 -
Figure 136 – Matlab script describing the Monte Carlo simulation	- 7 -
Figure 137	- 8 -
Figure 138	- 8 -
Figure 139	- 9 -
Figure 140	- 9 -
Figure 141	- 10 -

Figure 142	- 10 -
Figure 143	- 11 -
Figure 144	- 11 -
Figure 145	- 12 -
Figure 146	- 12 -
Figure 147	- 13 -
Figure 148	- 13 -
Figure 149	- 14 -
Figure 150	- 14 -
Figure 151	- 15 -
Figure 152	- 15 -
Figure 153	- 16 -
Figure 154	- 16 -
Figure 155	- 17 -
Figure 156	- 17 -
Figure 157	- 18 -
Figure 158	- 18 -
Figure 159	- 19 -
Figure 160	- 19 -

1. INTRODUCTION

1.1 RESEARCH TOPIC

In 1959, Stichting Bouwresearch (SBR) was founded as a research institute regarding innovation, development and knowledge implementation within the Dutch building sector (Proficient, 2012). SBR published the SBR richtlijn A (SBRCURnet, 2017), titled “Schade aan bouwwerken”, translated in English “Damage to structures”. This guideline states vibration measuring methods for structures and shows how these measurements or calculations can be judged. Moreover, this report states threshold values for the vibration speed of these structural vibrations. If the structural vibration speeds remain under this threshold value, the probability of failure is considered acceptable.

In 1997, ir. P.H. Waarts of Netherlands Organisation for Applied Scientific Research (TNO) published a report regarding the probability of damage of masonry structures due to vibrations (Waarts, 1997). This report states that if the threshold values from SBR richtlijn A are exceeded, it is not certain that failure can be expected. It also states that it could be feasible to know the probability of damage at vibrations that exceed the threshold value. The report attempts to quantify these probabilities.

1.2 PROBLEM STATEMENT

Although TNO published a report that states the relationship between vibration speed and the probability of failure, there is lack of a standard procedure for engineers to compute the probability of failure for vibration speeds that exceed the threshold values as stated in SBR richtlijn A. CRUX Engineering B.V. notices that construction companies experience challenges because of the lack of knowledge regarding this topic. Therefore, it is feasible to develop a procedure to evaluate the probabilities of failure for vibration speeds exceeding the threshold values stated in SBR richtlijn A. Moreover, the TNO report quantifies a lot of properties as stochastic parameters. By evaluating these parameters in a structural model, these parameters can be improved.

1.3 READING GUIDE

- Chapter 2 describes the goals and procedures of this project. This chapter also states the research questions.
- Chapter 3 shows a summary of the literature study.
- Chapter 4 describes the calculation procedure and the chosen models for this project.
- Chapter 5 elaborates the comparison between the TNO report and the results of this project’s procedure.
- Chapter 6 shows examples how the calculation procedure can be executed on the models described in chapter 4. This chapter also shows and discusses the results of these calculations.
- Chapter 7 describes comparative calculations with different model parameters.
- Chapter 8 discusses the conclusion of this report, by answering the research questions stated in chapter 2 and discusses the recommended future research.

2. GOALS AND PROCEDURES

2.1 RESEARCH QUESTIONS

The main research question is:

“How can the probability of failure for masonry structures be computed for vibration speeds exceeding the threshold values stated in SBR richtlijn A?”

Sub questions of this research project will be:

- *“Can a linear-elastic calculation lead to statements regarding cracking?”*
- *“Is it feasible to include stresses at the soil-masonry interface in calculating the probability of failure due to vibration speeds?”*
- *“Does a nonlinear approach lead to significantly other results than a linear-elastic calculation?”*

2.2 RESEARCH PROCEDURE

To answer the research questions stated in 2.1, a clear working plan is required, which states the various phases of the project, what will be executed in these phases, the questions that should be answered in these phases and the goals of those phases.

2.2.1. LITERATURE STUDY

At the start of the literature study, an assessment is made of the prior knowledge regarding the research topic. The results of this assessment shows both topics requiring further investigation and topics where the writer's knowledge is sufficient for this project. Following this, literature should be gathered and studied regarding the topics requiring further investigation. Moreover, various software packages should be investigated to determine if those software packages can contribute to a solution of the research problem. After these topics have been clarified, the next phase of the project can commence.

2.2.2 EXPERIMENTS

Firstly, the models from the TNO report will be remodeled in the structural model and the probabilistic model. When the results from both calculation methods are comparable, this means that these software packages are sufficient to produce qualitative results.

Secondly, using the knowledge gained in the literature study, choices should be made regarding the scope of the project, e.g. boundaries, definitions, the use of software and which (justified) assumptions should be made to successfully execute this experiment. Using this, the proposed procedure can be set up. By following this procedure on certain models, the results can help to improve the proposed procedure. This results in an iterative process where the procedure will be updated by executing it on different models, where certain parameters will be adjusted.

Once the quality of the proposed procedure is regarded acceptable, this procedure will be executed on chosen models and its results will be elaborated extensively, to produce a clear example for the future users of this procedure.



FIGURE 1 – PROJECT FLOWCHART

2.2.3 RESULTS AND COMPARISONS

By executing this procedure on the models, the results can be gathered. By using different facades, frequencies, vibration speeds and soil propagation speeds, the effect of these properties on the probability of failure can be described.

Furthermore, some comparative studies can be executed. Certain modeling parameters can be adjusted, like:

- Constraining.
- Stresses at the soil-masonry interface.
- Nonlinear approach.

The results due to calculations using these approaches can be compared to the results in the original situation. This leads to statements regarding these approaches, like what effect they produce, and recommendations for further research regarding these parameters. Note that these comparisons will be executed briefly and this will not lead to solid statements, but to a first set of findings. Therefore, further research should be recommended regarding these topics. After this step, conclusions can be drawn regarding the research subject.

3. LITERATURE STUDY

After consideration of the different aspects of the problem regarding the probability of failure of masonry structures due to vibration, the topics requiring extra attention are determined:

1. Soil mechanics/geodynamics.
2. Masonry properties.
3. Finite Element Method and crack models.
4. Probabilistic design.
5. Software possibilities.

3.1 GEODYNAMICS

Geodynamics is an important aspect of this study. It should be clear how vibrations from (sheet) piling will be transmitted in the soil and how this transmission affects the structure and can provoke damage. This section discusses the theory regarding geodynamics and soil mechanics.

3.1.1 GENERAL VIBRATIONS

Vibration is a phenomenon where there is an oscillatory movement around an equilibrium point. Different types of motions can occur. Some of these motions, the ones most applicable to this project, are discussed below.

Harmonic motion

According to Woods, the simplest form of vibratory motion is the harmonic motion. This is described as: (Woods, 1997)

$$z = A_m \sin(\omega t) \quad (1)$$

Where:

$$\begin{aligned} z &= \text{Vertical displacement (mm)} \\ A_m &= \text{Displacement amplitude (mm)} \\ \omega &= \text{Circular frequency (rad/s)} \\ t &= \text{time (s)} \end{aligned}$$

This equation is plotted in Figure 2. The frequency and the period correspond to the circular frequency in the following equations: (Woods, 1997)

$$f = \frac{\omega}{2\pi} \quad (2)$$

$$T = \frac{2\pi}{\omega} \quad (3)$$

Where:

$$\begin{aligned} f &= \text{Frequency (Hz)} \\ T &= \text{Period (t)} \end{aligned}$$

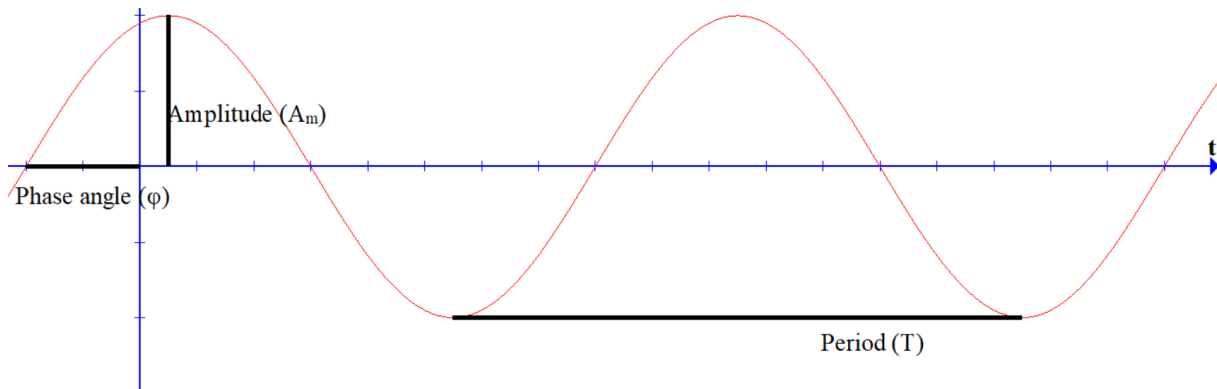


FIGURE 2 – HARMONIC MOTION

In Figure 2 the most important features of a harmonic motion are demonstrated; with these features every harmonic motion can be described:

- Amplitude A_m : This is the maximum oscillation that occurs relative to equilibrium. Sometimes, peak-to-peak or double amplitude is used, which is the vertical difference between the positive and negative peak and is equal to $2 * A_m$ (Richart, 1970).
- Period T : This is the duration of one harmonic motion. After one period the motion repeats itself. It holds narrow relations with circular frequency ω and frequency f . These relationships are shown in equations (2) and (3).
- Phase angle ϕ . This is the amount of time between the motion and a pure sine function.

Periodic motion

This is a motion that follows a repetitive pattern during a period T . The difference between a periodic and a harmonic motion is that a periodic motion does not have to be pure sinusoidal. It could be presented as the sum of sinusoidal functions, which is called a Fourier series. (Vrouwenvelder, Spijkers, & Klaver, 2006). A periodic motion is shown in Figure 3.

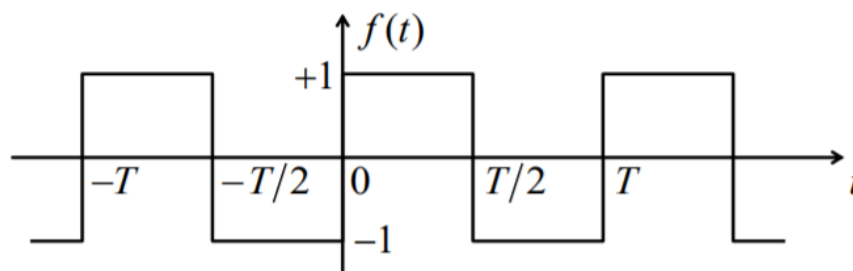


FIGURE 3 – BLOCK STYLE PERIODIC MOTION (VROUWENVELDER)

Random motion

A random motion is about the opposite of a periodic motion: it is a motion that never repeats itself. Examples could be earthquakes, wind or waves (Vrouwenvelder et al., 2006). An earthquake vibration is shown in Figure 4.

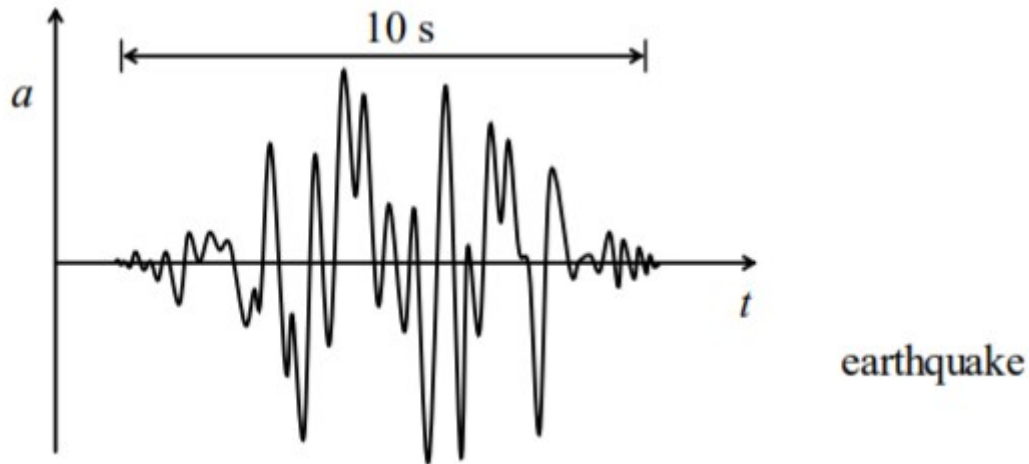


FIGURE 4 – RANDOM EARTHQUAKE VIBRATION (VROUWENVELDER)

Transient motion

A transient motion describes a short-term or passing motion. This means that it starts at a high intensity and gradually decreases in time. Things that can cause these kinds of motions are collisions, explosions or pile driving amongst others (Vrouwenvelder et al., 2006).

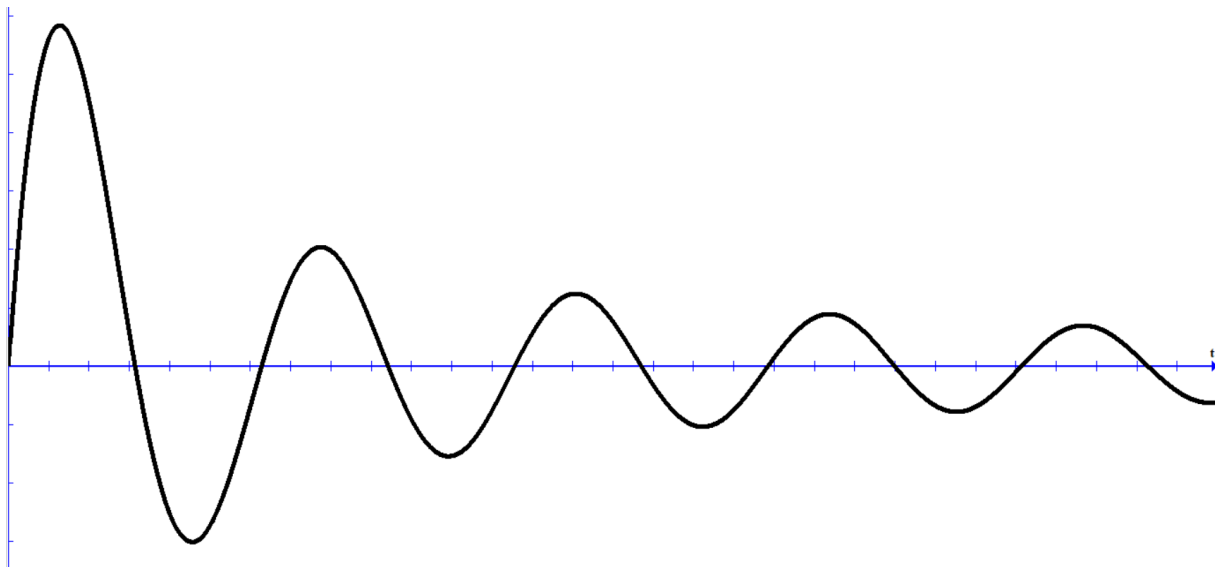


FIGURE 5 – TRANSIENT MOTION

3.1.2 WAVE PROPAGATION

If a vibration has commenced, waves in the soil will develop which will propagate through the soil. The simplest form of soil where it can propagate will be uniform soil, which means the same soil and its parameters are present anywhere. Important properties of wave propagation are wave propagation velocity c and particle velocity v . The wave propagation velocity is the speed at which the wave travels through the ground and the particle velocity is the speed of the motion of an individual particle. (Deckner, 2013)

Wave types

The two main types of waves are body waves and surface waves. Surface waves move along the surface of the soil, body waves also travel within the different soil layers.

Body waves

There are two kind of body waves, waves which travel through the earth's inner layers: primary (P-waves) and secondary (S-waves). These will be discussed separately.

P-waves

P-waves are the fastest kind of soil waves, so they are the first noticeable soil waves. The waves can move through liquids and solids. It pushes and pulls particles, which cause the wave. That is why they are sometimes also known as compressional waves. The particles move longitudinally in the direction the wave propagates (Braille, 2007). The velocity of a P-wave can be described as stated in equation (4) (Kramer, 1996).

$$v_p = \sqrt{\frac{G(2 - 2\nu)}{\rho(1 - 2\nu)}} \quad (4)$$

Where:

- v_p = Velocity of p-wave (m/s)
- G = Shear modulus (Pa)
- ρ = Material density (kg/m³)
- ν = Poisson's ratio (-)

Figure 6 shows the propagation of a P-wave in time.

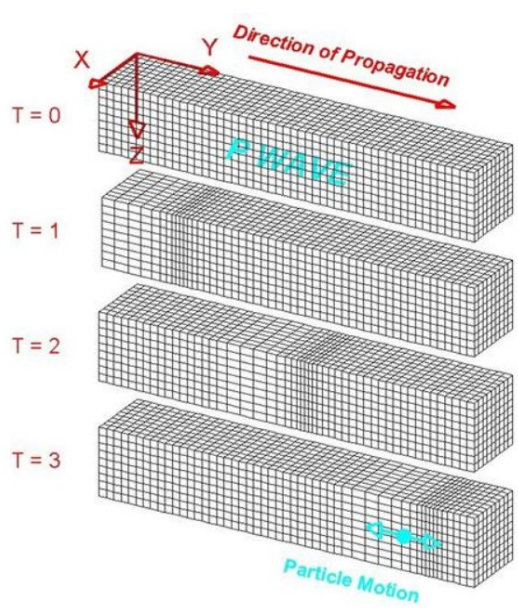


FIGURE 6 – P-WAVES (BRAILE, 2007)

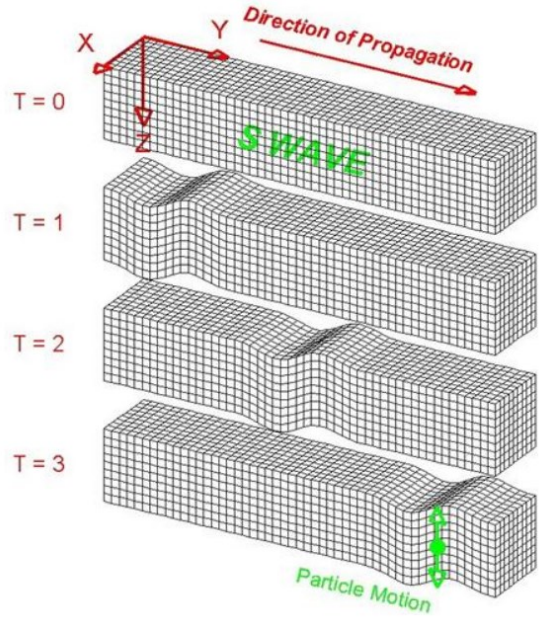


FIGURE 7 – S-WAVES (BRAILE, 2007)

S-waves

S-waves, also known as secondary waves, are slower than P-waves. In an S-wave, particles move perpendicular to the direction of wave propagation. This causes shearing deformations. It is not able to move through liquids, because liquids do not have any shearing stiffness. The waves can cause oscillation in both the vertical and horizontal plane (Braile, 2007). The velocity of S-waves is described as (Kramer, 1996):

$$v_s = \sqrt{\frac{G}{\rho}} \tag{5}$$

Where:

- v_s = Velocity of S-wave (m/s)
- G = Shear modulus (Pa)
- ρ = Material density (kg/m³)

Figure 7 shows the propagation of an S-wave in time.

Surface waves

Surfaces waves tend to have lower frequencies than body waves. These waves are the result of the interaction between body waves and the surface. The amplitude decreases the further the wave propagates. The most common surface waves are the Rayleigh waves (R-waves) and the Love waves.

R-waves

R-waves (abbreviation from Rayleigh waves, another name for this phenomenon), look a bit like rolling propagation of waves in the ocean. They move the ground up and down and side-to-side in the direction the wave is moving. Its motions tends to be larger than other kind of waves (Braile, 2007). Figure 8 shows the propagation of an R-wave in time. R-waves travel slightly slower than S-waves for all values of Poisson’s ratio except for $\nu = 0.5$ (Kramer, 1996) .

Love waves

Love waves are the fastest surface waves. These waves move the ground side-to-side in a completely horizontal motion (Braile, 2007). Figure 9 shows the propagation of a Love-wave in time. Love waves are frequency dependent, which makes them dispersive (Kramer, 1996).

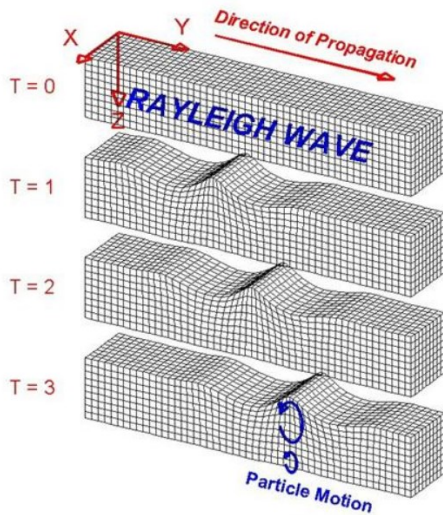


FIGURE 8 – R-WAVES (BRAILE, 2007)

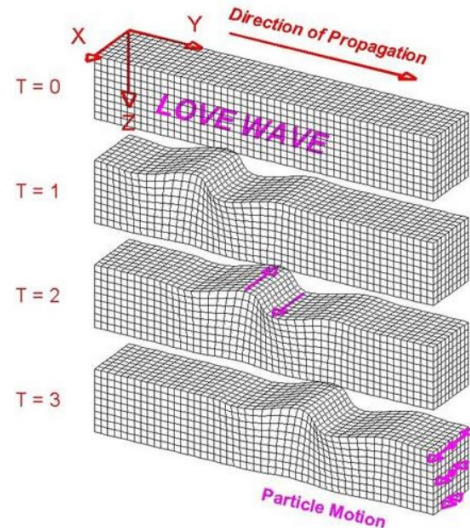


FIGURE 9 – LOVE WAVES (BRAILE, 2007)

Transmission

When a body wave in an elastic medium reaches the boundary that it shares with another elastic medium, some of the wave energy will be reflected and some of the wave energy will be transmitted to the other medium. It works about the same as light reflection and refraction according to Snell's law (Kramer, 1996). In Figure 10, the refracted and reflected waves from incident P-waves, SV-waves (vertical S-waves) and SH-waves (horizontal S-waves) are shown. Incident P- and SV-waves produce both reflected and refracted P- and SV-waves. Incident SH-waves only cause reflected and refracted SH waves, since there is no motion perpendicular to the interface (Kramer, 1996).

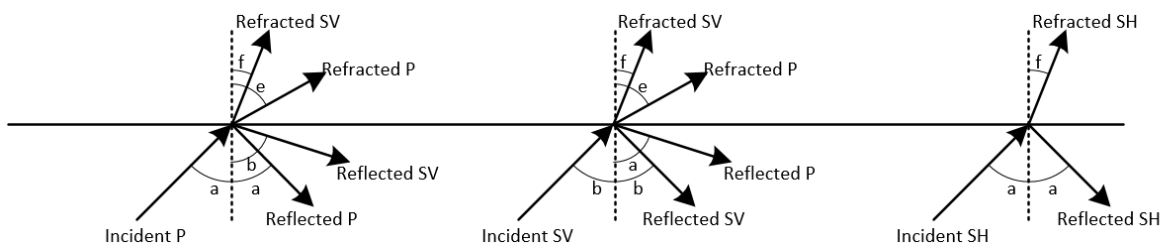


FIGURE 10 – REFLECTED AND REFRACTED RAYS FROM INCIDENT P, SV AND SH WAVES, MODIFIED AFTER DECKNER (2013)

The directions and amplitudes of the reflected and refracted waves rely on the direction and amplitude of the incident wave. Snell's law states (Kramer, 1996):

$$\frac{\sin(a)}{U} = \frac{\sin(b)}{V} = \frac{\sin(c)}{U} = \frac{\sin(d)}{U} = \frac{\sin e}{Y} = \frac{\sin(f)}{Z}$$

The meanings of the symbols are shown in .

Table 1.

TABLE 1 – SYMBOLS OF VELOCITY AND ANGLES OF WAVES, MODIFIED AFTER WOODS (1997)

Wave type	Velocity	Angle with normal
Incident P	U	a
Incident S	V	b
Reflected P	U	c
Reflected S	V	d
Refracted P	Y	e
Refracted S	Z	f

Geometric damping

As waves travel further through the soil, they pass larger volumes of ground. This leads to an energy reduction, which leads to a decay in the waves. This property is called geometric damping: as the waves travel further from the source, the amplitude of the wave decreases. This geometric damping can be described as in equation (6) (Woods, 1997):

$$A_2 = A_1 \left(\frac{r_1}{r_2} \right)^n \quad (6)$$

Where:

- A_2 = Amplitude of motion at distance r_2 from the source (m)
- A_1 = Amplitude of motion at distance r_1 from the source (m)
- r_2 = Distance from source to point of known amplitude (m)
- r_1 = Distance from source to point of unknown amplitude (m)
- n = $\frac{1}{2}$ for R-waves (-)
- 1 for body waves (-)
- 2 for body waves at the surface (-)

Material damping

Material damping is described as the damping capacity of the ground itself. Both the material damping and geometric damping can be described as in equation (7) (Woods, 1997):

$$A_2 = A_1 \left(\frac{r_1}{r_2} \right)^n \exp(-\alpha(r_2 - r_1)) \quad (7)$$

α is described as a variable that depends on the character of the grounds: the softer the ground, the greater the α -value. The α -value is also frequency dependent. However, it is linearly dependent on frequency, and therefore the formula for the α -value at another frequency can be computed as in equation (8) (Woods, 1997)

$$\alpha_2 = \alpha_1 \left(\frac{f_2}{f_1} \right) \quad (8)$$

where α_1 is the known frequency at f_1 and α_2 is the unknown frequency at f_2 . Table 2 describes the α -value at 5 Hz, for different types of soil. Therefore, the second part of the equation describes the material damping.

TABLE 2 – α -VALUE OF DIFFERENT SOILS, MODIFIED AFTER WOODS (1997)

Class	α -value at 5 Hz	Description of material
I	0.01 to 0.033	Weak or soft soils – loose sand, loose beach sand, organic soils, topsoil, dry or partially saturated peat and muck
II	0.0033 to 0.01	Competent soils – most sands, sandy clays, silty clays, gravel
III	0.00033 to 0.0033	Hard soils – dense compacted sand, dry consolidated clay
IV	<0.00033	Hard, competent rock – bedrock, freshly exposed hard rock

3.1.3 DYNAMIC PROPERTIES SOIL

The dynamic properties of soil are important when it comes to dynamic loading. In the next section a couple of dynamic properties will be discussed.

Shear modulus

The shear modulus, G , is a measure of the stiffness when it comes to shearing. The shear modulus is not constant: it varies with the strain. The shear modulus has its largest values (G_{max}) at small shear strains (Deckner, 2013). With increasing shear strains, the shear modulus decreases. Moreover, the plasticity index, PI , has an effect on the shear modulus. These relationships can be seen in Figure 11.

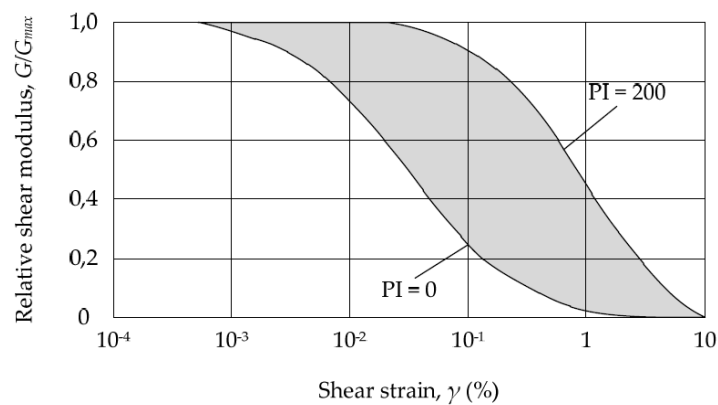


FIGURE 11 – RELATIONSHIP BETWEEN SHEAR MODULUS, SHEAR STRAIN AND PLASTICITY INDEX DECKNER (2013)

The shear modulus G is related to the elastic modulus E as described in equation (9):

$$E = 2G(1 + \nu) \quad (9)$$

Where:

- E = Elasticity modulus (Pa)
- G = Shear modulus (Pa)
- ν = Poisson's ratio (-)

Wave propagation properties

Waves keep on moving at the same propagation velocity c . At this velocity, the wave travels through the soil. The velocity of the various particles as the wave passes is the particle velocity v . The difference in the wave velocities are shown in .

Table 3.

TABLE 3 – VELOCITIES OF BODY WAVES IN DIFFERENT SOIL TYPES (HEAD & JARDINE, 1992)

Type of soil	c_p (P-wave velocity) (m/s)	c_s (S-wave velocity) (m/s)
Vegetal soil	300-700	100-300
Dry sands	400-1200	100-500
Wet sands	1500-2000	400-600
Saturated shales and clays	1100-2500	200-800
Marls	2000-3000	750-1500
Saturated shale and sand sections	1500-2200	500-750
Porous and saturated sandstones	2000-3500	800-1800
Water	1450-1500	-
Ice	3400-3800	1700-1900

According to Woods (1997), the wave velocity depends on Young's and shear moduli and density of the soil.

According to Massarsch & Fellenius (2008), the P-wave velocity is dependent on the water saturation. Below the groundwater table, this wave velocity corresponds to the 1450 m/s wave velocity of water. Shear wave velocity is not influenced by this, since liquids lack shear strength. R-wave velocity is usually unaffected by groundwater, but is generally lower in moist soil. The properties of different wave types are shown in Table 4.

TABLE 4 – SUMMARY OF PROPERTIES REGARDING WAVE PROPAGATION, MODIFIED AFTER HEAD & JARDINE (1992)

P-wave	S-wave	R-wave
Highest propagation velocity	Intermediate propagation velocity	Lowest propagation velocity
Longitudinal oscillation	Transverse oscillation	Vertical oscillation, but horizontal component develops with distance
Propagation velocity increases below groundwater level	Propagation velocity decreases below groundwater level	Propagation velocity unaffected by groundwater but generally lower in moist soil
Propagation velocity increases with material stiffness	Propagation velocity increases with material stiffness	Propagation velocity increases with material stiffness and is independent of frequency in homogeneous material
Energy proportion propagated is low	Energy proportion propagated is medium	Energy proportion propagated is high
Displacement amplitude is proportional to $\frac{1}{distance}$	Displacement amplitude is proportional to $\frac{1}{distance}$	Displacement amplitude is proportional to $\frac{1}{\sqrt{distance}}$

According to research performed by Woods (1997), the propagation velocity is dependent upon Poisson's ratio. P-wave velocity increases exponentially if Poisson's ratio increases.

S-wave velocity is also strongly dependent on void number, and usually increases in depth, soil usually has a greater pressure the deeper the measurement is taken (Massarsch & Fellenius, 2008). Lastly, the shear wave velocity decreases with increasing values of the shear strain (Whenham, 2011).

Impedance

Impedance is the ratio between force and velocity. This will be explained in the following section by elaborating 3 different types of impedance.

Pile impedance

The general formula for pile impedance is shown in equation (10):

$$Z_p = \frac{EA_p}{c_p} \quad (10)$$

Where:

- Z_p = Impedance of pile ($\text{Pa} \cdot \text{s} \cdot \text{m}^{-1}$)
- E = Elasticity modulus (Pa)
- A_p = Pile cross section area (m^2)
- c_p = Wave propagation speed in the pile (m/s)

The impedance limits the amount of force that can be transmitted along the pile. As can be seen in the formula, it is solely a function of the pile material and dimensions, which makes it independent of the soil it is driven in. The amount of pile impedance influences the amount of energy that can be transmitted into the soil (Woods, 1997).

Soil impedance

The soil impedance depends on the cross-section area of the pile toe with the soil. Equation (11) describes the soil impedance Z_s (Deckner, 2013):

$$Z_s = A_p c_p \rho_{soil} \quad (11)$$

Where:

- Z_p = Impedance of pile ($\text{Pa} \cdot \text{s} \cdot \text{m}^{-1}$)
- A_p = Pile cross section area (m^2)
- c_p = Wave propagation speed in the pile (m/s)
- ρ_{soil} = Density of the soil (kg/m^3)

With the soil impedance, the dynamic soil resistance along the pile shaft can be estimated, according to equation (12) (Massarsch & Fellenius, 2008):

$$R_s = z_s v_p S_p \quad (12)$$

Where:

- R_s = Dynamic soil resistance along the pile shaft (kN)
- z_s = Soil impedance for shear waves (kNs/m^3)
- v_p = Particle velocity of the pile (m/s)
- S_p = Contact area between shaft and soil (m^2)

Specific impedance

The specific impedance is used to relate the compressive stress and the particle velocity of a propagating wave. It is applicable to both P and S-waves. For S-waves, equation (13) is applicable (Massarsch & Fellenius, 2008):

$$z_s = c_s \rho_{soil} \quad (13)$$

Where:

$$\begin{aligned} c_s &= \text{Shear wave velocity of the soil at the pile/soil interface} \\ &\quad (\text{m/s}) \\ \rho_{soil} &= \text{Soil density (kg/m}^3\text{)} \end{aligned}$$

Using the specific impedance, the dynamic soil resistance along the pile shaft can be estimated, according to equation (14) (Massarsch & Fellenius, 2008):

$$R_s = z_s v_p S_p \quad (14)$$

Where:

$$\begin{aligned} R_s &= \text{Dynamic soil resistance along the pile shaft (kN)} \\ z_s &= \text{Soil impedance for shear waves (kNs/m}^3\text{)} \\ v_p &= \text{Particle velocity of the pile (m/s)} \\ S_p &= \text{Contact area between shaft and soil (m}^2\text{)} \end{aligned}$$

3.2 MASONRY

The scope of this section is to gather more knowledge regarding the vibrations from (sheet) piling on a masonry wall. Basic knowledge about masonry, and its dynamic properties is therefore required. This chapter will explain more about this material.

3.2.1 INTRODUCTION

In over half the houses built in the Netherlands, the load bearing walls are constructed using masonry. Masonry usually consists of bricks with measurement of around 50 x 100 x 210 mm. Mortar is used to connect these bricks. The horizontal parts of mortar are called the bed joints and the vertical ones are called the head joints. During the construction phase, this mortar is in the plastic phase, which enables it to flow into the irregularities in the contact area of the bricks. Following this, the mortar hardens and this way, forces can be transferred through the entire cross section. (Gerrits, 2008)

Masonry walls in the Netherlands usually consist of multiple leafs. For the outer layer, usually only clay brick is used. Inner layers can also consist of calcium silicate or aerated concrete. Between leafs there is usually a cavity which provides insulation. The standard mortar used is general purpose mortar, which is a mix of binder (cement), sand and water (Terwel, 2017).

The bricks can be stacked in various patterns. In Figure 12, Figure 13, Figure 14 and Figure 15, various common patterns are demonstrated.

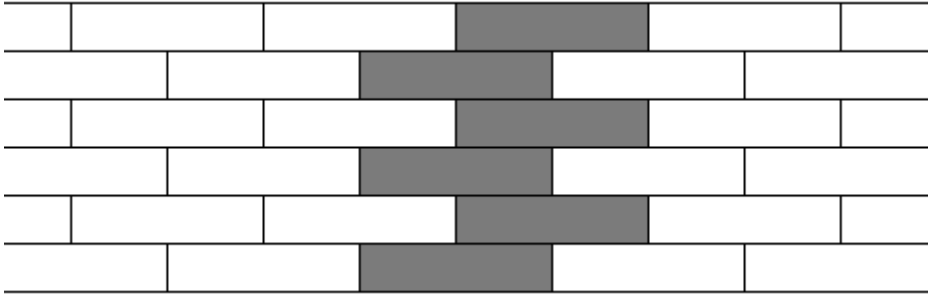


FIGURE 12 – STRETCHER BOND, MODIFIED AFTER GERRITS (2008)

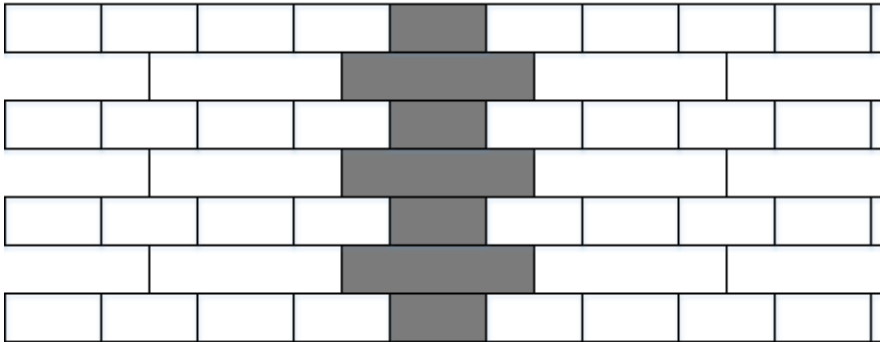


FIGURE 13 – ENGLISH BOND, MODIFIED AFTER GERRITS (2008)

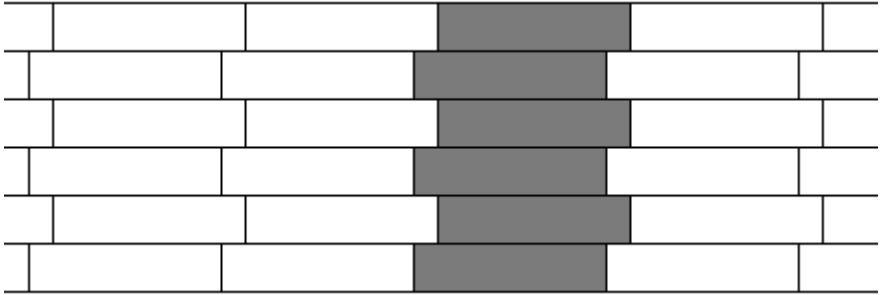


FIGURE 14 – RAKING STRETCHER BOND, MODIFIED AFTER GERRITS (2008)

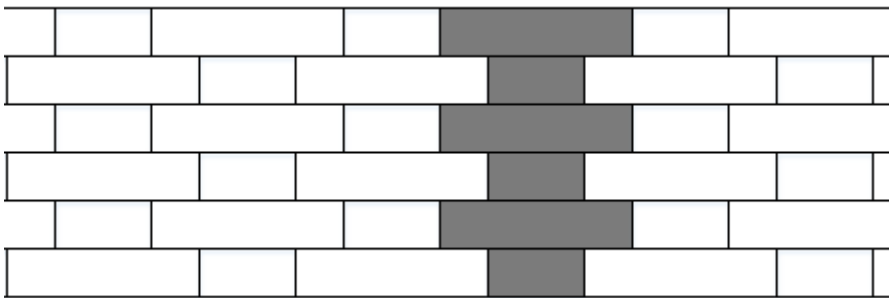


FIGURE 15 – FLEMISH BOND, MODIFIED AFTER GERRITS (2008)

In the Netherlands, as stated before, there are usually cavities between leafs. There is a difference between old buildings and new buildings regarding the width of the cavities. Historically, cavities were only used for ventilation, so a thickness of 30-40 mm was sufficient. Nowadays, structural designers tend to use thicker insulation materials, which leads to cavities with a thickness of 100-150mm. Between leafs, ties are used to keep the leafs together (Terwel, 2017).

3.2.2 PROPERTIES OF MASONRY

In this section, the properties of masonry are elaborated. This is helpful to understand how a masonry structure would be affected by vibrations acting on the system. Using the knowledge regarding these properties, the prediction of the effects of vibration can be improved.

Compressive strength

The height to width ratio can have large influence in the apparent compressive strength, because of the Poisson’s effect, which means that material tends to expand in the transverse direction when it is loaded under a uniaxial compressive load. This amongst other factors that affect the masonry strength are demonstrated in Table 5.

TABLE 5 – CHARACTERISTICS THAT INFLUENCE COMPRESSIVE STRENGTH (HENDRY, SINHA, & DAVIES, 1997)

Unit characteristics	Mortar characteristics	Masonry
Strength	Mixture	Bond
Type and geometry	Water/cement ratio	Direction of stressing
	Water retentivity	Local stress raisers
	Deformation characteristics	

According to various compression tests on masonry and other materials have stated a few conclusions about the compression strength (Hendry et al., 1997):

- Masonry will fail due to tension cracks parallel to the axis of loading or by failure along certain lines of weakness. This depends on the strength of the mortar compared to the strength of the brick.
- Strength of masonry in compression is smaller than the strength of the bricks in a standard compression test, but greatly exceeds the cube crushing strength of the mortar.
- Compressive strength varies roughly as the square root of the brick crushing strength and the third or fourth root of the mortar cube strength.

Usually, empirical relationships are used and are incorporated in practice. With these empirical relations, the strength of masonry can be shown. A good estimation of the compressive strength of masonry is 20 N/mm² (Hendry et al., 1997). This relation for various mortar strengths is shown in Figure 16.

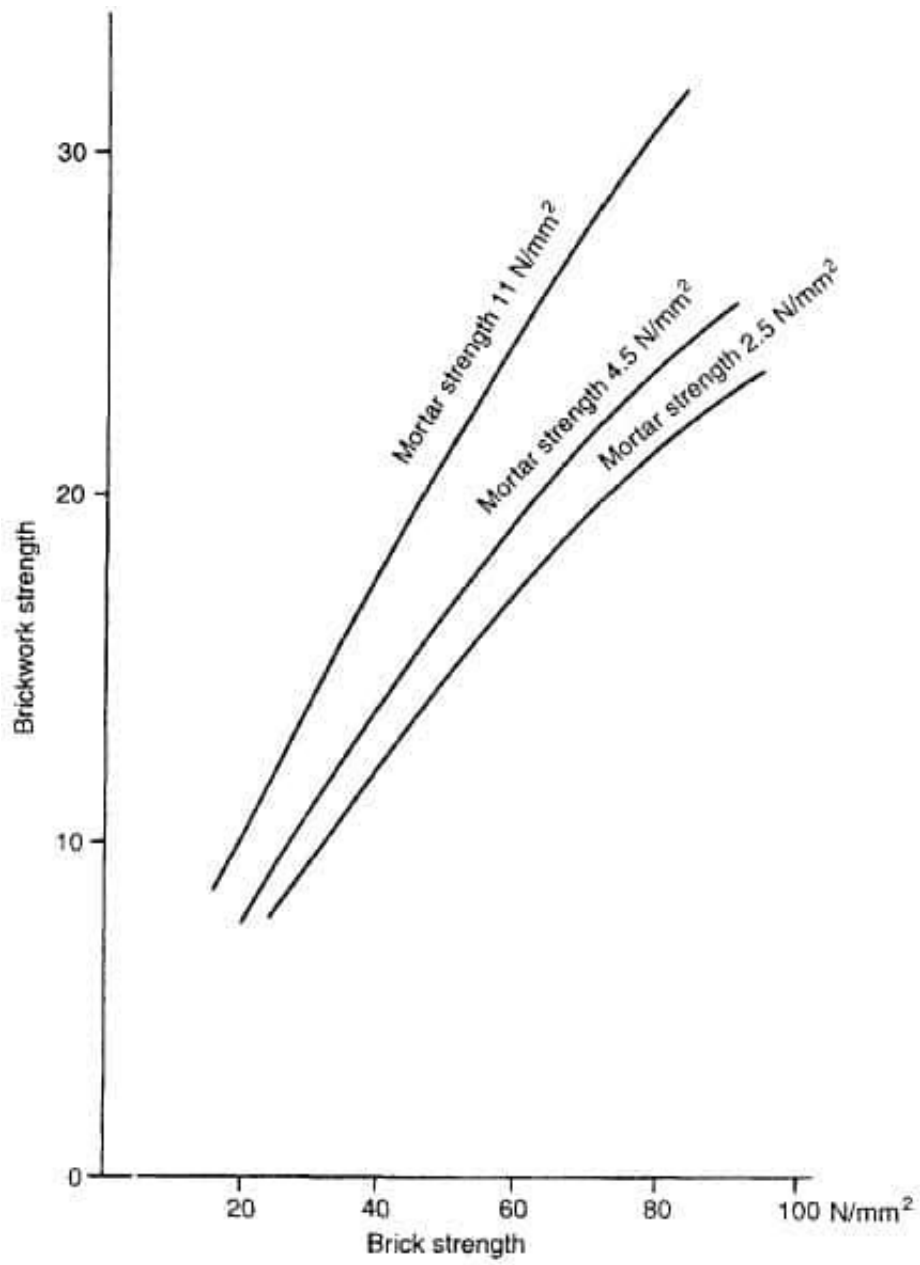


FIGURE 16 – BRICKWORK STRENGTH VS BRICK STRENGTH (HENDRY ET AL., 1997)

Modulus of Elasticity – Stress strain relationship

Although tests have shown that the stress – strain relationship of masonry is approximately parabolic, in service conditions it can be treated linear-elastically. This can be done because with typical structural deformations, it is only loaded until a fraction of its ultimate load. Young’s modulus for masonry is still an approximation, and equation (15) is assumed (Hendry et al., 1997):

$$E = 700\sigma'_c \tag{15}$$

where σ'_c is the crushing strength of masonry. Figure 17 demonstrates a typical stress – strain curve for masonry.

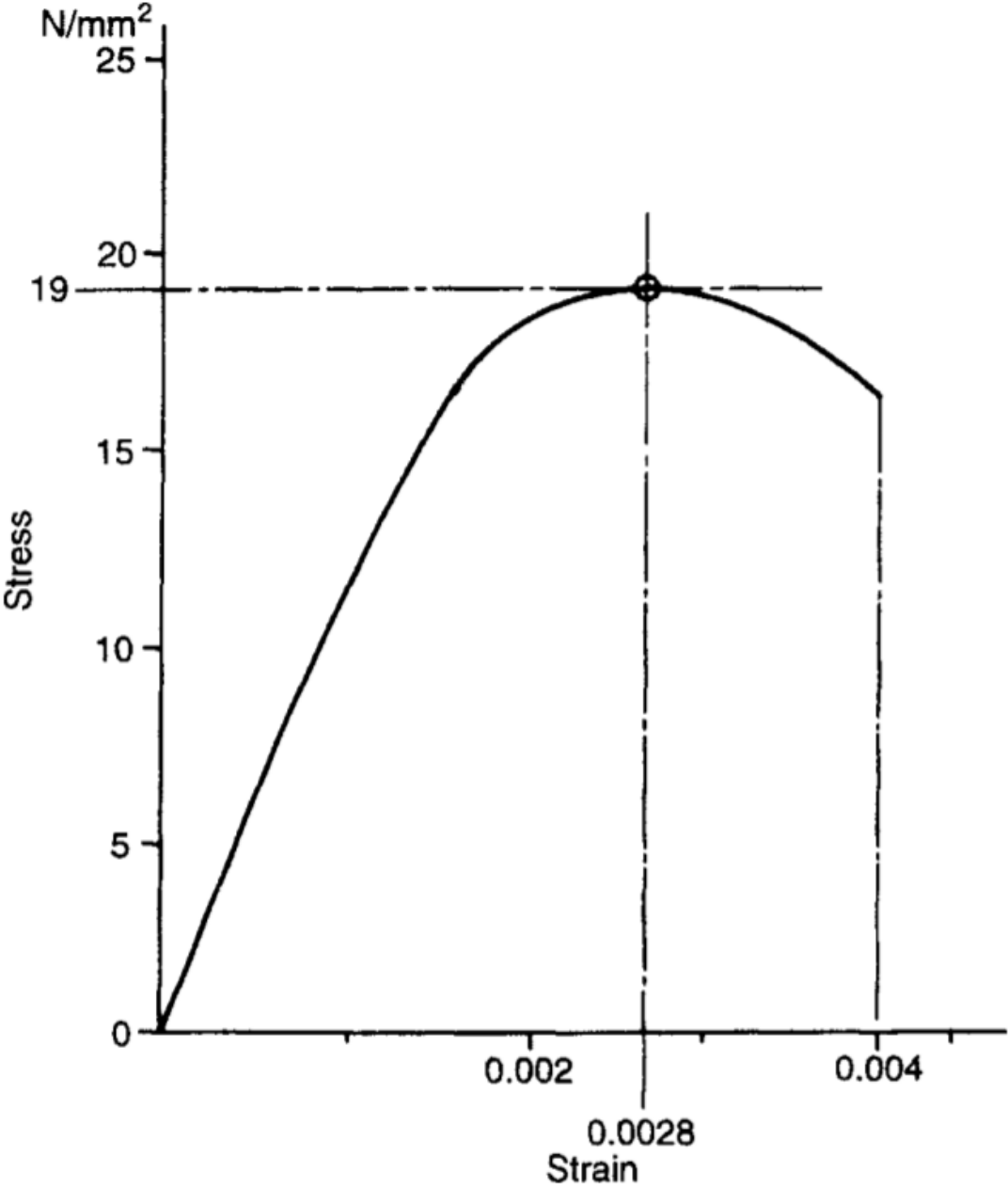


FIGURE 17 – STRESS-STRAIN CURVE FOR MASONRY LOADED IN COMPRESSION (HENDRY ET AL., 1997)

Tensile strength

There is a difference between direct tensile strength and the flexural tensile strength. The direct tensile strength is due to phenomena that cause in-plane deformations. Flexural tensile strength, can also be called bending strength, is caused by phenomena that cause out-of-plane deformations.

Direct tensile strength

Direct tensile stresses can be a result of in-plane loading effects. It can be caused by phenomena like wind loading and foundation movement among others. Masonry's tensile strength is generally quite low and should not be relied on. However, there should be some adhesion between the mortar and the bricks, to keep a solid material, and therefore, the masonry should have some tensile strength.

The grading of the mortar sand is important to the adhesion, very fine sands are unfavourable for this. For clay brickwork, also the moisture content is important: fully dry and fully saturated bricks are unfavourable.

Direct tensile strength is typically around 0.4 N/mm^2 at ideal conditions (Hendry et al., 1997), like an ideal moisture content. However, this ideal condition is not realistic and it would be an overestimation to assume this value of tensile strength.

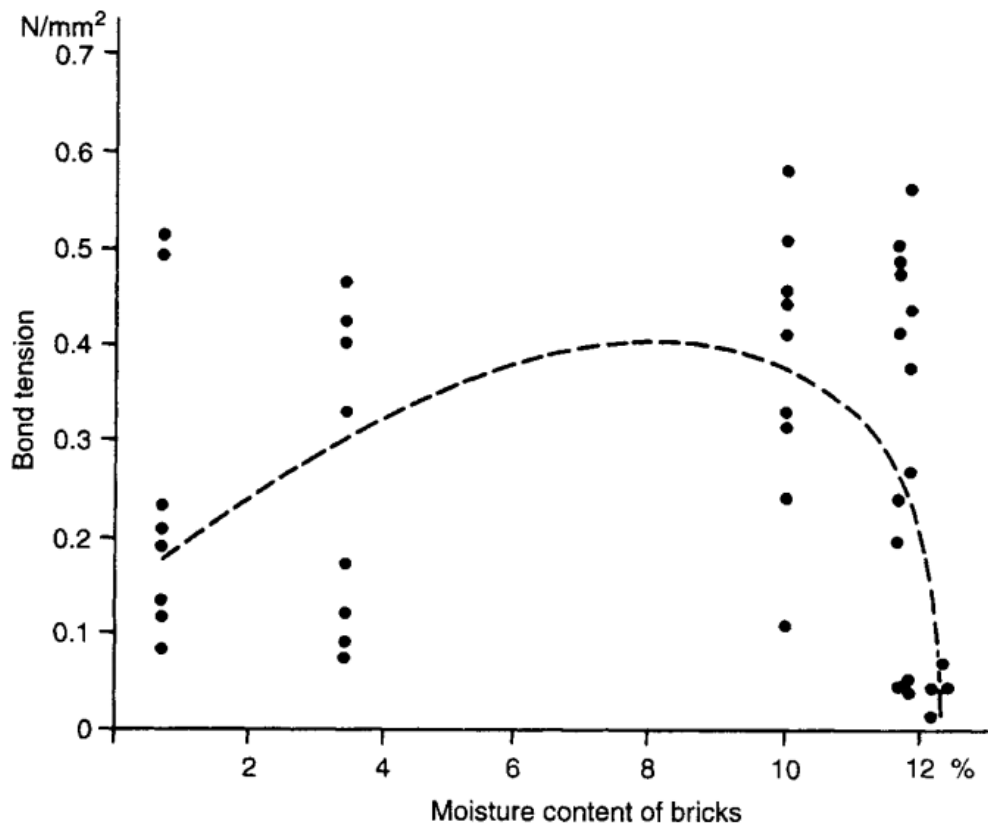


FIGURE 18 – RELATIONSHIP BETWEEN THE BOND TENSION AND THE MOISTURE CONTENT OF THE BRICKS (HENDRY ET AL., 1997)

Flexural tensile strength

Flexural tensile strength is required because a wall also has to withstand lateral wind pressures and suction. If the wall is only supported at its base and top, the bed joints will provide the lateral resistance and this resistance will depend on the flexural tensile strength of these joints. If it is also supported at its sides, also the brickwork in a straight angle with the bed joints will provide flexural tensile strength. This strength is usually three times larger than the direct tensile stress (Hendry et al., 1997). Also, the adhesion is important. A low adhesion will result in a lateral strength which depends on the shear strength of the brick-mortar interface. If this adhesion is sufficient, it will improve the flexural tensile strength of the brickwork.

The flexural tensile strength of clay brickwork is usually between 0.8 and 2.0 N/mm², while the strength in bending across bed-joints is usually between 0.3 to 0.7 N/mm² (Hendry et al., 1997). Calcium silicate and concrete brickwork tend to have a smaller flexural tensile strength than clay brickwork.

Shear strength

The shear strength of masonry is important, since walls are often exposed to both shear and compressive forces. There is a Coulomb type of relationship between shear strength and pre-compression, shown in Figure 19. The expression for this relationship can be formulated as in equation (16) : (Hendry et al., 1997)

$$\tau = \tau_0 + \mu\sigma_c \quad (16)$$

Here, τ_0 is the shear strength at no pre-compression, μ is the friction coefficient and σ_c is the vertical pre-compression stress. This shows that the greater the pre-compression, the better the wall can resist shear stresses. The shear strength also depends on the mortar strength. The shear strength at zero pre-compression (τ_0) usually has values between 0.2 and 0.3 N/mm².

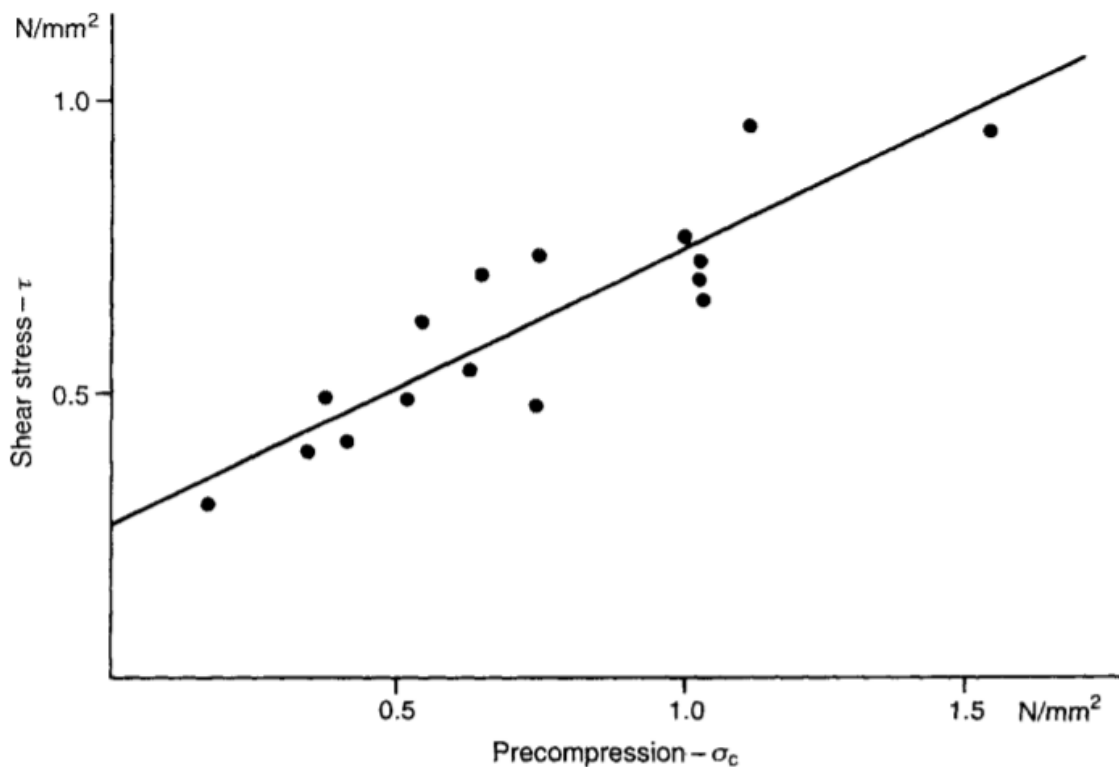


FIGURE 19 – RELATIONSHIP BETWEEN SHEAR STRENGTH AND PRECOMPRESSION. (HENDRY ET AL., 1997)

Absorption properties

Regarding the absorption, the initial rate of absorption (IRA) is important. This value should be in between 0.25 kg/min/m² and 2.05 kg/min/m² (Horng, 2010). If the IRA value is lower than 0.25 kg/min/m², this results in low-absorption units. This can produce a poor bond between mortar and brick. It affects the masonry's flexural strength but also the water tightness and therefore, the durability. If the IRA value is higher than 2.05 kg/min/m², the unit is highly absorptive. This results in a poor bond if the layer of mortar is thin or dry. Moreover, the mortar can stiffen very quickly, which causes trouble with the setting of the units. This problem can be prevented by wetting the brick before laying.

Durability

Durability can be regarded as the ability of a structure to remain functional after a period of time without excessive maintenance. Masonry itself is quite capable of this but it is important to select materials with the right properties regarding durability.

Factors that contribute to the durability are the ability to withstand frost action, salt crystallisation, sulphate attack and the attack of biological agents. Water is involved in all of those actions, so it is important for the structure to withstand the penetration of water.

3.2.3 FAILURE MODES

In-plane loading

In-plane loading can lead to failure in various ways: by tension (horizontal and vertical), shear and compression (horizontal and vertical).

Figure 20 shows the failure pattern when it is loaded in vertical tension. This leads to an exceedance of the maximum bond stress between the bricks and the mortar. This results in an almost horizontal crack in the mortar between two rows of bricks.

When tension forces are applied in the horizontal direction, as shown in Figure 21, this typically leads to exceedance of the maximum bond stress between the bricks and the mortar. This will result in an almost vertical crack. Sometimes, as shown in the figure, it will only cause a crack in the mortar, but sometimes the crack will propagate through the bricks as well.

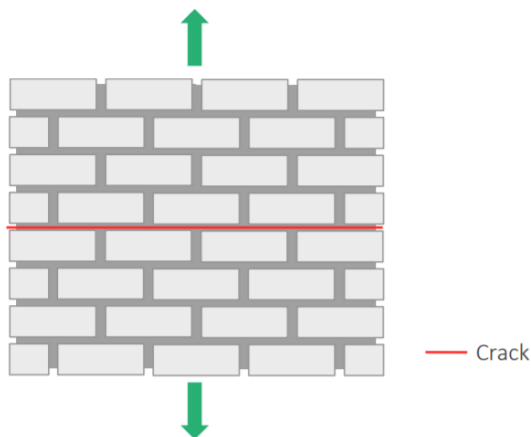


FIGURE 20 – VERTICAL TENSION (SCHIPPER, 2017)

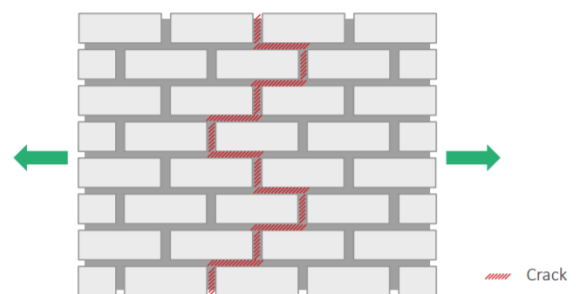


FIGURE 21 – HORIZONTAL TENSION (SCHIPPER, 2017)

If shear action is working on the wall, horizontal forces are working in opposite directions. This leads to sliding of these brick layers. When a vertical force is applied to the masonry, sliding of those brick layers can become more difficult and that way shear resistance can be increased. This sliding is shown in Figure 22. Another way a wall can fail due to shear loading, is when the structure is constrained at the top and the bottom of the structure, but is also subject to horizontal forces at the top or the bottom. This leads to shear stresses in the bottom and the top and to a horizontal tensile strength. This then leads to diagonal cracks along the wall. In Figure 23 this phenomenon is shown on a church in Quebec City in Canada. (EERI, 1988)

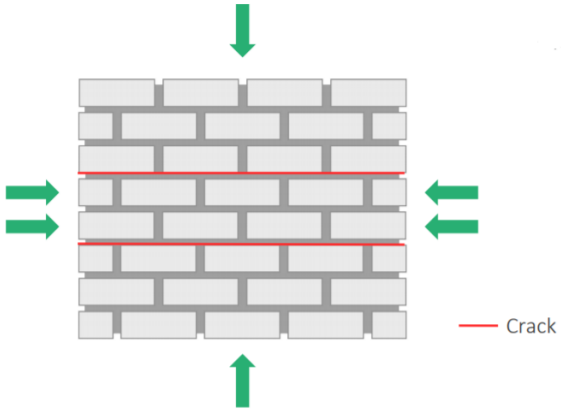


FIGURE 22 – SHEAR (SCHIPPER, 2017)



FIGURE 23 – DIAGONAL CRACK IN A CHURCH IN QUEBEC CITY , CANADA (EERI, 1988)

Of all types of loading, masonry is best at withstanding compressive forces. As shown in the section 3.2.2, good quality masonry can withstand compressive forces of about 20 N/mm². When the compressive lead to stress levels that exceed this level, the masonry will be crushed, in the bed joints or in the bricks, this depending on which is best at withstanding the forces. In Figure 24 and Figure 25, respectively vertical and horizontal compression vectors are shown, with the corresponding crushing zones. While horizontal compression is possible, usually vertical crushing is governing, due to the self-weight of the structure acting in vertical direction.

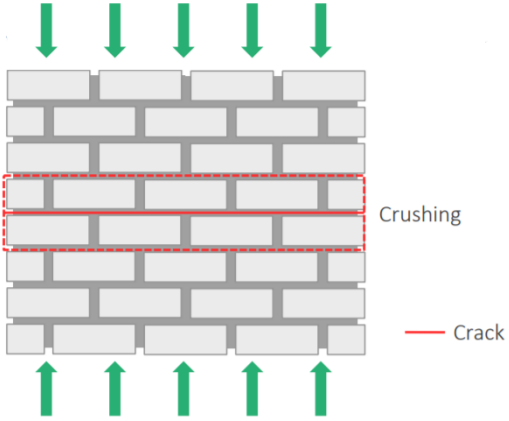


FIGURE 24 – VERTICAL COMPRESSION (SCHIPPER, 2017)

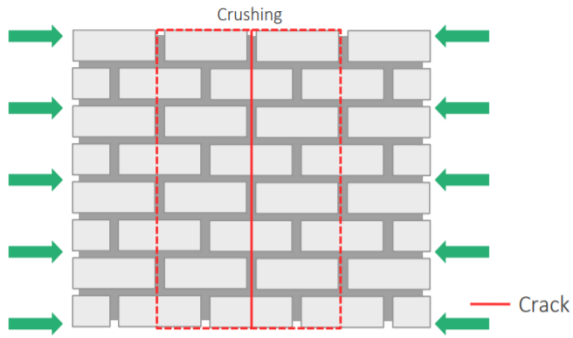


FIGURE 25 – HORIZONTAL COMPRESSION (SCHIPPER, 2017)

Out-of-plane loading

Out-of-plane loading can occur on different occasions, like the wind loading or when there are horizontal movements of the ground when the top and the bottom of the wall are restricted. In these cases, bending can occur. This leads to cracks in the side of the masonry which is stretched, due to the tension forces that occur in the mortar on this side.

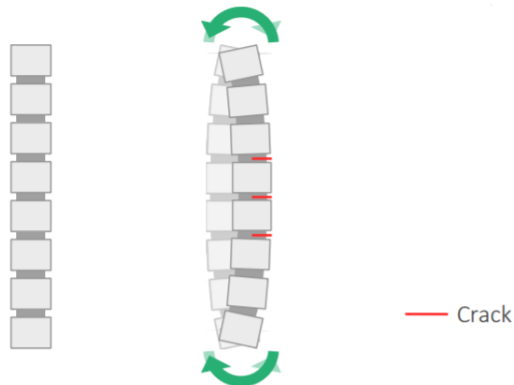


FIGURE 26 – BENDING (SCHIPPER, 2017)

3.3 FINITE ELEMENT METHOD AND CRACK MODELS

This project will require the modelling of different masonry walls and a method to calculate what the response of the structure on this load is, regarding stresses, strains and displacements/cracks. The Finite Element Method (FEM) could be a good tool to implement this into the project. Crack models can demonstrate how the cracks will develop in the structures, what can also be helpful regarding this project.

3.3.1 INTRODUCTION

The Finite Element Method has been created in the second half of the 20th century. The necessity for FEM was that a solution was needed to solve complex engineering problems. When computers came into use more and more, FEM was seen as a great possibility to solve these engineering problems, and this resulted in an increase in research regarding FEM, which led to ever improving calculation possibilities.

Nowadays, FEM is a numerical method that can be used for a wide variety of problems, not only structural, but also in electrical analysis and biomaterials. However, since it is the scope of the project, the focus will be on the structural problems.

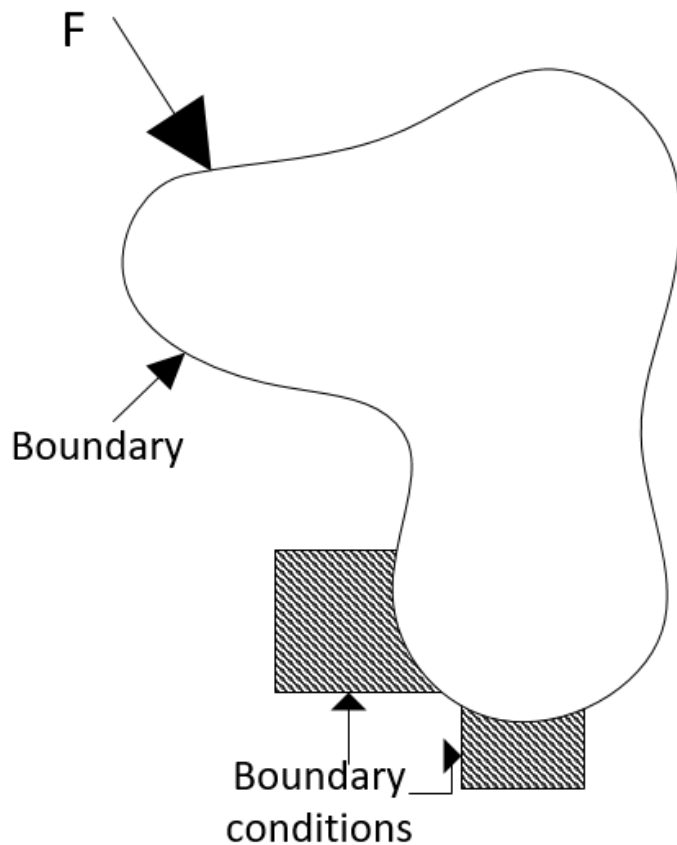


FIGURE 27 – BODY WITH FORCES AND BOUNDARY CONDITIONS, MODIFIED AFTER QI (2006)

Figure 27 shows a solid body, whereon a force is applied. The boundary conditions prescribe that the displacement at the point where those boundary conditions are applied should be equal to 0. Looking at this figure in a structural way, it would be helpful to know what the force’s effect would be the force on the structure’s stresses, strains and displacements. Figure 28 shows a flowchart for this operation.

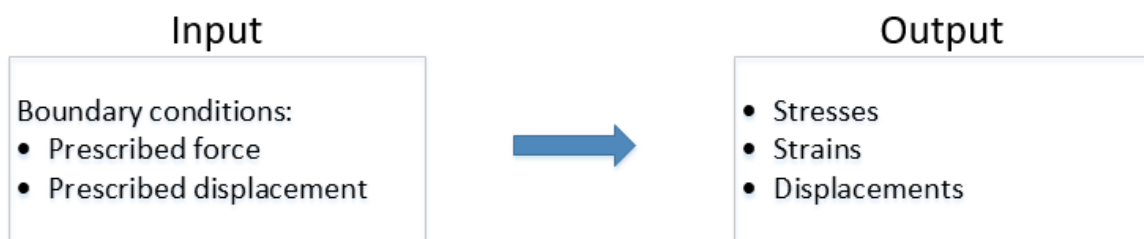


FIGURE 28 – INPUT AND OUTPUT, MODIFIED AFTER QI (2006)

To produce this output at all the material points, we have to solve a large set of equations if a lot of elements are used. Some of these equations are even partial differential equations. It would be extremely difficult, virtually impossible, to solve all of these equations analytically. The best way to tackle a problem like this would be to use the Finite Element Method. This gives a good *approximation* of the solution.

Using FEM-software, the structure will be divided in different *elements*. This elements can either be 1-D, 2-D or 3-D. The elements used in this project are limited to structural mechanics applications. This means that these elements relate stresses to displacements.

3.3.2 PREPROCESSING

Preprocessing is the process of creating the elements. Elements can be formed in many different ways. This section will show what has to be done regarding preprocessing.

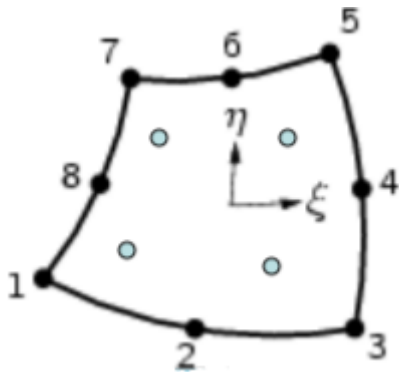


FIGURE 29 – PLANE STRESS ELEMENT (HENDRIKS & ROTS, 2015)

In Figure 29, a plane stress element is shown. In a finite element, the input will be the displacement at the nodes. The nodes in this figure are shown in numbers 1 to 8. The element will then produce an output, which are the internal forces at the nodes. Another output will be an estimate of the current element stiffness, this helps to find better displacement fields.

The steps of the calculation process will be the following:

- 1) Input: displacements at the nodes.
- 2) Interpolation from nodes to integration points (the 4 grey points in the middle of the element, in Figure 29).
- 3) With a stress-strain relationship, the displacements and the stresses can be linked.
- 4) With integration, the internal forces at the nodes and the element stiffness can be determined.

TABLE 6 – FINITE ELEMENT CHARACTERISTICS

Characteristic	Examples
Dimension of the shape	<ul style="list-style-type: none"> • 0-D point mass • 1-D straight line • 2-D flat shell • 3-D wedge
Topological dimension	<ul style="list-style-type: none"> • 0-D point • 1-D straight or curved line • 2-D quadrilateral or triangle • 3-D brick or wedge
Assumptions for displacements, stress and strain field	<ul style="list-style-type: none"> • Plane strain • Plane stress
Interpolation for the displacement, strain and stress field	<ul style="list-style-type: none"> • Linear • Quadratic • Cubic
Types of degrees of freedom	<ul style="list-style-type: none"> • Displacement • Rotation
Calculation method	<ul style="list-style-type: none"> • Numerical integrated • Analytical

Table 6 describes different characteristics of finite elements. The plane stress element of Figure 29 is for example a 2-D flat shell, a 2-D quadrilateral and a plane stress element. The other characteristics depend on the amount of integration points and/or the choice of the user.

When the elements are chosen, the structure can be *meshed*. This means that the structure will be divided into elements. Usually, a software program will create the mesh, although it can be done by hand.

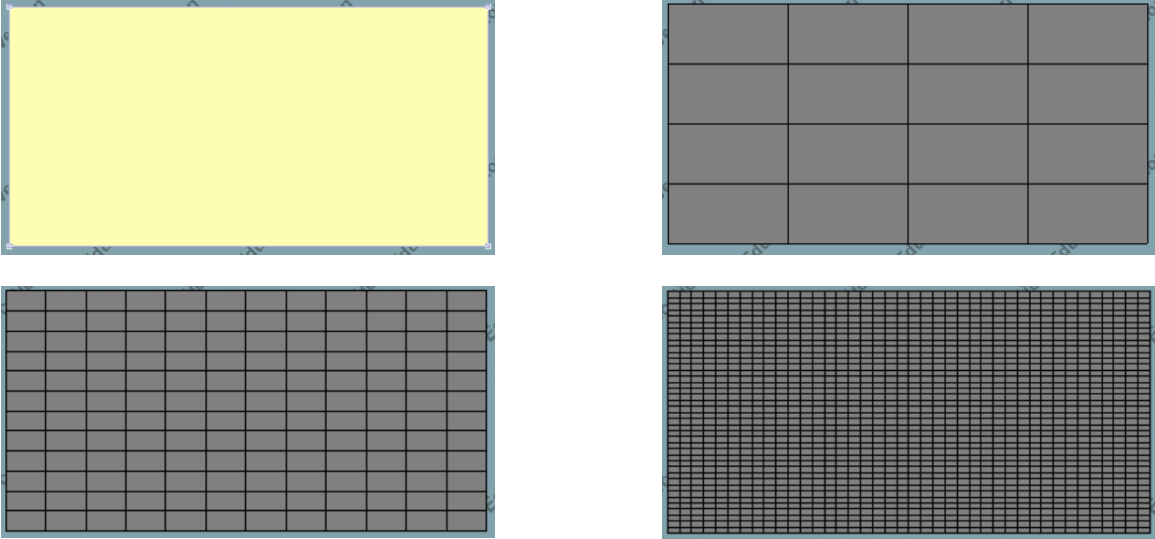


FIGURE 30 – MESHES. TOP LEFT IS THE ORIGINAL STRUCTURE, THE OTHERS SHOW MESHES WITH DIFFERENT ELEMENT SIZES.

3.3.3 ANALYSIS

The analysis phase follows the preprocessing phase. The software program will read the input data from the previous phase. The program will then start to interpolate the displacements and strains from the nodes to the integration points. With a stress-strain relation the link between those properties will be set. Lastly during this phase, the internal forces and element stiffness will be integrated over the volume of this element (Wells, 2009).

In this phase, not much is required from the programs user. However, attention should be paid to a few things during this phase by the user:

- Sometimes, errors can occur. In most FEM-programs, a log-file can be generated which will show warnings and error messages. It is the user's responsibility to check this file if something odd occurs.
- Sometimes it is useful to check the generated stiffness matrix to see if there is indeed a concentration of terms on the diagonal (Wells, 2009).
- If necessary, check the convergence for nonlinear calculation.

3.3.4 POST-PROCESSING

The post-processing phase follows the analysis phase. In this phase, the results of the analysis will be evaluated. This can be done according to the following properties:

- Plots of displacements, stresses and strains.
- See if the results produces results that were expected, qualitative.
- Check if the equilibrium total load is in correspondence with the reaction forces.
- Quantitative interpretation.
- Hand calculation.

Figure 31 and Figure 32 show the stress and displacement contours of a simple structure supported on 2 points where a distributed load is applied on top. Inspecting this kind of plots is the first step of post-processing, because you can compare the plot with expected results and thus, perform a first qualitative check.

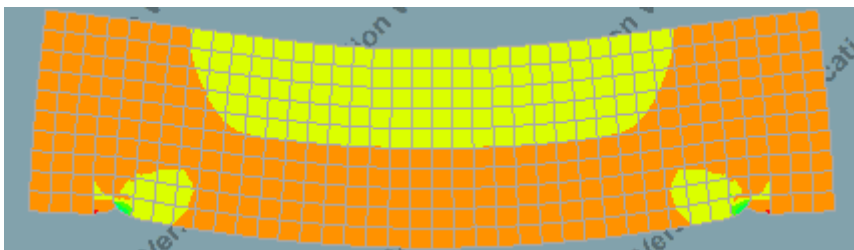


FIGURE 31 – STRESS CONTOUR FOR A SIMPLE DISTRIBUTED LOAD

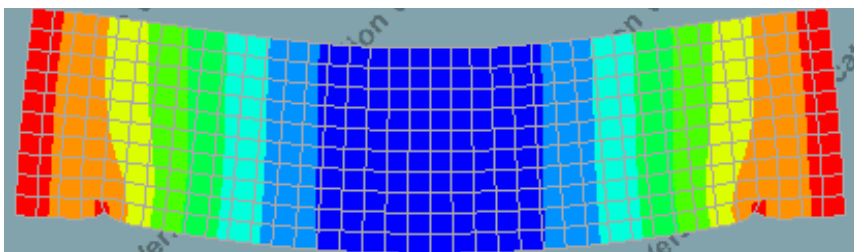


FIGURE 32 – DISPLACEMENTS FOR A SIMPLE DISTRIBUTED LOAD.

After post-processing, one can decide the results are sufficient, or to modify their pre-processing to get more accurate results. This can be done by changing the amount of integration points, changing the element size or using other integration methods.

Moreover, one should be careful in using *nodal averaging*. This can be explained in the following way: a node is at the edge of 2 adjacent elements. This results in the fact that the stress in the nodes is calculated in two different elements, which results in two different values. Graphically, this is shown as a gap between those two values. Nodal averaging takes both values and calculates the average of those values, which it graphically represents. Thus, this is a big improvement visually, since the graphs can get a lot clearer, but it can lead to great differences with the exact value. This is the reason why one should be very careful using this function in the post-processing phase of a project.

3.3.5 DISCRETE VS SMEARED CRACKING

For a good understanding of the failure mechanisms, crack models should be applied in a FEM-analysis. Two models will be discussed: discrete cracking and smeared cracking.

Using *discrete* crack models, there are springs or interface elements placed in the model, which leads to cracking in that point. This means that prior knowledge is required where the crack may occur. This can be done by engineering judgement, like the knowledge engineers are supposed to have that concrete will crack in the tensile zone, or that plastic hinges usually form at locations of supports or the point loads. At these locations, springs or interfaces are modeled in the FEM-model. This leads to the main structure (blocks) are kept linear, and the springs and interfaces respond nonlinearly (Willam & Carol, 1996). This is one way to include nonlinearity in the model.

Smeared cracking spreads the effect of cracking over the area that belongs to an integration point. The advantage of smeared cracking is that the cracks can occur anywhere in the mesh and in any direction. The crack is initiated when the principal tensile strength exceeds the value of maximum tensile strength. The direction of this crack is perpendicular to the direction of the principal tensile strength. Smeared cracking can be categorized in fixed and rotating crack concepts. In a fixed concept, the orientation of the crack is fixed during the entire process, whereas in the rotating concept, the crack can rotate with the axes of principal strain.

It has to be noted that both of these crack mechanisms occur using a nonlinear analysis, not in a linear-elastic approach.

3.4 PROBABILISTICS

Since this research project is about the *probability* of failure after applying vibrations on a masonry structure, the probabilistic properties are another point of attention of this project. The following section discusses the way these properties will be applied.

3.4.1 RELIABILITY

In reliability calculation, a verification has to be made if the resistance is larger than the load that can act on a structure. In terms where R represents the resistance and S represents the load, this results in equation (17):

$$R > S \quad (17)$$

These effects, resistance and load, are not deterministic but random variables. The aim in designing is to minimize the probability of having high loads and small resistances. The failure probability P_f can be written as:

$$P_f = P(S > R) \quad (18)$$

A *limit state function* is written as a limit state Z , which should not be smaller than 0:

$$Z = R - S \quad (19)$$

The failure probability can then be written as:

$$P_f = P(S > R) = P(Z < 0) \quad (20)$$

A general formulation for the limit state would be (Steenbergen, 2016):

$$g(\underline{X}) = Z = 0 \quad (21)$$

The vector \underline{X} consists of different structural variables, like material properties, loads, and uncertainties. These can be deterministic, when there is no variation in time or space, but can also be random, normal or lognormal distributed.

Figure 33 should shed more light on this case. On the x-axis, R is plotted, the resistance, which has a normal distribution. On the y-axis, S is plotted, which also has a normal distribution. In the figure, the limit state function and lines of equal probability of the functions R and S are plotted. The chance of failure P_f is equal to the volume of the joint probability density function in the region where $Z < 0$.

Mathematically, this can be written as:

$$P_f = \iiint_{Z < 0} f_R(r) f_S(s) dr ds \quad (22)$$

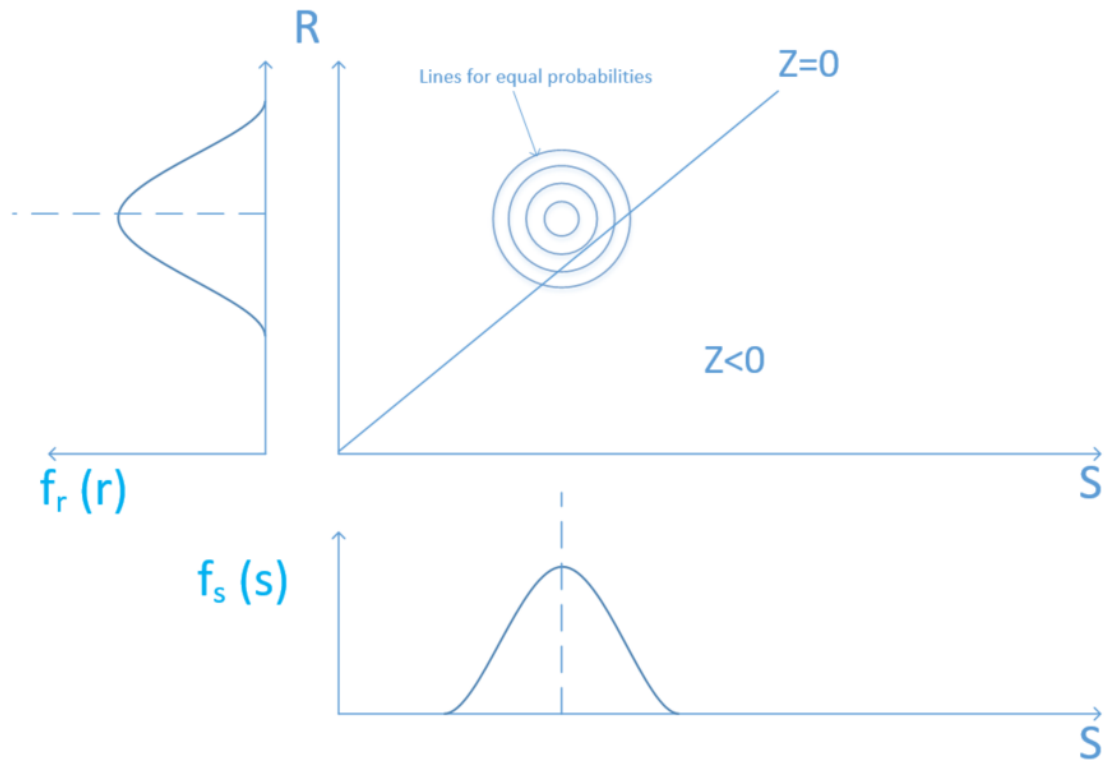


FIGURE 33 – FAILURE PROBABILITY

3.4.2 RELIABILITY METHODS

There are different levels of reliability methods, in a range from 0 to IV, as shown in Table 7 (Steenbergen, 2016).

TABLE 7 – RELIABILITY LEVELS

Level	Brief explanation
Level 0	Deterministic method, no reliability analysis
Level I	Semi-probabilistic, because of the use of safety factors
Level II	Probabilistic with approximations, i.e. the limit state function
Level III	Fully probabilistic method, i.e. Monte Carlo
Level IV	Costs are also taken into account.

Level 0, I and IV methods will not be investigated in this project. The reason level 0 and I will not be taken into account is that these methods will not lead to results reliable enough for these calculations. Level IV calculations will not be taken into account because costs will not be considered. For the level II method, the FORM-method will be investigated, while a Monte Carlo simulation will be considered as a level III method.

3.4.3 POSSIBLE RELIABILITY METHODS REGARDING THE PROJECT

FORM-method

The FORM-method is a reliability method of level II, which means that only the mean values of the basic variables and the moments of the first and second order are used in most cases. The probability density function is simplified and nonlinear limit state functions will be linearized in the design point using a Taylor series approximation (Steenbergen, 2016). This design point is the most probable point of failure. This point is found with an iterative procedure. After that, a failure probability graph as in Figure 33 can be made, which then can lead to an estimation of the probability of failure. This, because the iterative process leads to a constant value of the reliability index β , which can be translated to a probability of failure through a well-known table, based on the standard normal distribution. The reliability index β is the result of a division of the mean value and the standard deviation of Z .

TABLE 8 – RELIABILITY INDEX TO CHANCE OF FAILURE

β	P_f	β	P_f	β	P_f
3.00	0.001358	2.00	0.022853	1.00	0.159127
2.95	0.001598	1.95	0.025702	0.95	0.171553
2.90	0.001877	1.90	0.028842	0.90	0.184581
2.85	0.002199	1.85	0.032294	0.85	0.198207
2.80	0.002570	1.80	0.036081	0.80	0.212424
2.75	0.002997	1.75	0.040224	0.75	0.227219
2.70	0.003486	1.70	0.044749	0.70	0.242578
2.65	0.004047	1.65	0.049668	0.65	0.258482
2.60	0.004687	1.60	0.055013	0.60	0.274910
2.55	0.005415	1.55	0.060802	0.55	0.291837
2.50	0.006243	1.50	0.067057	0.50	0.309233
2.45	0.007180	1.45	0.073798	0.45	0.327069
2.40	0.008240	1.40	0.081046	0.40	0.345308
2.35	0.009434	1.35	0.088818	0.35	0.363914
2.30	0.010778	1.30	0.097132	0.30	0.382846
2.25	0.012285	1.25	0.106004	0.25	0.402062
2.20	0.013971	1.20	0.115447	0.20	0.421519
2.15	0.015853	1.15	0.125472	0.15	0.441169
2.10	0.017948	1.10	0.136090	0.10	0.460964
2.05	0.020275	1.05	0.147307	0.05	0.480857
				0.00	0.500798

Monte Carlo Simulation

Using the Monte Carlo method, random numbers are drawn from a probability density function. These random numbers from a number of probability density functions can be inserted into a limit state function. This limit state function returns if these numbers lead to failure or if they will not lead to failure. Naturally, one of those calculations using random numbers will not lead to a solid conclusion if a structure will fail or not. This is why this random calculation has to be repeated quite a few (n) times, and using all these calculations, it can be calculated how many times it fails over the n times the simulation was executed. This gives, when the size of n is sufficient, a solid conclusion regarding the probability of failure.

Comparison

The main advantage of the FORM-method over the Monte Carlo simulation, is that the FORM-method is a faster method regarding the computation time. Moreover, the results tend not to differ that much from each other. However, it is less used in industry because it takes some time to understand the mathematical complexity of this method. It is less difficult to model a Monte Carlo simulation than a model which uses the FORM-method, using a computing environment like MATLAB.

3.5 SOFTWARE POSSIBILITIES

The software that is useful in this project should be classified in different categories. Firstly, software programs that can be used for Finite Element Analysis should be considered. Secondly, useful programs regarding probabilistic design, more specifically the FORM-method, should be considered.

3.5.1 FINITE ELEMENT ANALYSIS

DIANA FEA

DIANA FEA is a finite element solver which is developed by TNO, a Dutch research institute which is specialized in applied sciences. It is a multipurpose program, and has special options for civil and building engineering. Nonlinear analysis can be applied. It is oriented on structural engineering, so it can model materials like concrete, steel and masonry quite good. It is sometimes difficult to model some characteristics, like a support which is modeled as a line spring, but with certain preprocessors (FX+ for DIANA) it can be easier to process these characteristics. The student license prohibits the usage of this preprocessor but it is accessible through Delft University of Technology.

SCIA

SCIA Engineer is a 2- and 3-dimensional calculation software program for analyzing and designing structures. It is widely used in the construction industry. Taking into account the proposed procedure, it is very convenient if SCIA can be used for the evaluation of this project's problem. This program is able to do finite element analysis. The student version contains all the functionalities that the standard version contains (SCIA, 2018). The only difference between those versions is that files are not interchangeable. The program is very convenient in its usage. For this project, dynamic analysis is important. SCIA Engineer has functionalities for dynamic analysis, however, there are limitations regarding the input of loads and the implementation of springs for a flexible soil-structure connection.

ANSYS

ANSYS is another program that is specialized in finite element analysis. Just like DIANA FEA, it is a multipurpose program and it is very useful in structural engineering. However, setting up a line spring support has proven being difficult, just like in DIANA FEA. Regarding this project, the student license is quite comprehensive.

TABLE 9 – COMPARISON FEM-SOFTWARE

Functionality	DIANA FEA	SCIA	ANSYS
Purpose	Multipurpose	Construction	Multipurpose
Convenience	Standard version reasonably, preprocessor would help a lot	Very convenient	Reasonably convenient
Student license	Only standard version, no preprocessors	Full functionality	Quite comprehensive
Line spring	Difficult to implement	Easy to implement	Difficult to implement
Sinusoidal load	Model as multifold trapezoidal load	Model as multifold trapezoidal load	Model as multifold trapezoidal load
Mesh refinement	No difficulties	Difficulties around corners	Difficulties around corners

3.5.2 PROBABILISTIC DESIGN

MATLAB

MATLAB is a multi-paradigm numerical computing environment developed by MATHWORKS. Using the toolbox created by the Computational Design of Engineering Systems (CODES) at the University of Arizona, a FORM analysis can be executed, where the probability of failure will be calculated. The program MATLAB is quite fast and convenient, however, it takes some time to gain a good command of the program. Moreover, codes can be written which enable the possibility of a Monte Carlo simulation. Another advantage of using MATLAB is that one can change codes easily because the program has to be written by the user.

Prob2B

The program Prob2B is designed by TNO and its function is that it can quickly calculate risk probabilities for various events. It can perform full probabilistic calculations, with various types of random variables. It is also able to use various methods to come up with a solution, like the FORM-method and a Monte Carlo analysis.

Microsoft Excel

Using Excel from Microsoft Office, it is possible to perform a FORM analysis. A great advantage is that Microsoft Office is used widely in all kinds of industries and a lot of people are able to work with it. This ability will be advantageous for the proposed procedure. Since Excel has a lot of functionalities it is possible to perform a wide range of operations in the FORM analysis. A disadvantage is that in comparison to a program like Prob2B, it is not a program that is directly focused on the probabilistic design.

4. COMPUTATIONAL EXPERIMENTS

4.1 CHOICE OF BOUNDARIES, DEFINITIONS, SOFTWARE, LOADS, PROCEDURES

4.1.1 BOUNDARIES

The investigated structures are assumed to be in the Netherlands. Given this fact, this results in some boundaries for this problem, which are investigated in this section.

Soil

The soil will be assumed a clay or sandy soil. This means material properties of these soils will be used in the project. The main material property that is used in this project will be the propagation velocity. In the experiments, different models will be used for sand and clay. Two different models will be created, one will perform the calculation with a sandy soil, while the other one will perform the calculation using a clay soil. The difference between those models will be the propagation velocity of the soil. For the sandy soil the propagation velocity is assumed to be 300 m/s, and for the clay soil it is assumed this property is 600 m/s, according to Head & Jardine (1992)

Vibrations

The considered vibrations are due to construction work. These can be caused by either sheet pile or pile driving. The frequencies of the vibrations depend on what method is used. For pile driving, lower frequencies will be assumed (3, 4 and 5 Hz) (Soede, 2009). For sheet pile driving, higher frequencies will be assumed (10, 15, 20 and 25 Hz) (Soede, 2009). These properties, combined with the propagation velocity of the different soils (300 or 600 m/s) will result in various wave lengths, as shown in Table 10. This occurs due to equation (23):

$$\lambda = \frac{v}{f} \quad (23)$$

Where λ is the wave length (m), v is the propagation velocity (m/s) and f is the frequency (Hz).

For the lower frequencies (pile driving) the amplitude of the vibration will dampen in time. The amplitudes of the higher frequency vibrations will remain the same in time.

TABLE 10 – WAVE LENGTHS FOR VARIOUS PROPAGATION VELOCITIES AND FREQUENCIES

Frequency (Hz)	Wave length for sand ($v=300$ m/s) (m)	Wave length for clay ($v=600$ m/s) (m)
3	100	200
4	75	150
5	60	120
10	30	60
15	20	40
20	15	30
25	12	24

Masonry properties

The masonry facades where the procedure will be tested upon will be based on current masonry structures in Delft, the Netherlands. Assumed is that the masonry consist of clay bricks and mortar with Portland cement as its binder. It is assumed that damage occurs in the masonry if the tensile strength is exceeded. According to the literature study in section 3.2, the tensile stress is assumed to be 0.3 N/mm^2 , while Young's Modulus is assumed to be 5000 N/mm^2 . Their variation coefficients are assumed to be 30%, according to the TNO report (Waarts, 1997).

TABLE 11 – MASONRY PROPERTIES

Property	Value
Tensile strength (f_t)	0.3 N/mm^2
Variation coefficient	30%
Young's modulus (E)	5000 N/mm^2
Variation coefficient	30%
Poisson coefficient	0.2

In-plane loading will be considered, whereas out-of-plane loading will not be considered. The principal tensile stresses will lead to failure of the masonry (i.e. cracking).

The masonry is considered isotropic, so the brick and mortar are not considered individually. The walls consists of a single leaf and the tensile strength that is considered is *direct* tensile strength.

4.1.2 DEFINITIONS

Damage

Three types of damage will be distinguished (Boscardin & Cording, 1989):

- 1) Architectural damage.
- 2) Functional damage.
- 3) Structural damage.

Architectural damage is considered to be damage that is visible. Examples can be small cracks in a wall, but these cracks will not limit the functionality of the structures in any way. Functional damage is considered damage that is severe that some of the functions of the building cannot be carried out anymore. This means that, due to the cracks that have developed in the structure, things like isolation can be prevented. Also, it can lead to jammed doors or windows or urban vermin is able to enter the structure. Structural damage is considered damage that leads to a defect in the bearing structure. This means that the damage is so severe that there is danger of collapsing of the structure or of structural elements. This project will be focused on functional damage. This implies that small cracks that lead to esthetical devaluation will not be considered as failure.

Failure

When the principal stresses exceed the tensile stresses stated in Table 11, the structure cannot provide for any tensile strength at this point anymore. However, when it reaches this tensile stress level at one point, it does not mean that the structure fails, it only produces a slight crack. As discussed before, this will not lead to failure in the model: the structure fails when there is functional damage. Therefore the following assumption is made: in the model, the principal tensile stress may exceed the maximum tensile stress, but this stress peak cannot be any longer than 210 mm (width of a brick). This is assumed because according to the study performed by Boscardin & Cording (1989), strain has to be taken as the limiting factor for failure of masonry, where a strain of

0.0005 leads to functional damage. A longer stress peak has been chosen because a short crack will not be wide, and will therefore not result in functional damage.

4.1.3 CHOICE OF SOFTWARE

The software used for the structural calculation of the structures will be SCIA Engineer. The choice for this software program is made because this program is widely used in the construction industry. To provide a clear procedure, it is best to do this in a known environment for engineers. The program has possibilities for the finite element method and dynamic calculations. As discussed in section 3.5.1, there are some problems regarding dynamic calculations in SCIA. However, it is possible to create a workaround regarding these problems. Moreover, the fact that SCIA Engineer is widely used in the construction industry is considered a more important factor than this disadvantage. The feasibility of SCIA will be investigated by comparing the results to those produced by the TNO report.

For the probabilistic calculation, a Monte Carlo simulation will be performed. This will be done by using MATLAB codes that provide for the stochastic properties in this project. The reason to prefer the Monte Carlo simulation over the FORM-analysis, is because of the ease of use of MATLAB. Because multiple simulations have to be run (i.e. for many different vibration speeds), it is easier to implement this in a MATLAB code, than to manually adjust this property while using Prob2B. This saves more time than the time that is lost because of a Monte Carlo simulation. Also for the probabilistic calculation, a comparison should be made with the results provided by the TNO report. This will determine if the Monte Carlo simulation and/or the FORM-analysis will be useful for this calculation.

4.1.4 LOADS

Two types of loads will affect the structure: initial loads and the vibration load.

Initial loads

The initial loads are static loads present in the façade. These are loads due to self-weight, mobile floor loads and mobile roof loads. It is assumed that the roof is a tile roof, while the floors are timber floors.

The self-weight of a tile roof is 0.5 kN/m² (Oosterhoff, 2008). The self-weight of a timber floor is 0.3 kN/m² (Oosterhoff, 2008).

According to Eurocode 1991-1-1, the mobile loads are 1 kN/m² for the roof, while they are 1.75 kN/m² for the floors (NEN, 2002b). To create a representative loading situation, only 50% of these loads are taken into account (NEN, 2002a).

For a bearing wall, a span of 7 meters is assumed.

This results in the following formula for the weight on a floor or roof level:

$$q_{tot} = Q_{sw} * 0.5 * s + Q_{mob} * \gamma_{mob} * 0.5 * s \quad (24)$$

Where:

q_{tot}	= total load (kN/m)
Q_{sw}	= self-weight (kN/m ²)
s	= span (m)
Q_{mob}	= mobile load (kN/m ²)
γ_{mob}	= mobile load factor (-)

The self-weight of the masonry ($\gamma = 2000 \text{ kg/m}^3$) with a wall thickness of 200 mm results in a vertical surface load on the façade of 3.92 kN/m^2 .

TABLE 12 – INITIAL LOADS

	Self-weight (kN/m ²)	Self-weight (kN/m ¹)	Mobile load (kN/m ²)	Mobile load factor (-)	Mobile load (kN/m ¹)	Representative loading situation
Floor	0.3	1.5	1.75	0.5	2.6125	4.1125 (kN/m)
Roof	0.5	2.5	1	0.5	1.75	3.5 (kN/m)
Self-weight masonry	3.92	-	-	-	-	3.92 (kN/m ²)

Vibration load

A vibration source results in a wave at the soil-surface interface. As stated before, the frequencies in this project are 3 to 25 Hz, these are the frequencies that usually occur during construction work and the low frequencies (3-5 Hz) are close to the natural frequencies (Ceroni, 2004). The frequency of vibration and the propagation speed determine the wave length of the wave in space. The displacement amplitude depends on the vibration speed and the frequency. The vibration load is explained using the example below:

Example

A vibration source causes a wave with a vibration speed of 3 mm/s while its frequency is 5 Hz. This all occurs in clay soil ($v = 600 \text{ m/s}$). The vibration in time can be written as:

$$v(t) = 3 * \sin(5 * 2\pi * t)$$

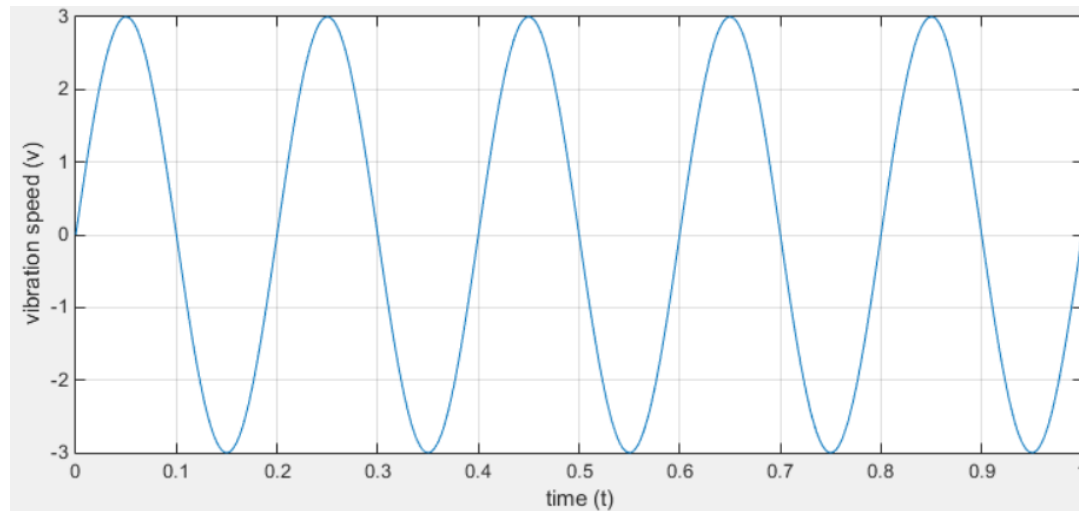


FIGURE 34 – VIBRATION IN TIME

The displacement follows after integrating:

$$v(t) = u'(t) \rightarrow u(t) = \frac{-3}{5 * 2\pi} * \cos(5 * 2\pi * t) = -\frac{3}{10\pi} \cos(10\pi * t) = -0.0955 * \cos(10\pi * t)$$

Example

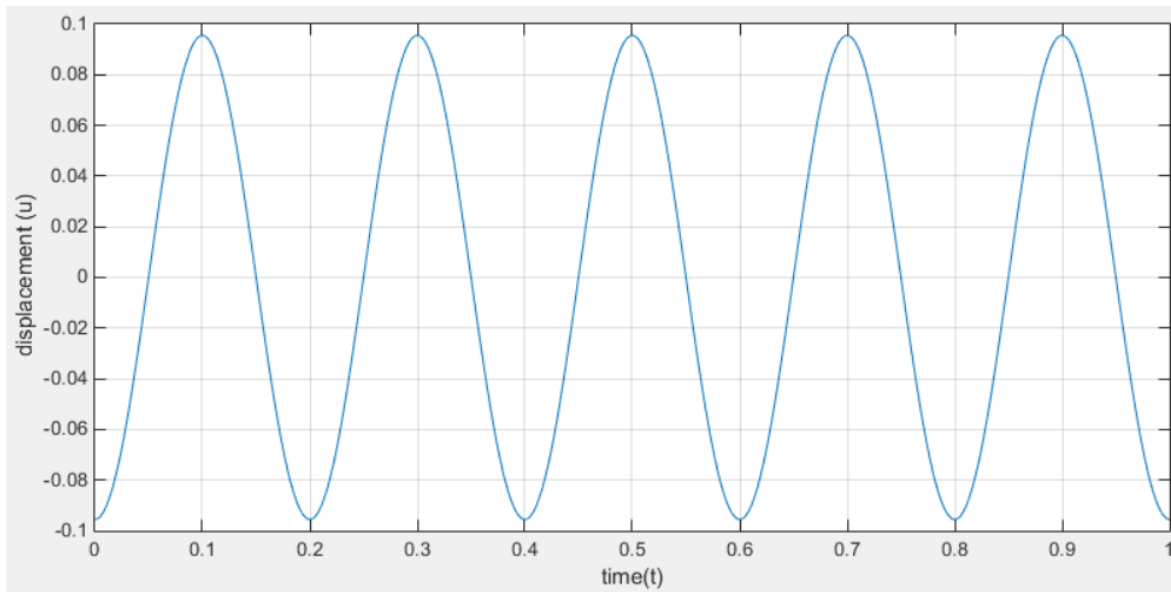


FIGURE 35 – DISPLACEMENT IN TIME

Since there is wave propagation in the soil, there has to be a parameter for space in the formula. For every meter further from the source, the phase difference should be 1 meter divided by the propagation speed. This leads to:

$$u(t, x) = -0.0955 * \cos\left(10\pi * \left(t - \frac{x}{v}\right)\right) = -0.0955 * \cos\left(10\pi * \left(t - \frac{x}{600}\right)\right)$$

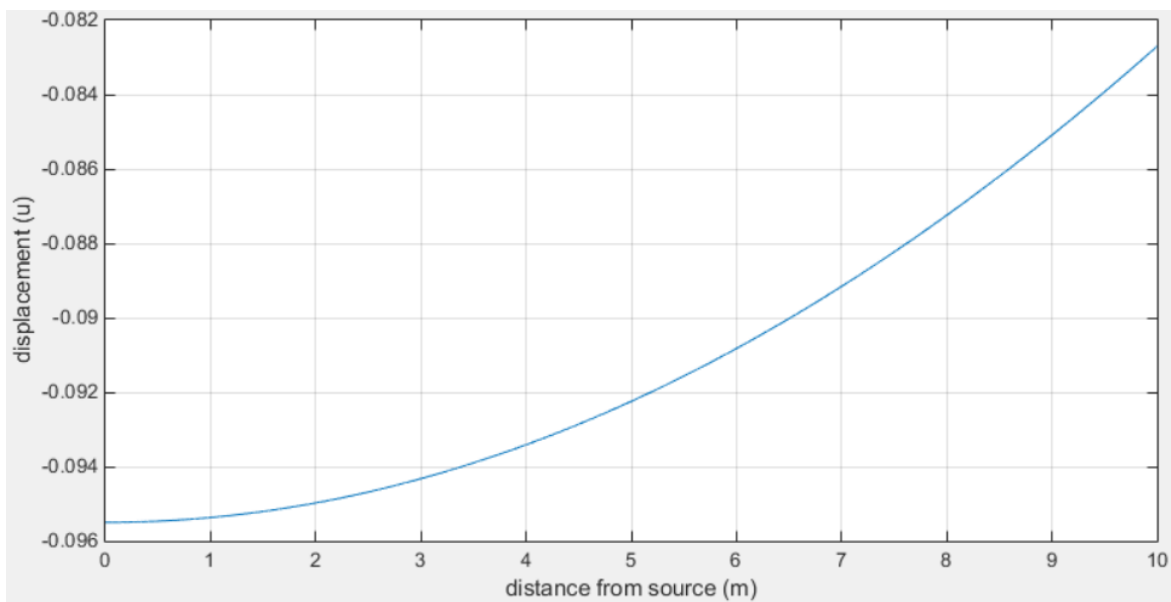


FIGURE 36 – DISPLACEMENT IN SPACE (FROM 0 TO 10 M) FOR T=0

Example

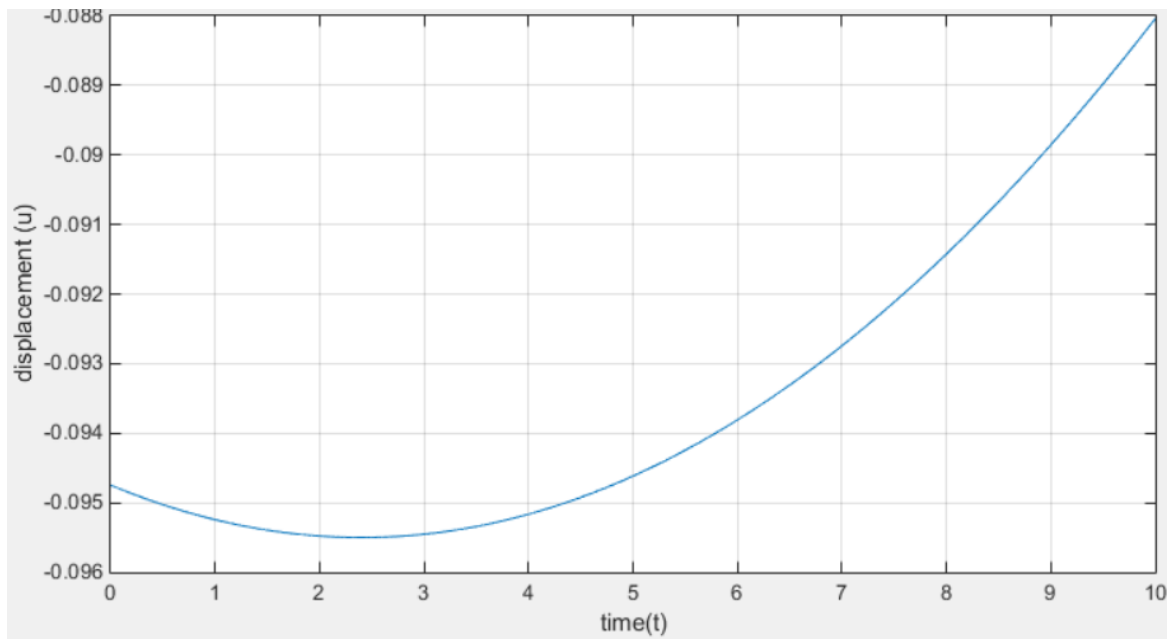


FIGURE 37 – DISPLACEMENT IN SPACE (FROM 0 TO 10 M) FOR T=0.04

It is emphasized that the sine-cosine integration is performed solely to gather the displacement amplitude that is required for the further calculation. The displacement will be put in like a sine function, but with the displacement amplitude that is gained through integration.

Furthermore, for the low frequencies (3, 4 and 5 Hz) it is assumed that the vibration dampens. This is assumed because these vibration frequencies occur due to haying, and after a blow the vibration is initiated. However, it is not vibrating constantly. For the higher frequencies (10, 15, 20 and 25 Hz) the vibration does not dampen.

The duration of the vibrations is set at 10 seconds. The parabolic damping will be applied using the following equations:

$$v_{damp} = 0.04 * t^2 - 0.4 * t + 1 \quad t = 0..5 \quad (25)$$

$$v_{damp} = 0 \quad t = 5..10 \quad (26)$$

These equations should be multiplied with the displacement formula, which results in a damped sinusoidal wave.

4.1.5 CALCULATION PROCEDURE

Calculation steps

There are a couple of steps to be taken in modeling the structures:

- 1) Initial loads

In this case, the structure is loaded by its initial loads. The structure has a rigid support with the soil.

2) Initial load and vibration loads, no stresses at the soil-masonry interface

In this case, there is still a rigid connection between soil and structure. During this phase, besides the initial load, the vibration load is added too. Multiple wave lengths and phase variations are used in this calculation, to represent different vibration frequencies and soils. This way it can be seen what the effect of those properties is on the probability of failure. This step is the main focus of this project, what means that most conclusions will be drawn from this step. It should be noted that in reality stresses at the soil-masonry interface occur, and this step is therefore a somewhat simplified version of reality.

3) Initial load and vibration loads, including stresses at the soil-masonry interface

The rigid soil-structure connection is replaced by a flexible soil-structure connection (springs). This results in stresses at the soil-masonry interface, what gives a good view of what to expect during soil vibrations due to construction work. This phase will be executed briefly, and will result in a recommendation for further research regarding this topic. Therefore, this topic will be discussed in the comparative section in chapter 0.

4) (possibly) Nonlinear springs/nonlinear material behavior

It could be feasible to do perform a nonlinear analysis. The nonlinear approach is focused on nonlinear material behavior. This can be done by using a smeared crack model (e.g. using DIANA FEA) or using a sequential elastic calculation. In this project, chosen is to perform a sequential elastic calculation. This step is also executed briefly, and will not be a main focus of the project, but can provide some recommendations for further research. Therefore, also this topic will be discussed in the comparative section in chapter 0.

Calculation outline

In Chapter 5, a comparison will be made between the report from TNO and the modeling of that structure in SCIA Engineer and the probabilistic calculation using the Monte Carlo simulation. This can ensure that the model in SCIA and the Monte Carlo analysis in MATLAB produce sufficient results.

In Chapter 6, steps 1 and 2 of the calculation will be executed. As stated before, step 2 is the main focus of the project. Therefore, the results discussed in this chapter will be the most elaborated and important. In Chapter 7 comparative studies regarding different modeling parameters will be presented, executed and discussed. Chapter 8 will summarize the conclusions that can be drawn from the entire project, and will discuss possible further research on the topic.

4.2 CHOICE OF MODELS

Three structures have been chosen to be examined. These are actual facades in Delft, one built around 1900, one around 1960 and one built recently. These structures are used solely for the geometry of the models. The geometries of these facades vary in two ways: the dimensions of the façade (height and width) and also on the opening pattern. The proposed procedure will be applied as a test on these façades.

4.2.1 OUDE DELFT 81



FIGURE 38 – OUDE DELFT 81

The building at Oude Delft 81 is a residential building, built in 1907 (DUWO, 2016). It has monumental value and its façade is made of masonry. The building has two floors. On the bottom floor there are 3 windows and one door, while on the top floor there are four windows.

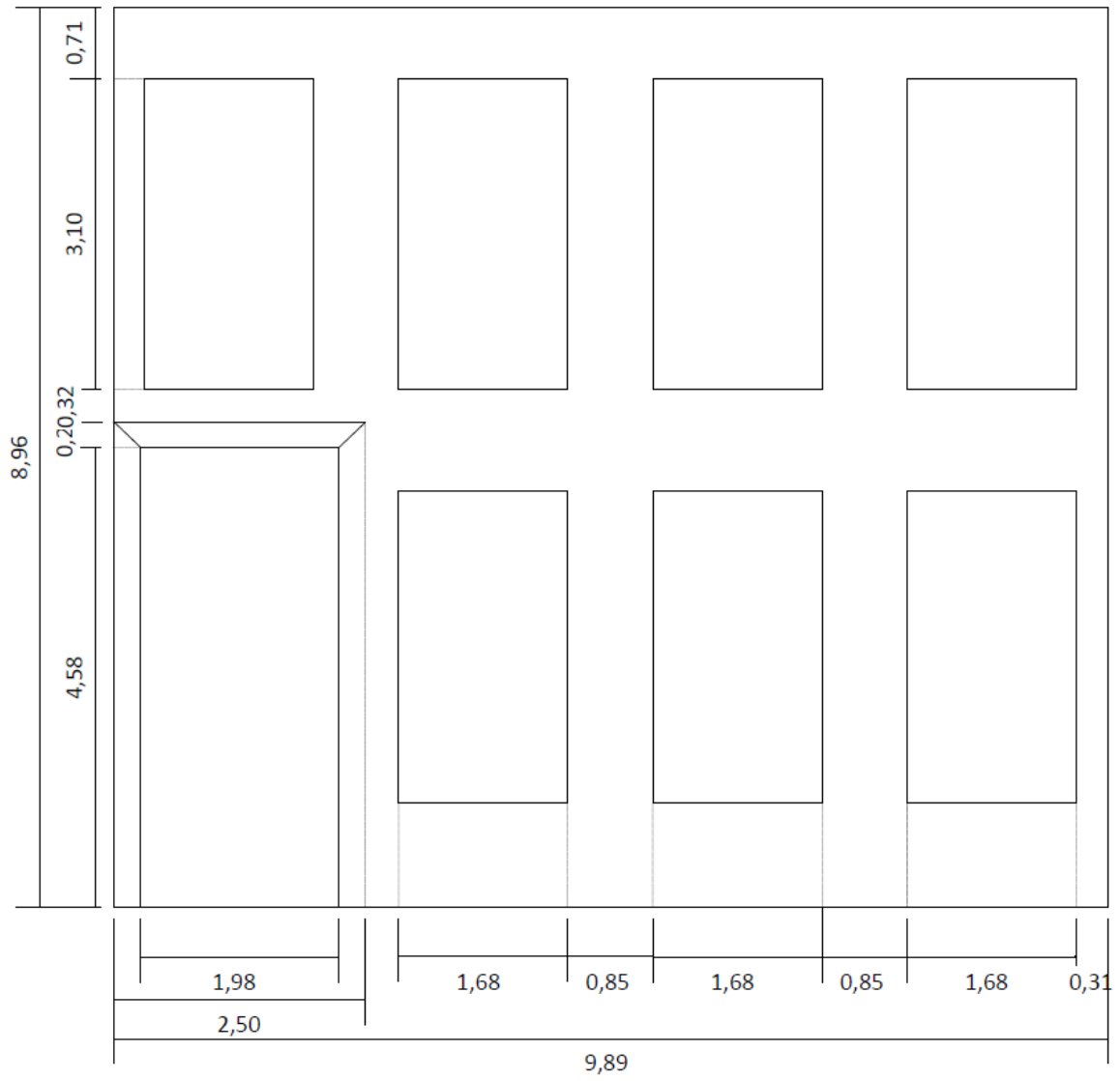


FIGURE 39 – GEOMETRY OUDE DELFT 81

4.2.2 BIESLANDSEKADE 22



FIGURE 40 – BIESLANDSEKADE 22

Bieslandsekafe 22 is a masonry residential building, and it is built around 1960. It has 3 floors, on ground level there is one door and a double window in the façade, while on the other two floors there are two single windows next to each other.

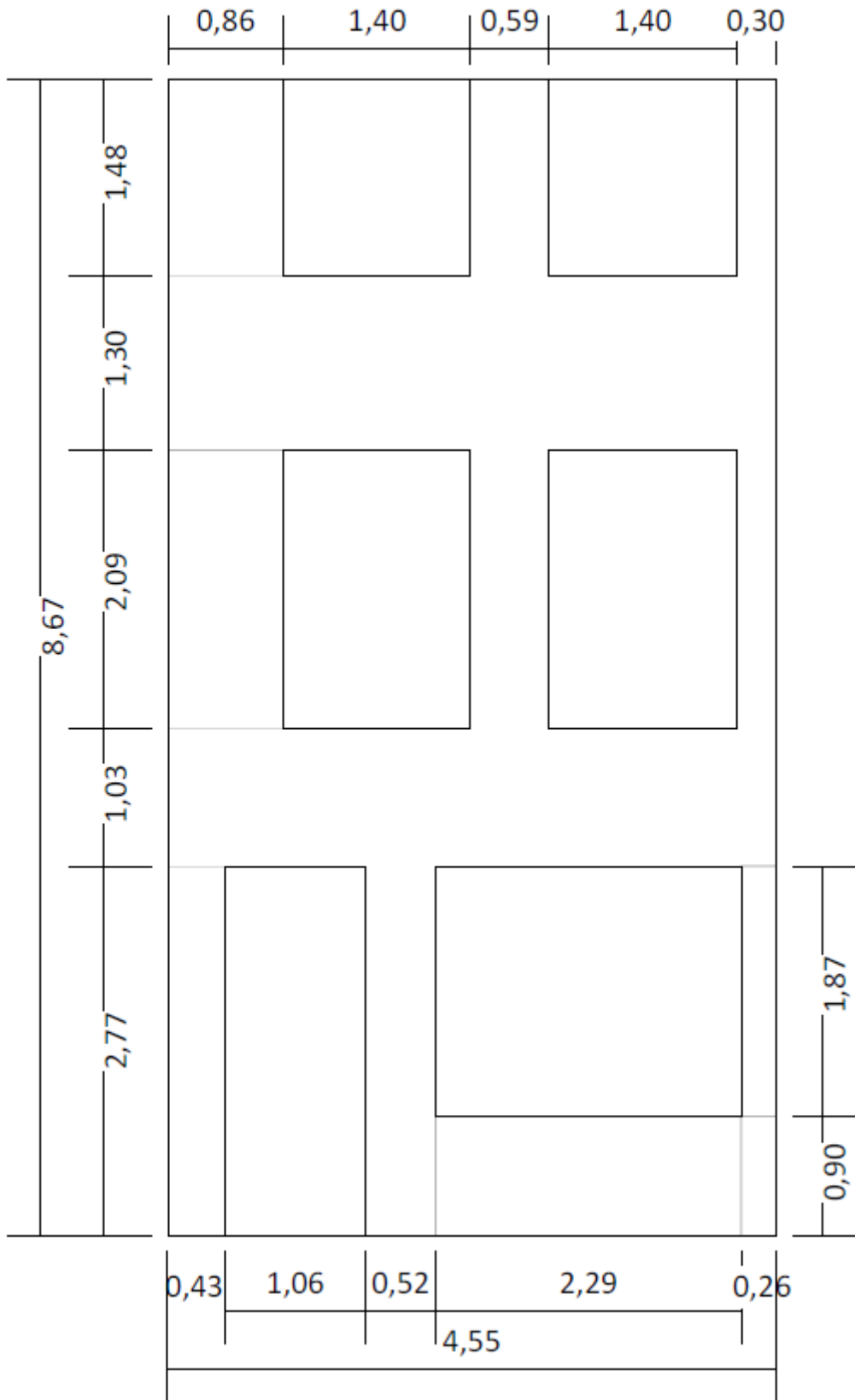


FIGURE 41 – GEOMETRY BIESLANDSEKADE 22

4.2.3 VAN TIJENSTRAAT 8

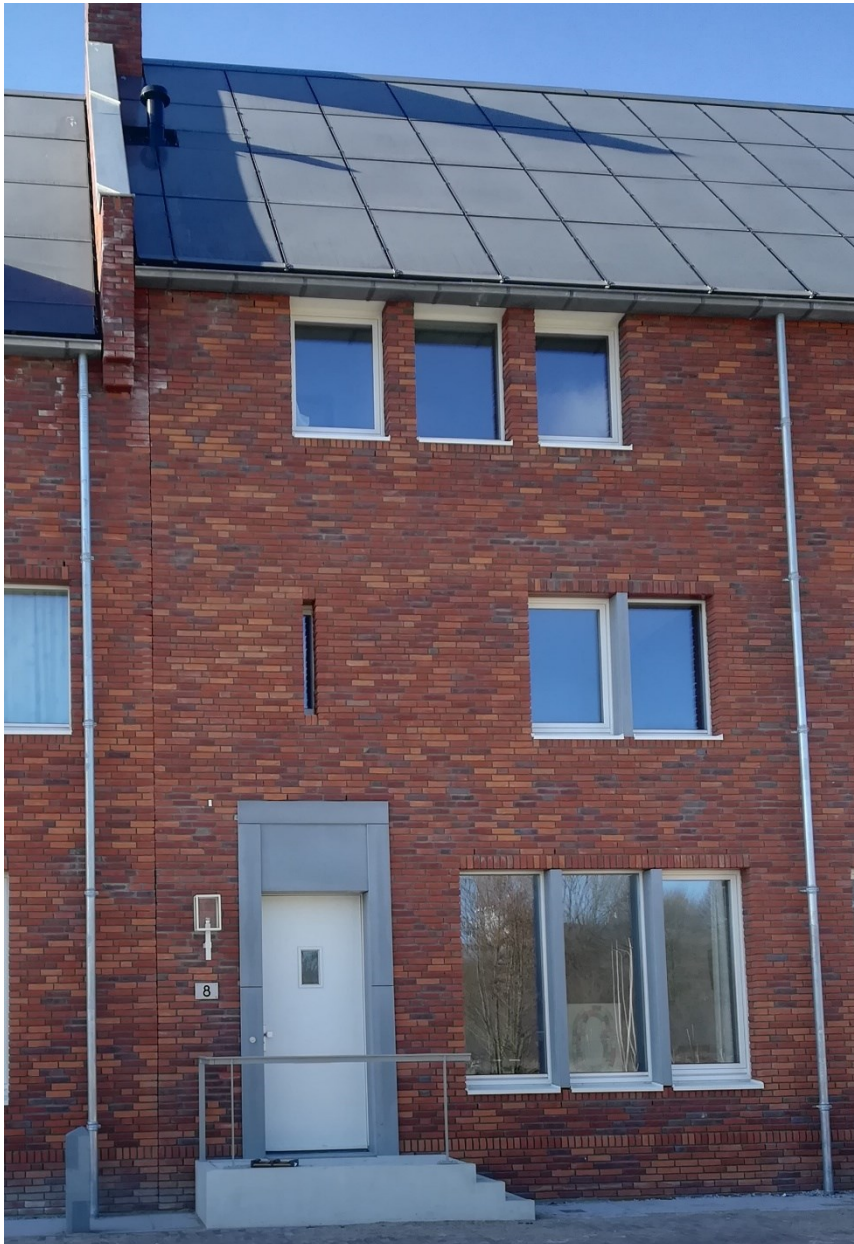


FIGURE 42 – VAN TIJENSTRAAT 8

Van Tijenstraat is part of a new residential building project (Silfhout, 2016), and is located east from the Delft University of Technology. It has a masonry façade and three floors. On the bottom floor, there is a door and a three-part window. The door is not on ground level, there is a small stairway up a few decimetres. On the first floor, there is one double window and there is one very narrow window. On the top floor, three single windows are placed.

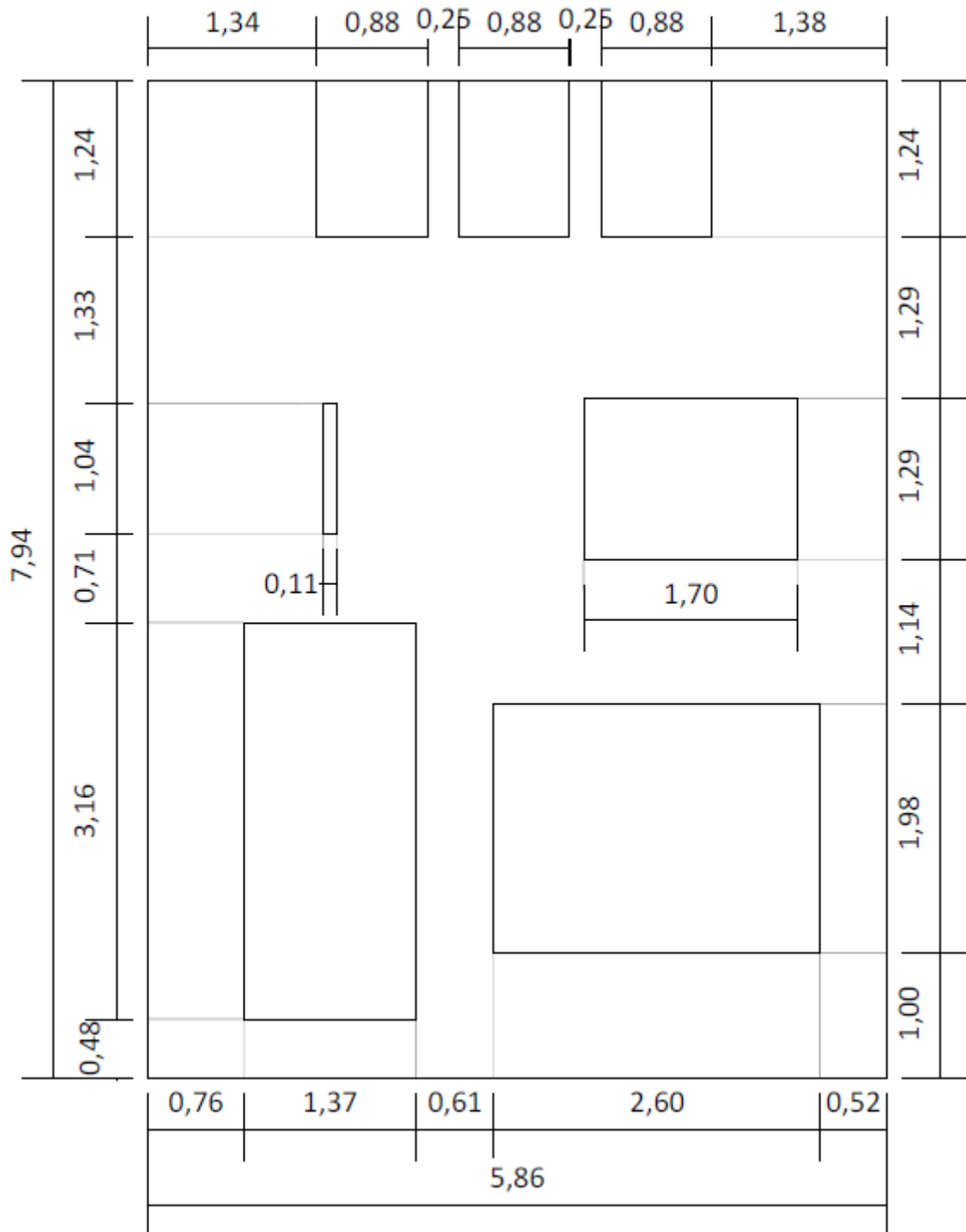


FIGURE 43 – GEOMETRY VAN TIJENSTRAAT 8

4.3 PROPOSED PROCEDURE

This section describes the calculation procedure extensively. Hence, this section describes the proposed procedure for practical analysis.

Designing the model

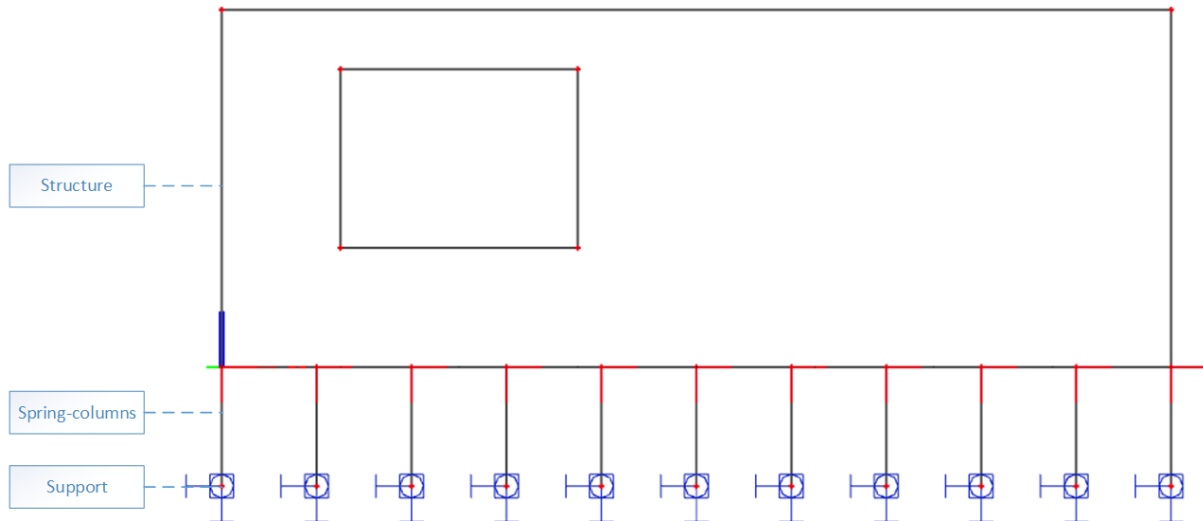


FIGURE 44 – STRUCTURE

The model in Figure 44 shows the model that will be constructed using an imaginary structure. The structure will be the façade that has to be examined. Due to limitations of SCIA Engineer it has been chosen to model the structures this way. SCIA is not able to produce a sinusoidal dynamic displacement. The only load available in dynamic calculations are point forces. This section explains the workaround that is used to provide for a sinusoidal dynamic calculation.

Firstly, the examined structure is labeled *Structure*. Below this, eleven *spring-columns* are placed, each $1/10^{\text{th}}$ structure width away from the adjacent spring-column(s), and each 1 meter in length. The support at the bottom side (*Support*) prevents translation in horizontal direction but does not prevent translation in the vertical direction nor rotation. The spring-columns are used to translate a point force into a displacement in the structure. Using a dynamic vertical point force at the ground level, using the known stiffness of the spring-column, the displacement at the bottom can be produced.

To ensure the displacement at the bottom of the structure will not be influenced by the inertia of the façade, but also ensure numerical accuracy, the spring stiffness of the spring-columns should be set accurately. Therefore, assumed is that the difference between the theoretical displacement and the displacement in the SCIA calculation should be 1% maximum. See appendix A.1 for a more detailed explanation regarding the structural modeling

Inputting the loads

Initial loads

The initial loads will be added to the corresponding floor levels/roof levels/façade in the structure. This process is quite convenient in SCIA. The corresponding stresses will be calculated by performing a linear-elastic calculation.

Vibration loads

For the desired load case, dynamic load functions (DLF's) have to be created. The dynamic load function describes the value of the point force in time. The vibration load is placed on the spring-columns. For a more detailed elaboration regarding the vibration load, see appendix A.2.

Combining the stresses

Another disadvantage of SCIA Engineer is that it is very cumbersome to add the results of a dynamic load case to those of a static load case. From the envelope of results in a dynamic load case, the specific load case that leads to the maximum tensile stress has to be investigated manually. Only after that, it is possible to combine the load cases.

Therefore, a different approach has been applied. The maximum stresses in x- (σ_{xx}) and y-direction (σ_{yy}) from the load case of initial loads will be exported to a Microsoft Excel file. The same will be done for the load case of vibration loads. Using the following equations, the principal stresses will be gathered:

$$\sigma_{1,2} = \frac{1}{2} \left(\sigma_{xx} + \sigma_{yy} \pm \sqrt{(\sigma_{xx} - \sigma_{yy})^2 + 4 * \sigma_{xy}^2} \right) \quad (27)$$

$$\alpha = \frac{1}{2} \arctan \frac{2\sigma_{xy}}{\sigma_x - \sigma_y} \quad (28)$$

Using this, it is possible to find the maximum principle tensile stress in the structure. However, the nodes at the bottom of the structure will not be taken into consideration. This is chosen, because at those points at the bottom, the displacement will be applied, which results in large values in the singularities and therefore unrealistic results.

The envelope of the stress results of the vibration load may be too small because stresses at another time, where the principal stresses may be in a different direction, might result in higher total principal stresses when the initial loads are added. Therefore, numerous other points in time which also produce high principal stresses for the vibration load have been investigated. From those checkups follows that these do not produce higher principal stresses than the envelope.

Probabilistic approach

Limit state function

The limit state function for the probabilistic approach is shown in the following equation (see section 5.2.2):

$$Z = f_t - \frac{\sigma_E(E)}{\sigma_\mu} * \sigma \quad (29)$$

With the stochastic parameters as shown in Table 13:

TABLE 13 – STOCHASTIC PARAMETERS

Parameter	Symbol	Distribution	Mean value (μ)	Variation coefficient
Young's Modulus	E	Lognormal	5000 N/mm ²	0.3
Maximum tensile strength	f_t	Lognormal	0.3 N/mm ²	0.3

Chosen is to use lognormal distributions so it is not possible for the distribution to compute a negative value.

E , $\sigma_E(E)$ and σ_μ

Masonry Young's Modulus has a mean value $\mu = 5000 \text{ N/mm}^2$ and a variation coefficient of 0.3, as described in section 4.1. However, Young's Modulus's effect on the principal tensile strength should be added to the limit state function. Therefore, for different Young's modulus values ($\mu - 3\sigma$, $\mu - 2\sigma$, $\mu - \sigma$, μ , $\mu + \sigma$, $\mu + 2\sigma$, $\mu + 3\sigma$) the resulting principal tensile strength should be gathered. These can be put in a scatterplot, with Young's Modulus on the x-axis and the maximal principal tensile strength on the y-axis. A curve-fit that is applicable to this scatter should be computed. The equation of this curve describes the stress as a function of Young's Modulus. This formula, divided by the stress produced at the mean value of Young's Modulus, describes Young's Modulus's effect on the principal tensile strength, and can therefore be added to the limit state function. Appendix A.3 provides an example regarding this topic.

f_t

The maximum tensile stress for masonry, as stated in section 4.1, is 0.3 N/mm². However, as also has been stated in section 4.1: in the model, the principal tensile stress may exceed the maximum tensile stress, but this stress peak cannot be any longer than 210 mm (width of a brick). Using this failure criterion, and its elaboration described in section 4.4, the mesh size has to be adjusted so the principal tensile strength will be 0.3 N/mm². This can be computed as follows:

- 1) Input the loads that lead to a fracture zone of 210 mm.
- 2) Adjust the mesh size to the point that the peak stress is 0.3 N/mm².

Coding in MATLAB

The information gathered in the previous sections is all gathered together in a MATLAB script. This script can calculate the probability of failure. The script is further elaborated in appendix A.4.

A flowchart of the procedure is shown in Figure 45.

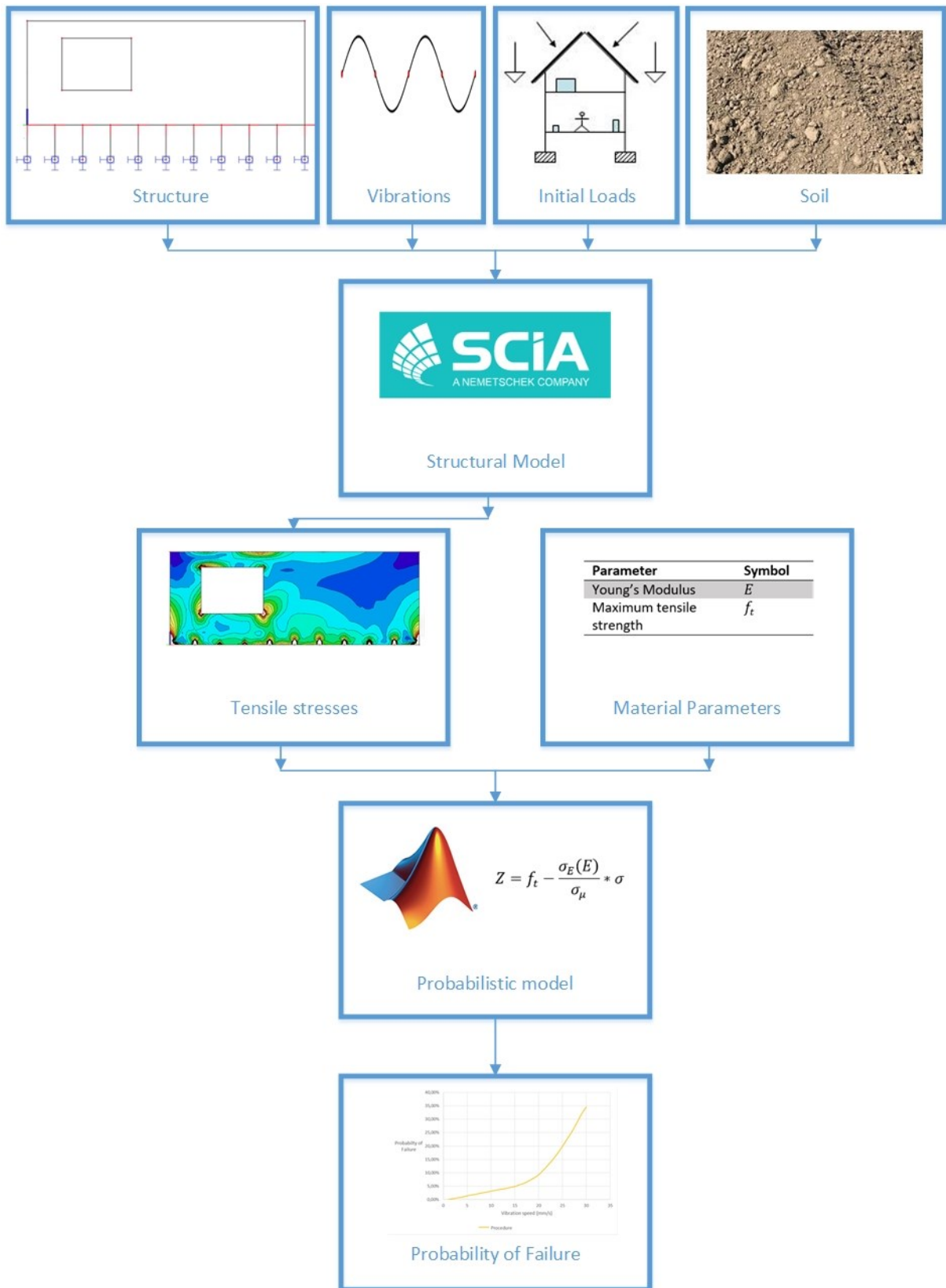


FIGURE 45 – FLOWCHART OF THE PROCEDURE

4.4 FAILURE CRITERION

In the linear-elastic calculation, it is assumed that the structure will fail if the principal tensile stress will exceed the tensile strength over a length of 210 mm, as stated in section 4.1.2. The peak stress in that failure zone can be used as the tensile strength of the structure. However, the mesh size is a very decisive factor in this calculation. The peak stress will be influenced by the mesh size. Therefore, a comparative study should be executed to make a statement regarding this phenomenon.

Two elaborations of this statement will be investigated to see what will result in the most reliable failure criterion.

- 1) The peak stress in that failure zone will be used as the tensile strength of the structure in the probabilistic approach.
- 2) A failure zone of 210 mm will be computed for a structure with a mesh size of 100 mm. Following this, the mesh will be enlarged until the peak stress at the point of failure will be equal to the tensile strength of the masonry. This mesh size will be used in the calculation for the probability of failure.

The structure that is used for the comparison with the TNO report is chosen for this calculation. This structure is shown in Figure 46.

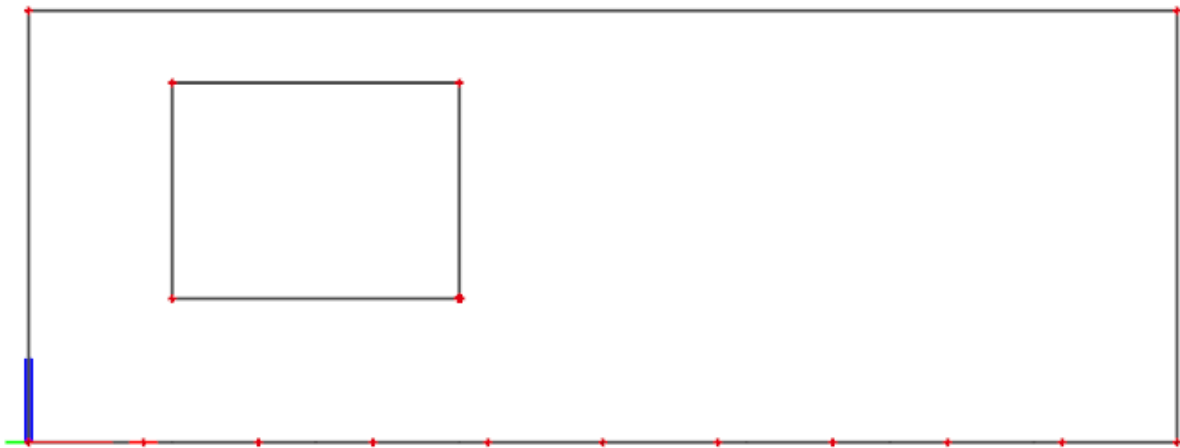


FIGURE 46 – STRUCTURE USED FOR COMPARISON WITH NONLINEAR MATERIAL PARAMETERS

First, option 1 (peak stress method) will be investigated. Following this option 2 (mesh size method) will be investigated. The results will be compared to each other, and the decision regarding the best method will be made.

Option 1 – Peak stress method

Example

For a 10 Hz vibration, in a sandy soil, with a mesh size of 100 mm, a 5 mm/s vibration speed leads to a situation where the tensile stress of 0.3 N/mm^2 is exceeded over a length of 210 mm. This is shown in Figure 47 and Figure 48.

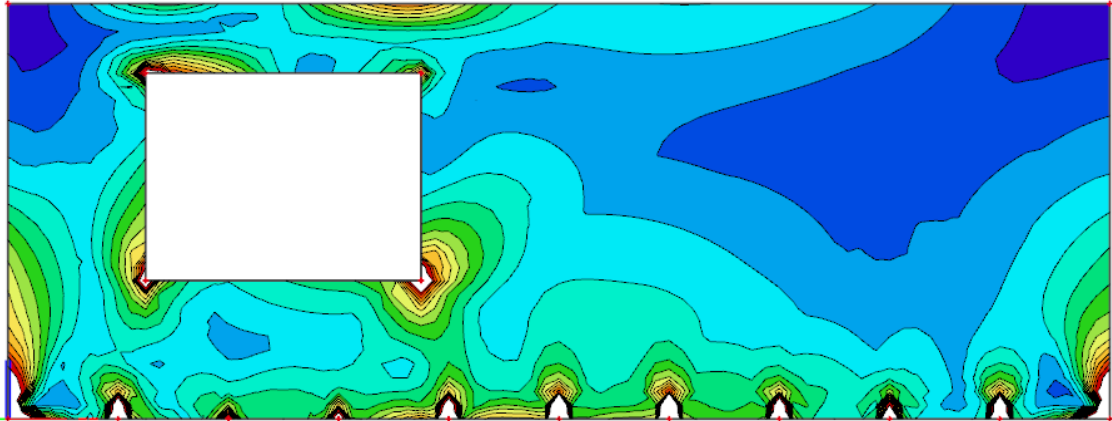


FIGURE 47 – STRESS CONTOUR 100 MM MESH

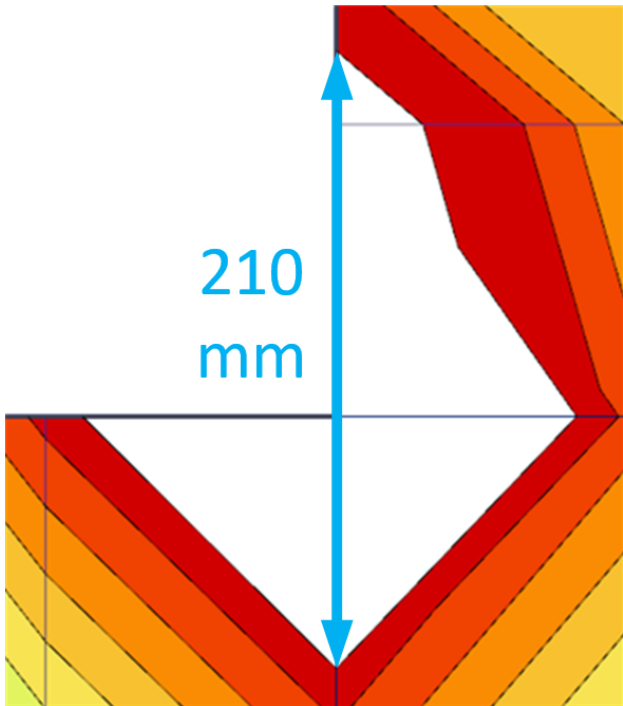


FIGURE 48 – STRESS CONTOUR ZOOMED IN AT BOTTOM RIGHT CORNER OF THE WINDOW

This means that is the situation where the structure fails. One mesh block is 100 mm, so Figure 48 shows the situation where the crack will reach 210 mm. When the peak tensile stress at the corner is investigated, it follows that the maximum tensile stress in that corner is 0.53 N/mm^2 . This is the value that will be taken for the mean value in the probabilistic approach.

Option 2 – mesh size method

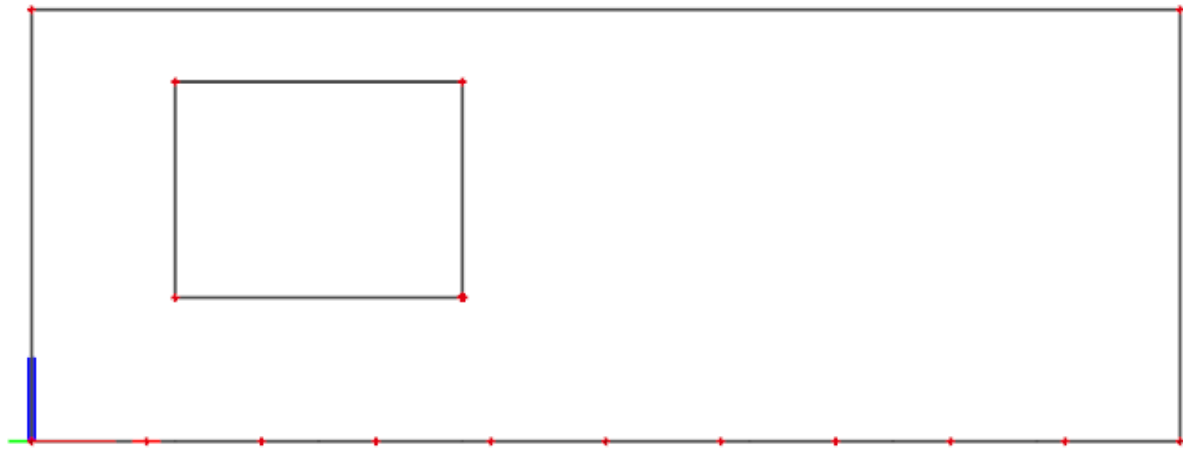


FIGURE 49 – STRUCTURE USED FOR COMPARISON WITH NONLINEAR MATERIAL PARAMETERS

The mesh size used in in option 1 is 100 mm. To compare the results of other mesh sizes, the following mesh sizes have been chosen for this comparison

- 40 mm
- 50 mm
- 65 mm
- 80 mm
- 100 mm
- 150 mm
- 200 mm

After following the procedure for various mesh sizes (40, 50, 65, 80, 100, 150 and 200 mm), the results shown in Figure 50 and Figure 51 are obtained.

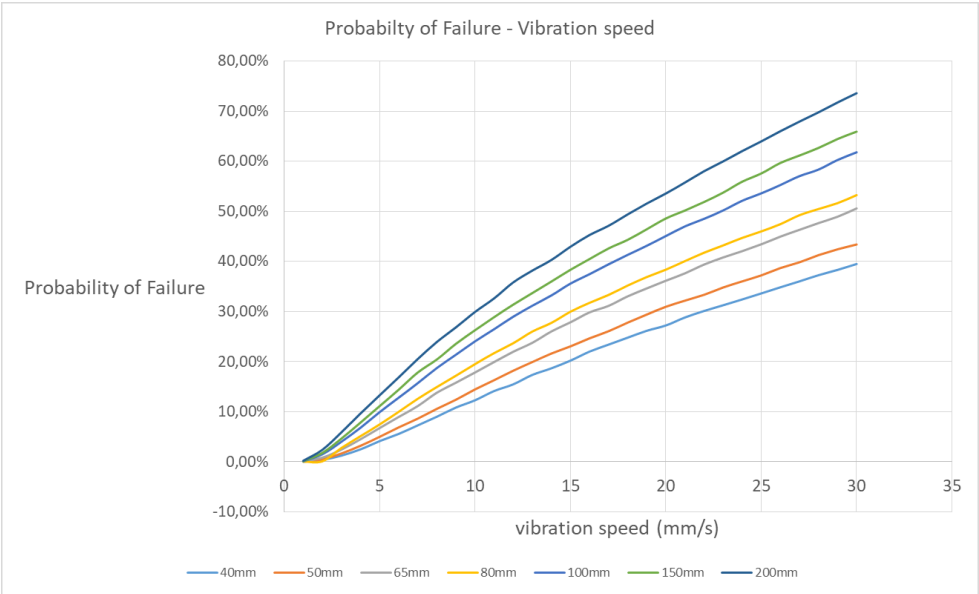


FIGURE 50 – PROBABILITY OF FAILURE FOR VARIOUS MESH SIZES

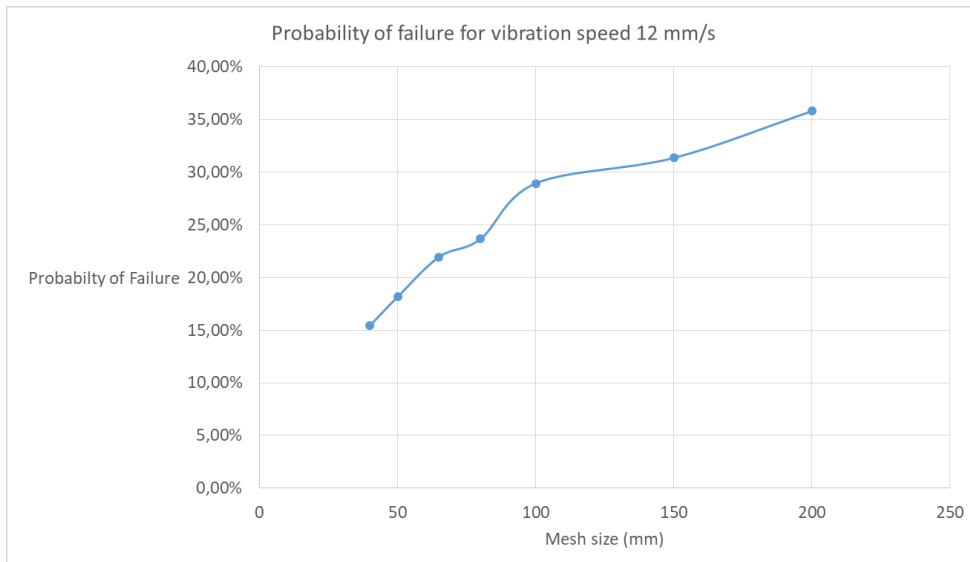


FIGURE 51 – PROBABILITY OF FAILURE FOR A 12 MM/S VIBRATION SPEED

As shown in these figures, it can be seen that the mesh size has quite some effect on the probability of failure. This probability of failure is calculated using the peak stress method. It is important to investigate this more thoroughly.

The size of the fracture zone (the zone where the tensile strength is exceeded in the linear-elastic calculation) is also investigated for the different mesh sizes. This results of this comparison are demonstrated in Figure 52.

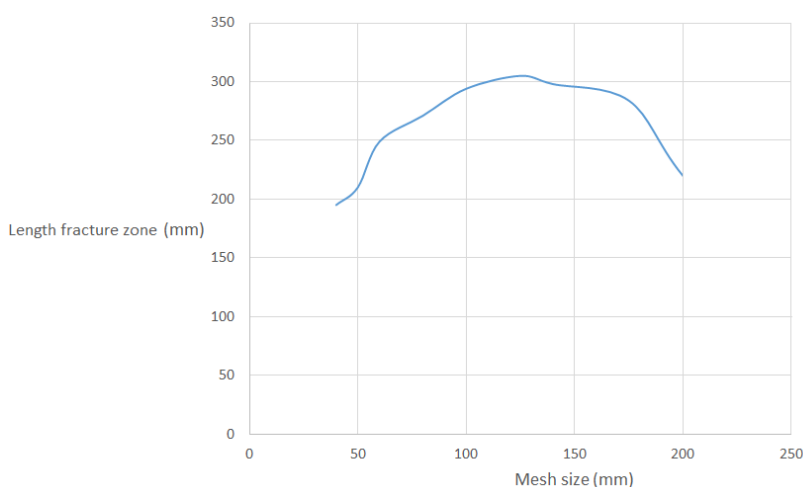


FIGURE 52 – LENGTH OF THE FRACTURE ZONE VS MESH SIZE

As can be seen in the figure, the biggest fracture zone occurs when the mesh size is around 100 mm. It seems that for smaller mesh sizes, the fracture zone will converge towards zero. The length of the fracture zone is not constant. Different mesh sizes lead to different probabilities of failure because these result in different fracture zone sizes. However, this is not the only limiting factor, since the peak stresses in the fracture zone determine the different maximum tensile stresses in the probabilistic model.

According to the FEM-theory, the integral of the stresses over a certain length is independent of the mesh size. It has to be verified if this is the case for this model.

To verify this, the stresses over a section of 210 mm is investigated, for mesh sizes of 40, 50, 80 and 100 mm. This section is in the bottom right corner of the window of the structure shown in Figure 53.

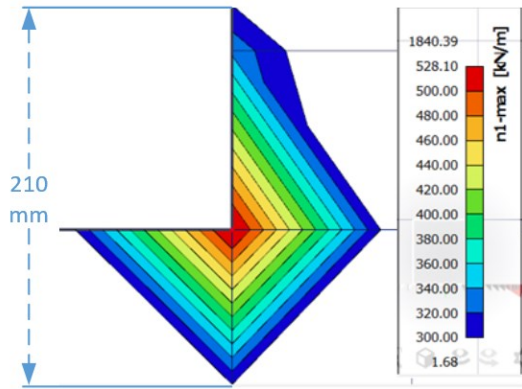


FIGURE 53 – 210 MM SECTION, 100 MM MESH SIZE

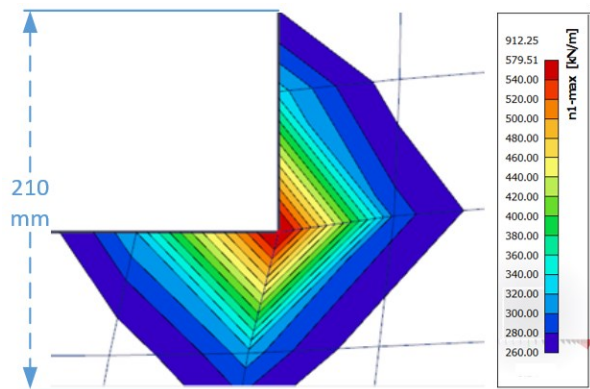


FIGURE 54 – 210 MM SECTION, 80 MM MESH SIZE

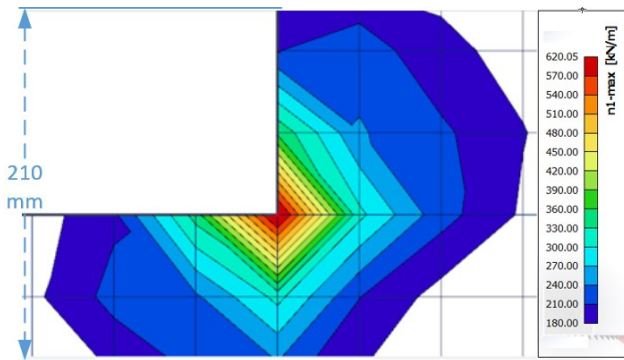


FIGURE 55 – 210 MM SECTION, 50 MM MESH SIZE

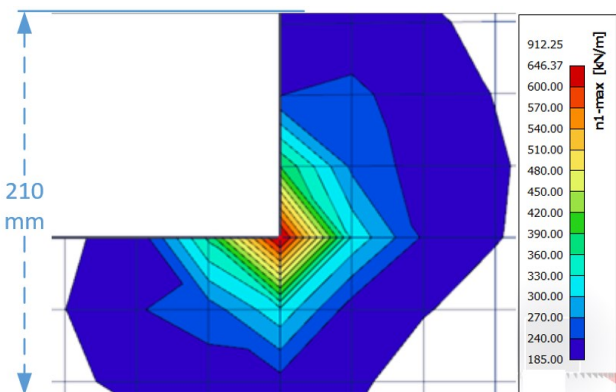


FIGURE 56 – 210 MM SECTION, 40 MM MESH SIZE

The average stress in the 210 mm section is calculated. The results are shown in Table 14.

TABLE 14 – AVERAGE TENSILE STRESSES FOR A 210 MM SECTION

Mesh size (mm)	40	50	80	100
Average tensile stress (N/mm ²)	349,1096	360,2472	388,2643	409,5422

The average stress in the 210 mm section is not constant for the various mesh sizes. Therefore the statement cannot be verified for this section. However, using a 100 mm section (around the peak stress) leads to the results as shown in Table 15.

TABLE 15 – AVERAGE TENSILE STRESSES FOR A 100 MM SECTION

Mesh size (mm)	40	50	80	100
Average tensile stress (N/mm ²)	538,384	541,038	542,49	538,966

These results lead to a constant average tensile stress, since the difference between the average tensile stresses do not exceed 1%. This way the second failure criterion can be computed: 0.3 N/mm² peak tensile stress calculated using a mesh size x . x can be computed as follows:

The peak tensile stress at a mesh size of 100 mm is calculated. The mesh size will be adjusted until the peak stress becomes 0.3 N/mm². The mesh size that leads to this mesh size is equal to x .

Comparison

The example below shows that both failure criteria lead to nearly the same probabilities of failure. This comparison shows that by using the failure criterion using the “mesh size method” will lead to results independent of the mesh size that is chosen initially.

Therefore, the mesh size method is the preferred method. The user inputs the loads that lead to a fracture zone of 210 mm. Following this, the user adjusts the mesh size in a way that the peak tensile stress becomes 0.3 N/mm². This value is used for the structural calculation.

Example

For a 10 Hz vibration, in a sandy soil, with a mesh size of 100 mm, a 5 mm/s vibration speed leads to a situation where the tensile stress of 0.3 N/mm² is exceeded over a length of 210 mm. This is shown in Figure 57 and Figure 58.

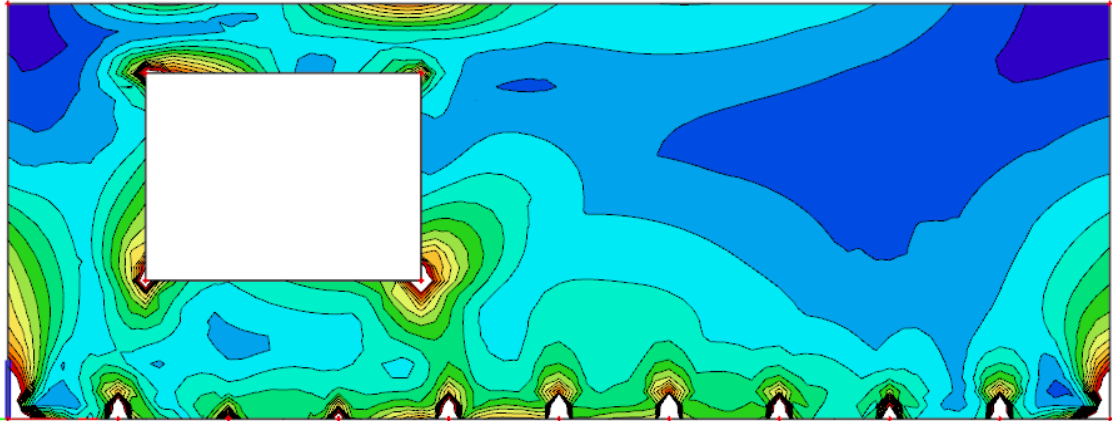


FIGURE 57 – STRESS CONTOUR 100 MM MESH

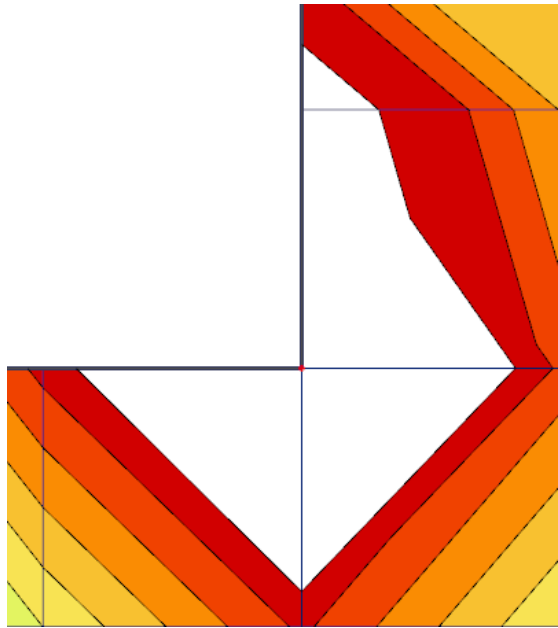


FIGURE 58 – STRESS CONTOUR ZOOMED IN AT BOTTOM RIGHT CORNER OF THE WINDOW

Example

The peak stress in the area shown in Figure 58 is 0.53 N/mm². This value can be added to the probabilistic model in the proposed procedure and the probability of failure can be calculated this way.

Using the fail criterion in this calculation, the mesh size is increased until the peak stress at this point will become 0.3 N/mm². This is the case when the mesh size is 216 mm.

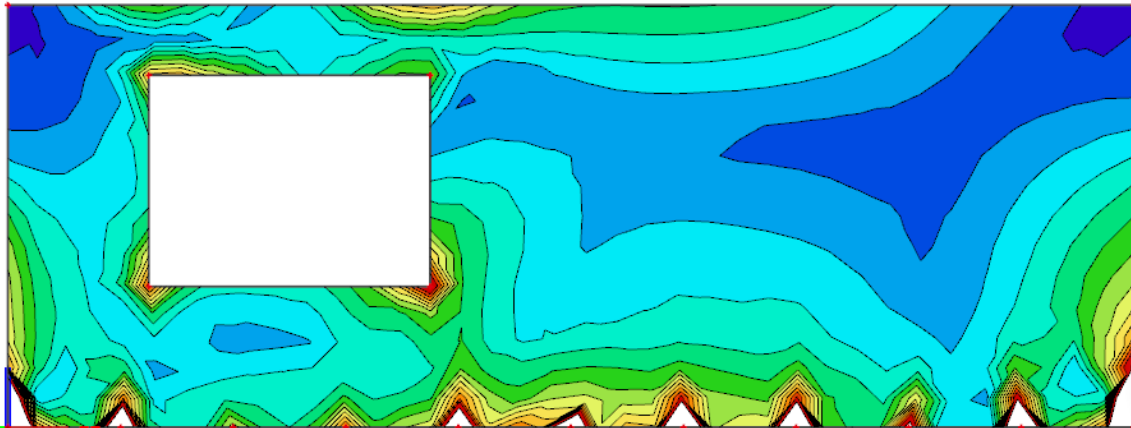


FIGURE 59 – STRESS CONTOUR 216 MM MESH

This mesh size is then used to calculate the stresses that occurred due to the vibration loads. These values can be added to the proposed procedure and the probability can also be calculated this way.

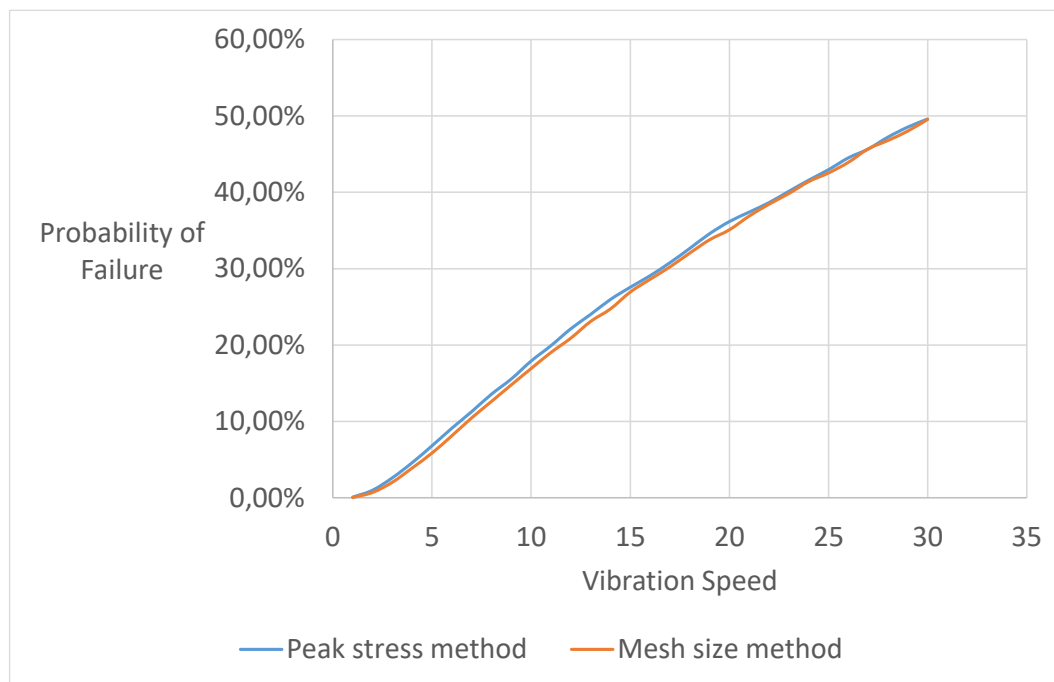


FIGURE 60 – COMPARED METHODS

As can be seen in Figure 60, both methods lead to nearly the same results.

5. COMPARISON TNO REPORT

This section describes how the results from the TNO report are compared if the same structure is examined according to the calculation procedure described in section 4. However, a few things have to be noted:

- The TNO report only uses a static calculation, while the procedure described in section 0 uses a dynamic calculation.
- There are less stochastic parameters in the proposed procedure than in the TNO report (Table 21, section 5.2.2). These are covered for in the SCIA calculations of the proposed procedure.
- The TNO report uses a sinusoidal force at the bottom of the structure, with an amplitude of 1 N/m². A static calculation is used for this calculation. The proposed procedure uses a dynamic calculation and will use the displacement at the bottom of the structure as the load.

To perform a comparison between the two methods of sufficient quality, two steps have to be executed:

- 1) The first step is to see if the SCIA calculation will produce the same results as the results in the TNO report. This is done by implementing the same loads and structural parameters which are used in the TNO report, in the SCIA structure. The results will be compared, and the results shall be compared. This results in a statement if the usage of SCIA is feasible.
- 2) The second step is to execute the procedure as described in section 0. This results in a probability of failure of this structure by using vibration speeds from 1 to 30 mm/s.

5.1 STEP 1: STRUCTURAL ANALYSIS

The goal of this step is to see if the SCIA calculation and the TNO report will produce comparable results. Using this information, it can be determined if SCIA is feasible to produce the structural results needed for the probabilistic calculation.

5.1.1 STRUCTURAL PARAMETERS

The parameters shown in Table 16 are used in the report made by ir. P.H. Waarts from TNO (Waarts, 1997).

TABLE 16 – PROPERTIES MODEL TNO REPORT

Property	Value
Wall width (b)	8 m
Wall height (h)	3 m
Window width (b_w)	2 m
Window height (h_w)	1.5 m
Window placement (from left) (s)	2 m (situation 1), 4 m (situation 2)
Load (F)	Half-sinus, max 1 N/m
Young's Modulus masonry (E)	$1.5 \cdot 10^9$ N/m ²
Poisson coefficient (ν)	0.2 (-)
Density (ρ)	2000 kg/m ³

In SCIA, these parameters are used to model the structure. The dimensions of the wall and the window, masonry Young's Modulus, Poisson coefficient and the density are easy to implement in the model. Since it is difficult to implement a sinusoidal load, this load has been translated to a tenfold trapezoidal load, by using the values of the sinuses of $0.1 \cdot \pi$, $0.2 \cdot \pi$ etc. This resulted in the load scheme shown in Figure 61.

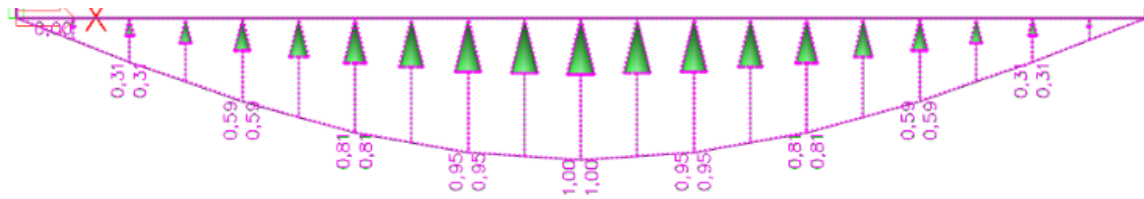


FIGURE 61 – TRANSLATION SINUSOIDAL LOADS TO TRAPEZOIDAL LOAD.

The TNO report is not very clear how the supports are modeled. It is chosen to implement the support as a line spring support over the entire bottom of the structure. The spring constant of this spring support was set at 1 MN/m².

Regarding the mesh, the TNO report used quite a large refinement around the edges of the window. This has been tested in SCIA. Very fine meshes around the edges lead to a visualization of the singularities around the corners of the window. That is why the choice was made to use a fine mesh for the entire structure. The element size was set to 0.05 m, since this is the size of one edge of brick elements and decided is not to use mesh sizes smaller than this size. The mesh is shown in Figure 62.



FIGURE 62 – MESH

Figure 62 does not show the window opening in the structure. Naturally, these will be present in the structure. In situation 1 this opening will be on the left side of the structure, in situation 2 this will be in the middle of the structure.

5.1.2 STRUCTURAL RESULTS

Opening on left side

Stresses in x-direction

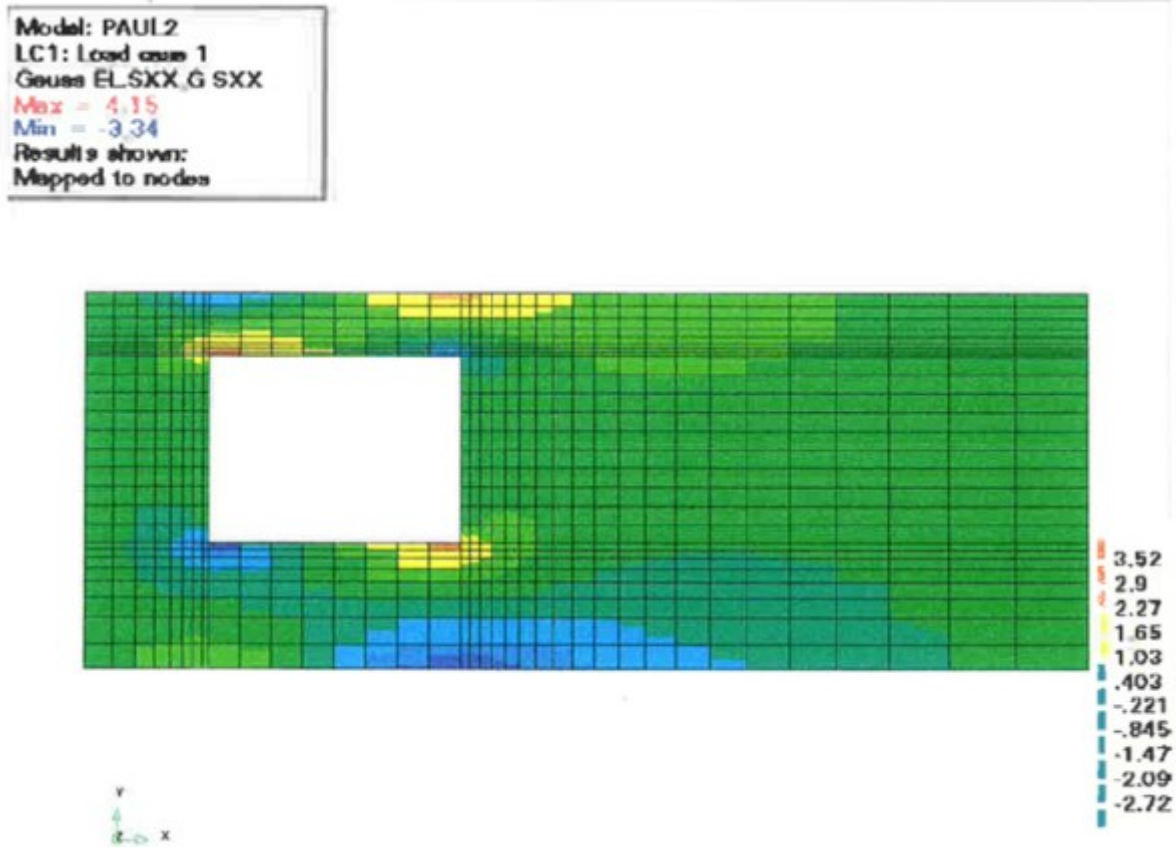


FIGURE 63 – TNO REPORT X-STRESSES. OPENING ON LEFT SIDE

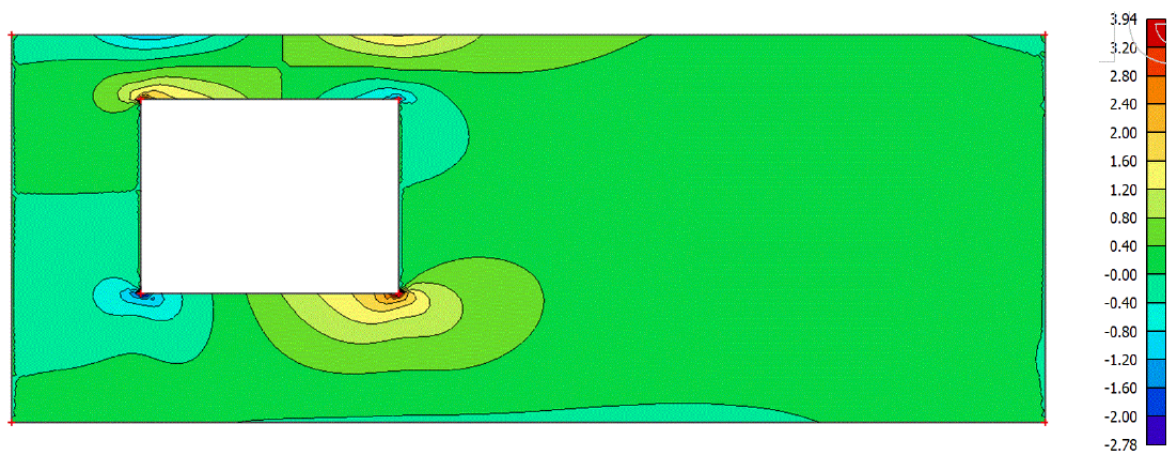


FIGURE 64 – SCIA RESULTS X-STRESSES. OPENING ON LEFT SIDE.

The figures above show the comparison between the x-stresses with an opening on the left side.

Stresses in y-direction

Model: PAUL2
LC1: Load case 1
Gauss EL SXX, G SYY
Max = 2.65
Min = -3.9
Results shown:
Mapped to nodes

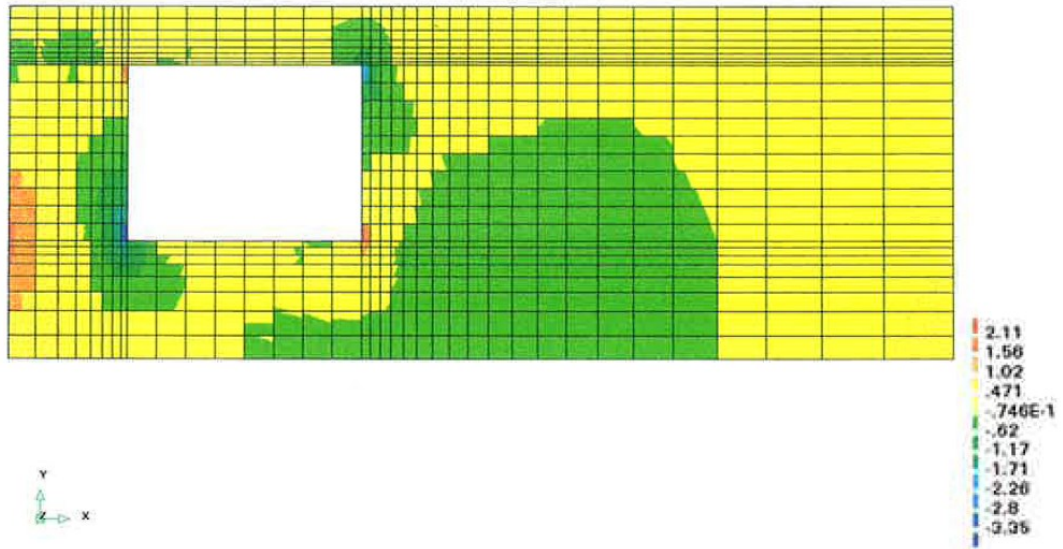


FIGURE 65 – TNO REPORT Y-STRESSES. OPENING ON LEFT SIDE.

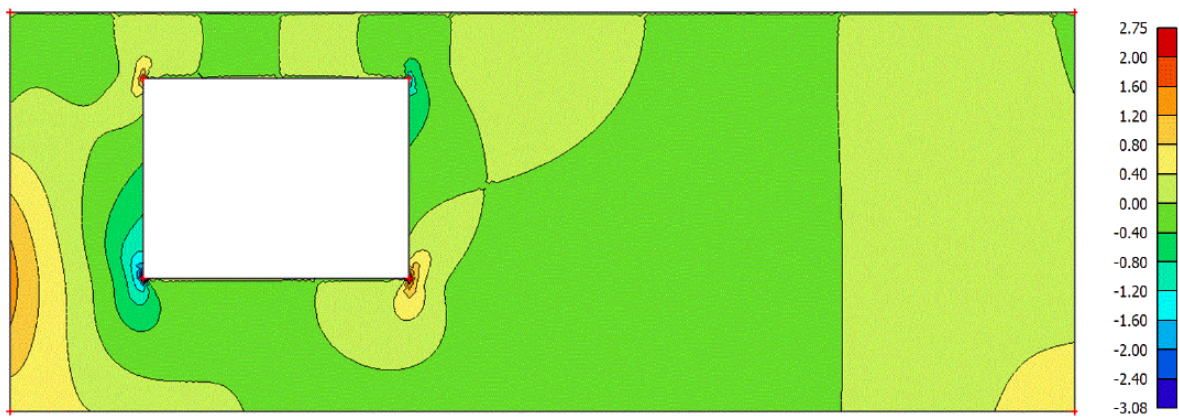


FIGURE 66 – SCIA RESULTS Y-STRESSES. OPENING ON LEFT SIDE.

The figures above show the comparison between the y-stresses with an opening on the left side.

Opening in the middle

Stresses in x-direction

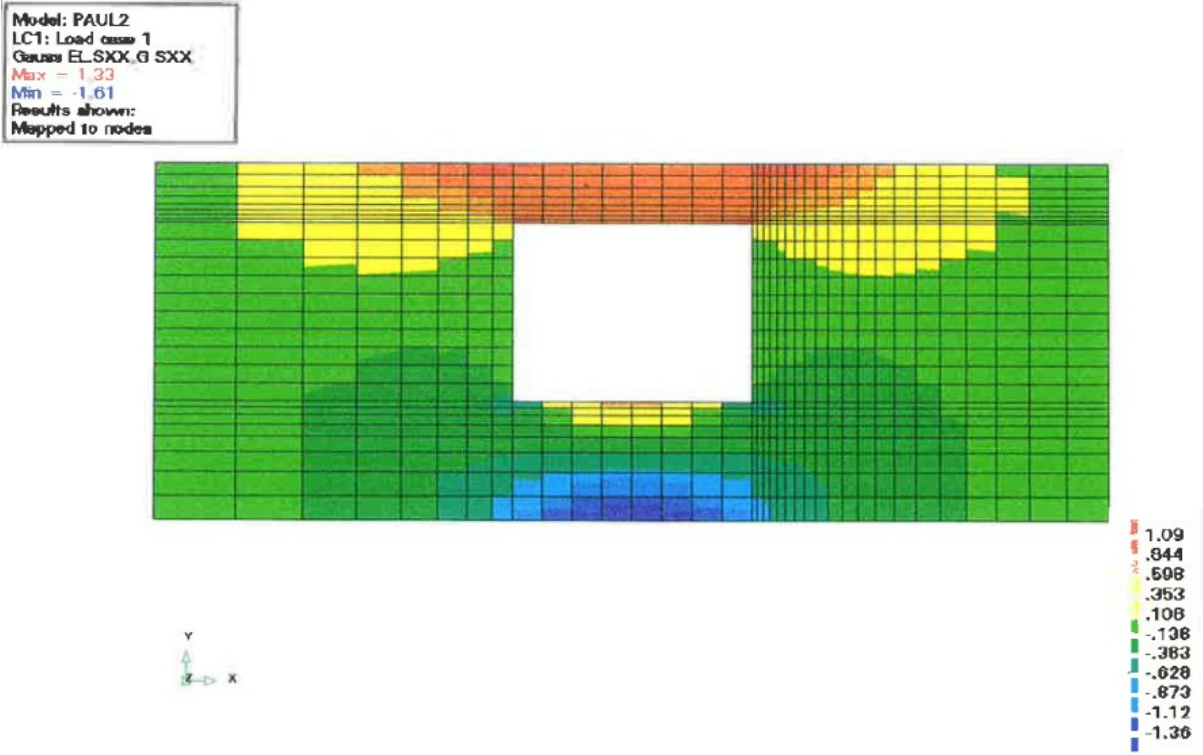


FIGURE 67 – TNO REPORT X-STRESSES. OPENING IN THE MIDDLE

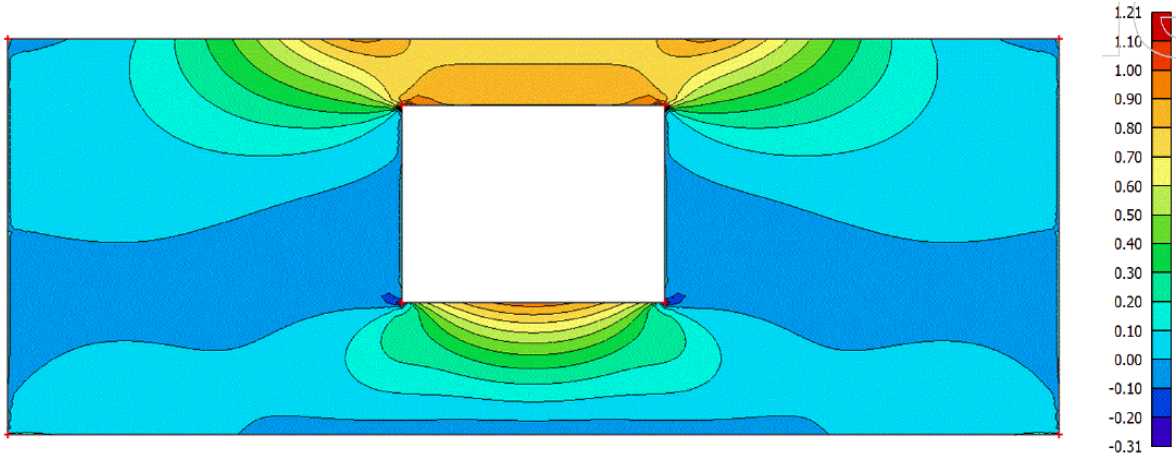


FIGURE 68 – SCIA RESULTS X-STRESSES. OPENING IN THE MIDDLE

The figures above show the comparison between the x-stresses with an opening in the middle.

Stresses in y-direction

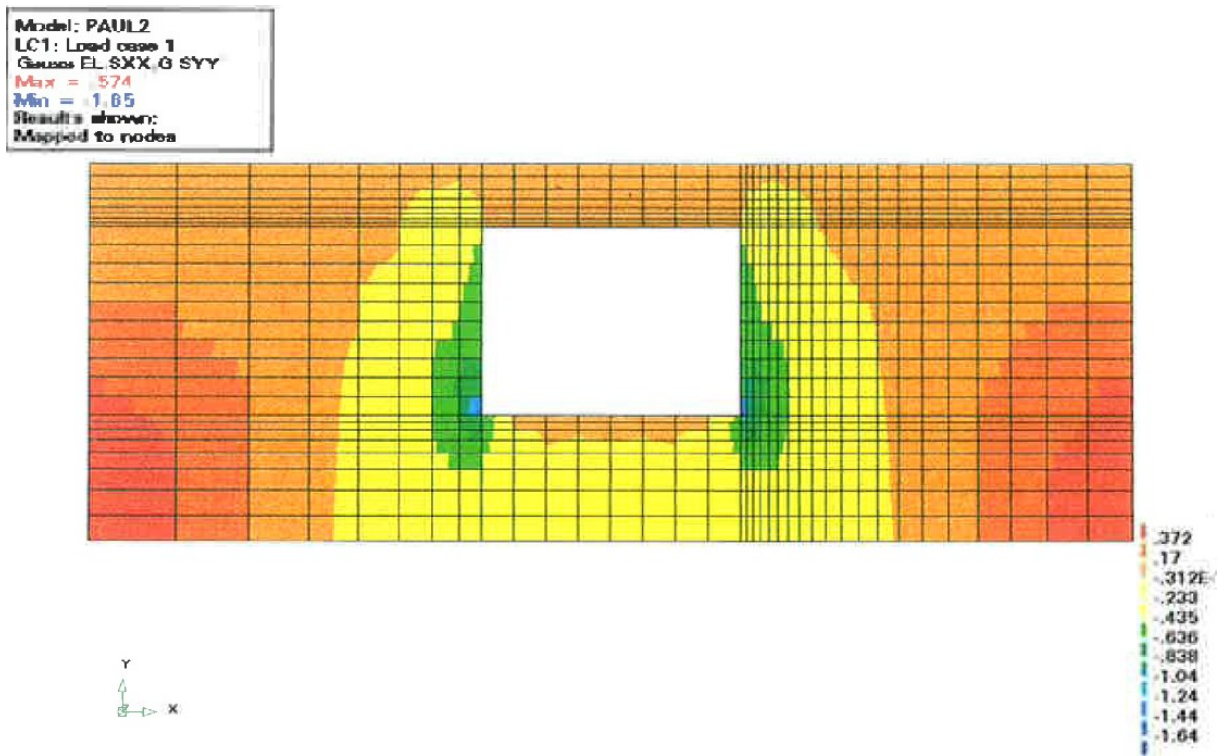


FIGURE 69 – TNO REPORT Y-STRESSES. OPENING IN THE MIDDLE

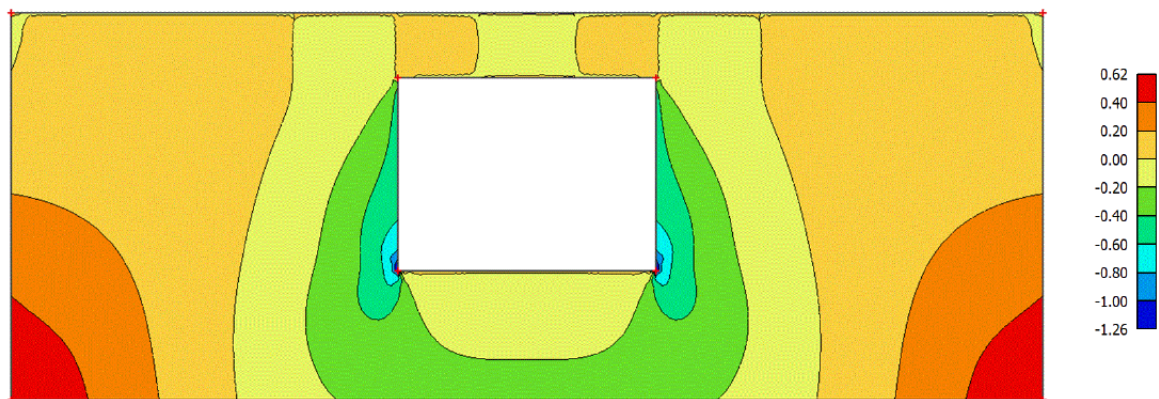


FIGURE 70 – SCIA RESULTS Y-STRESSES. OPENING IN THE MIDDLE.

The figures above show the comparison between the y-stresses with an opening in the middle.

5.1.3 CONCLUSION

The plot contours are compared to each other. It has been chosen to compare these properties to each other because it shows if the structure will respond the same way as the TNO-calculation. The maximum and minimum stresses are not compared since these are the results in singularities and will lead to different results, since there are different mesh sizes, element types and software programs amongst others.

It can be seen that the order size of the stresses are about the same for both calculations. Therefore, the results produced in SCIA will be applicable to this situation.

The contours produced by SCIA have comparable patterns as those from the TNO report. This means that the distribution of stresses will follow the same patterns in both situations.

These two compared properties lead to the fact that SCIA will produce comparable results to the TNO-report, which means that this software program can be used.

5.2 STEP 2: PROBABILISTIC METHODS

The probabilistic method is tested by using the parameters of the TNO report for two reasons:

- The first reason is to see if the Monte Carlo simulation or the FORM-method is more applicable to this project.
- The second reason is to see if the chosen method in the proposed procedure will lead to probable results for this research project.

The TNO report has used the program VAP, developed by ETH Zurich for probabilistic calculations. This program is used mainly for educational purposes and it could perform analyses using the FORM-method as well as Monte Carlo simulations. However, support for the program ended and therefore it is currently not available for usage.

In the TNO report, the following limit state function is used (Z is the limit state):

$$Z = f_t - \sigma_{ini} - \sigma_{dyn} \quad (30)$$

Where:

$$\sigma_{dyn} = E * \epsilon \quad (31)$$

And:

$$\epsilon = k * H * v_{measurement} \quad (32)$$

Table 17, Table 18 and Table 19 demonstrate these properties for good quality, bad quality and monumental masonry, as used in the TNO report.

TABLE 17 – STOCHASTIC PROPERTIES FOR GOOD QUALITY MASONRY

Type	Parameter	Mean value (μ)	Standard deviation (σ)	Unit	Distribution type
Young's Modulus	E	1505	1161	N/mm ²	Lognormal
Tensile strength	f_t	0.28	0.086	N/mm ²	Lognormal
Transfer ratio	H	$3.3 * 10^{-7}$	$2.2 * 10^{-7}$	s/mm	Lognormal
Initial stress	σ_{ini}	0.0	0.1	N/mm ²	Normal
Multiplying factor for opening in walls	k	8	2	-	Lognormal
Vibration speed	$v_{measurement}$	5	0.1	mm/s	Normal

TABLE 18 – STOCHASTIC PROPERTIES FOR BAD QUALITY MASONRY

Type	Parameter	Mean value (μ)	Standard deviation (σ)	Unit	Distribution type
Young's Modulus	E	1505	1161	N/mm ²	Lognormal
Tensile strength	f_t	0.28	0.086	N/mm ²	Lognormal
Transfer ratio	H	$3.3 \cdot 10^{-7}$	$2.2 \cdot 10^{-7}$	s/mm	Lognormal
Initial stress	σ_{ini}	0.14	0.13	N/mm ²	Lognormal
Multiplying factor for opening in walls	k	8	2	-	Lognormal
Vibration speed	$v_{measurement}$	3	0.06	mm/s	Normal

TABLE 19 – STOCHASTIC PROPERTIES FOR MONUMENTAL MASONRY

Type	Parameter	Mean value (μ)	Standard deviation (σ)	Unit	Distribution type
Young's Modulus	E	1505	1161	N/mm ²	Lognormal
Tensile strength	f_t	0.28	0.086	N/mm ²	Lognormal
Transfer ratio	H	$3.3 \cdot 10^{-7}$	$2.2 \cdot 10^{-7}$	s/mm	Lognormal
Initial stress	σ_{ini}	0.0	0.13	N/mm ²	Normal
Multiplying factor for opening in walls	k	8	2	-	Lognormal
Vibration speed	$v_{measurement}$	3	0.06	mm/s	Normal

5.2.1 MONTE CARLO OR FORM

In order to compare the Monte Carlo simulation to the FORM-analysis, the parameters for the different types of masonry are implemented in the simulations. Afterwards, these will be compared to one another and to the results from the TNO report. This should result in a statement which probabilistic method is the most useful for this project.

Monte Carlo Simulation

As said before, support has ended for the program VAP which was used in the TNO report. Therefore, it was not possible to use this program for a Monte Carlo simulation, so a Monte Carlo simulation was performed using MATLAB. The script for the bad quality masonry is shown in Figure 71.

```

clear all;
n=100000;
for i=1:n
%E
mu=log((1505^2)/sqrt(1161^2+1505^2));sigma=sqrt(log(1161^2/(1505^2)+1));E(i)=lognrnd(mu,sigma);
%ft
mu=log((0.31^2)/sqrt(0.086^2+0.31^2));sigma=sqrt(log(0.086^2/(0.31^2)+1));ft(i)=lognrnd(mu,sigma);
%H
mu=log((0.00000033^2)/sqrt(0.00000022^2+0.00000033^2));sigma=sqrt(log(0.00000022^2/(0.00000033^2)+1));H(i)=lognrnd(mu,sigma);
%sigmaini
mu=log((0.14^2)/sqrt(0.13^2+0.14^2));sigma=sqrt(log(0.13^2/(0.14^2)+1));sigmaini(i)=lognrnd(mu,sigma);
%k
mu=log((8^2)/sqrt(2^2+8^2));sigma=sqrt(log(2^2/(8^2)+1));k(i)=lognrnd(mu,sigma);
vmeet(i)=normrnd(3,0.06);
R(i)=ft(i);
S(i)=sigmaini(i)+E(i)*k(i)*vmeet(i)*H(i);
Z(i)=R(i)-S(i);
end
sum(Z<0)/n

```

ans =

0.1111

FIGURE 71 – MATLAB SCRIPT FOR BAD QUALITY MASONRY

In Table 20, the results due to different sample sizes are compared. It can be seen that a sample size of 10000 will not lead to a mean value and differences comparable to the results by using a sample size of 1000000. A sample size of 100000 leads to results comparable to those produced by a sample size of 1000000, while the computational time is limited. Therefore this sample size has been chosen.

TABLE 20 – SAMPLE SIZES

N	Max value	Min value	Mean value	Difference
10000	0.1149	0.1090	0.1226	3.2%
100000	0.1119	0.1107	0.1113	0.5%
1000000	0.1117	0.1111	0.1114	0.27%

By editing parts of this script, other scripts can be written which would be applicable to good quality masonry and monumental masonry. Using various values of vibration speed, a figure can be drawn for the probability of failure against the vibration speed, which is elaborated further in the comparison section.

FORM-analysis

The FORM-method is explained in Chapter 4. As stated before, the support for VAP has ended, therefore, another software package had to be investigated. TNO created the program Prob2B, which can perform a FORM-analysis using the normal and lognormal distributions and uses the limit state function to calculate the probability of failure. In the comparison section the results will be elaborated further.

Comparison

Comparing the results of the Monte Carlo simulation and the FORM-analysis to each other, it can be seen that in all cases the bad state masonry leads to the highest probabilities of failure, and the monumental masonry experiences the lowest probabilities of failure. For the low values for vibration speed, the probability of failure of the Monte Carlo simulation and the TNO report are comparable. Taking a look at the high values for vibration speed, it can be seen that the probability of failure is higher in the TNO report than in the Monte Carlo simulation.

Figure 72, Figure 73 and Figure 74 show the probability of failure versus the vibration speed of bad state masonry, good state masonry and monumental masonry respectively. The graphs show that for the low values of the vibration speed, both the FORM and the Monte Carlo simulation produce results which are comparable to the results in the TNO report. If the value of the vibration speed increases, the differences between the results of the TNO report, FORM and Monte Carlo simulation diverge a bit. It is clear that the Monte Carlo simulation produces results more comparable to the TNO report. However, even the results of the Monte Carlo simulation are not that close to the results of the TNO report. The difference is between 4 and 10 percentage points. However, since the project focuses on the lower values of vibration speed (1-30 mm/s), and the differences are smaller for those values, the Monte Carlo method is sufficient to produce acceptable results.

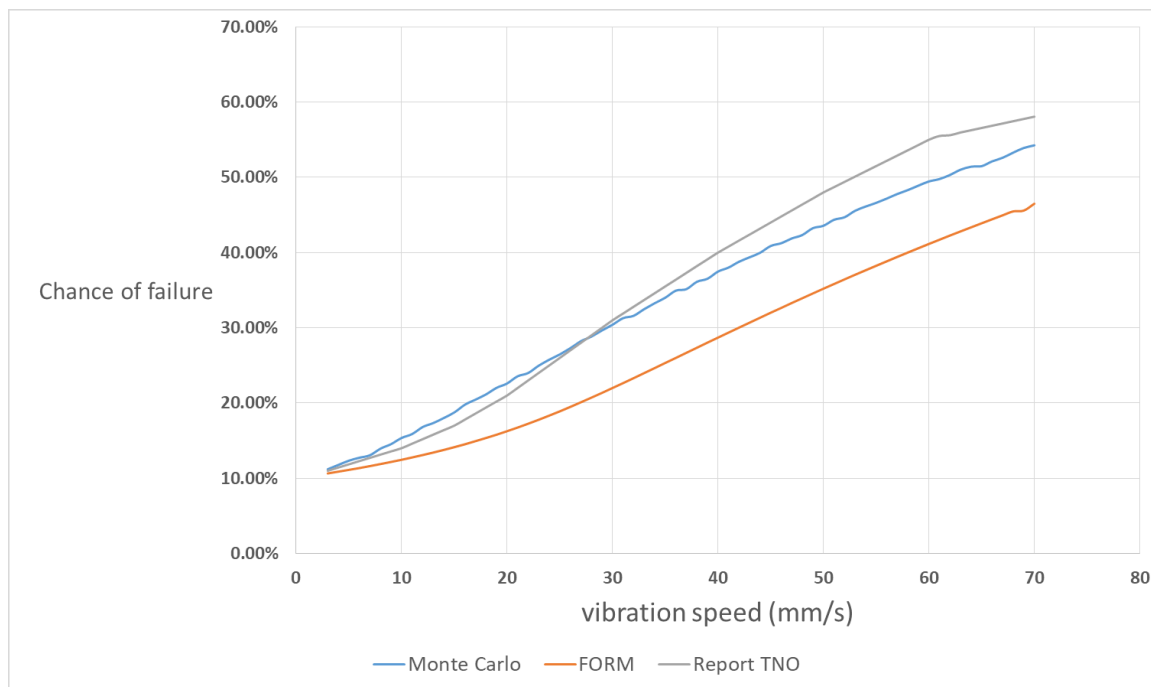


FIGURE 72 – PROBABILITY OF FAILURE OF BAD STATE MASONRY

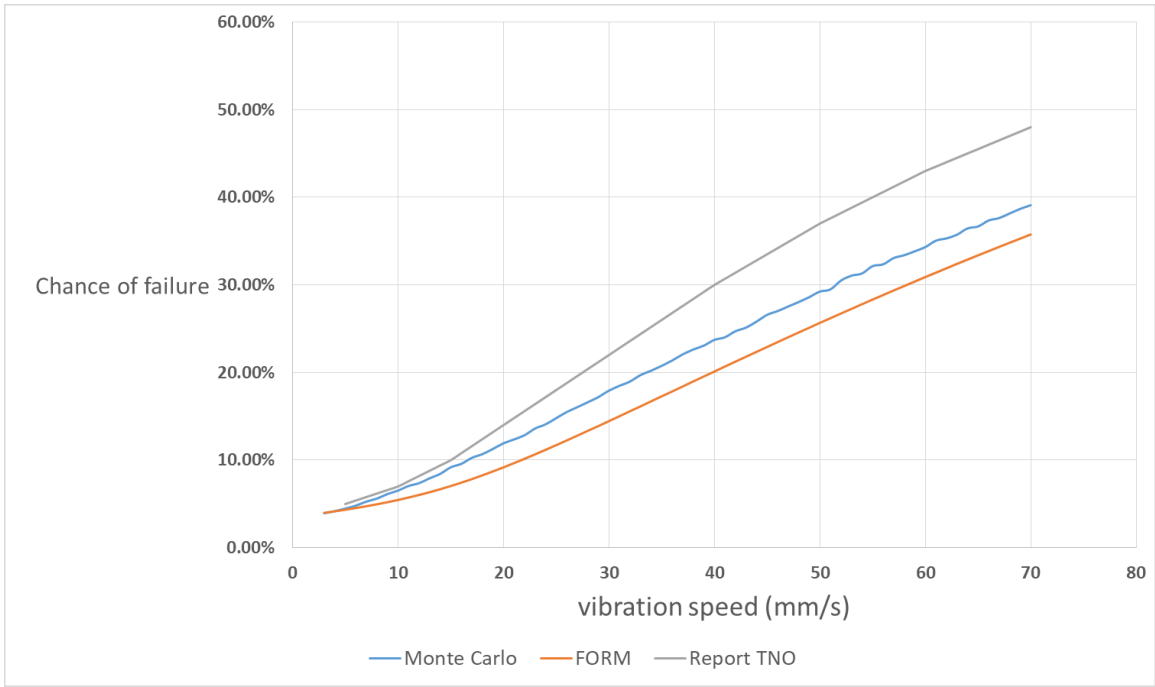


FIGURE 73 – PROBABILITY OF FAILURE OF GOOD STATE MASONRY

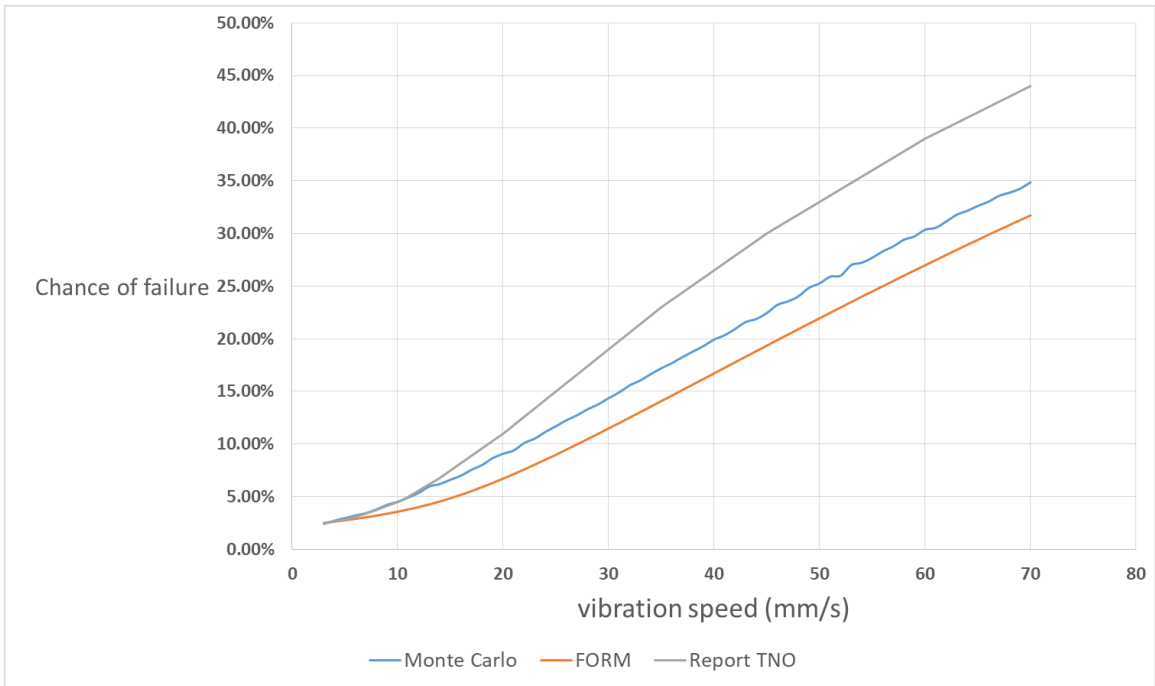


FIGURE 74 – PROBABILITY OF FAILURE OF MONUMENTAL MASONRY

5.2.2 PROPOSED PROCEDURE AND TNO METHOD

The calculation in the TNO-report leads to the results shown in Figure 75.

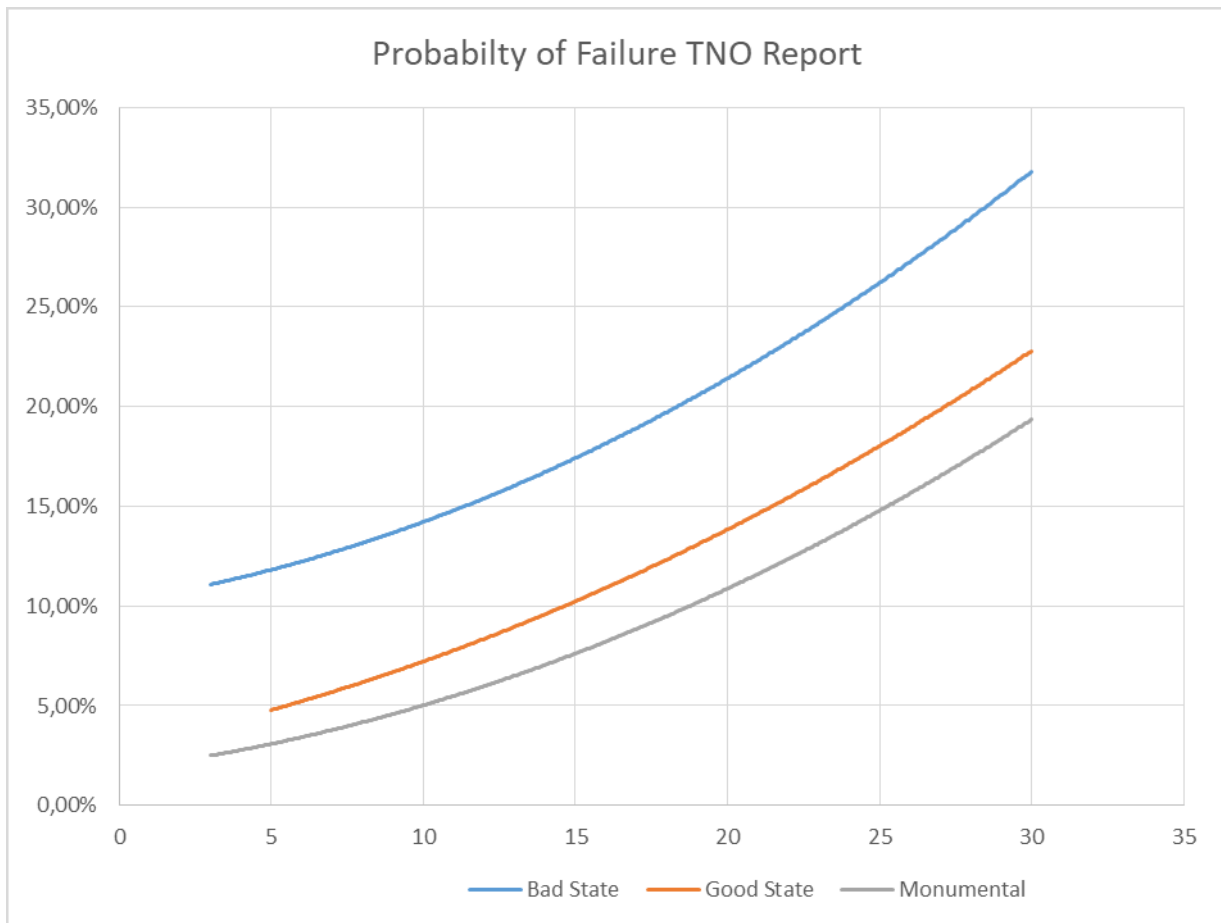


FIGURE 75 – RESULTS ACCORDING TO THE TNO REPORT, MODIFIED AFTER WAARTS (1997)

These are only the results for vibration speeds from 1 to 30 mm/s. Greater values for vibration speed will be unlikely and are therefore disregarded.

The parameters that have been used in the TNO report are stated in Table 21.

TABLE 21 – STOCHASTIC PARAMETERS TNO REPORT (WAARTS, 1997)

Parameter	Symbol	Distribution
Young's Modulus	E	Lognormal
Maximum tensile strength	f_t	Lognormal
Transmission formula	H	Lognormal
Initial stress	σ_{ini}	Normal
Multiplying factor for openings	k	Lognormal
Vibration speed	v_{meet}	Normal

The TNO report's aim was to perform a calculation where many uncertainties were covered by using stochastic parameters. In the current project, those uncertainties are covered using more advanced finite element calculations:

- The transmission formula was used to cover for the uncertainty of the frequency of the vibration speed. However, the engineer knows which frequencies to expect, which can be described in the SCIA model. Moreover, this project covers the bandwidth of stresses by using multiple frequencies (ranging from 3 to 25 Hz)
- The initial stress is covered by adding the stresses that result from the initial loads to the stresses produced by the vibration load.
- The multiplying factor for openings is not necessary since the engineer knows which façade he has to draw in the FEM-model.
- The vibration speed is covered by using various vibration speeds in the calculations.

This leaves two stochastic parameters: the maximum tensile stress and Young’s modulus.

The stochastic parameters of these properties are described in Table 22.

TABLE 22 – STOCHASTIC PARAMETERS

Parameter	Symbol	Distribution	Mean value (μ)	Variation coefficient
Young’s Modulus	E	Lognormal	5000 N/mm ²	0.3
Maximum tensile strength	f_t	Lognormal	Depends on situation	0.28

To find out the mean value of the maximum tensile stress for this structure, it has to be investigated what maximum tensile stress leads to an exceedance of 0.3 N/mm² tensile stress over a length of 210 mm. This situation is shown in Figure 76 and Figure 77.

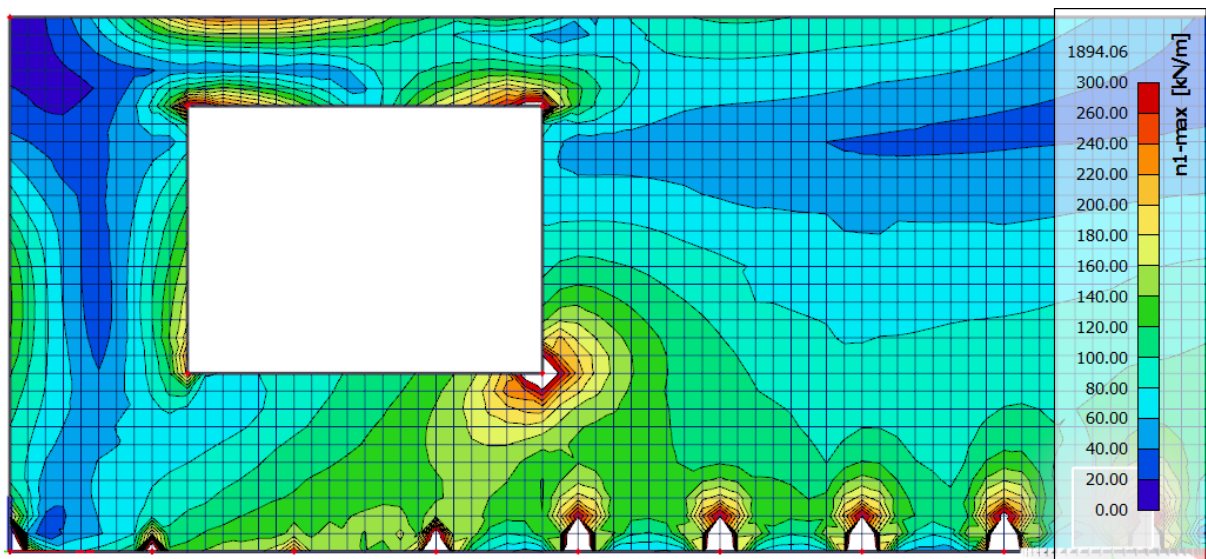


FIGURE 76 – ENVELOP STRUCTURAL TENSILE STRESSES

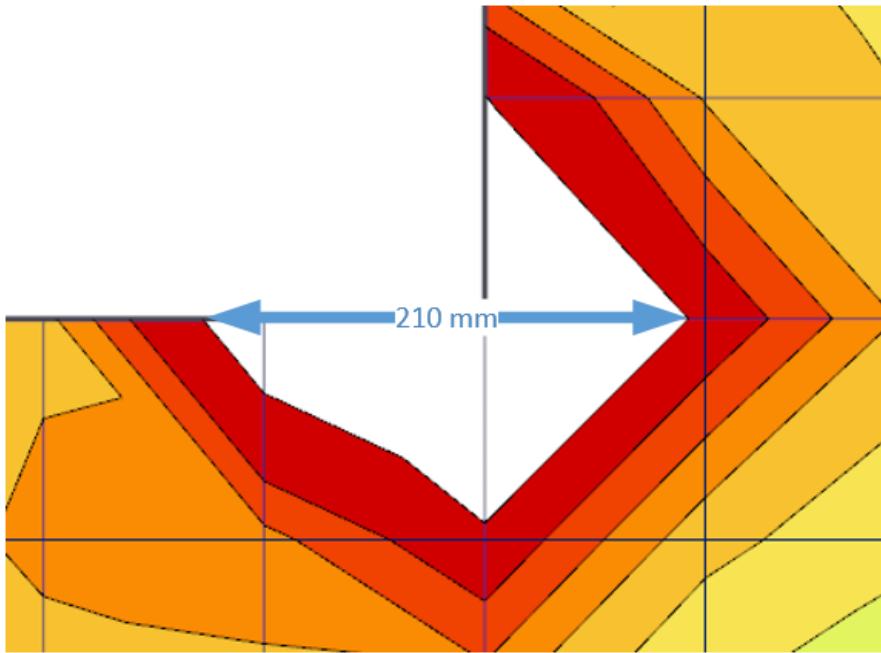


FIGURE 77 – ZOOMED IN CORNER AT MOMENT OF FAILURE (MESH SIZE: 100 MM)

This investigation leads to a tensile stress at the corner at moment of failure of 0.741 N/mm^2 . This will be the mean value of the tensile strength in the probabilistic calculation. (NOTE: failure criterion option 1 is used here (see 4.4). However, as also can be seen in this section, the difference is negligible, and therefore this option can be applied. It is done because earlier during this project this phase had been covered, before setting up the second failure criterion.)

The frequency for the calculation in this example will be set at 10 Hz. A clay soil is chosen, which propagation velocity is 600 m/s. For a 12 mm/s vibration speed, this leads to a displacement amplitude of $\frac{3}{5\pi} \text{ mm}$ ($\approx 0.191 \text{ mm}$), according to the following formula:

$$v(t) = u'(t) = 12 * \sin(10 * 2\pi * t) \rightarrow u(t) = -\frac{12}{20\pi} \cos(10 * 2\pi * t) \quad (33)$$

This value is implemented in the SCIA model. The value here leads to a maximum tensile stress in the structure in principal direction (n1) of 0.237 N/mm . This is shown in Figure 78.

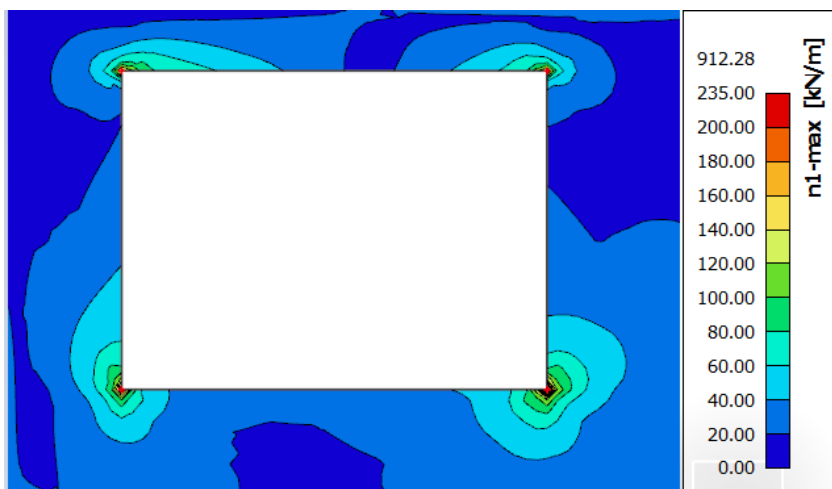


FIGURE 78 – STRESS CONTOUR AROUND OPENING FOR A VIBRATION SPEED OF 12 MM/S

It should be noted that in the figure the stress values in SCIA are written as kN/m. However, since it is a linear-elastic calculation and the wall thickness is 1000 mm (=1 m), the value of kN/m can be divided by 1000 to gain the results in N/mm². This thickness does not affect the stress in the structure in 2D but it will lead to an easier user experience.

Moreover, the other values (n_2, α) have to be gathered for the probabilistic calculation. This has to be done for both the initial load case and the vibration loads. These are demonstrated in Table 23.

TABLE 23 – STRESS VALUES FOR THE BOTTOM RIGHT CORNER OF THE OPENING

	$n1(N/mm^2)$	$n2(N/mm^2)$	$\alpha(deg)$
Initial load	-0.00968	-0.0446	56
Vibration load	0.237	0.0815	42.7

To complete the MATLAB code, the effect of Young’s Modulus of masonry on the maximum tensile stress needs to be described and implemented in the code using a formula. For different values of Young’s Modulus ($\mu - 3 * \sigma, \mu - 2 * \sigma \dots \mu + 3 * \sigma$) the values of the maximum tensile stress have been gathered, using the SCIA model. These are divided by the value of the tensile stress when Young’s Modulus is equal to the mean Young’s Modulus of masonry (5000 N/mm²).

This results in the scatterplot as shown in Figure 79. A curve-fit is made for this scatterplot. In this figure, the solid line is the scatter while the dotted line is the curve-fit (3rd order) of this scatter. This curve-fit results in a third order equation to describe this curve, which is also shown in the figure. Therefore, the equation which can be implemented in the MATLAB-script reads:

$$\sigma(E) = 1.54 * 10^{-11} * E^3 - 1.75 * 10^{-7} * E^2 + 6.689 * 10^{-4} * E - 0.1553 \tag{34}$$

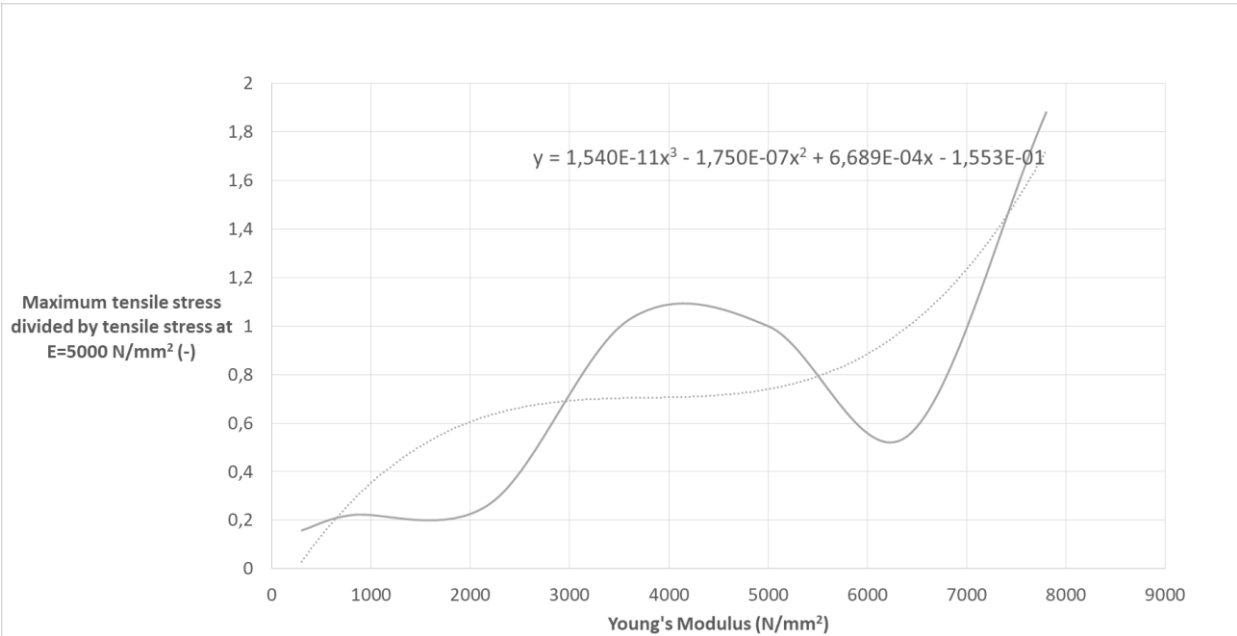


FIGURE 79 – TENSILE STRESS VERSUS YOUNG’S MODULUS

However, equation (34) is not a good representation of the actual relationship between Young’s Modulus and maximum tensile stress. Therefore, two curve-fits should be computed, one for $E < 3600$ N/mm² and one for $E > 3600$ N/mm². These are shown in Figure 80 and Figure 81.

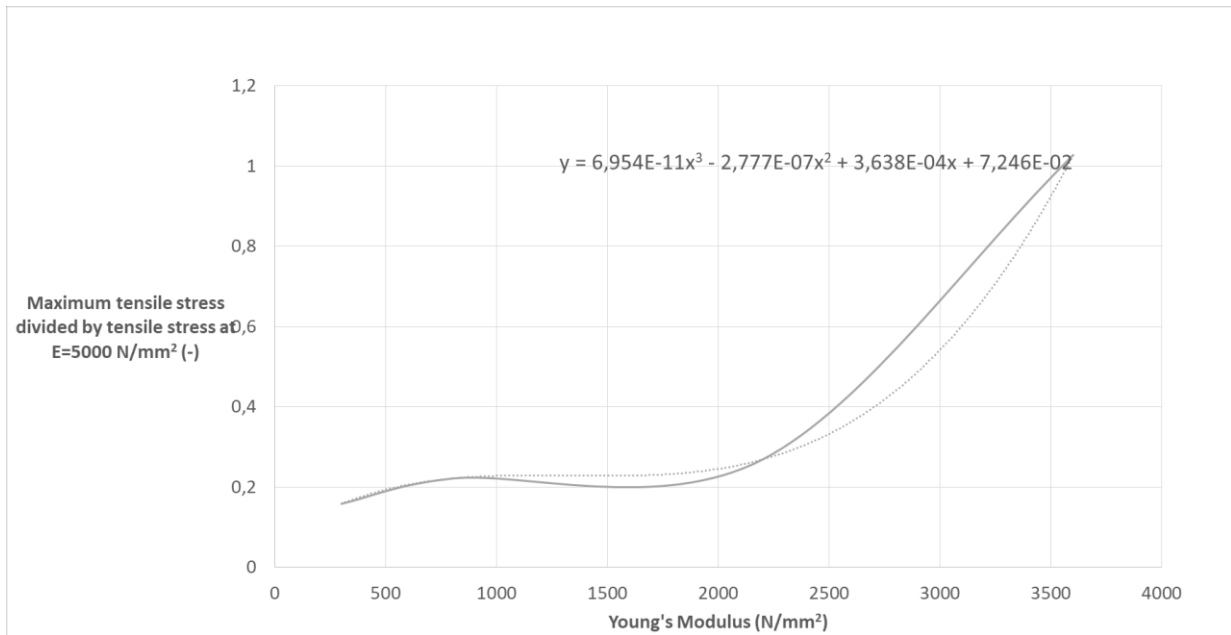


FIGURE 80 – CURVE-FIT FOR E<3600 N/MM²

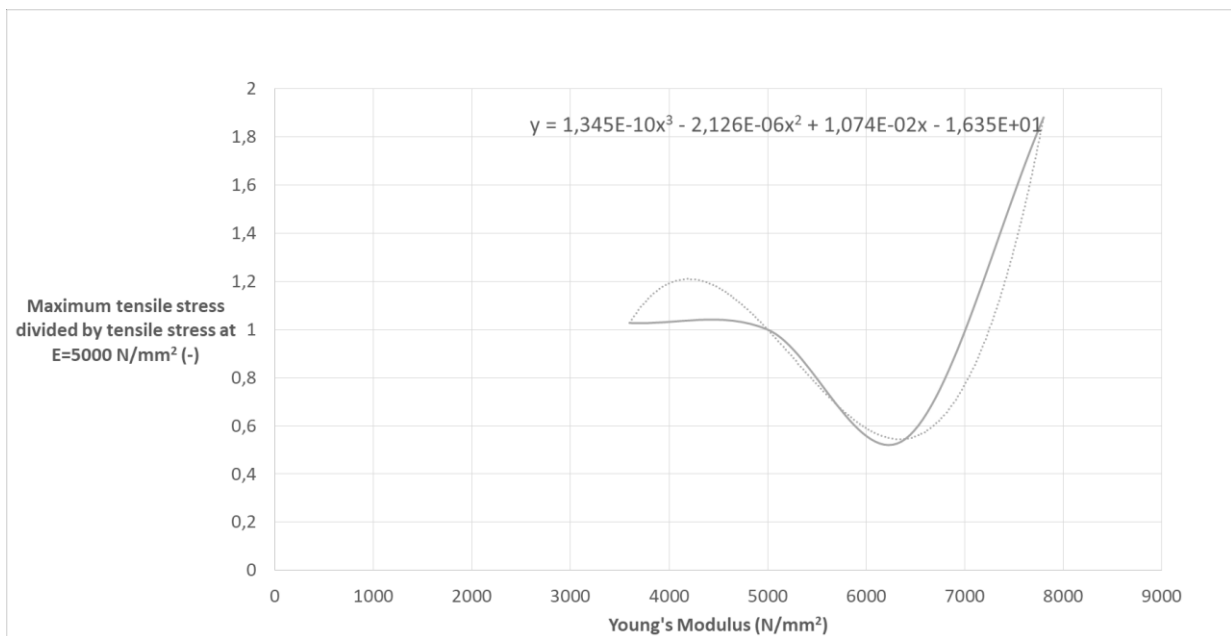


FIGURE 81 – CURVE-FIT FOR E>3600 N/MM²

This results in following equations to describe the relationship between Young's Modulus and maximum tensile stress:

$$\sigma(E) = 6.954 * 10^{-11} * E^3 - 2.77 * 10^{-7} * E^2 + 3.638 * 10^{-4} * E + 0.07246 \quad E < 3600 \text{ N/mm}^2 \quad (35)$$

$$\sigma(E) = 1.345 * 10^{-10} * E^3 - 2.126 * 10^{-6} * E^2 + 1.074 * 10^{-2} * E - 16.35 \quad E > 3600 \text{ N/mm}^2 \quad (36)$$

These values are implemented in the probabilistic model, and a Monte Carlo simulation can be executed. The Monte Carlo simulation results in the probability of failure/vibration speed curve as shown in Figure 82.

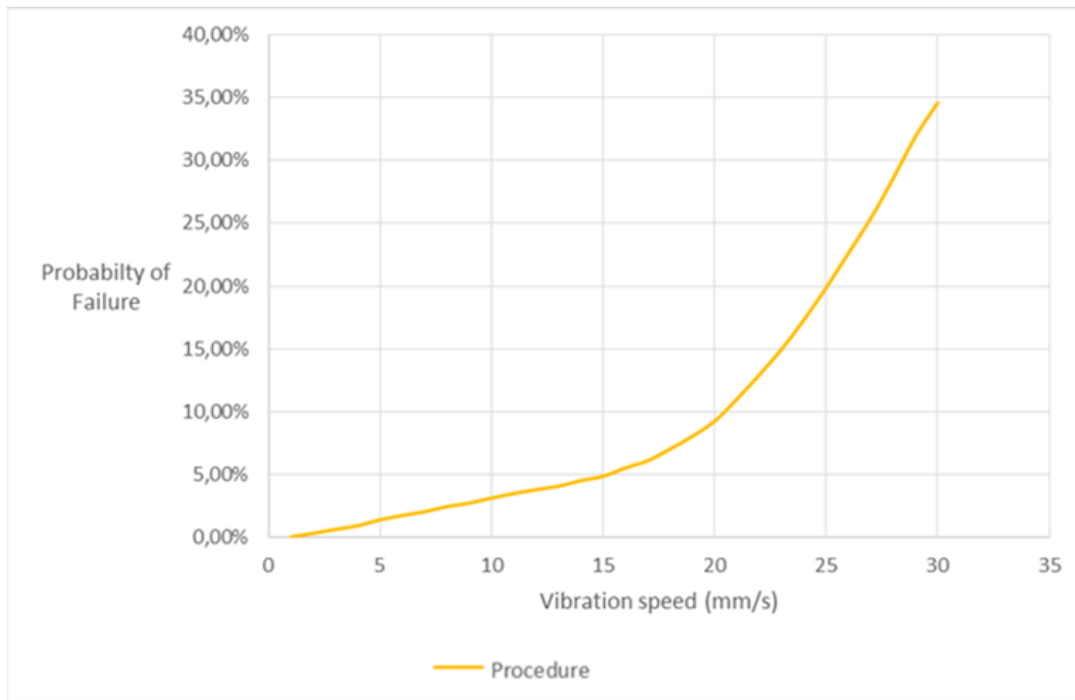


FIGURE 82 – PROBABILITY OF FAILURE FOR A 10 HZ VIBRATION IN A SANDY SOIL

Comparison

The probability of failure that has been gathered using the proposed procedure is compared to those from the TNO report. A few things can be noted according to this comparison (Figure 83):

- At lower vibration speeds, the probability of failure is lower than the probabilities which are gathered in the TNO report.
- If the vibration speeds exceed roughly 20 mm/s, probability of failure gathered from the proposed procedure will rise sharply, and the values from the TNO report are exceeded.

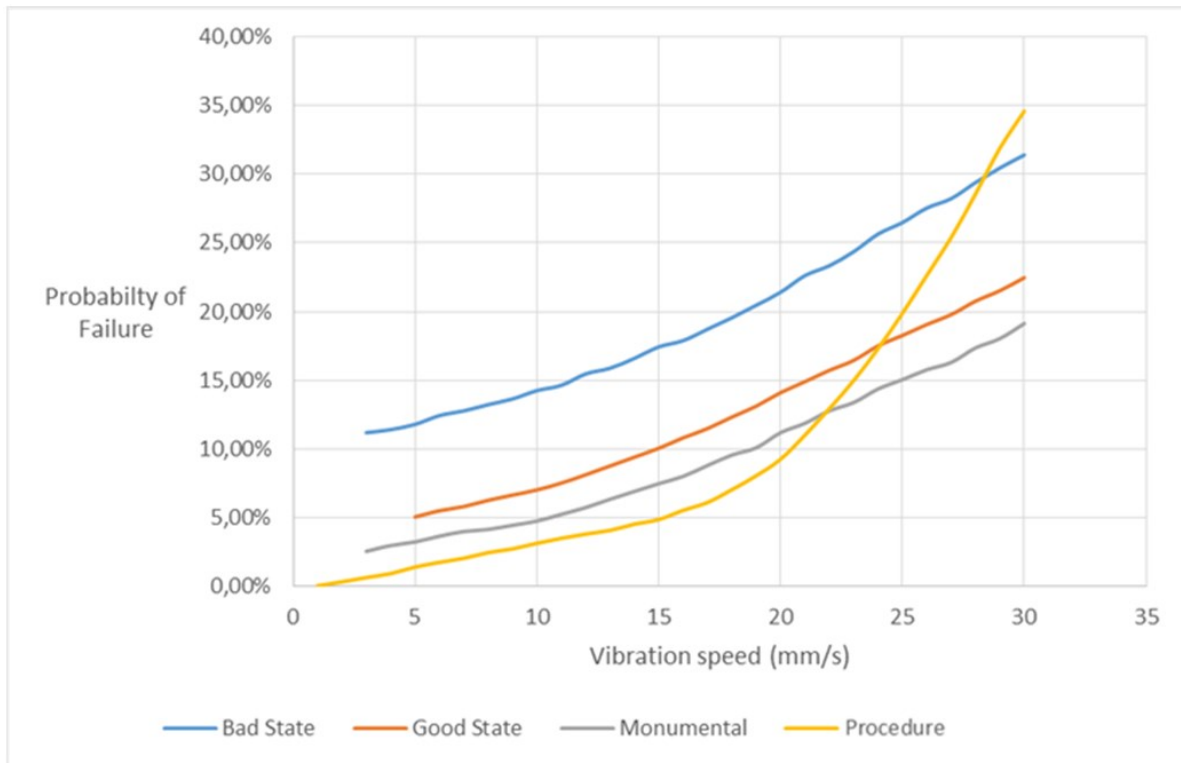


FIGURE 83 – COMPARISON TNO REPORT AND PROPOSED PROCEDURE

The main focus of this comparison is to see if the probabilistic method leads to probable results, which means if this method is applicable to this situation. Since the probabilities of failure are around the same order size, it seems that the method is applicable for these vibration speeds.

The project only focuses on the vibrations between 1 and 30 mm/s. If higher vibration speeds will be investigated (31-80 mm/s), another comparison has been made, since the probabilities of failure are starting to rise sharply. On the other hand, this can be expected, since those unlikely high vibration speeds will most likely lead to a significant increase in the probability of failure.

For the bandwidth of this project, (1-30 mm/s), the proposed procedure leads to probable results and is therefore applicable.

A flowchart regarding the calculation is shown in Figure 84.



FIGURE 84 – FLOWCHART OF THE CALCULATION

6. MODELING AND RESULTS

This phase will describe the modeling of the chosen structures (see section 4.2). The case “Oude Delft” will be elaborated extensively, while the others follow the same path, but for clarity purposes only the results will be shown.

6.1 OUTLINE

As stated before (section 4.1), there are 4 steps in the calculation procedure:

- 1) Initial loads.
- 2) Initial loads and vibration loads, no stresses at the soil-masonry interface.
- 3) Initial loads and vibration loads, with stresses at the soil-masonry interface.
- 4) (possibly) Nonlinear springs/nonlinear material behavior.

The main focus of this project is the initial loads and vibration loads, without stresses at the soil-masonry interface. These steps will be described in their respective sections in this chapter.

6.2 MODEL

As stated before, the case “Oude Delft” will be elaborated extensively, while the results of the other cases will be demonstrated.

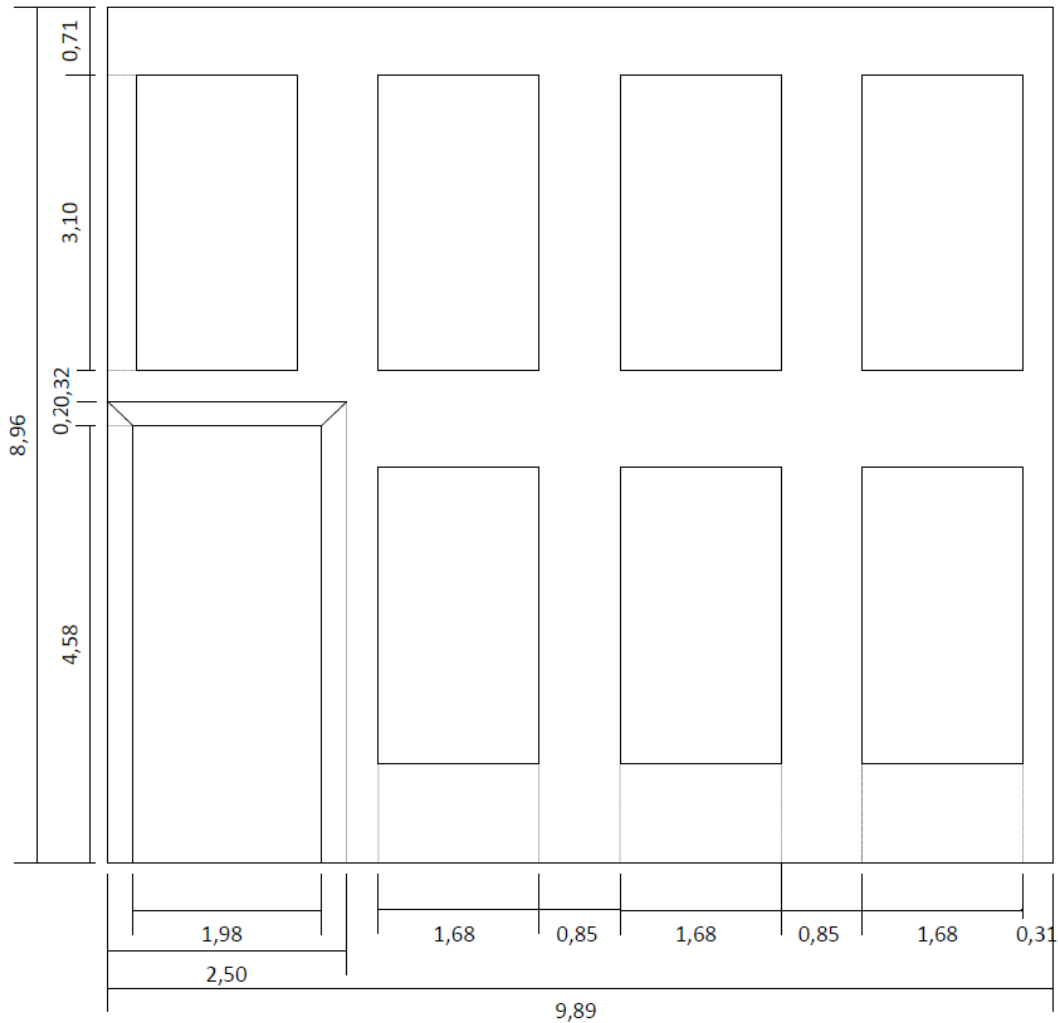


FIGURE 85 – OUDE DELFT DIMENSIONS

A few things have to be noted

- The structure is 9.9 meters wide. There are 11 spring-columns evenly distributed, with the outer spring-columns placed at the bottom corners of the structure. Therefore, they are placed 0.99 meters from one another.
- To ensure that the spring-columns are attached to the bottom of the structure, there is some façade material added at the bottom of the door.
- There is a floor level between the door and the top window, at 4.9 meters from the bottom of the structure.
- The mesh size is 100x100 mm.

This leads to the model in SCIA as shown in Figure 86.

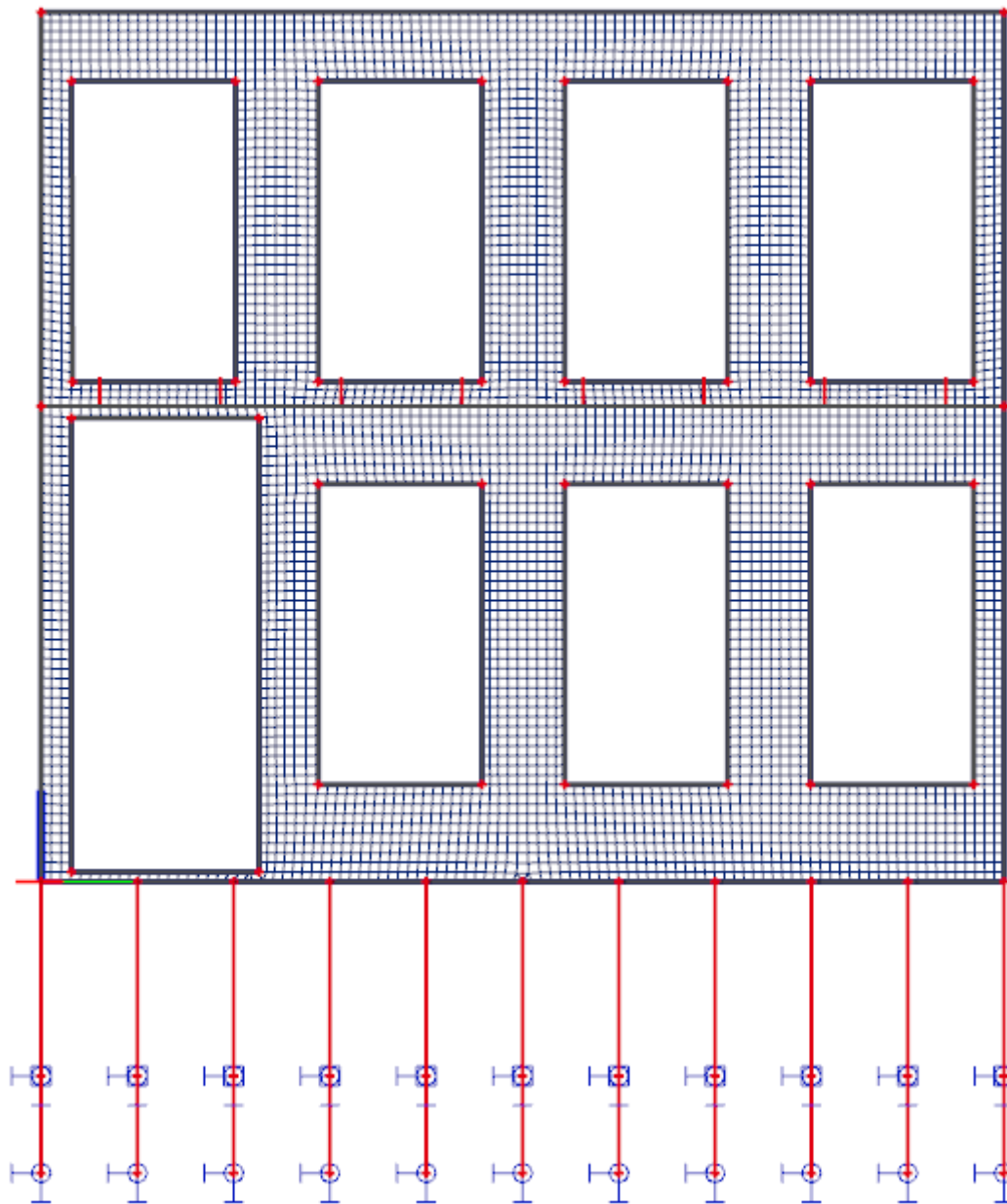


FIGURE 86 – SCIA MODEL OUDE DELFT

6.3 LOADS

6.3.1 INITIAL LOADS

The initial loads, as specified in section 4.1, are shown in Table 24, Figure 87 and Figure 88.

TABLE 24 – INITIAL LOADS

	Representative loading situation
Floor	4.1125 (kN/m)
Roof	3.5 (kN/m)
Self-weight masonry	3.92 (kN/m ²)

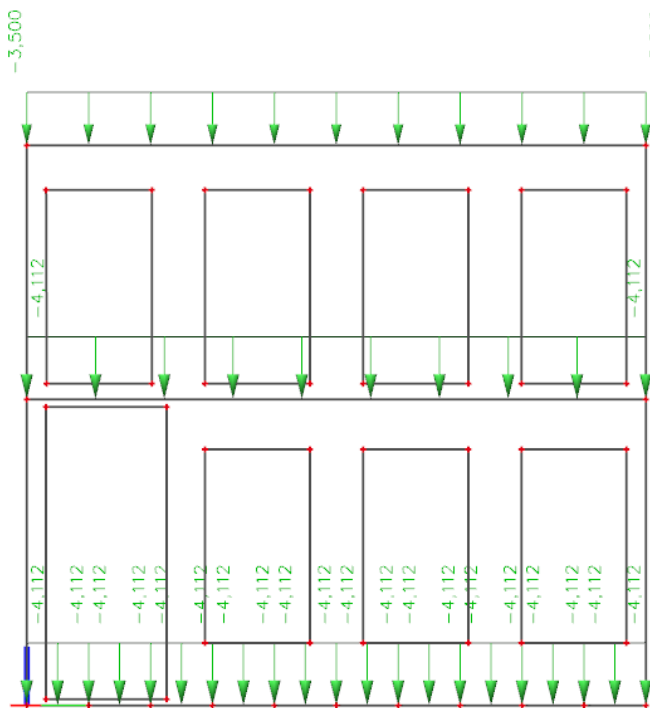


FIGURE 87 – FLOOR AND ROOF LOADS

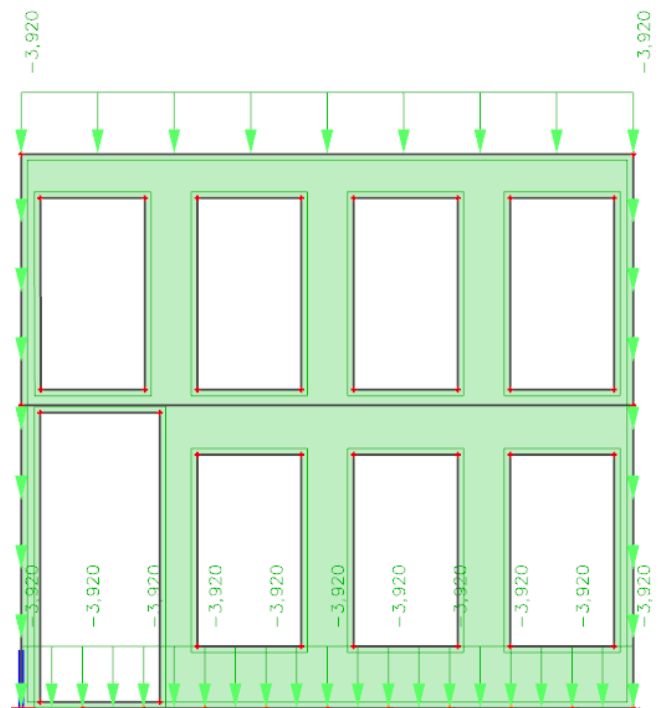


FIGURE 88 – SELF-WEIGHT MASONRY

6.3.2 VIBRATION LOADS

For the vibration loads, the phase differences depend on the propagation velocity v and the distance d between two spring-columns:

$$\Phi = \frac{d}{v} \quad (37)$$

Where:

- Φ = Phase difference (s)
- d = Distance (m)
- v = Propagation speed (m/s)

This results in the phase differences for the spring-columns as shown in Table 25.

TABLE 25 – PHASE DIFFERENCES

Spring-column no.	Distance from left side (m)	Phase difference for sand ($v = 300 \text{ m/s}$)	Phase difference for clay ($v = 600 \text{ m/s}$)
1	0	0	0
2	0.99	0.0033	0.00165
3	1.98	0.0066	0.0033
4	2.97	0.0099	0.00495
5	3.96	0.0132	0.0066
6	4.95	0.0165	0.00825
7	5.94	0.0198	0.0099
8	6.93	0.0231	0.01155
9	7.92	0.0264	0.0132
10	8.91	0.0297	0.01485
11	9.9	0.033	0.0165

The calculation for the vibration loads will be executed using a vibration speed of 12 mm/s. To calculate the displacement amplitude these speeds have to be integrated according to the following formula:

$$v(t) = u'(t) = 12 * \sin(f * 2\pi * t) \rightarrow u(t) = -\frac{12}{2 * f * \pi} \cos(f * 2\pi * t) \tag{38}$$

This calculation results in the displacement amplitudes as shown in Table 26, which should be used in the SCIA model.

TABLE 26 – DISPLACEMENTS PER FREQUENCY

Frequency (Hz)	Displacement amplitude (mm)
3	0.638
4	0.477
5	0.382
10	0.191
15	0.127
20	0.095
25	0.0764

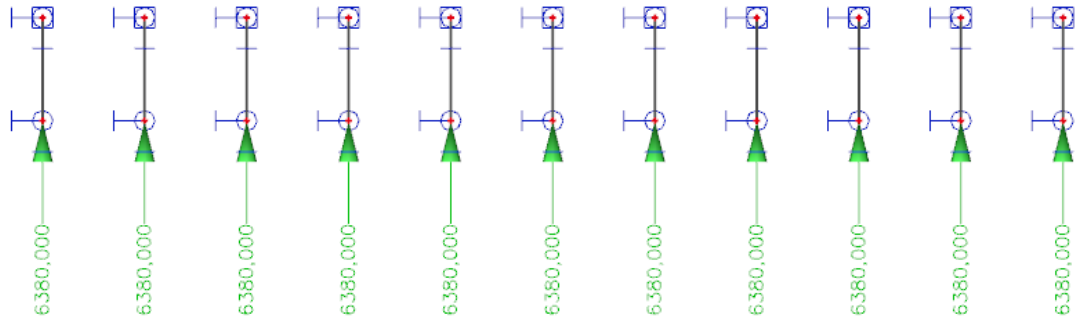


FIGURE 89 – LOADS FOR 3 HZ

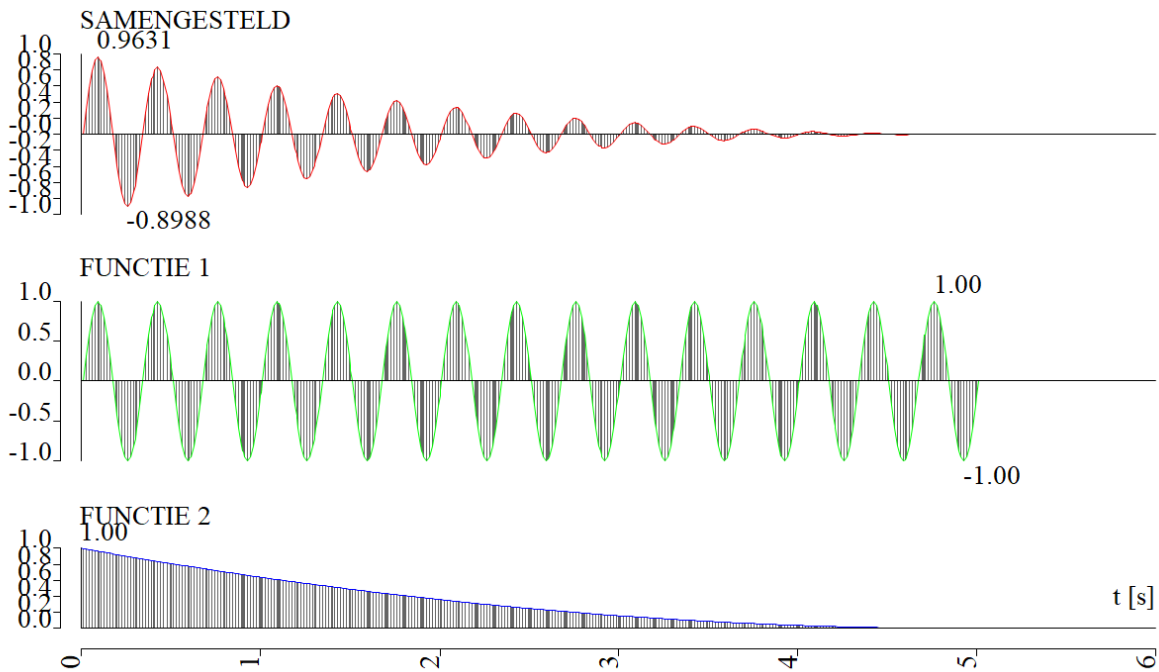


FIGURE 90 – DYNAMIC LOAD FUNCTION FOR 3 HZ, FOR SPRING-COLUMN 6

Figure 89 and Figure 90 show respectively the load that is applied for a 3 Hz vibration and a dynamic load function for this situation.

6.4 MAXIMUM TENSILE STRESS AND RELATION WITH YOUNG'S MODULUS

6.4.1 MAXIMUM TENSILE STRESS

As stated in section 4.1, the structure fails when the value of 0.3 N/mm^2 tensile stress is exceeded for a length of 210 mm. This happens in the situation shown in Figure 91. The value is exceeded in the top left window in the bottom left corner. In this situation the tensile stress in that corner is equal to 0.437 N/mm^2 . This is taken as the mean value of the maximum tensile stress in the Monte Carlo simulation. (NOTE: failure criterion option 1 is used here (see 4.4). This means that the peak stress method is chosen instead of the more general mesh size method. It is executed this way because this method was used in an earlier stage and since the difference in numerical results (see 4.4) is not significant, it would be too cumbersome to repeat the calculations.)

The Monte Carlo parameters are now stated in Table 27.

TABLE 27 – OUDE DELFT STOCHASTIC PARAMETERS

Parameter	Symbol	Distribution	Mean value (μ)	Variation coefficient
Young's Modulus	E	Lognormal	5000 N/mm ²	0.3
Maximum tensile strength	f_t	Lognormal	0.437 N/mm ²	0.3

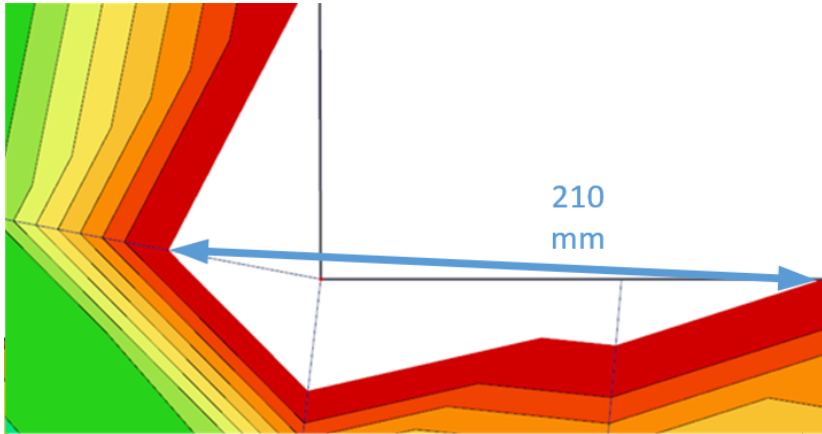


FIGURE 91 – EXCEEDANCE OVER A LENGTH OF 210 MM. TOP LEFT WINDOW, BOTTOM LEFT CORNER

6.4.2 RELATION TENSILE STRESS – YOUNG’S MODULUS

As explained in section 4.1, the values of the tensile stress for different Young’s Moduli have to be gathered to describe the relation between maximum tensile stress and Young’s Modulus. This relationship is shown in Figure 92.

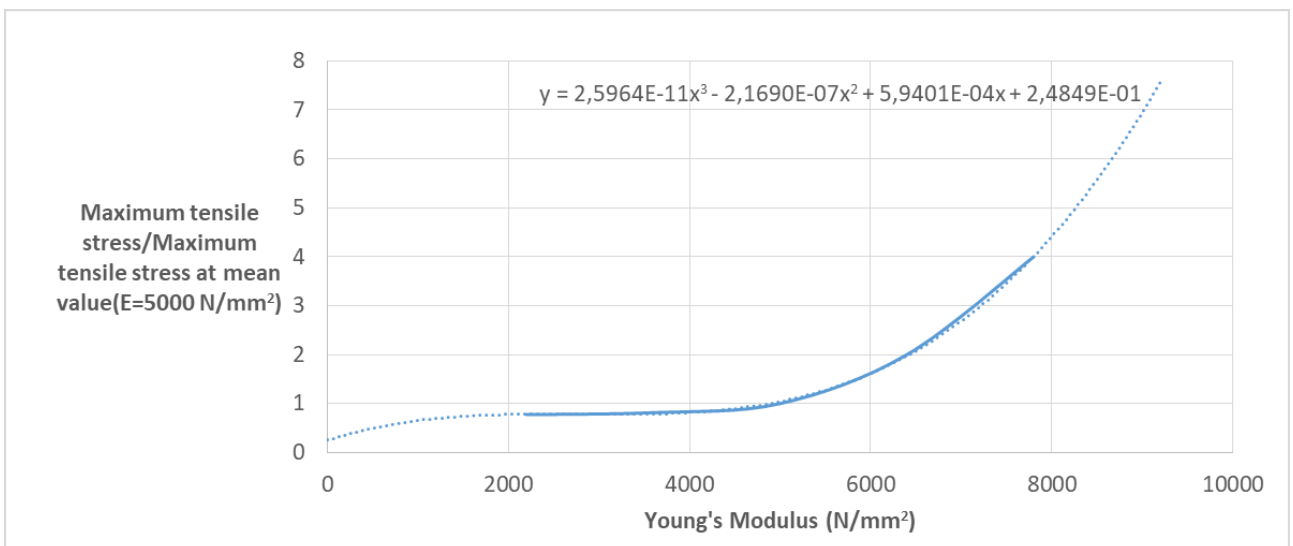


FIGURE 92 – RELATIONSHIP MAXIMUM TENSILE STRESS-YOUNG’S MODULUS OUDE DELFT

The following equation is therefore added to the Monte Carlo simulation:

$$\sigma(E) = 2.5964 * 10^{-11} * E^3 - 2.169 * 10^{-7} * E^2 - 5.94 * 10^{-4} * E + 0.24849 \quad (39)$$

6.5 STEP 1: INITIAL LOADS

For the situation where only the initial loads are applied, the floor and roof loads are added to the structure and also the self-weight is taken into account. A linear-elastic calculation produces the following results:

6.5.1 OUDE DELFT

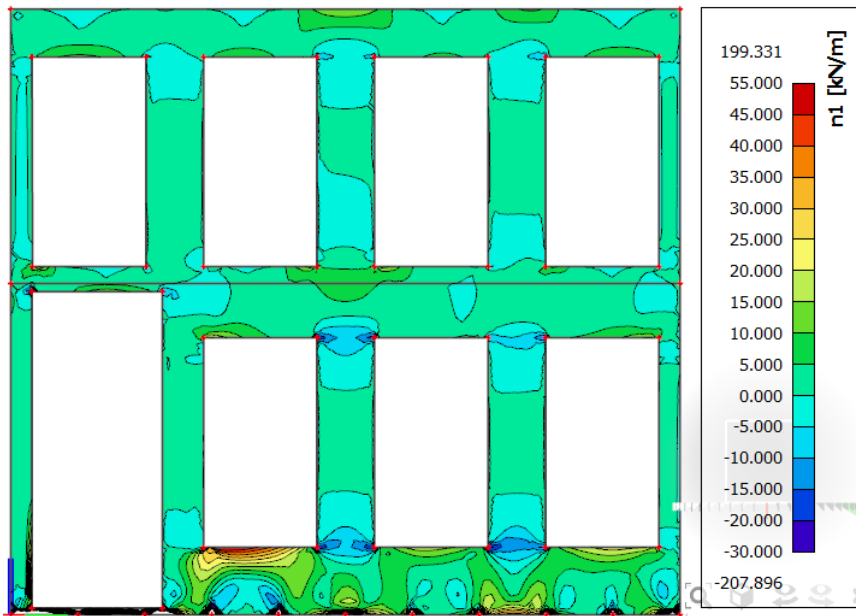


FIGURE 93 – STRESSES DUE TO INITIAL LOADS OUDE DELFT

This leads, in the point of interest (under the left bottom window) to maximum stresses as shown in Table 28.

TABLE 28 – MAXIMUM INITIAL STRESSES OUDE DELFT

Property	Value
σ_1	0.0552 N/mm ²
σ_2	0.001732 N/mm ²
α	-0.83°

These lead to a failure probability according to the Monte Carlo simulation (see section 4) of 0.0088%.

6.5.2 VAN TIJENSTRAAT

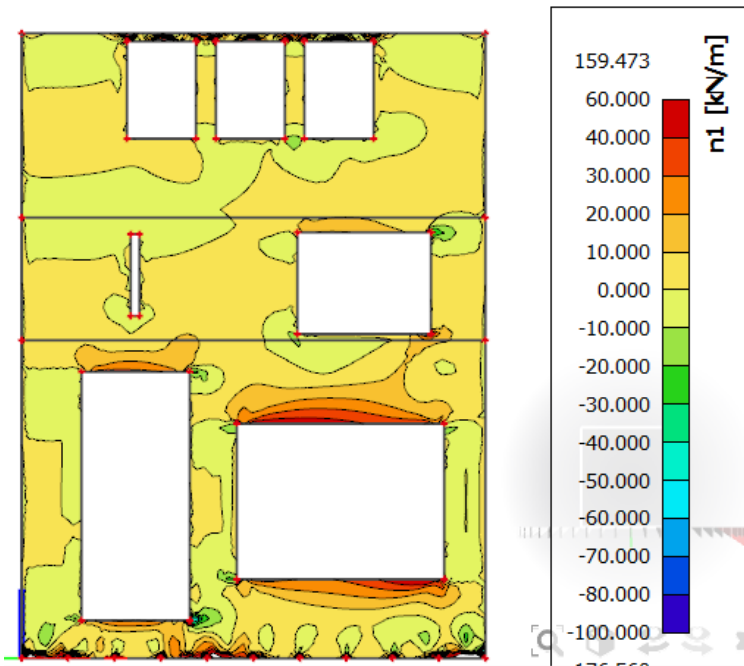


FIGURE 94 – STRESSES DUE TO INITIAL LOADS VAN TIJENSTRAAT

TABLE 29 – MAXIMUM INITIAL STRESSES VAN TIJENSTRAAT

Property	Value
σ_1	0.0594 N/mm ²
σ_2	0.00844 N/mm ²
α	-1.84°

These lead to a failure probability according to the Monte Carlo simulation (see section 4) of 0.0042%.

6.5.3 BIESLANDSEKADE

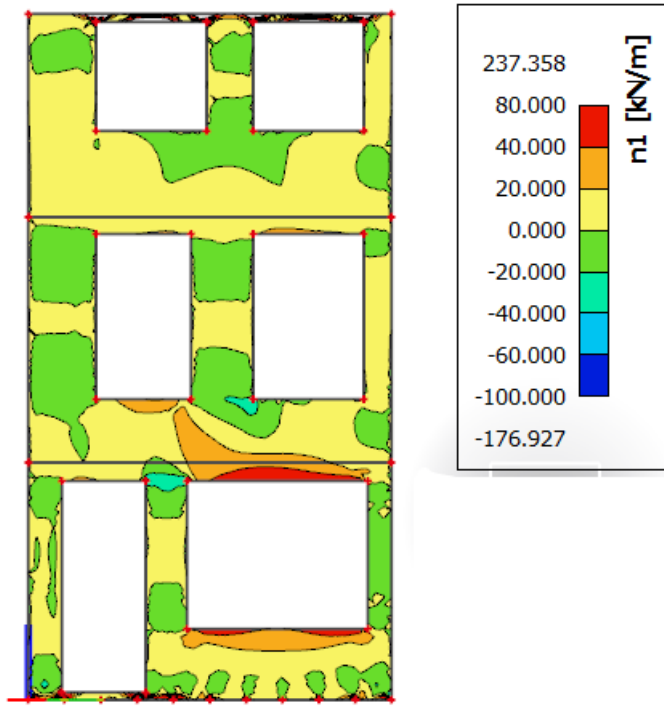


FIGURE 95 – STRESSES DUE TO INITIAL LOADS VAN TIJENSTRAAT

TABLE 30 – MAXIMUM INITIAL STRESSES VAN TIJENSTRAAT

Property	Value
σ_1	0.0657 N/mm ²
σ_2	0.000502 N/mm ²
α	0.08°

These lead to a failure probability according to the Monte Carlo simulation (see section 4) of 0.011%.

6.6 INITIAL LOAD AND VIBRATION LOAD, NO SOIL-STRUCTURE INTERACTION

This section will demonstrate the results of the situation where besides the initial loads, the structure is also loaded by vibration loads. For every structure (Oude Delft, Van Tijenstraat and Bielandsekade), 14 analyses will be performed. They differ in:

- Clay ($v = 600 \text{ m/s}$) or sandy ($v = 300 \text{ m/s}$) soil
- Frequency (3, 4, 5, 10, 15, 20 and 25 Hz)

For the situation Oude Delft, 10 Hz, sandy soil, the procedure will be explained, a contour plot will be shown and the results are presented. For Van Tijenstraat and Bieslandsekade, a contour plot will be shown for 10 Hz, sandy soil and the results will be presented. For all other cases, only the results will be presented.

6.6.1 ELABORATED EXAMPLES

Oude Delft, 10 Hz, sandy soil

The loads will be added according to section 6.3. The structure and mesh size are discussed in section 6.2. This results in the contour plot shown in Figure 96, for a vibration speed of 12 mm/s. The maximum principal tensile stress occurs in the top left corner of the door, see Figure 97.

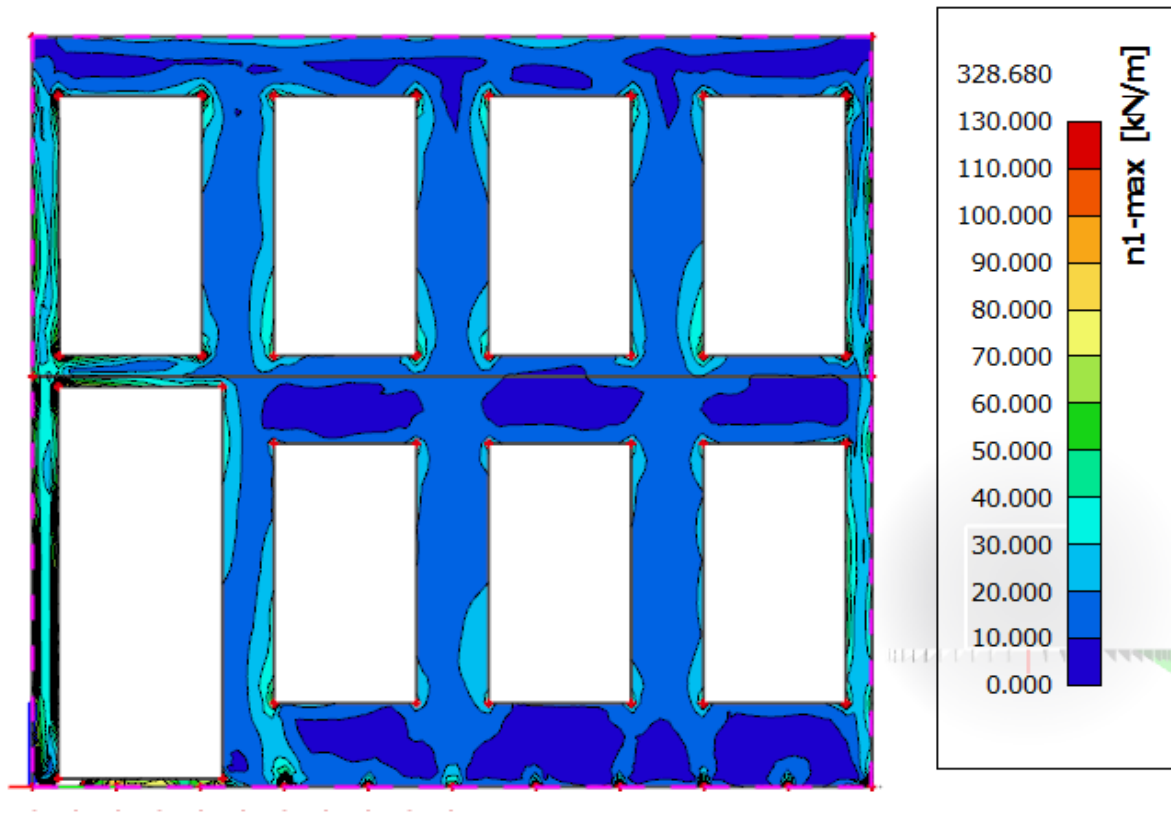


FIGURE 96 – CONTOUR PLOT OUDE DELFT 10 HZ, SANDY SOIL, 12 MM/S VIBRATION SPEED

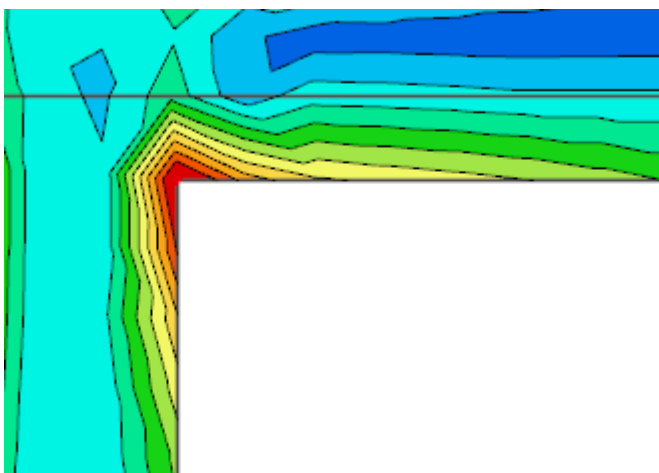


FIGURE 97 – TOP LEFT CORNER DOOR

The principal values in this corner are gathered, see Table 31. Also the initial stresses in this point are gathered, see Table 32.

TABLE 31 – PRINCIPAL STRESSES TOP LEFT CORNER DOOR

Property	Value
σ_1	0.1291 N/mm ²
σ_2	0.05402 N/mm ²
α	53.91°

TABLE 32 – INITIAL STRESSES TOP LEFT CORNER DOOR

Property	Value
σ_1	-0.0533 N/mm ²
σ_2	-0.1733 N/mm ²
α	-17.1°

It has to be noted that theoretically another point in the structure can produce higher total principal stresses, since the maximum tensile stress is only sought for in the contour of the vibration loads. However, other points with high principal tensile stresses due to the vibration speed have been investigated to see if they produce higher total results. This is not the case, so this leads to the assumption that the point which produces the highest principal tensile stress due to vibration load will have the highest total principal tensile stresses.

The values of Table 31 and Table 32 are added to the MATLAB script which executes the Monte Carlo simulation.

```

close all+
no1=129.149;
no2=54.021;
ao=53.91;
n=100000;
for p=1:30
    ini1(p)=0;
    ini2(p)=0;
    inia(p)=-17.1;
    n1(p)=no1*p/12;
    n2(p)=no2*p/12;
    a(p)=ao;
    f1(p)=0.5*(n1(p)+n2(p)+ini1(p)+ini2(p))-0.5*(n1(p)-
n2(p))*cos(2*a(p)*pi/180)-0.5*(ini1(p)-ini2(p))*cos(2*inia(p)*pi/180);
f2(p)=0.5*(n1(p)+n2(p)+ini1(p)+ini2(p))+0.5*(n1(p)-
n2(p))*cos(2*a(p)*pi/180)+0.5*(ini1(p)-ini2(p))*cos(2*inia(p)*pi/180);
    fa(p)=0.5*(ini1(p)-ini2(p))*sin(2*inia(p)*pi/180)+0.5*(n1(p)-
n2(p))*sin(2*a(p)*pi/180);
    N1(p)=0.5*(f1(p)+f2(p)+sqrt((f1(p)-f2(p))^2+4*fa(p)^2));
    N2(p)=0.5*(f1(p)+f2(p)-sqrt((f1(p)-f2(p))^2+4*fa(p)^2));
    A(p)=0.5*atan(2*fa(p)/(f1(p)-f2(p)))*180/pi;
    for i=1:n
        % ft;
mu=log((0.437^2)/sqrt(0.437^2+0.1311^2));sigma=sqrt(log(0.1311^2/(0.437^2
)+1));ft(i)=lognrnd(mu,sigma);
        %E
mu=log((5000^2)/sqrt(5000^2+1500^2));sigma=sqrt(log(1500^2/(5000^2)+1));E
(i)=lognrnd(mu,sigma);
        stressE(i)=2.5964*10^-11*E(i)^3-2.169*10^-7*E(i)^2+5.94*10^-
4*E(i)+0.24849;
S(i)=stressE(i)*N1(p)/1000;
Z(i)=ft(i)-S(i);
    end

```

```

P (p) =sum (Z<0) /n;
end
P
plot (1:30,P)

```

FIGURE 98 – MATLAB SCRIPT FOR MONTE CARLO SIMULATION

This leads to the probability of failure against vibration speed as shown in Figure 99.

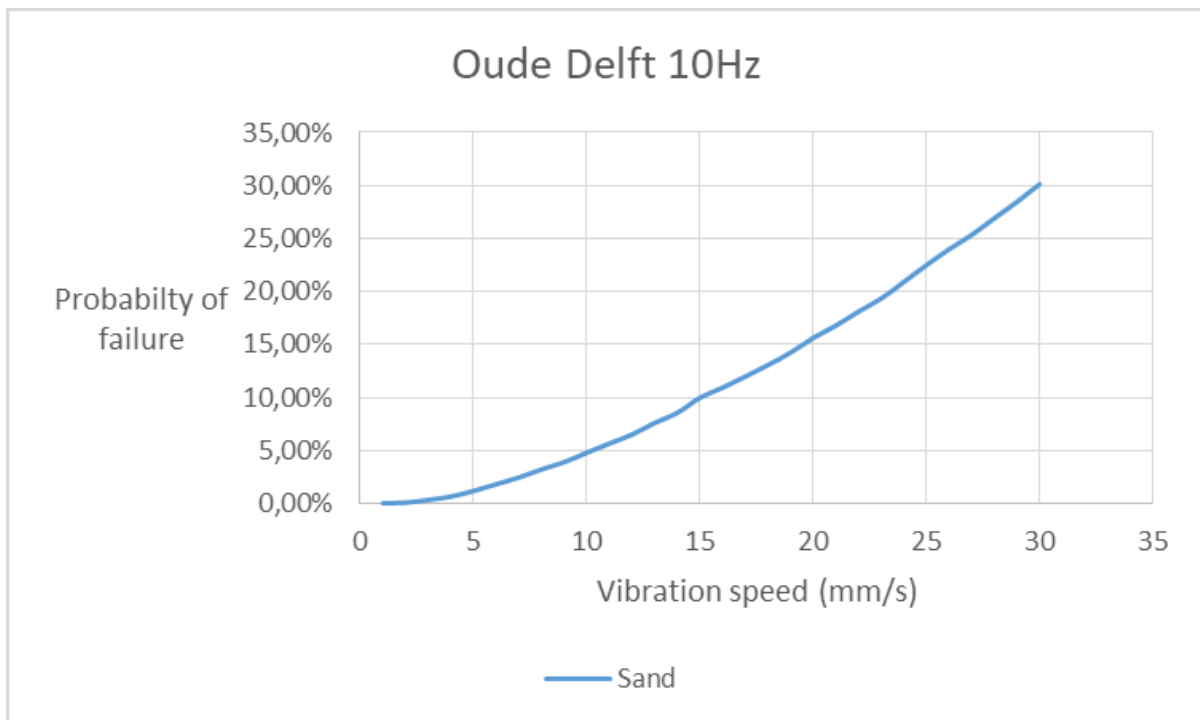
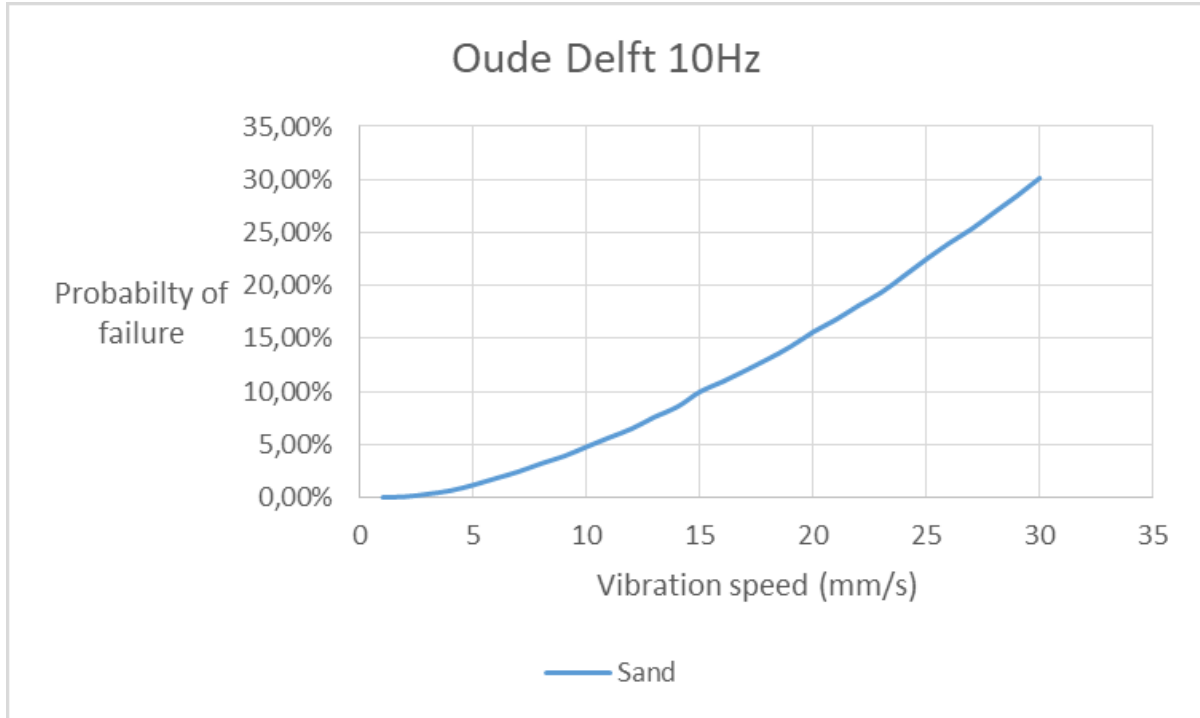


FIGURE 99 – PROBABILITY OF FAILURE VS VIBRATION SPEED OUDE DELFT, 10 HZ, SANDY SOIL

Van Tijenstraat, 10 Hz, sandy soil

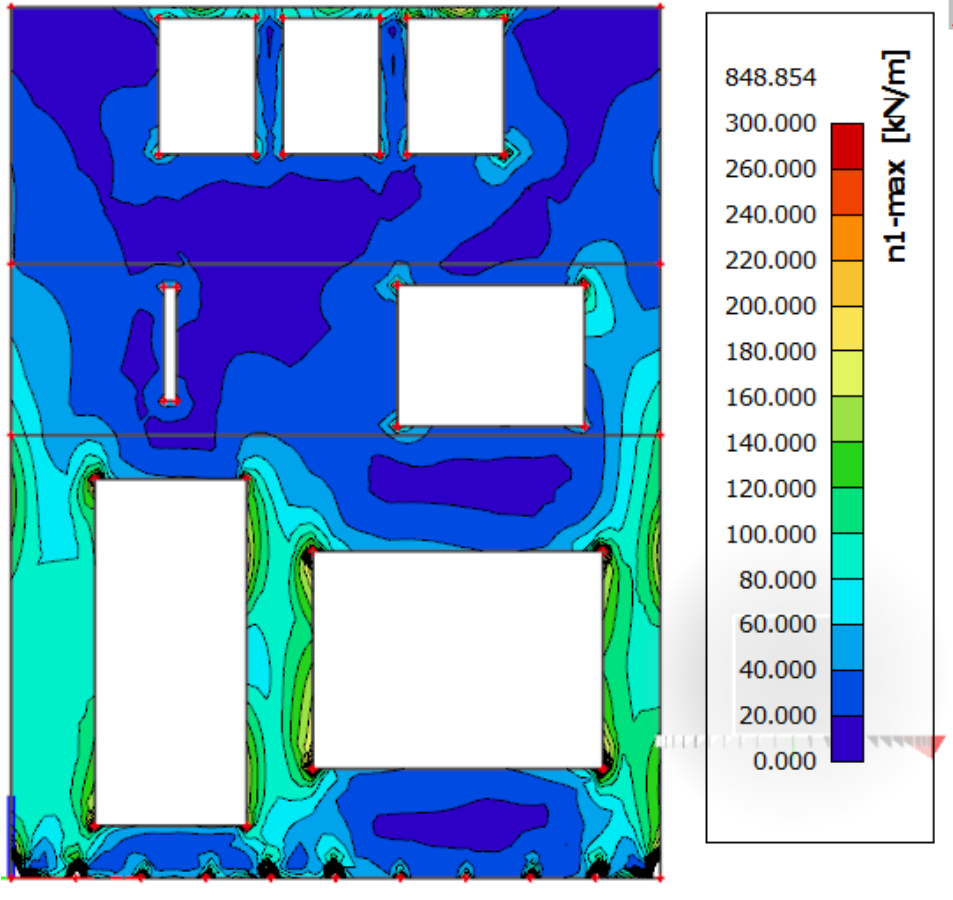


FIGURE 100 – CONTOUR PLOT VAN TIJENSTRAAT 10 HZ, SANDY SOIL, 12 MM/S VIBRATION SPEED

Bieslandsekade, 10 Hz, sandy soil

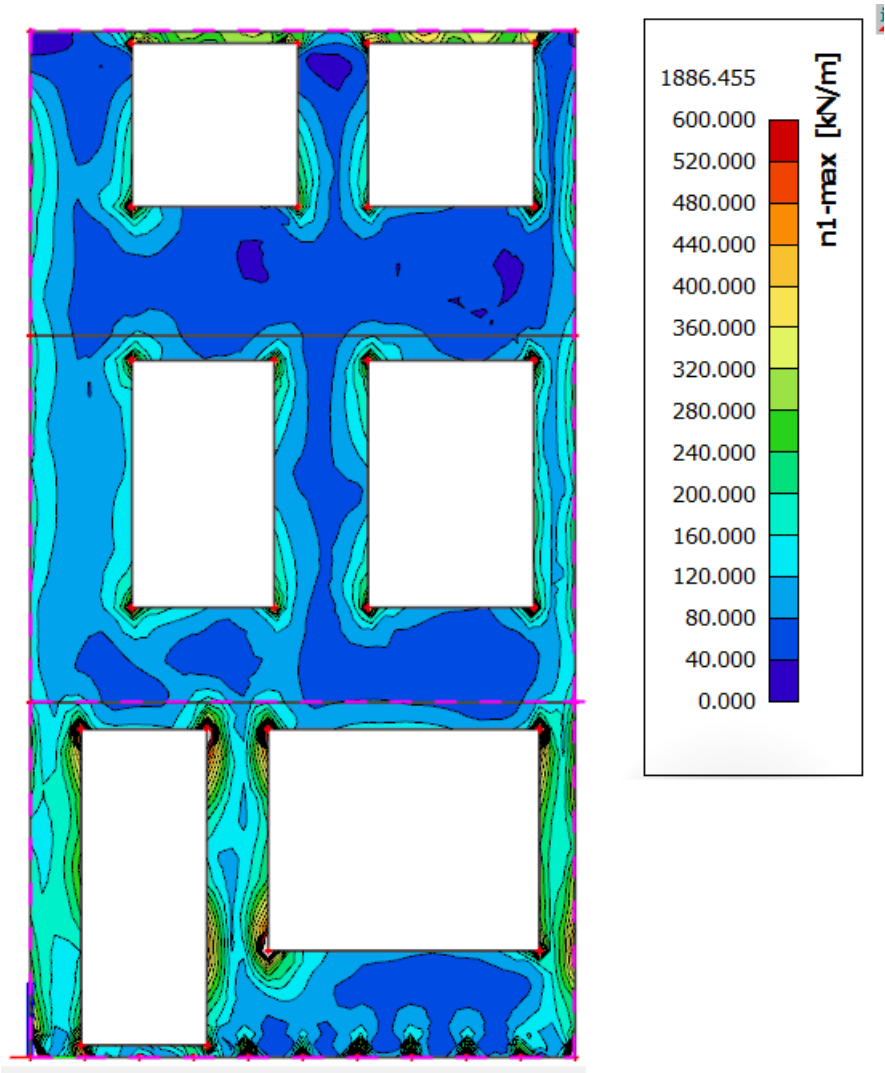


FIGURE 101 – CONTOUR PLOT BIESLANDSEKADE 10 HZ, SANDY SOIL, 12 MM/S VIBRATION SPEED

6.6.2 RESULTS

In this part, the results will be discussed. All the results are added in Appendix A. This section describes mainly the 10 Hz results of the façade “Oude Delft”, some comparisons with other facades and with the results from the TNO report. These are used to state some conclusions regarding the study performed in this chapter.

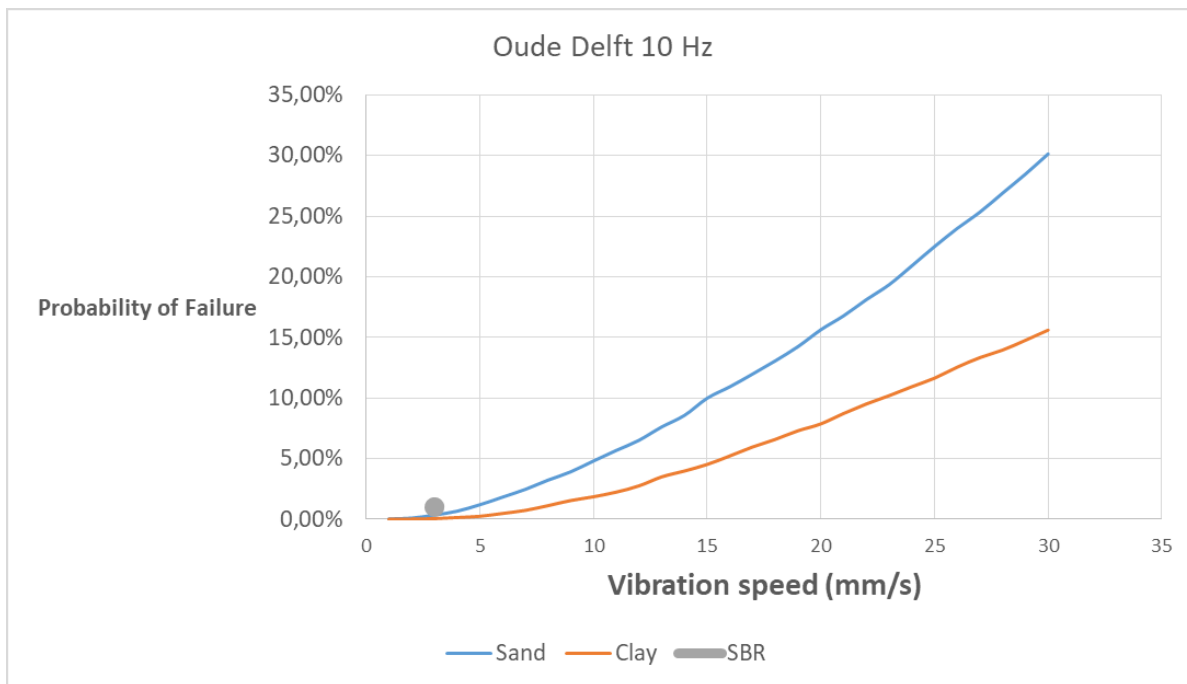


FIGURE 102 – RESULTS OUDE DELFT

Figure 102 shows the results of the 10 Hz calculation, for both clay and sandy soils, for the façade “Oude Delft”. Noticeable in this plot is:

- The sandy soil results in clearly higher probabilities of failure than the clay soil.
- The value of the SBR-richtlijn (1% probability of failure at 3 mm/s vibration speed) corresponds more for the sandy soil than the clay soil, but they are both very close to this value.

It is interesting to see that the sandy soil produces higher probabilities of failure than the clay soil. To investigate this more, Figure 103 is plotted, which consists of all the cases for Oude Delft.

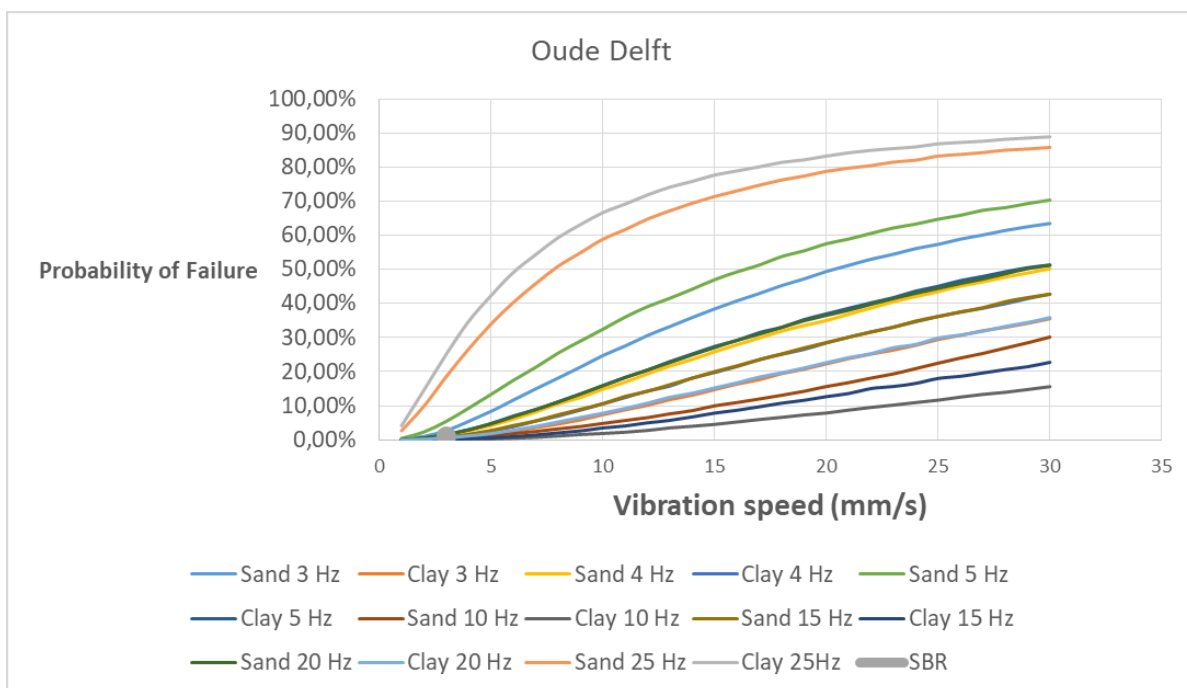


FIGURE 103 – RESULTS OUDE DELFT, ALL CASES

Using this plot, it is noticeable that for nearly all the different frequencies, sandy soils produce higher probabilities of failure than clay soil. The provisional conclusion can be: the lower the wave probation, the higher the stresses and thus the probability of failure will be. It is also noticeable that either the higher frequencies (25 Hz) or the low frequencies (3, 4 Hz) will lead to the highest probabilities of failure. The middle frequencies (like 10 Hz) usually result in a lower probability of failure. Resonance can be a reason for this phenomenon.

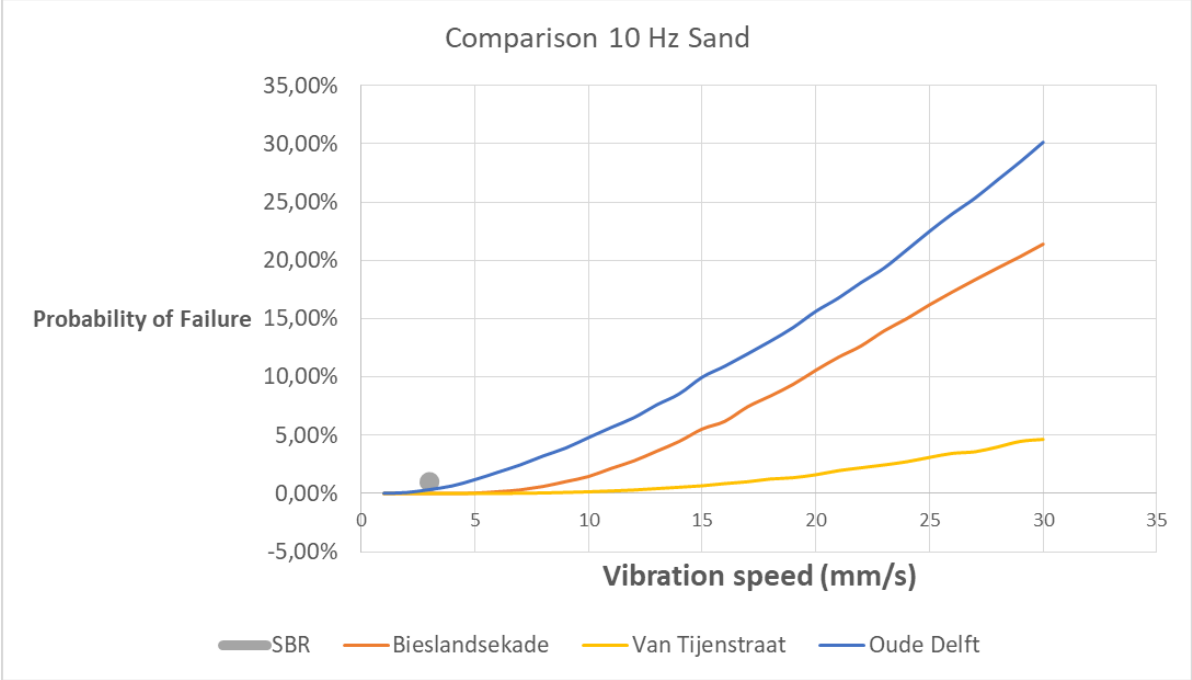


FIGURE 104 – 10 HZ SAND

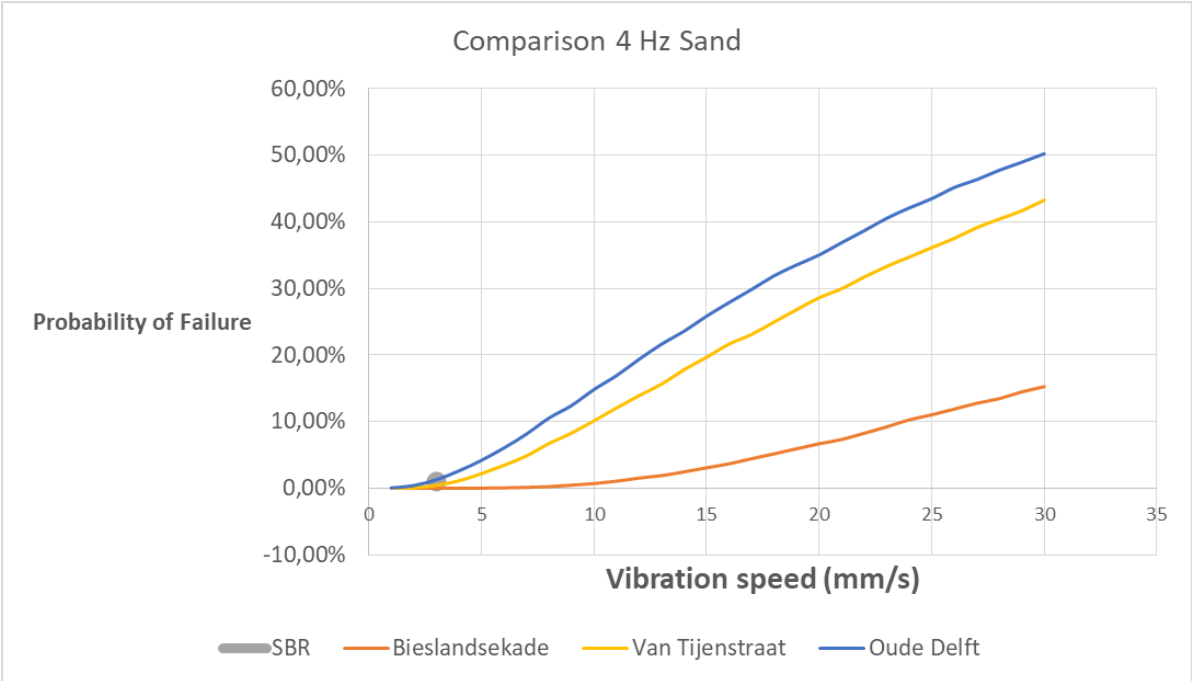


FIGURE 105 – 4 HZ SAND

If we look into Figure 104, which is a comparison for all 3 facades for the 10 Hz, sandy soil case, it is noticeable that the façade “Van Tijenstraat” produces way lower probabilities of failure than the other two facades. Therefore, for comparative reasons, Figure 105 has been plotted as well, that shows that the 4 Hz, sandy soil

case, “Bieslandsekade” produces lower probabilities of failure than the other two façades. Resonance, again, may be an explanation for this phenomenon: because the façades are different, other frequencies can lead to the structure being more or less responsive.

However, it can be noted that for a lot of the cases, “Oude Delft” produces relatively high probabilities of failure. The big differences between this façade and the other two façades are:

- Oude Delft has two floors, the other façades have three.
- Oude Delft has more door and window space on the façade compared to the other two façades.

These differences could be explanations why this phenomenon is noticeable for most cases.

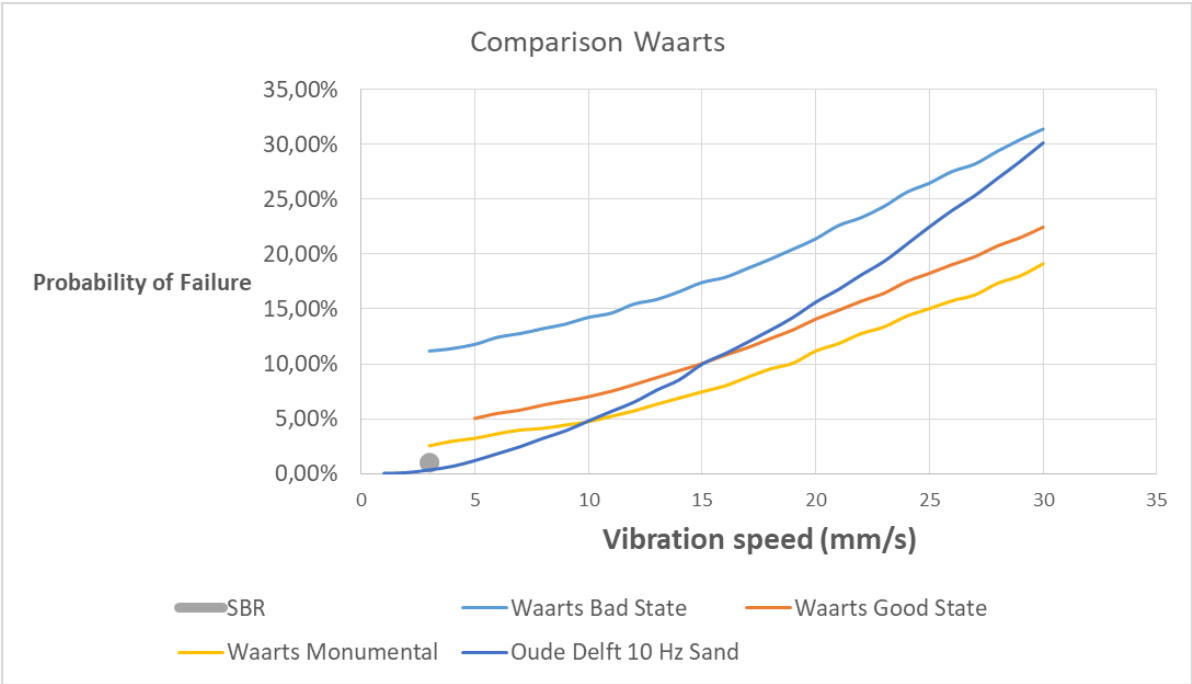


FIGURE 106 – COMPARISON TNO REPORT WAARTS

Figure 106 shows a comparison between the 10 Hz, sandy soil case for “Oude Delft” and the results produced in the TNO report. It can be seen that for the lower values of vibration speed, the proposed procedure results in a lower probability of failure but for higher vibration speeds, the increase of the probability of failure is higher. At 30 mm/s, the results produced by the procedure get close to those of bad state masonry from the TNO report. However, it can be seen that the curve produced by the proposed procedure is closer to the SBR-richtlijn. Moreover, the results from the procedure are realistic if compared to the TNO report.

7. COMPARISON STUDIES

This section describes some comparisons executed for some more in-depth conclusions about this subject. The performed comparative calculations are stated below:

- Comparison regarding the constraining of the structure.
- Comparison regarding stresses at the soil-masonry interface.
- Comparison regarding nonlinear material parameters.

These comparisons will be discussed in different subsections. The calculation procedure will be demonstrated, the results will be presented and statements and conclusions will be drawn up regarding these comparisons

7.1 CONSTRAINTS

An example of a structure is shown in Figure 107.

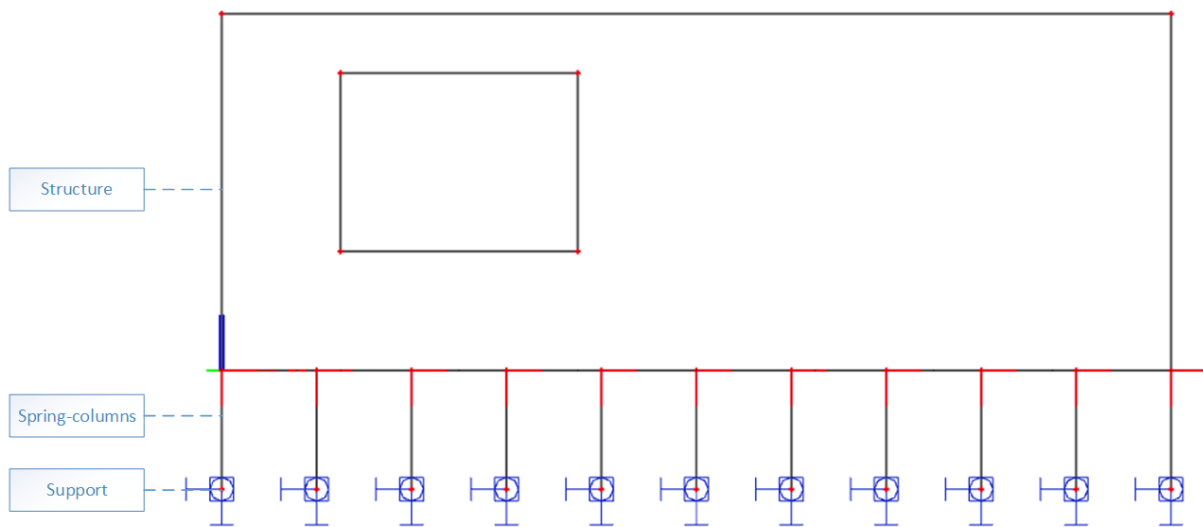


FIGURE 107 – EXAMPLE STRUCTURE

It is useful to see what the effect is if the structure is not constrained in x-direction. Therefore, this comparative study is set up. The situations that will be compared are the following situations

- Constrained: In this situation, all 11 spring-columns are constrained in x-direction at the top and bottom of the spring-columns.
- Single unconstrained: In this situation, all 11 of the spring-columns are constrained in x-direction at the bottom. The left spring-column is also constrained in x-direction at the top, while all other spring-columns are unconstrained in x-direction at the top.
- Double unconstrained: In this situation, the outermost left spring-column is constrained in x-direction in both the top and the bottom of the spring-column, while all other spring-columns are unconstrained at the top and the bottom.

The comparative study is executed on the façade “Oude Delft”. The comparison is made for a 5, 10 and 20 Hz frequency, a 12 mm/s vibration speed, for both sandy and clay soils. Moreover, one comparison is made using the façade “Van Tijenstraat”, to see if it applies for other facades as well. The comparison is mainly focused on the structural results. A probabilistic comparison is only made for the 10 Hz case with the sandy soil. The 10 Hz

sandy soil situation is therefore elaborated extensively, using contour plots, structural results and the probabilistic comparison, while for the other cases only the structural results are discussed.

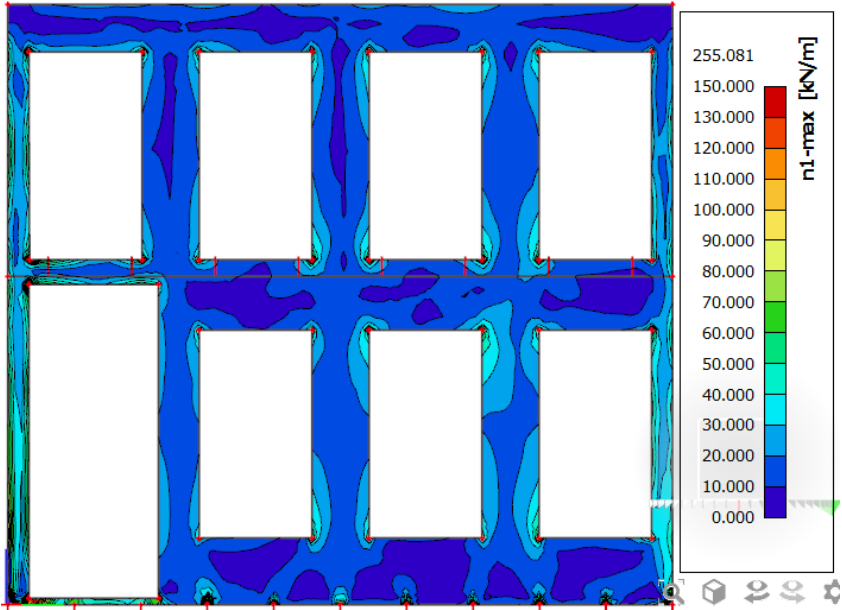


FIGURE 108 – CONTOUR PLOT 10 HZ, SANDY SOIL, CONSTRAINED

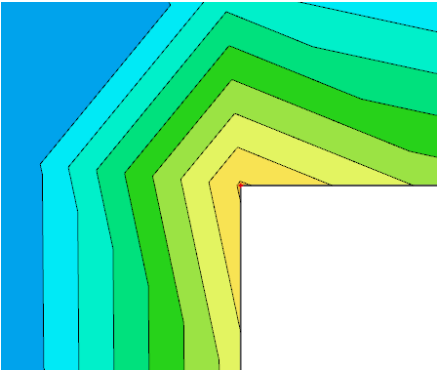


FIGURE 109 – ZOOMED IN AT TOP LEFT CORNER DOOR, 10 HZ, SANDY SOIL, CONSTRAINED

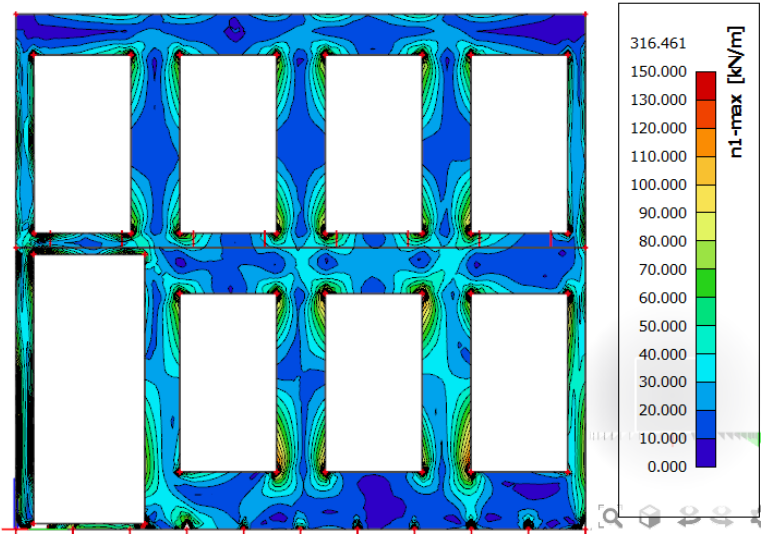


FIGURE 110 – CONTOUR PLOT 10 HZ, SANDY SOIL, SINGLE UNCONSTRAINED

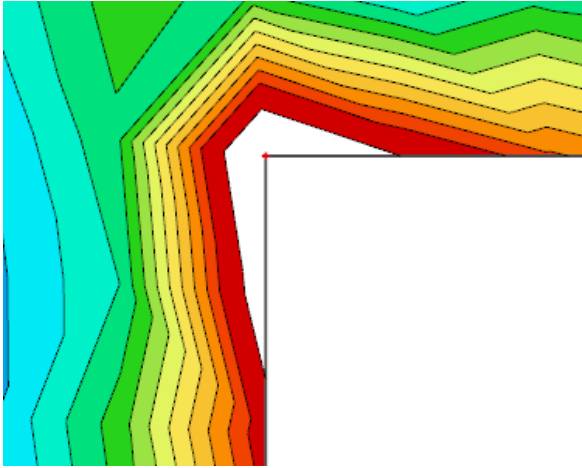


FIGURE 111 – ZOOMED IN AT TOP LEFT CORNER DOOR, 10 HZ, SANDY SOIL, SINGLE UNCONSTRAINED

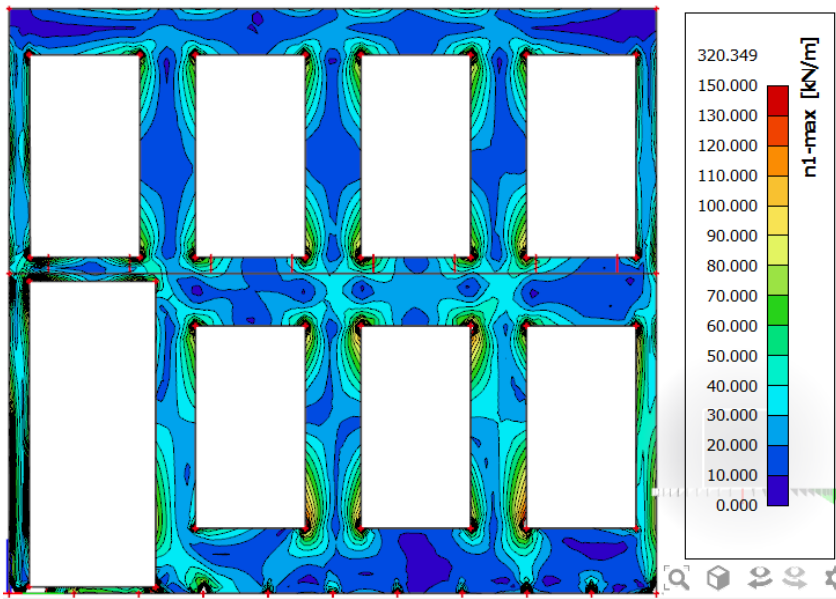


FIGURE 112 – CONTOUR PLOT 10 HZ, SANDY SOIL, DOUBLE UNCONSTRAINED

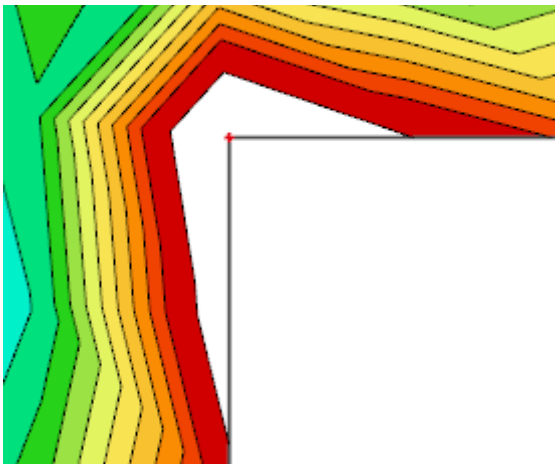


FIGURE 113 – ZOOMED IN AT TOP LEFT CORNER DOOR, 10 HZ, SANDY SOIL, DOUBLE UNCONSTRAINED

The stress contours are plotted in Figure 108, Figure 109, Figure 110, Figure 111, Figure 112 and Figure 113. The maximum principal tensile stresses in these situations are shown in Table 33.

TABLE 33 – MAXIMUM STRESSES 10 HZ, SANDY SOIL, 12 MM/S VIBRATION SPEED

Constraining	Node	n1 (N/mm ²)	n2 (N/mm ²)	α(°)
Constrained	K17	0.129	0.05402	53.91
Single unconstrained	K24	0.203	0.079	36.35
Double unconstrained	K23	0.208	0.074	50.85

From the results in Table 33, it is interesting to see the difference in maximum principal tensile stress. For the unconstrained situations, the maximum value is about twice the stress than the stress that is generated in the constrained situation. Another interesting property is that the maximum tensile stress occurs at a different place: For the constrained situation this is in Node K17 (bottom left corner of the top left window), while for the single unconstrained situation this occurs in node K24 (top right corner of the middle bottom window) and in the double unconstrained situation in node K23 (bottom right corner of the middle bottom window). Therefore, the type of constraining has effect on the location of the maximum tensile stress and on the value of this maximum tensile stress. The effect of the constraining on one specific node (K42) is shown in Table 34.

TABLE 34 – MAXIMUM TENSILE STRESS IN NODE K42 FOR DIFFERENT CONSTRAINING SITUATIONS

K42	Constrained	Single unconstrained	Double unconstrained
Maximum tensile stress (N/mm ²)	0.091	0.126	0.137

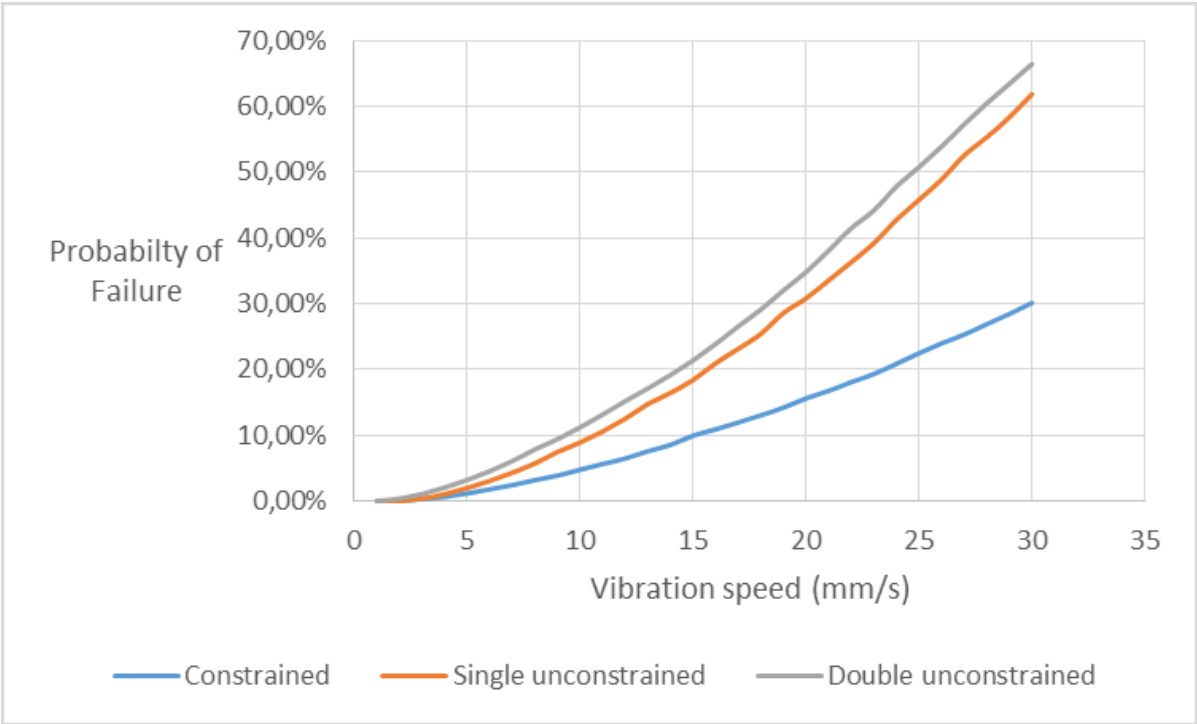


FIGURE 114 – PROBABILITY OF FAILURE FOR DIFFERENT CONSTRAINT CONFIGURATIONS

From the results shown in Table 34 and Figure 114, one can see that the constraint configuration is very important in the structural results, hence the big difference in probabilities of failure. It is therefore important to see if this also occurs at other frequencies, propagation velocities and facades. These results are shown in Table 35, Table 36, Table 37, Table 38 and Table 39.

TABLE 35 – MAXIMUM STRESSES 10 HZ, CLAY SOIL, 12 MM/S VIBRATION SPEED

Constraining	Node	$n1 (N/mm^2)$	$n2 (N/mm^2)$	$\alpha(^{\circ})$
Constrained	K26	0.077	0.027	55.54
Single unconstrained	K26	0.176	0.064	53.75
Double unconstrained	K26	0.18	0.064	54.33

TABLE 36 – MAXIMUM STRESSES 5 HZ, SANDY SOIL, 12 MM/S VIBRATION SPEED

Constraining	Node	$n1 (N/mm^2)$	$n2 (N/mm^2)$	$\alpha(^{\circ})$
Constrained	K42	0.138	0.057	49.95
Single unconstrained	K42	0.143	0.059	50.56
Double unconstrained	K42	0.140	0.059	50.41

TABLE 37 – MAXIMUM STRESSES 5 HZ, CLAY SOIL, 12 MM/S VIBRATION SPEED

Constraining	Node	$n1 (N/mm^2)$	$n2 (N/mm^2)$	$\alpha(^{\circ})$
Constrained	K18	0.733	0.024	34.75
Single unconstrained	K18	0.734	0.024	35.22
Double unconstrained	K18	0.73	0.024	35.01

TABLE 38 – MAXIMUM STRESSES 20 HZ, SANDY SOIL, 12 MM/S VIBRATION SPEED

Constraining	Node	$n1 (N/mm^2)$	$n2 (N/mm^2)$	$\alpha(^{\circ})$
Constrained	K39	0.048	0.016	52.65
Single unconstrained	K39	0.051	0.016	53.12
Double unconstrained	K39	0.049	0.016	52.48

TABLE 39 – MAXIMUM STRESSES 20 HZ, CLAY SOIL, 12 MM/S VIBRATION SPEED

Constraining	Node	$n1 (N/mm^2)$	$n2 (N/mm^2)$	$\alpha(^{\circ})$
Constrained	K42	0.061	0.026	44.64
Single unconstrained	K42	0.064	0.027	48.36
Double unconstrained	K42	0.062	0.026	48.28

According to the results, it seems that the only cases where big differences in structural results occur, are in the case a 10 Hz frequency is used. For the other frequencies, the difference in structural results are minimal. If the comparison is made between stresses due to the 5 Hz and the 20 Hz frequencies at one side and the stresses due to the 10 Hz frequencies for the façade “Oude Delft”, it is very clear that only the vibrations at the 10 Hz frequency will lead to big differences in probabilities failure.

Thus, it is helpful to investigate the configuration of constraints on other facades. For the façade “Bieslandsekaade”, the principal tensile stresses for various configurations have been investigated, as can be seen in Table 40 and Table 41.

TABLE 40 – MAXIMUM STRESSES 10 HZ, SANDY SOIL, 12 MM/S VIBRATION SPEED, BIESLANDSEKADE

Constraining	Node	$n1 (N/mm^2)$	$n2 (N/mm^2)$	$\alpha(^{\circ})$
Constrained	K18	0.831	0.303	39.58
Single unconstrained	K18	0.825	0.302	40.21
Double unconstrained	K18	0.828	0.302	40

TABLE 41 – MAXIMUM STRESSES 5 HZ, SANDY SOIL, 12 MM/S VIBRATION SPEED, BIESLANDSEKADE

Constraining	Node	$n1 (N/mm^2)$	$n2 (N/mm^2)$	$\alpha(^{\circ})$
Constrained	K18	1.747	0.616	34.75
Single unconstrained	K18	1.791	0.635	35.09
Double unconstrained	K18	1.797	0.653	35.92

The findings from the investigation of the façade “Bieslandsekade” show that for a 5 and 10 Hz frequency, the differences in maximum tensile stresses are minimal once again. This will result in a minimal difference in probability of failure for the various configurations of constraints for this façade.

This comparative study shows that for most cases, the constraining has minimal influence on the maximum tensile stresses, and therefore on the probability of failure. However, it has to be noted that for one case (10 Hz vibration frequency, façade “Oude Delft”), the constraining does have great influence on the maximum tensile stress and the probability of failure. It is possible that resonance leads to these differences for this specific case. Therefore, this comparative study leads to the recommendation that more research has to be conducted to form a substantiated statement regarding resonance and the configuration of constraining.

7.2 STRESSES AT THE SOIL-MASONRY INTERFACE

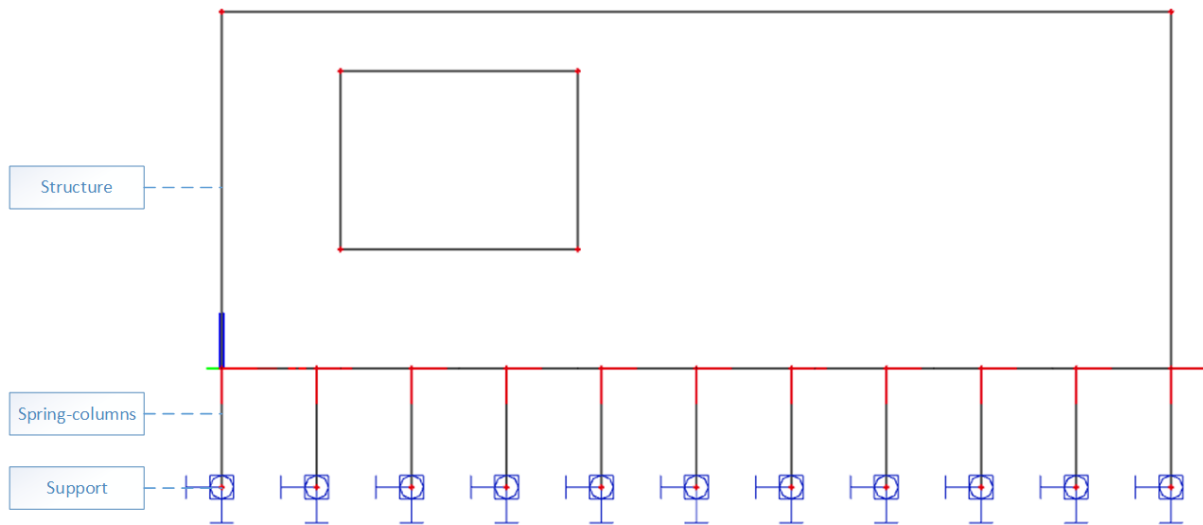


FIGURE 115 – EXAMPLE STRUCTURE

In the proposed procedure, the ground vibration is modeled as a displacement in time on the soil-structure interface. To ensure the inertia of the façade does not influence these displacements, the spring-columns (as shown in Figure 115) have a very high stiffness. Because of the difference in stiffness of the soil (spring-columns) and the structure, no stresses at the soil-masonry interface are present in this model. However, in reality, these stresses will occur.

In theory a sine wave will ‘push’ the soil upwards and then the soil will move downwards again. However, the soil will not ‘pull’ the structure downwards again: the structure will move freely and due to forces elsewhere in the structure and gravity, the structure will move downwards again. At some point after that, the soil will hit the structure again and interact with structure again. This procedure will repeat itself until the vibration has stopped and the static loading situation has reoccurred.

To ensure that the structure follows this behavior, there has to be a spring-connection between the soil and the structure, but which only supports this behavior in compression. Basically, the connection between the structure and the spring-columns in Figure 115 has to be a connection that behaves elastically in compression but can extend (almost) freely in tension. This because there can be a small tensile force between the soil and the masonry due to saturated soil or the vacuum of air. To implement this in the system the following :

- Pressure-only springs.
- Nonlinear springs (where the parameters are adjusted so it behaves like a pressure-only spring).

Unfortunately, since SCIA’s functionalities regarding dynamic calculation are limited, it does not allow nonlinear calculations to combine with dynamic calculations. Therefore, SCIA is very limited using stresses at the soil-masonry interface. For acceptable results, other software packages should be investigated.

However, there has been an attempt to include some stresses at the soil-masonry interface in the system. This interaction is implemented by applying a line spring support on the bottom of the structure, as shown in Figure 116. The spring stiffness is set at 80 MN/m². (Obrzud & Truty, 2012). This spring is a linear spring support. This means that the translation in z-direction is not prevented, but is prevented by a spring that is set between the bottom of the structure and the interface z=0.

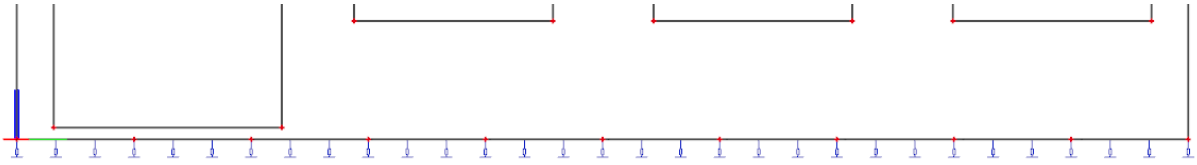


FIGURE 116 – LINE SPRING SUPPORT

To show a comparison, Figure 117 shows the contour plot without a spring support, while Figure 118 shows a contour plot with a spring support. Table 42 shows a comparison for the nodes that result in the highest results. Again, the self-weight (static) calculation has been added to the dynamic calculation.

TABLE 42 – PRINCIPAL TENSILE STRESSES FOR NODES WITH HIGHEST STRESSES

Node	$n1 (N/mm^2)$, no spring support	$n1 (N/mm^2)$, spring support
K14	0.103	0.083
K17	0.101	0.071
K42	0.090	0.088
K39	0.087	0.063
K30	0.082	0.065
K34	0.080	0.072
K35	0.080	0.062

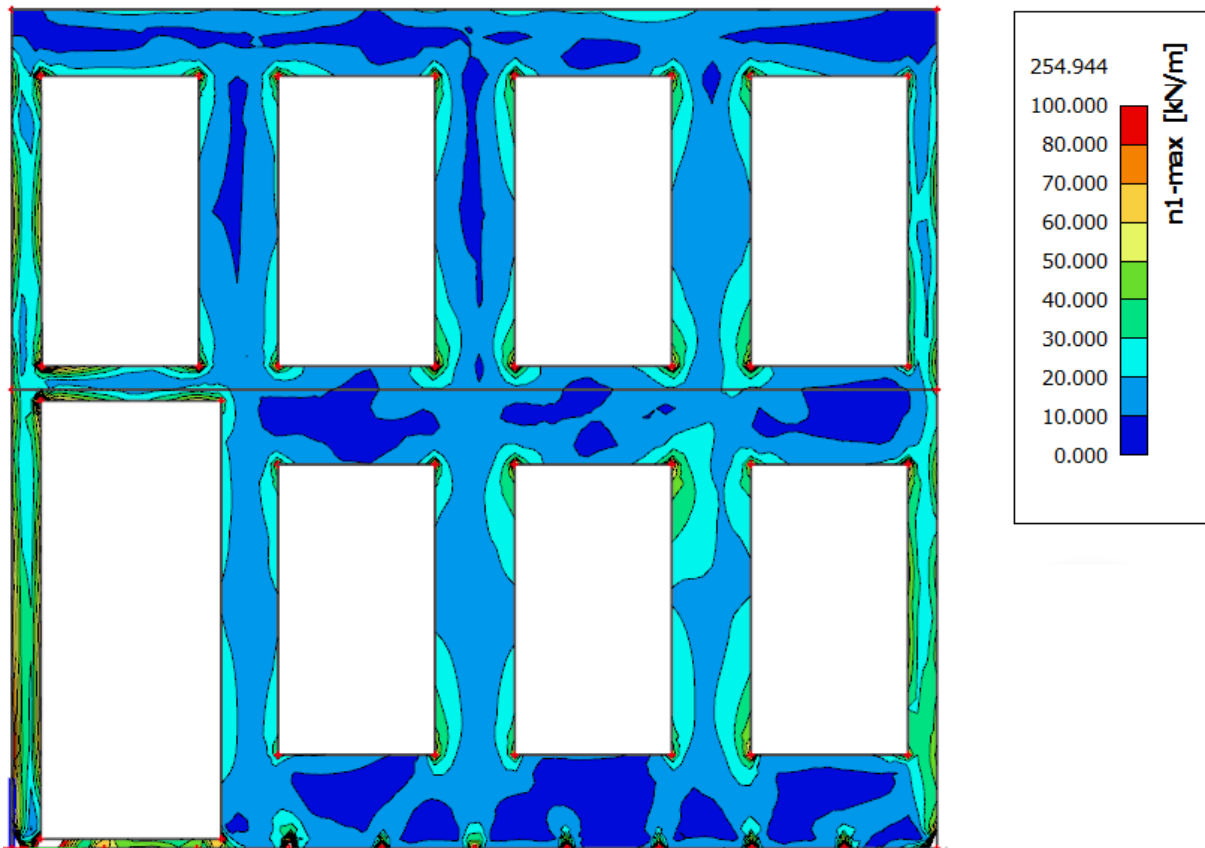


FIGURE 117 – CONTOUR PLOT 10 HZ, SANDY SOIL, 12 MM/S, WITHOUT SPRING SUPPORT

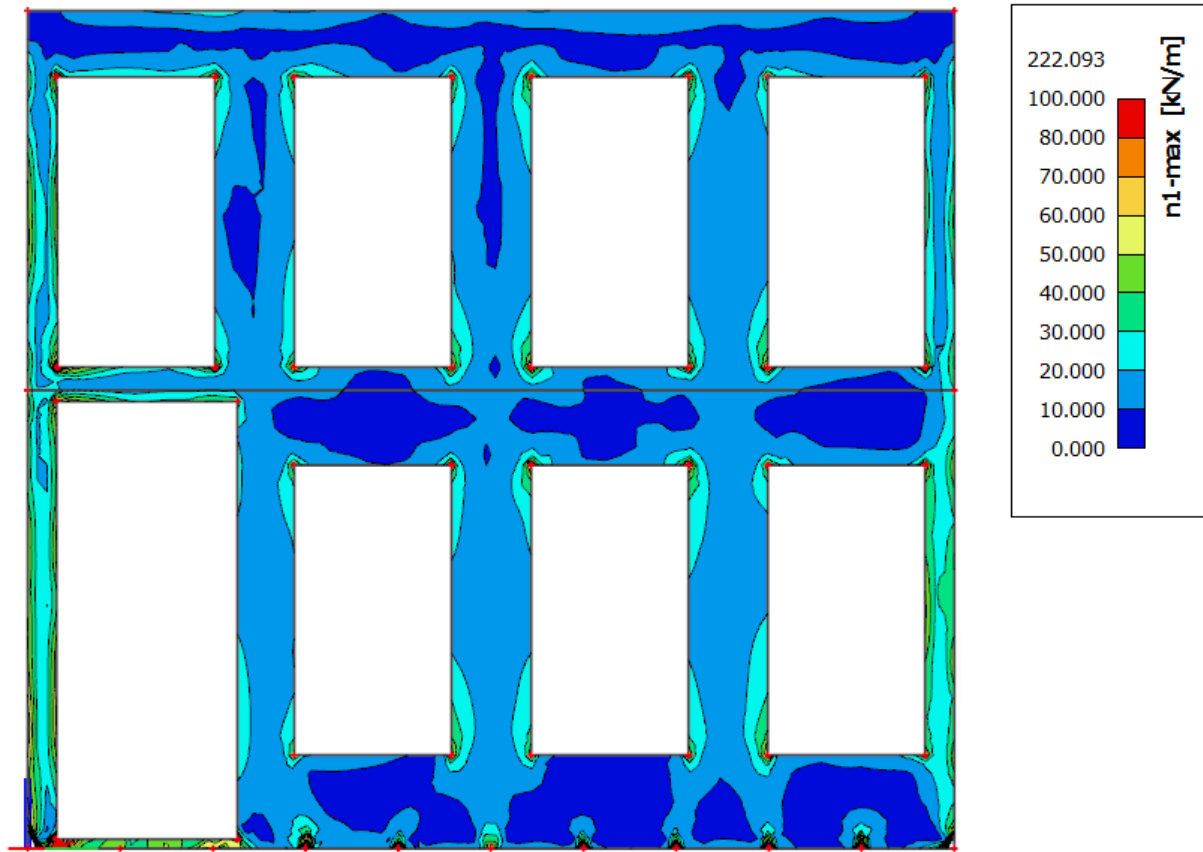


FIGURE 118 – CONTOUR PLOT 10 HZ, SANDY SOIL, 12 MM/S, WITH SPRING SUPPORT

It can be seen that using the line spring, the principal tensile stresses tend to become lower. Provisionally, it can be concluded that including stresses at the soil-masonry interface will lead to lower values of the maximum tensile stresses, which would ultimately result in lower probabilities of failure. However, Figure 119 shows that at certain points, they react on tensile forces. Tensile forces can occur in this interface, due to the saturation in the soil or the vacuum of air, but those require very small forces. Also, Figure 120 shows that larger tensile stresses can develop, which are larger than the tensile stresses that can be expected due to these effects. Therefore, the results of this method are not sufficient to provide a substantiated statement regarding this topic. To determine a substantiated statement, one of the following methods have to be followed:

- The use of nonlinear springs (pressure only springs),
- Modeling the soil in a FEM-environment.

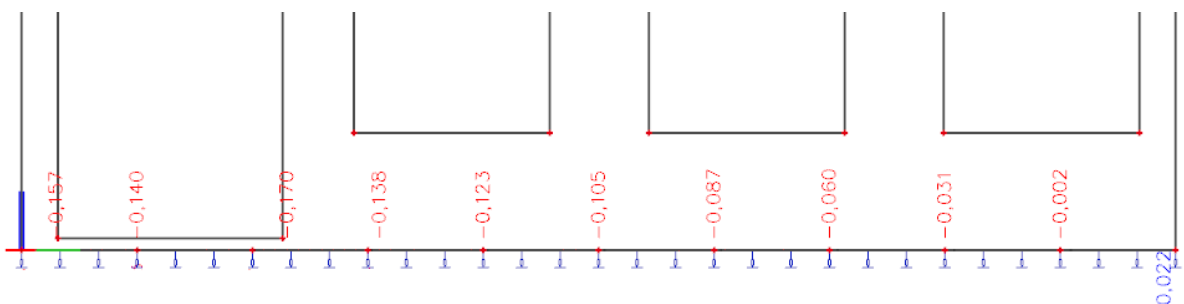


FIGURE 119 – REACTION FORCES AT T=0,17 S.

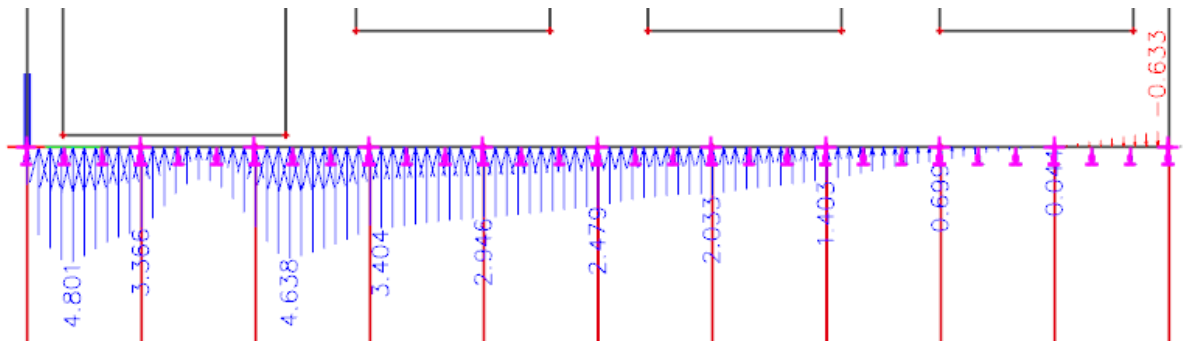


FIGURE 120 – REACTION FORCES AT T=0,37 S

7.3 NONLINEAR MATERIAL PARAMETERS

It is feasible to look into the nonlinear behavior of the masonry material. Since the structure fails due to the exceedance of the tensile strength, a crack will develop in the masonry structure. In this crack, the structure will not be able to produce tensile strength. The cracking of the structure leads to a different distribution of the stresses, which then may lead to further crack propagation or the tensile stresses to be located at another point in the structure.

In the linear-elastic calculation, it is assumed that the structure will fail if the principal tensile stress will exceed the tensile strength over a length of 210 mm. The nonlinear calculation that will be executed will be a sequential linear calculation. This means that the following steps will be taken in the calculation:

1. The structure will be loaded in a way that the calculation will produce a principal tensile stress that will just exceeds the tensile strength. This means a tiny crack will develop.
2. The properties of the masonry in the area of the crack will be edited: Young's Modulus of masonry will be reduced severely. This operation 'models' the crack. The structure is barely able to produce tensile strength at that point.
3. The calculation will be executed again. If the crack propagates (e.g. a greater area will exceed the tensile strength), step 2 will be repeated. If not, the tensile stress at the crack tip will be used for further calculation: the loads will be increased until the structure now fails at this point, and a tiny crack develops there. After that, step 2 will be executed again.
4. When the crack reaches a length of 210 mm, it is assumed the structure fails.

The goal of this comparison is to test the assumption used in the linear-elastic calculation: The structure fails if the principal tensile stress will exceed the tensile strength over a length of 210 mm.

The structure that is used for the comparison with the TNO report is chosen for this calculation. This structure is shown in Figure 121.

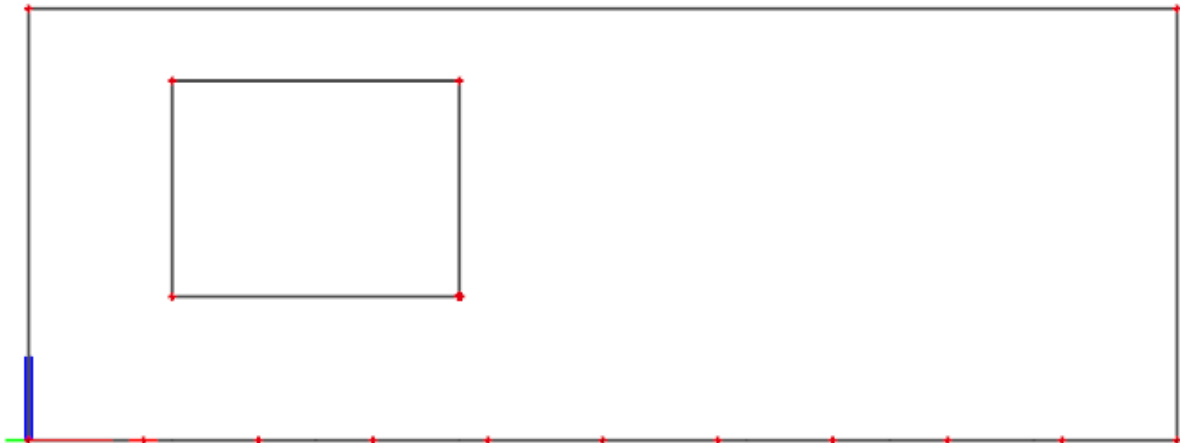


FIGURE 121 – STRUCTURE USED FOR COMPARISON WITH NONLINEAR MATERIAL PARAMETERS

A 10-Hz vibration speed will be used in a sandy soil (300 m/s propagation speed). The displacement amplitude will be adjusted to ensure a tiny crack develops in the structure. Following this, a displacement amplitude of 0.26 mm will lead to a tiny crack in the bottom right corner of the opening, as shown in Figure 122 and Figure 123.

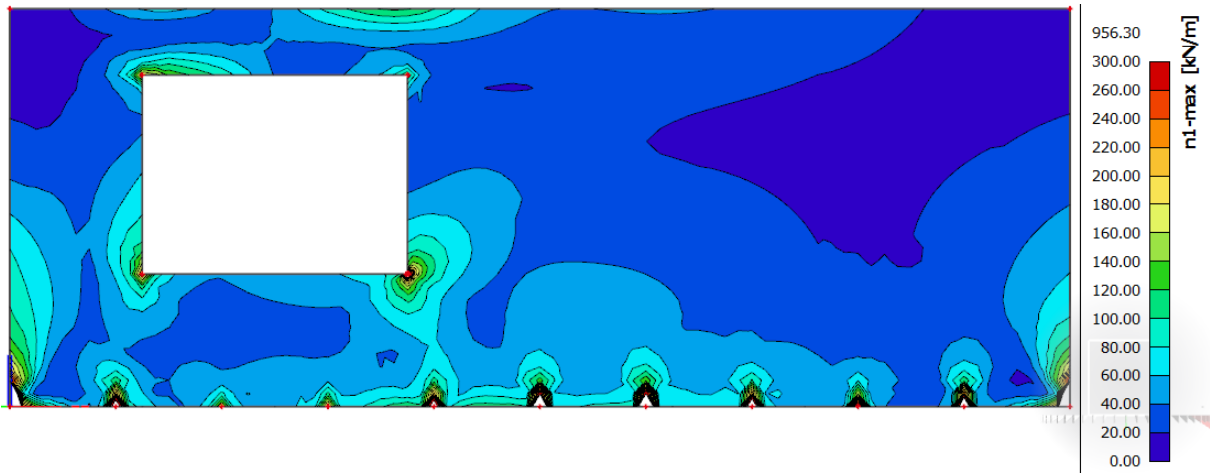


FIGURE 122 – CONTOUR PLOT SAND 10 HZ (0.26 MM DISPLACEMENT AMPLITUDE)

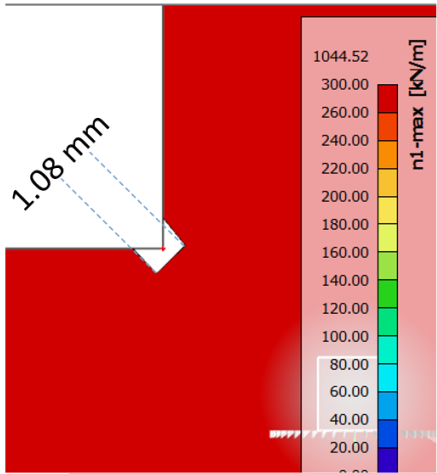


FIGURE 123 – ZOOMED IN AT BOTTOM RIGHT CORNER WINDOW, SAND 10 HZ (0.26 MM DISPLACEMENT AMPLITUDE)

The white part in Figure 123 is the part where the crack has developed. Masonry Young’s Modulus in this area is therefore adjusted: $E = 50 \text{ N/mm}^2$. With this adjustment, the calculation is executed again. This leads to the crack shown in Figure 124. The same displacement amplitude is used here, but with an area with a reduced Young’s Modulus, visually shown as the light blue color in Figure 124. Again, the white zone is the cracked area.

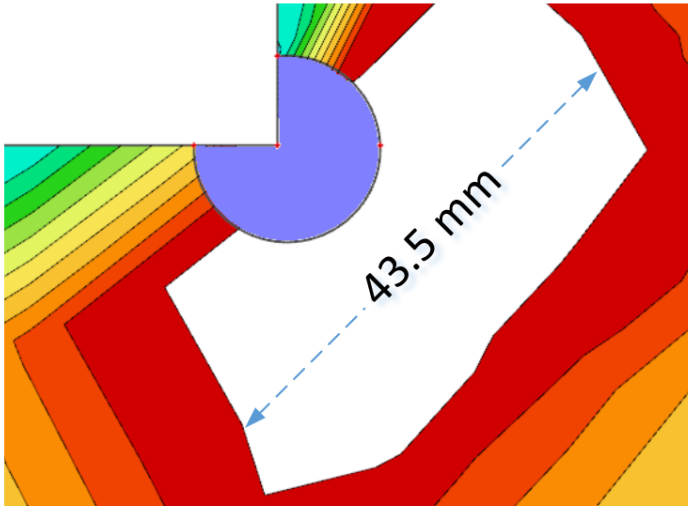


FIGURE 124 – ZOOMED IN AT BOTTOM RIGHT CORNER WINDOW, REDUCED YOUNG’S MODULUS, SAND 10 HZ (0.26 MM DISPLACEMENT AMPLITUDE)

Following this, in the white zone (cracked area) in Figure 124 Young’s Modulus has to be reduced. The calculation, with again the same displacement amplitude (there was still crack propagation) leads to the stress distribution as shown in Figure 125. Again, the light blue area is the area with the reduced Young’s Modulus.



FIGURE 125 – ZOOMED IN AT BOTTOM RIGHT CORNER WINDOW, REDUCED YOUNG’S MODULUS, SAND 10 HZ (0.26 MM DISPLACEMENT AMPLITUDE)

The crack has not propagated again. This means that the tensile stress at the crack tip has to be used to adjust the displacement amplitude, which can lead to a propagation of the crack. The tensile stress at the bottom right corner of the fracture zone (the maximum tensile stress) is 0.22 N/mm^2 . Since the crack occurs at $\sigma_t = 0.3 \text{ N/mm}^2$, the displacement amplitude can be raised to $\frac{0.3}{0.22} * 0.26 \text{ mm} = 0.355 \text{ mm}$. The same procedure is used again, and the result is shown in Figure 126. Again, the light blue area is the area with the reduced Young’s Modulus. The reason the area is a narrow diagonal stretch from the corner is that the crack will develop this way due to tensile stresses, as can be seen in section 3.2.

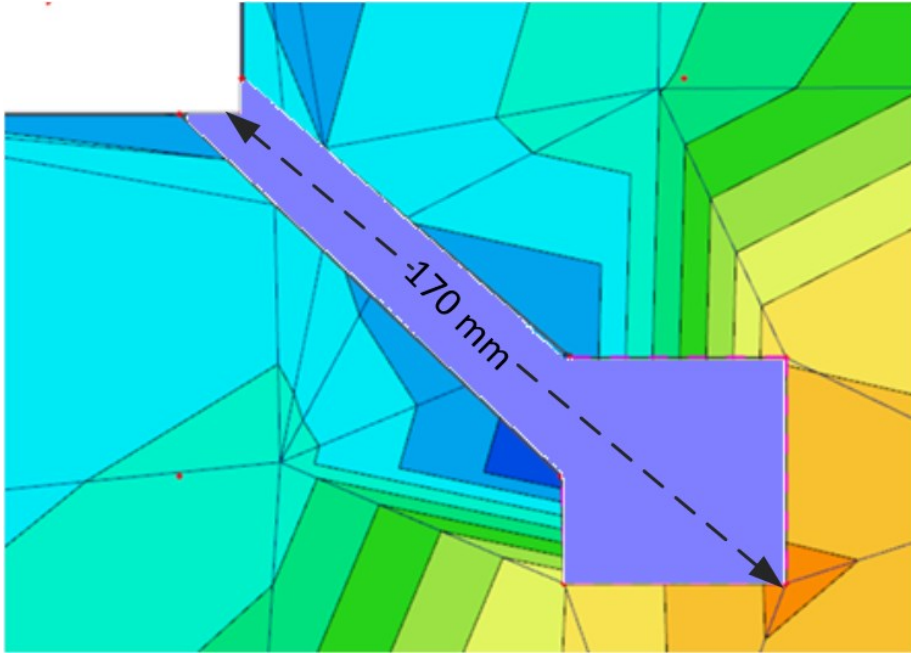


FIGURE 126 – ZOOMED IN AT BOTTOM RIGHT CORNER WINDOW, REDUCED YOUNG’S MODULUS, SAND 10 HZ (0.355 MM DISPLACEMENT AMPLITUDE)

The stress in the bottom right corner of the area with the reduced Young’s Modulus is 0.225 N/mm^2 , which now leads to a new displacement amplitude of 0.476 mm . The same procedure is used again, and the result is shown in Figure 127.

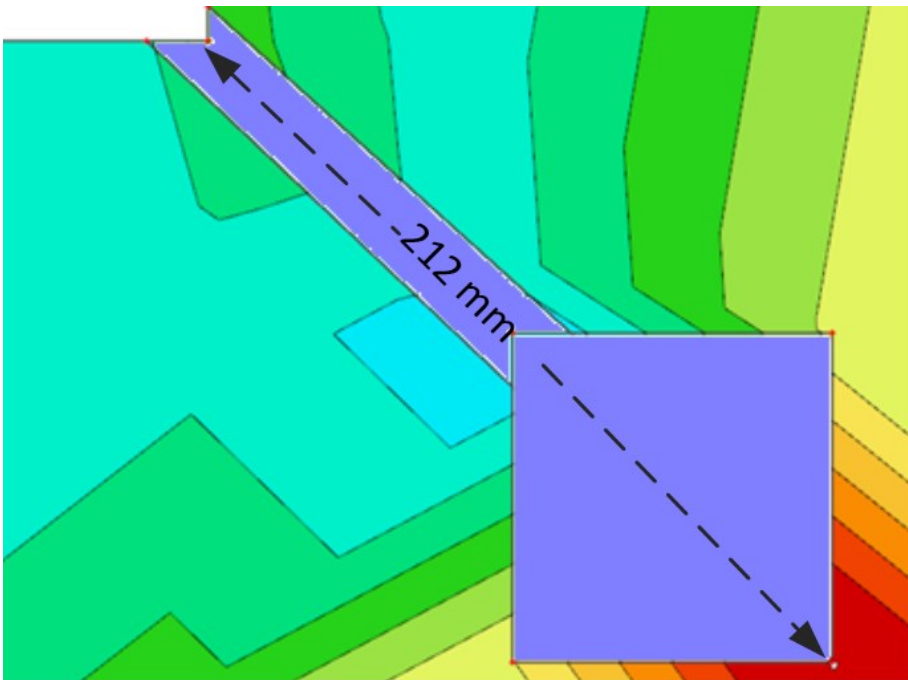


FIGURE 127 – ZOOMED IN AT BOTTOM RIGHT CORNER WINDOW, REDUCED YOUNG’S MODULUS, SAND 10 HZ (0.476 MM DISPLACEMENT AMPLITUDE)

At this point, the crack has reached the limit value of 210 mm . This means that this is value has exceeded the value of the failure criterion.

To compare this nonlinear result, the linear-elastic calculation with the same displacement amplitude has to be considered. These results can then be compared to each other.

The linear-elastic calculation with a displacement amplitude of 0.476 mm and, naturally, the same propagation speed and frequency, produces the results as shown in Figure 128 and Figure 129.

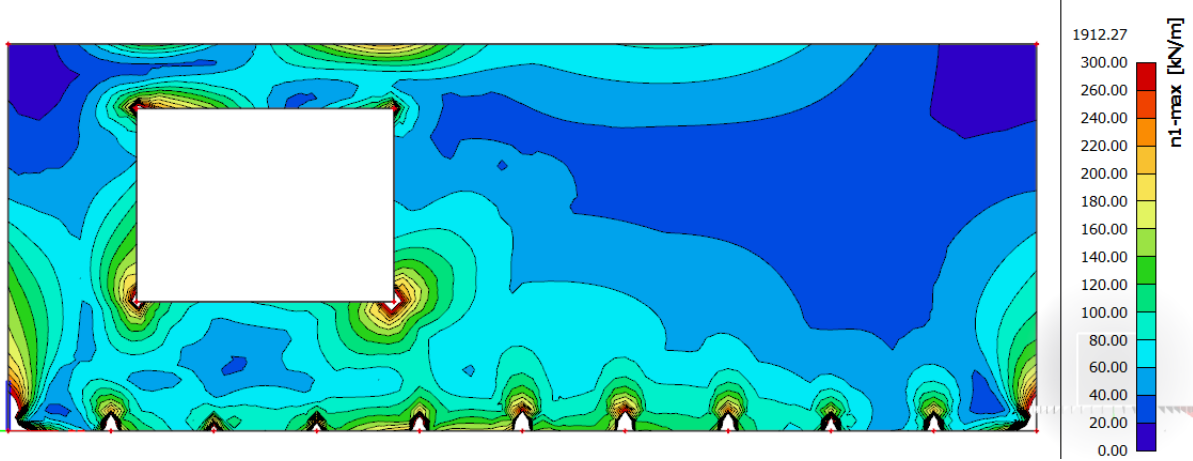


FIGURE 128 – CONTOUR PLOT SAND 10 HZ (0.476 MM DISPLACEMENT AMPLITUDE)

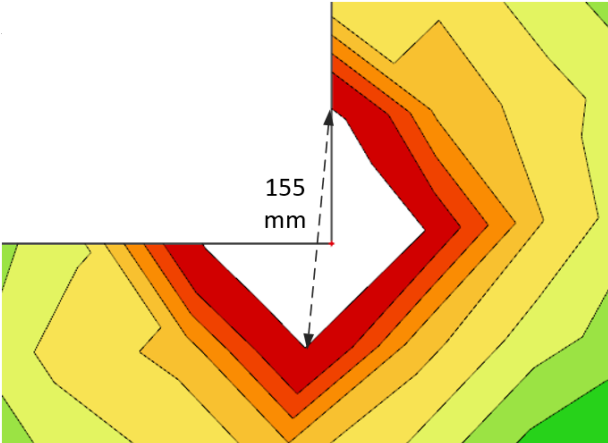


FIGURE 129 – ZOOMED IN AT BOTTOM RIGHT CORNER WINDOW, SAND 10 HZ (0.476 MM DISPLACEMENT AMPLITUDE)

This shows that, according to the sequential linear calculation, the assumption that the structure fails if the principal tensile stress will exceed the tensile strength over a length of 210 mm is not sufficient. The displacement amplitude in which the structure fails due to the sequential linear calculation will result in a length of the failure zone of only 155 mm. This means that if this assumption is considered true, the failure criterion according to the sequential nonlinear calculation will already be exceeded.

However, it has to be noted that this nonlinear approach is also a simplified version of reality. To perform an extensive nonlinear calculation, it is useful to apply the smeared crack model to this calculation. However, this model is not considered to be in the scope of this project. More research is recommended to produce a substantiated statement regarding this assumption and the nonlinear approach.

Using this comparison, it is recommended that the 210-mm assumption from section 4.3 should be changed to 155 mm. However, since this comparison is not enough for a substantiated statement, this is not yet applied in this report.

8. CONCLUSION AND RECOMMENDATION

This section describes the concluding statements that follow from this report. These are presented by answering the main research question and the sub-questions of this project, which were stated in section 2.1

“How can the probability of failure for masonry structures be computed for vibration speeds exceeding the threshold values stated in SBR richtlijn A?”

The project shows that it is possible to compute these vibration speeds. The procedure that has been set up in this project is basically the answer to this question. The procedure is described and demonstrated in sections 3.4 and 5.2. Briefly summarized:

- 1) The structural designer models the concerning façade in a FEM-preprocessing environment.
- 2) According to the use of the building, the span and the construction materials, the structural designer adds the self-weight, dead loads and mobile loads on the façade.
- 3) The structural designer adds a vibration load to the façade. This depends on the expected vibration speed, frequency and propagation speed in the soil (which depends on the type of soil).
- 4) The developed tensile stress that follows from a FEM-calculation is input for the stochastic model, a Monte Carlo simulation. Together with the other parameters (i.e. tensile strength and Young’s Modulus), this results in a statement regarding the probability of failure.

This can be executed for any vibration speed. Therefore, the procedure can provide for an estimation of the probability of failure.

The procedure is partly based on previous research. However, the procedure is also based on some assumptions. Moreover, some properties that could influence the probability of failure are not included in this study. To ensure the soundness of the procedure, more research on the following topics is recommended:

- Young’s Modulus’s effect on the maximum tensile stress.
- The effect of initial deformations, stresses and damage on the structure.
- The repetitiveness of the vibration.
- The stochastic parameters of the tensile strength and Young’s Modulus.

Summarized, the procedure gives an estimation of the probability of failure, but more research has to be conducted to justify the procedure and improve its quality.

“Can a linear-elastic calculation lead to statements regarding cracking?”

This project was mainly focused on the tensile stress that a linear-elastic calculation produces. To produce these results, a few assumptions were necessary to make this calculation feasible, for example:

- The structure fails when the maximum tensile stress is exceeded over a length of 210 mm.

By using these kind of assumptions, it is possible to follow this procedure in a linear-elastic way. However, this study did not investigate the soundness of this assumption. More research regarding this topic has to be executed to justify this assumption. This can be done by comparing the results to the results of a nonlinear approach, i.e. by using a smeared crack model.

Summarized, the linear-elastic calculation results in feasible results, but an extensive comparison to a nonlinear approach is necessary to ensure the soundness of this calculation.

“Is it feasible to include stresses at the soil-masonry-interface in calculating the probability of failure due to vibration speeds?”

The software package for structural calculations used in this project (SCIA) lacked possibilities of applying pressure-only springs or other nonlinear calculations in combination with dynamic loads. Therefore, it was not possible to implement stresses at the soil-masonry interface in a way that represents reality.

Linear springs are used to give an approximation of the consequences of stresses at the soil-masonry interface. This is not a realistic representation of the actual situation, but this approach can provide knowledge regarding these stresses. The results of this approach show that stresses at the soil-masonry interface result in a beneficial effect regarding the tensile stresses, and from this follows that applying these stresses will lead to lower probabilities of failure.

However, it has to be noted that this approach is not an actual representation of reality. Further research regarding this topic is necessary to form a solid statement regarding stresses at the soil-masonry interface. To form this statement, research should be conducted on one of the following properties:

- The use of nonlinear (pressure only) springs to represent soil.
- Implementing a soil model in the same model as the structure.

“Does a nonlinear approach lead to significantly other results than a linear-elastic calculation?”

A comparison of the nonlinear approach (sequential linear) and the linear-elastic approach tested the failure criterion that has been used in the linear-elastic calculation (The structure fails when the maximum tensile stress is exceeded over a length of 210 mm). This comparison shows that the nonlinear approach will reach this failure criterion due to a lower vibration speed than the vibration speed that leads to failure for the linear-elastic approach. When the failure criterion is reached using the linear-elastic approach, the structure would have already failed if the nonlinear approach had been used. Therefore, a nonlinear approach will lead to another failure criterion and the probability of failure will lead to other results

The sequential linear approach is a simplified version of reality. To produce a solid statement regarding the nonlinear approach, other models should be used, for example the smeared crack model. More research into this topic is recommended regarding the nonlinear approach.

APPENDICES

APPENDIX A: ELABORATION OF THE MODEL

A.1 EXAMPLE SPRING-COLUMNS

Example

One wants to place a sinusoidal load at the bottom of the structure, with an amplitude of 1 mm. The stiffness of the spring-columns (EA) is $1 \cdot 10^{10}$ N, and its length is 1m. This results in a spring stiffness of 10^{10} N/m. 10^7 N of force results therefore in a displacement of 1 mm. To produce a sinusoidal load, the following forces (in kN) should be placed on the spring-columns:

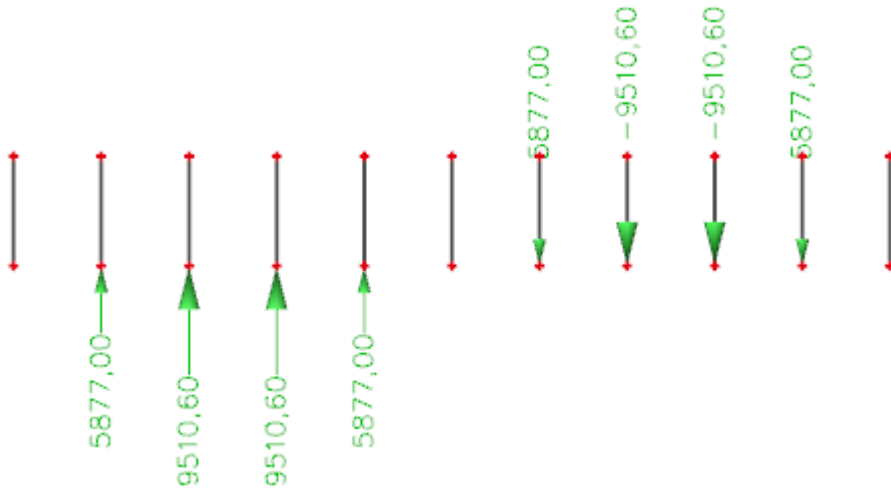


FIGURE 130 – LOADS ON SPRING-COLUMNS

Which results in these displacements at the bottom of the structure (when the inertia of the structure can be neglected, because of the great stiffness of the spring-columns):

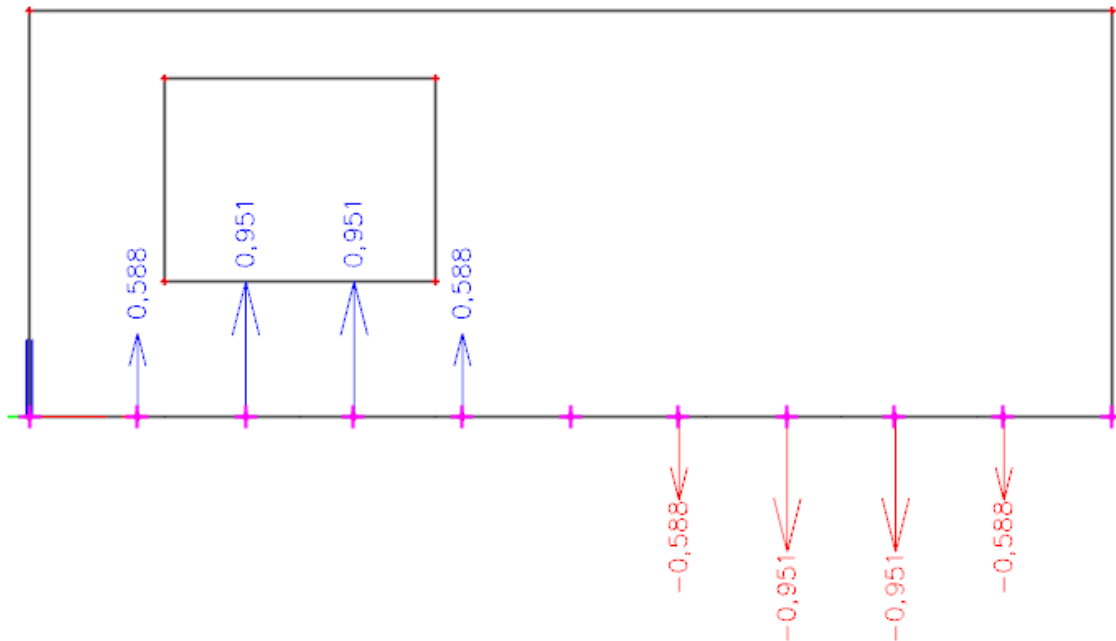


FIGURE 131 – RESULTING DISPLACEMENTS

The stiffness of the spring-columns is set very high, and the point forces that act on them are set very high as well. This choice has been made to ensure that the displacement at the bottom of the structure will not be influenced by the inertia of the façade. However, it cannot be set too high, since the numerical accuracy will decrease due to the bad condition of the system of equations. Assumed is that the difference between the theoretical displacement and the displacement in the SCIA calculation should be 1% maximum. The value of the stiffness of the spring-columns should ensure that this difference will not be any higher than 1%. Calculations regarding this matter result in a spring stiffness $k = 10^{10} \text{ N/m}$. This is explained in the example below.

Example

The results of a dynamic load acting on the structure in Figure 131 for both $k = 10^{18} \text{ N/m}$ and 10^{10} N/m have been investigated in Figure 132 and Figure 133. It can be seen that the displacements in the second situation will lead to differences with the first situation of about 1% for the highest values of displacement. This shows that a spring stiffness of 10^{10} N/m will lead to situations which result in numerical accurate results and the inertia of the façade will not influence the computational results too much, as stated in this paragraph.

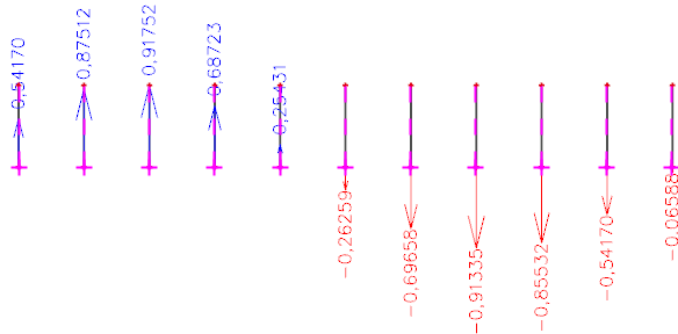


FIGURE 132 – RESULTS K=10¹⁸ N/M

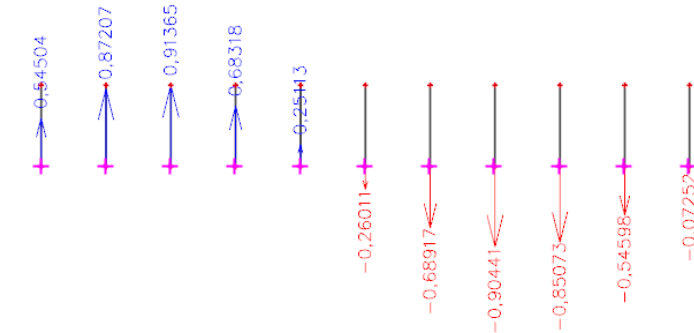


FIGURE 133 – RESULTS K=10¹⁰ N/M

A.2 VIBRATION LOADS

For the desired load case, dynamic load functions (DLF's) have to be created. The dynamic load function describes the value of the point force in time. The example below shows the development of a DLF.

Example

For a frequency of 5Hz a dynamic load function has to be developed. Since it is a low frequency (haying), the wave has to damp in time. Therefore, two functions are created, shown in Figure 132. The function "Samengesteld" is the product of "Functie 1" and "Functie 2"

$$\text{Functie 1} = \sin(5 * 2\pi * t)$$

$$\text{Functie 2} = 0.04 * t^2 - 0.4 * t + 1$$

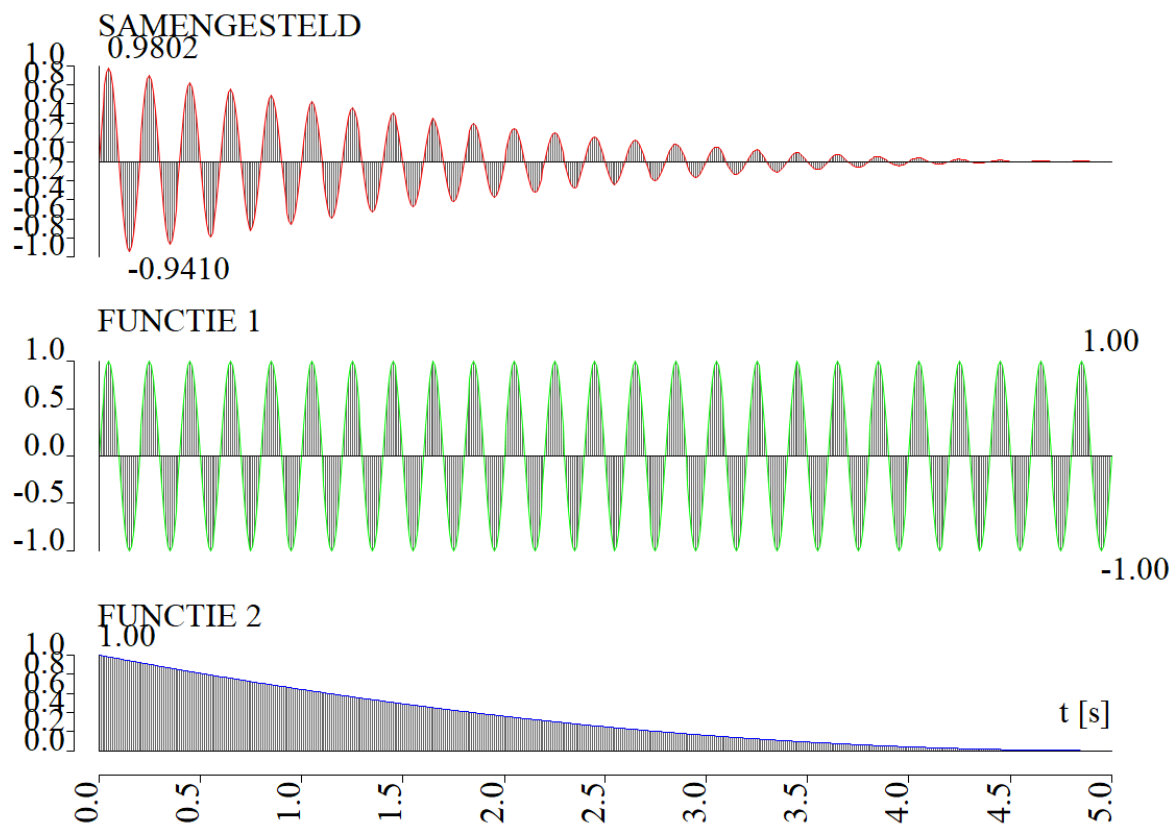


FIGURE 134 – DYNAMIC LOAD FUNCTION

The vibration source is placed left of the structure. The dynamic load functions for the eleven different spring-columns will be the same in frequency and amplitude, only there will be a phase difference. The phase difference depends on the propagation velocity v and the distance d between two spring-columns:

$$\Phi = \frac{d}{v}$$

i.e. when, the distance between two spring-columns is one meter and the propagation velocity is 300 m/s, the phase difference for the second spring-column is: $\Phi = \frac{d}{v} = \frac{1}{300} = 0.00333$ s. The phase difference for the third spring-column is: 0.00666 s etc.

A.3 EXAMPLE CURVE-FIT

Example

For an imaginary structure, the maximum tensile stresses are gathered from different Young's Moduli ($\mu = 5000 \text{ N/mm}^2$, $\sigma = 1500 \text{ N/mm}^2$). These results are shown in Table 43 and Figure 135.

TABLE 43 – MAXIMUM TENSILE STRESSES FOR DIFFERENT YOUNG'S MODULI

E (N/mm ²)	500	2000	3500	5000	6500	8000	9500
σ (N/mm ²)	0.540	0.575	0.625	0.830	1.550	3.240	6.000

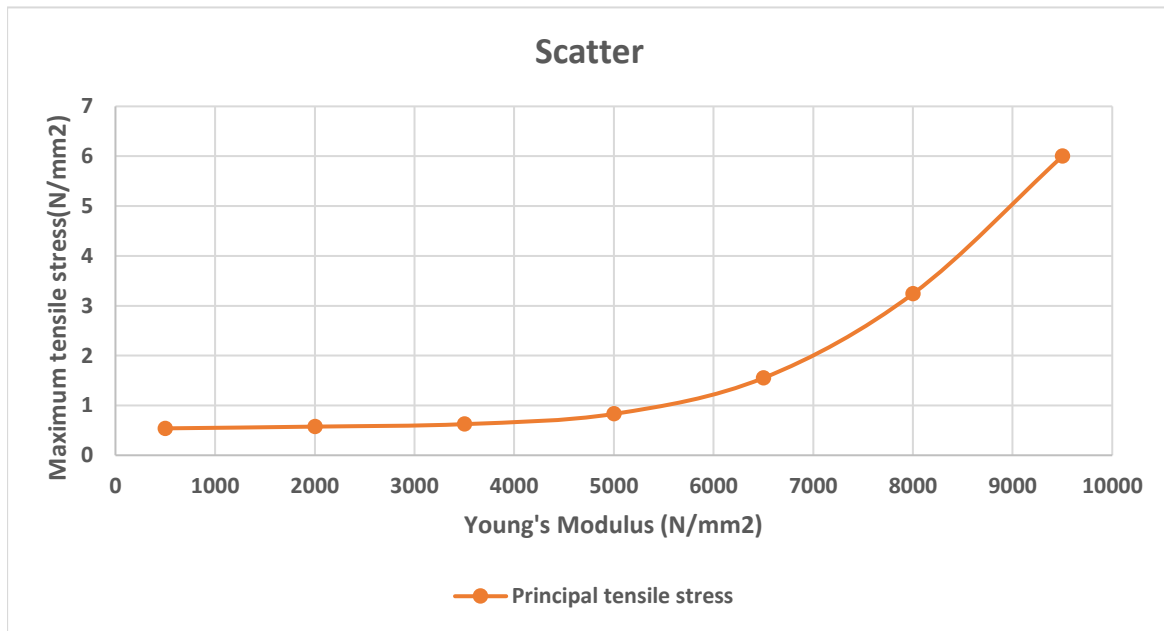


FIGURE 135 – MAXIMUM TENSILE STRESSES – YOUNG'S MODULUS SCATTER

A curve-fit has been made for this curve, using Microsoft Excel. This results in the following formula:

$$\sigma_E(E) = 1.5391 * 10^{-11} * E^3 - 1.0994 * 10^{-7} * E^2 + 2.4158 * 10^{-4} * E + 0.43691$$

This is divided by the stress for $E=5000$ (0.830 N/mm^2), and can be added to the limit state function. Therefore, the limit state function becomes:

$$Z = f_t - \frac{\sigma_E(E)}{0.830} * \sigma$$

A.4 EXAMPLE MATLAB SCRIPT

A few notes for the script:

- Row 2,3 and 4: The values of the maximum stresses at a vibration speed of 12 mm/s should be inputted here. These are the values of the point of interest (the point, usually a corner, where the structure fails).
- Rows 5-8: The mean value of the maximum tensile strength for failure, the variation coefficient of the tensile strength, the mean value of masonry Young's Modulus and the variation coefficient of masonry Young's Modulus should be inputted here, respectively.
- Row 9: amount of Monte Carlo simulations.
- Rows 11-13: the initial stresses at the point of interest should be inputted here.
- Rows 14-16: the maximum stresses due to the vibration load will be calculated at different vibration speeds. This is possible, because it is a linear calculation.
- Rows 17-22: the sum of the initial stress and the stress due to vibrations will be gathered for σ_x , σ_{xy} and σ_y . Following this, they will be translated into principal stresses.
- Rows 23: Monte Carlo Simulation starts.
- Rows 25-29: Random numbers are drawn from the distributions for f_t and E .
- Rows 31 and 32: the value for E will be inputted in the formula for $\sigma_E(E)$.
- Rows 33-35: The limit state function will be calculated.
- Row 36: The calculation of the probability of failure will be performed.
- Row 39: A scatter will be developed that plots the probability of failure against the vibration speed.

```

1  close all;
2  nx=;
3  ny=;
4  nxy=;
5  mft=;
6  vft=;
7  mE=;
8  vE=;
9  n=100000;
10 for p=1:30
11     ininx(p)=-.044583;
12     ininy(p)=-.195209;
13     ininxy(p)=-.050891;
14     nx(p)=nx*p/12;
15     ny(p)=ny*p/12;
16     nxy(p)=nxy*p/12;
17     f1(p)=nx(p)+ininx(p);
18     f2(p)=ny(p)+ininy(p);
19     fa(p)=nxy(p)+ininxy(p);
20     N1(p)=0.5*(f1(p)+f2(p)+sqrt((f1(p)-f2(p))^2+4*fa(p)^2));
21     N2(p)=0.5*(f1(p)+f2(p)-sqrt((f1(p)-f2(p))^2+4*fa(p)^2));
22     A(p)=0.5*atan(2*fa(p)/(f1(p)-f2(p)))*180/pi;
23     for i=1:n
24         % ft;
25         mu=log((mft^2)/sqrt(mft^2+(vft*mft)^2));sigma=sqrt(log((vft*mft)^2
26         /(mft^2)+1));ft(i)=lognrnd(mu,sigma);
27         %E;
28         mu=log((mE^2)/sqrt(mE^2+(mE*vE)^2));sigma=sqrt(log((mE*vE)^2/(mE^2
29         )+1));E(i)=lognrnd(mu,sigma);
30         %mu=5000;sigma=2800;E(i)=normrnd(mu,sigma);
31         stressE(i)=5.80967*10^-12*E(i)^3-3.8228*10^-
32         8*E(i)^2+0.000156517*E(i)-0.260209;
33         S(i)=stressE(i)*N1(p);
34         Z(i)=ft(i)-S(i);
35     end
36     P(p)=sum(Z<0)/n;
37     end
38     P
39     scatter(1:30,P)

```

FIGURE 136 – MATLAB SCRIPT DESCRIBING THE MONTE CARLO SIMULATION

APPENDIX B: RESULTS TEST FAÇADE

RESULTS OUDE DELFT

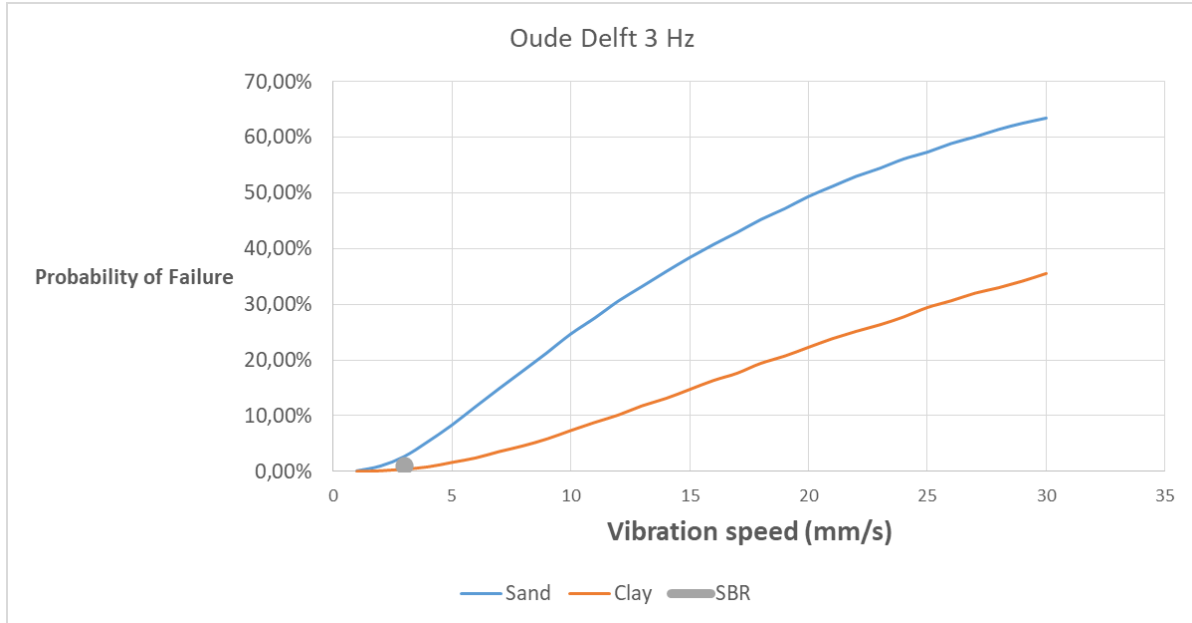


FIGURE 137

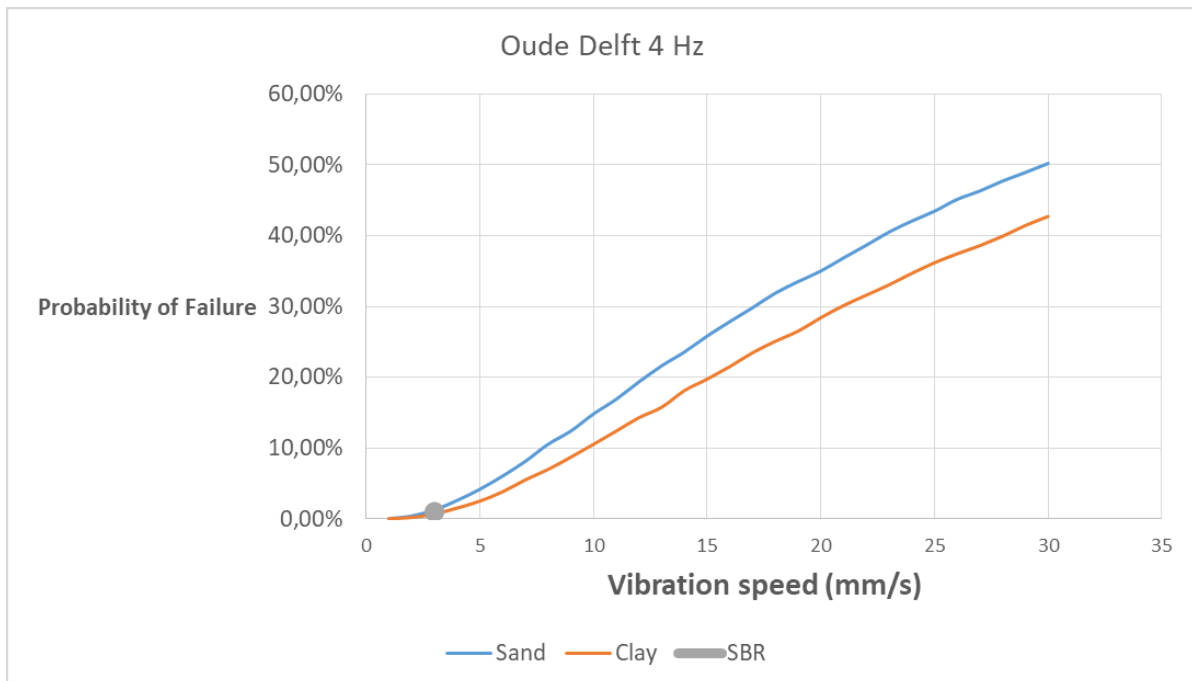


FIGURE 138

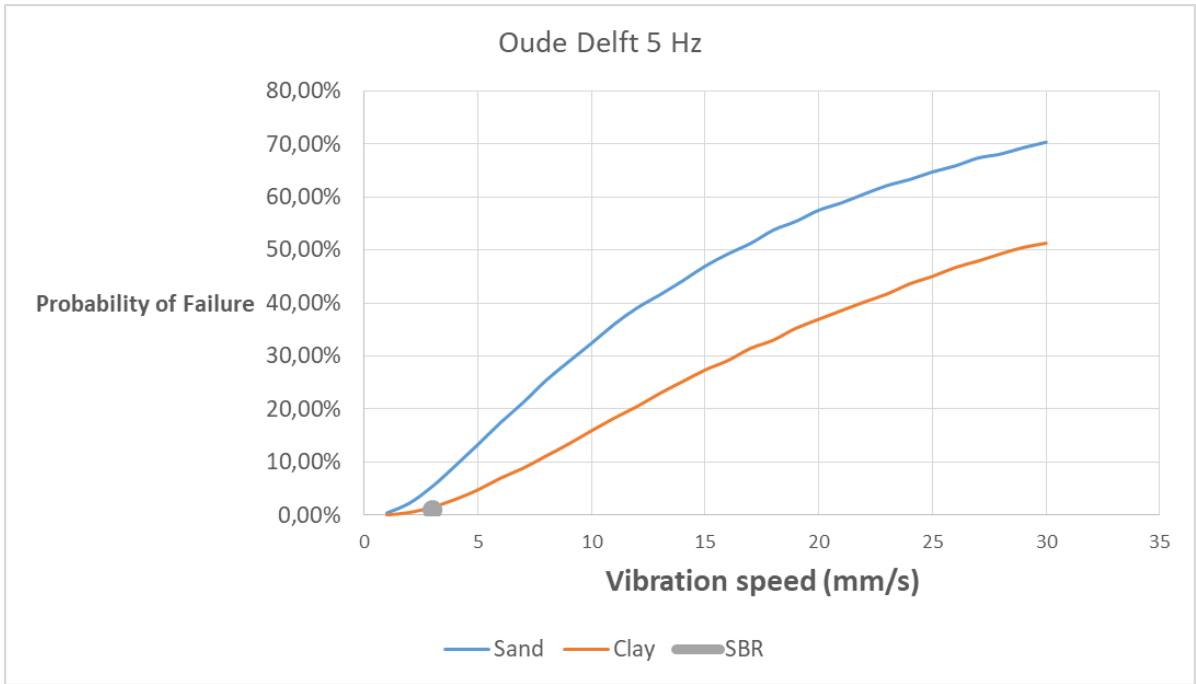


FIGURE 139

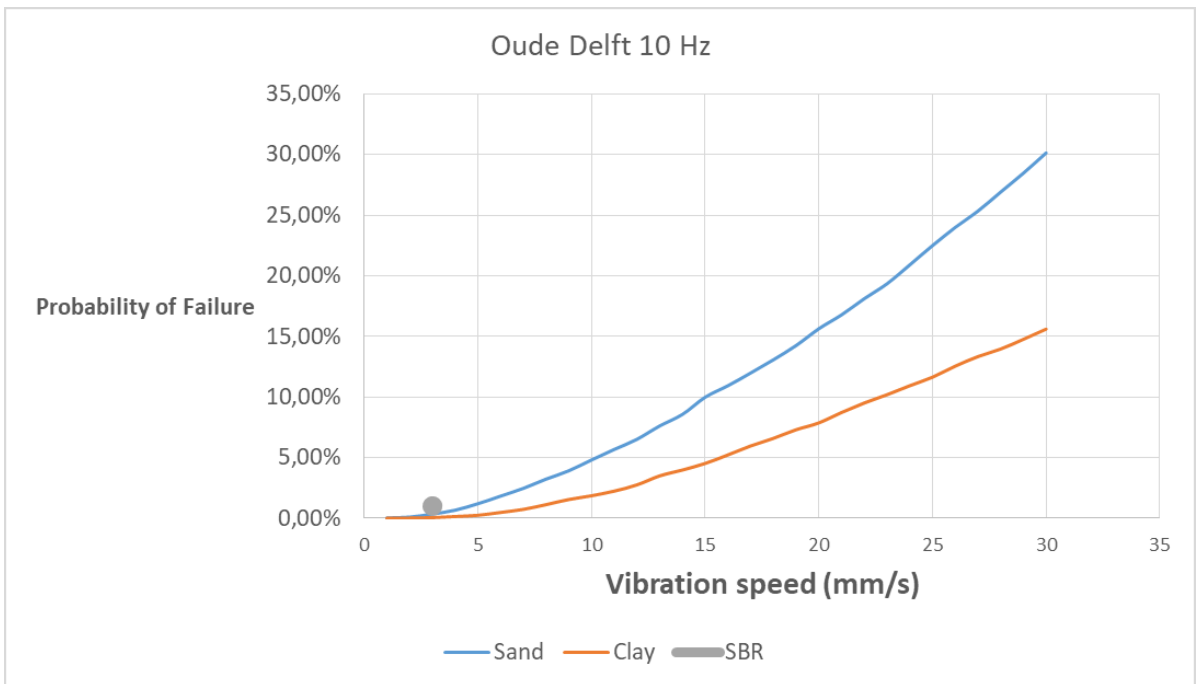


FIGURE 140

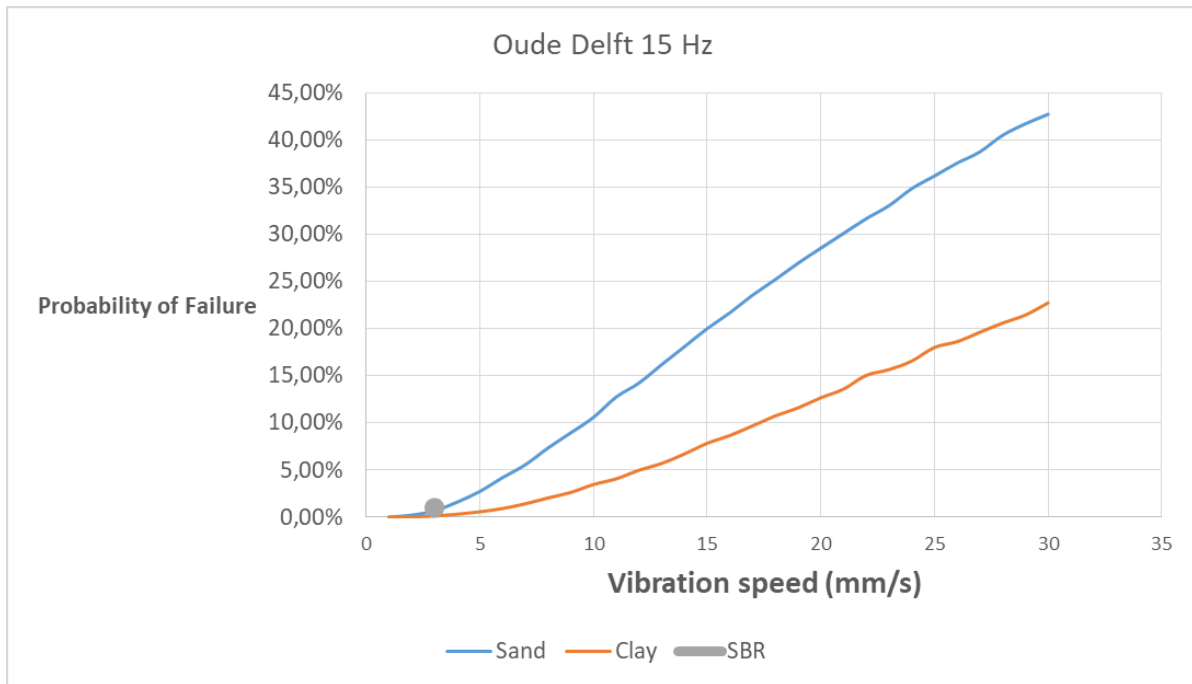


FIGURE 141

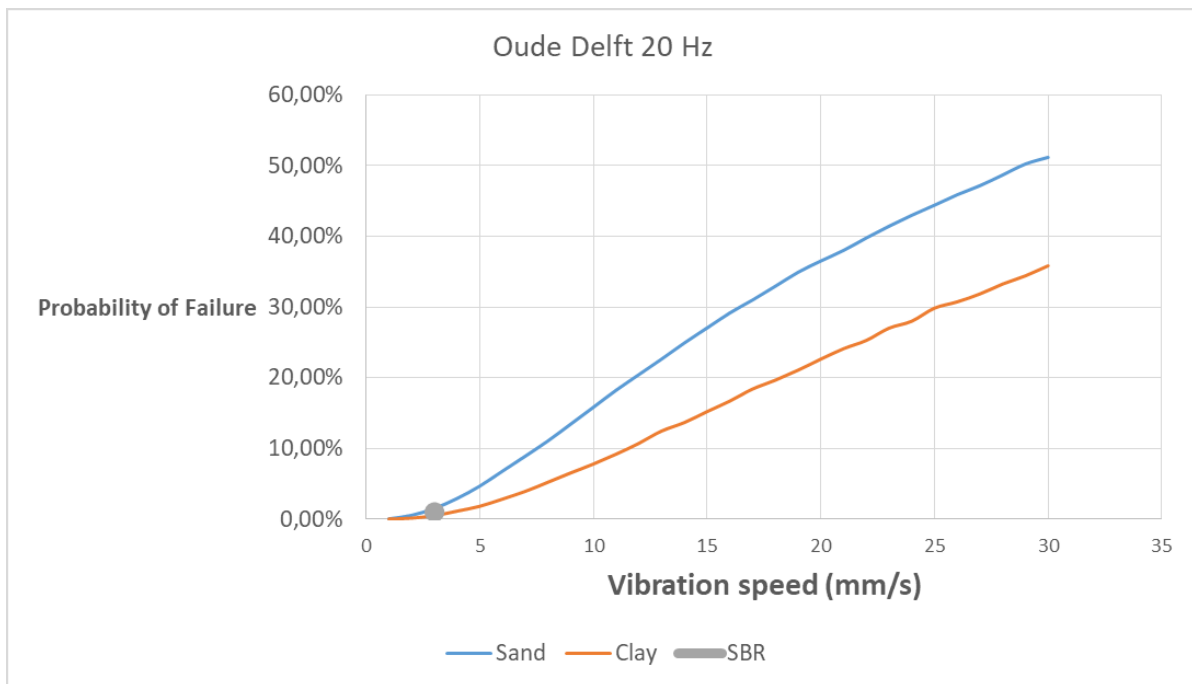


FIGURE 142

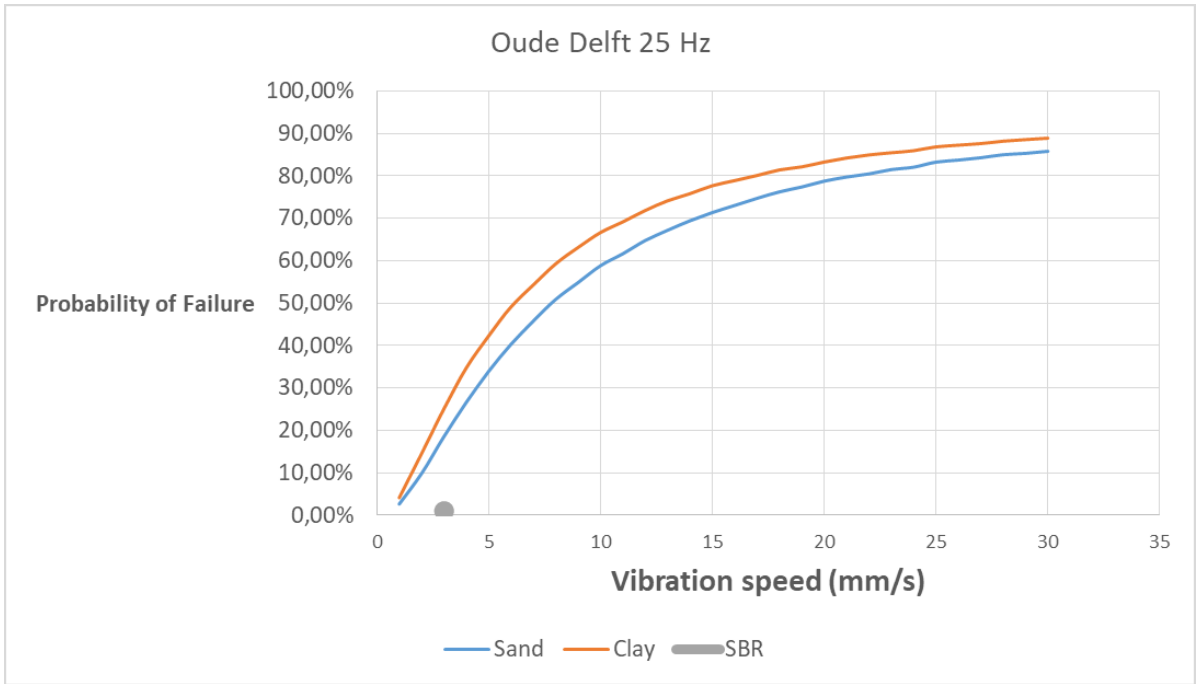


FIGURE 143

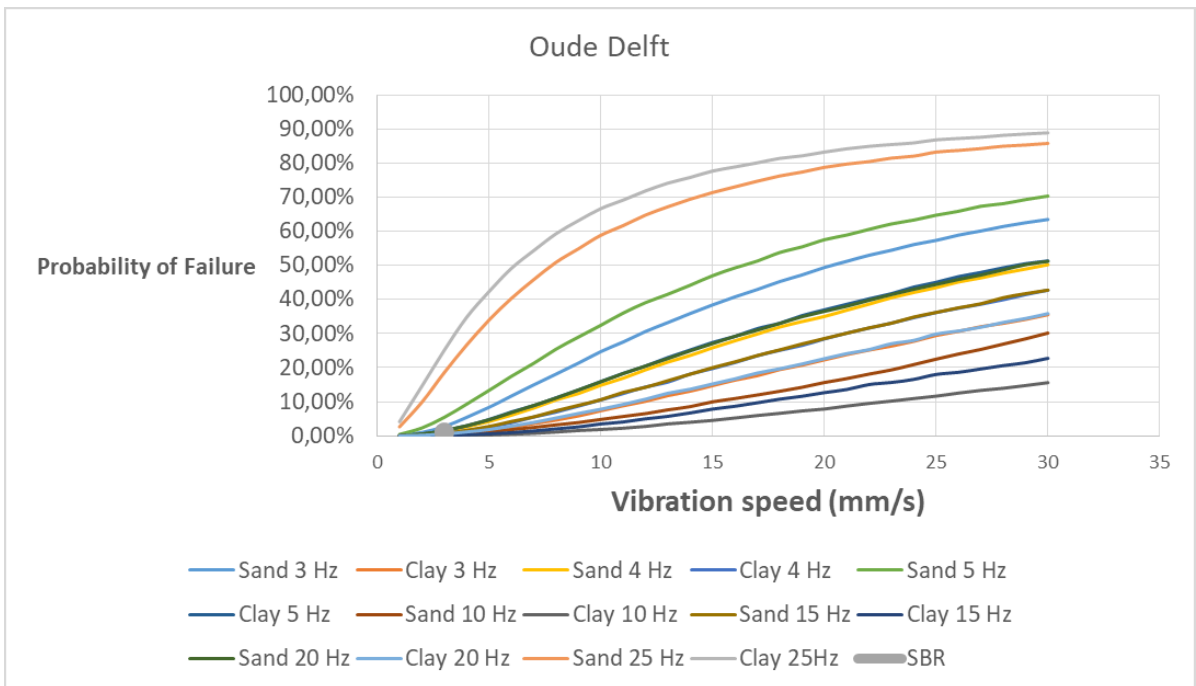


FIGURE 144

RESULTS VAN TIJENSTRAAT

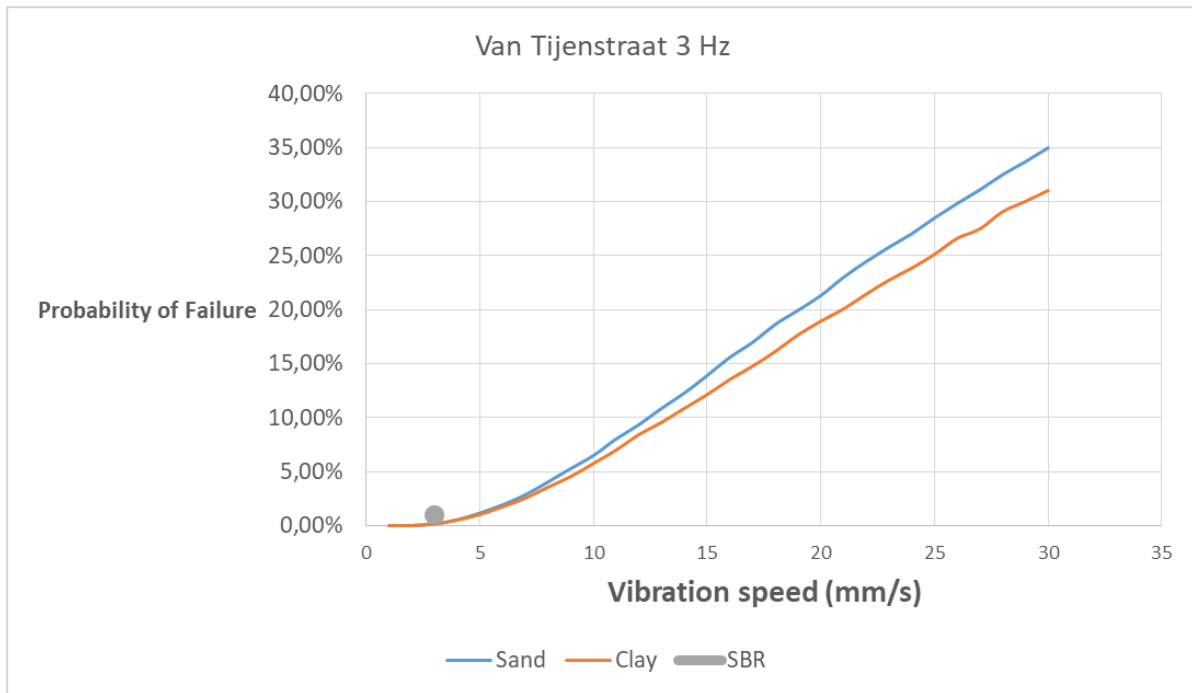


FIGURE 145

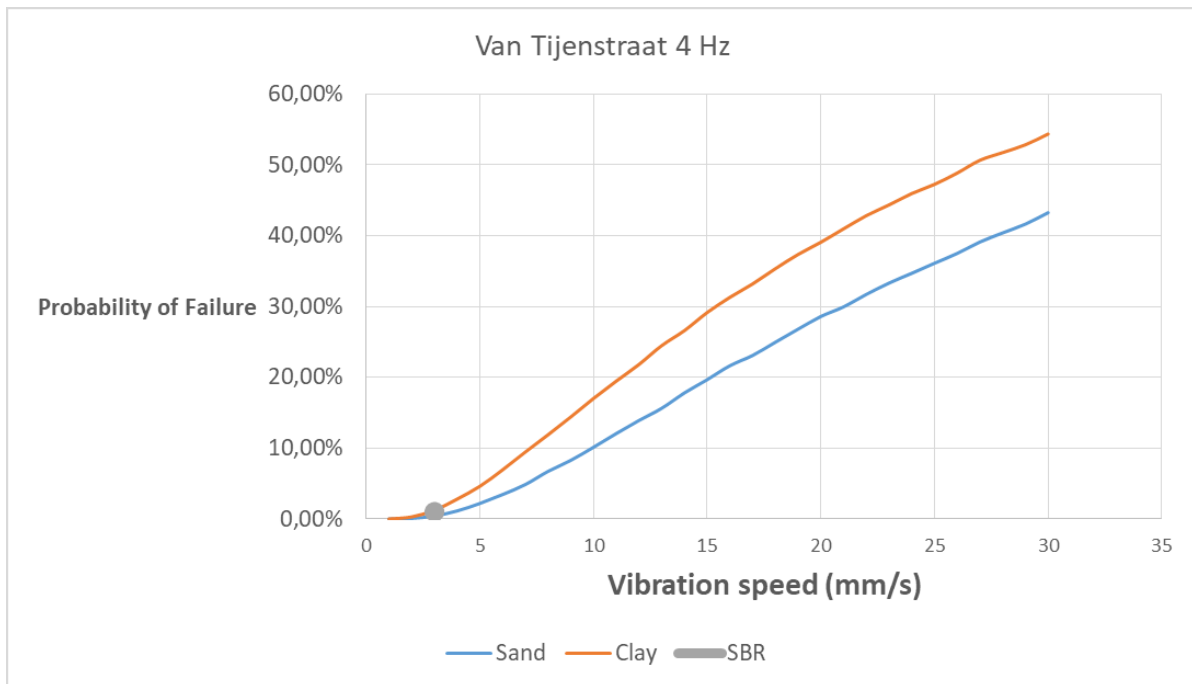


FIGURE 146

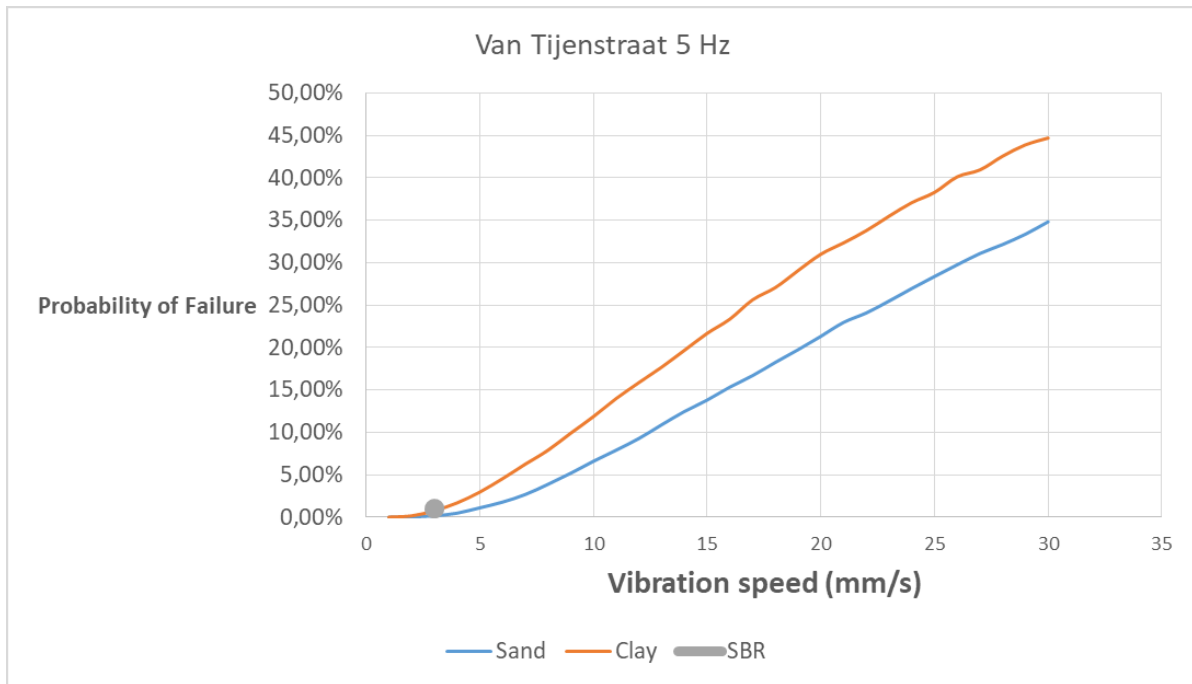


FIGURE 147

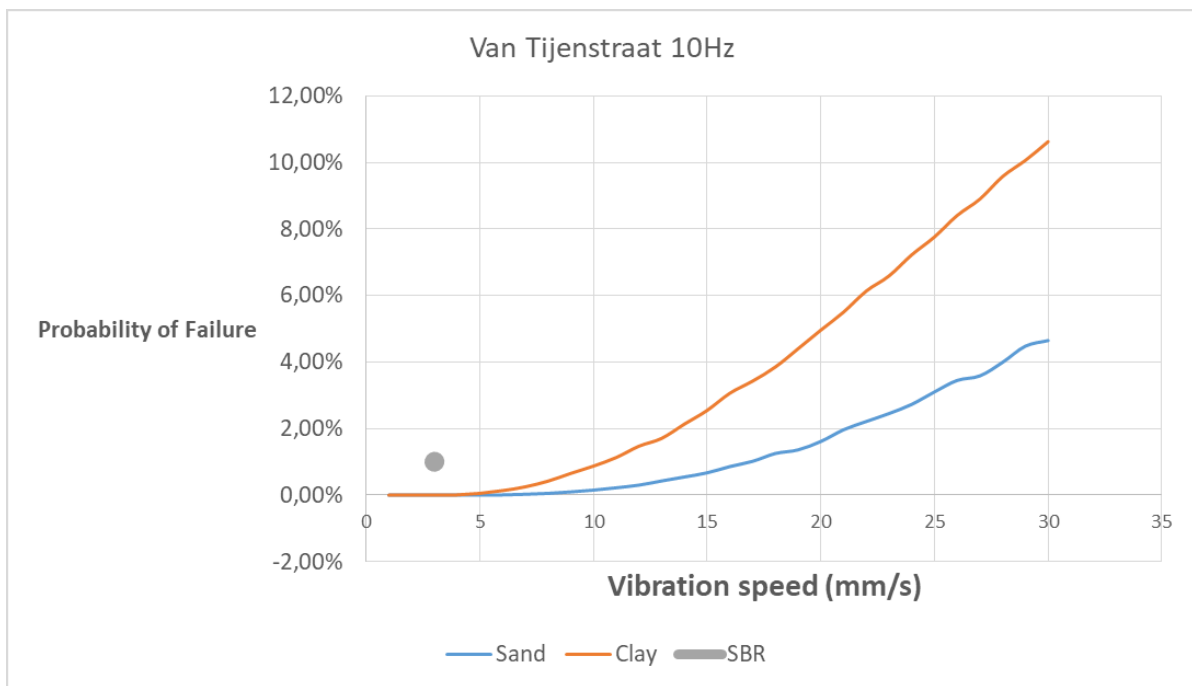


FIGURE 148

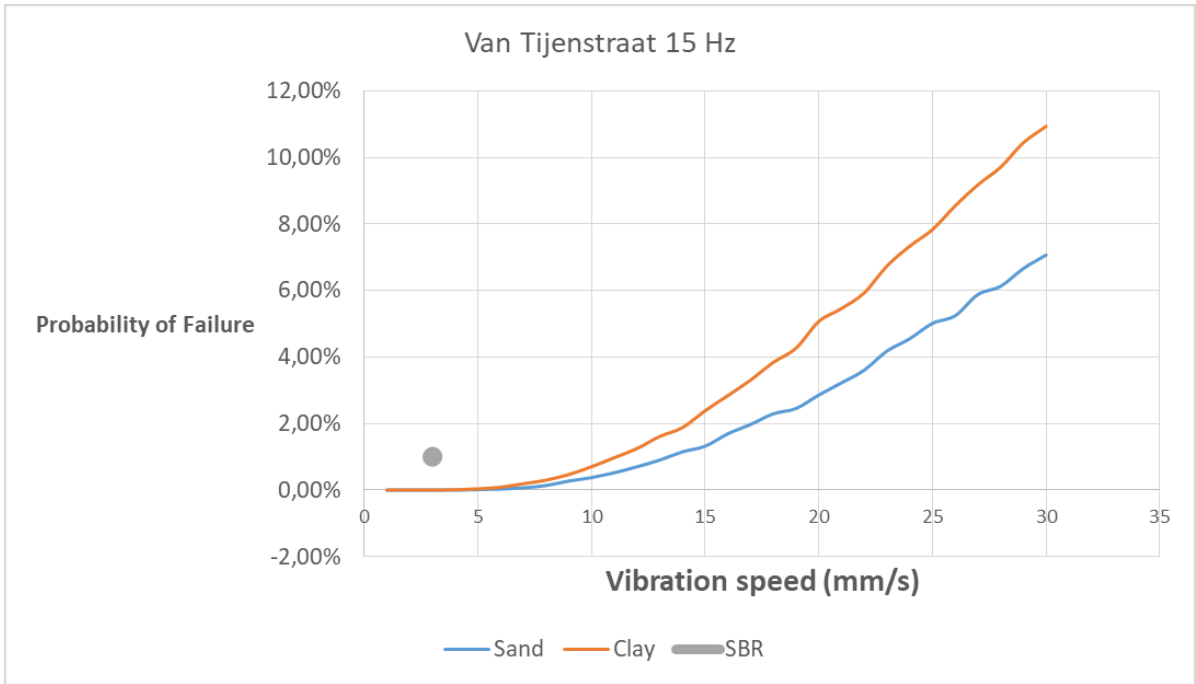


FIGURE 149

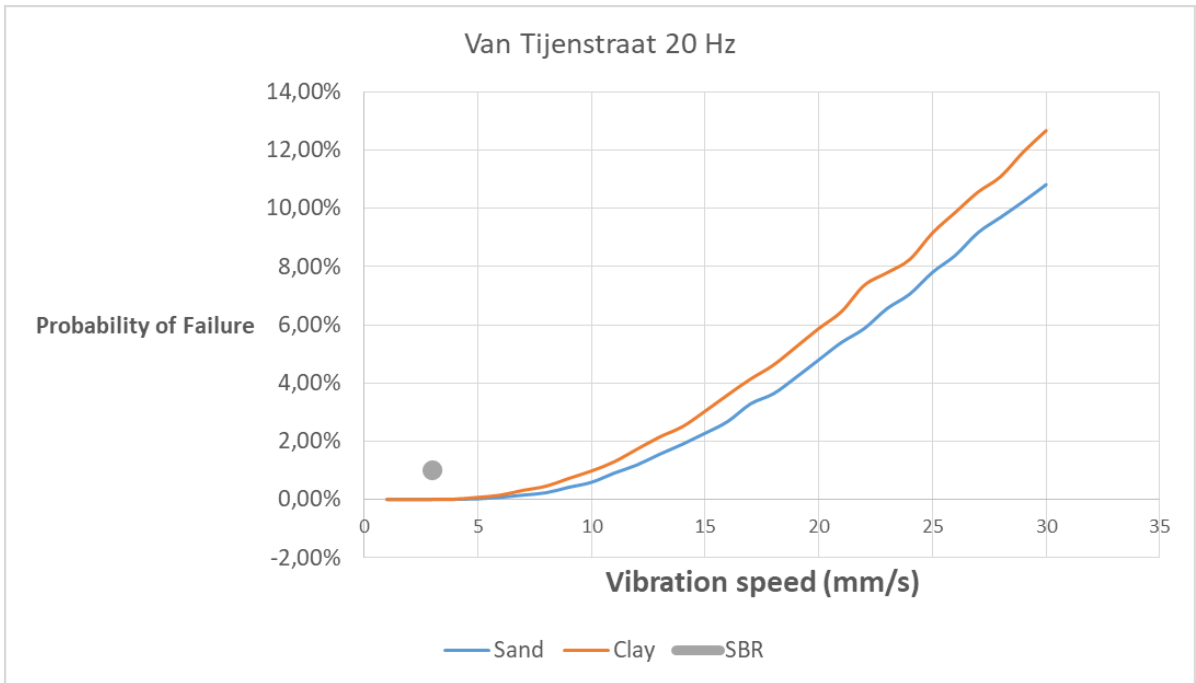


FIGURE 150

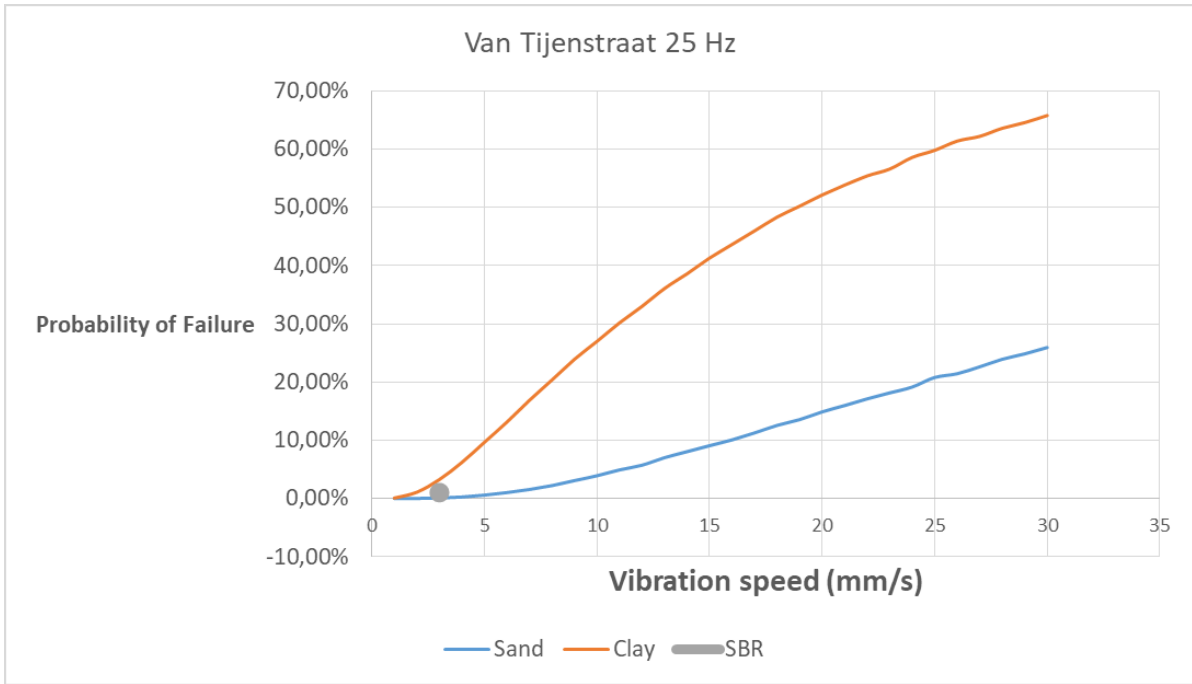


FIGURE 151

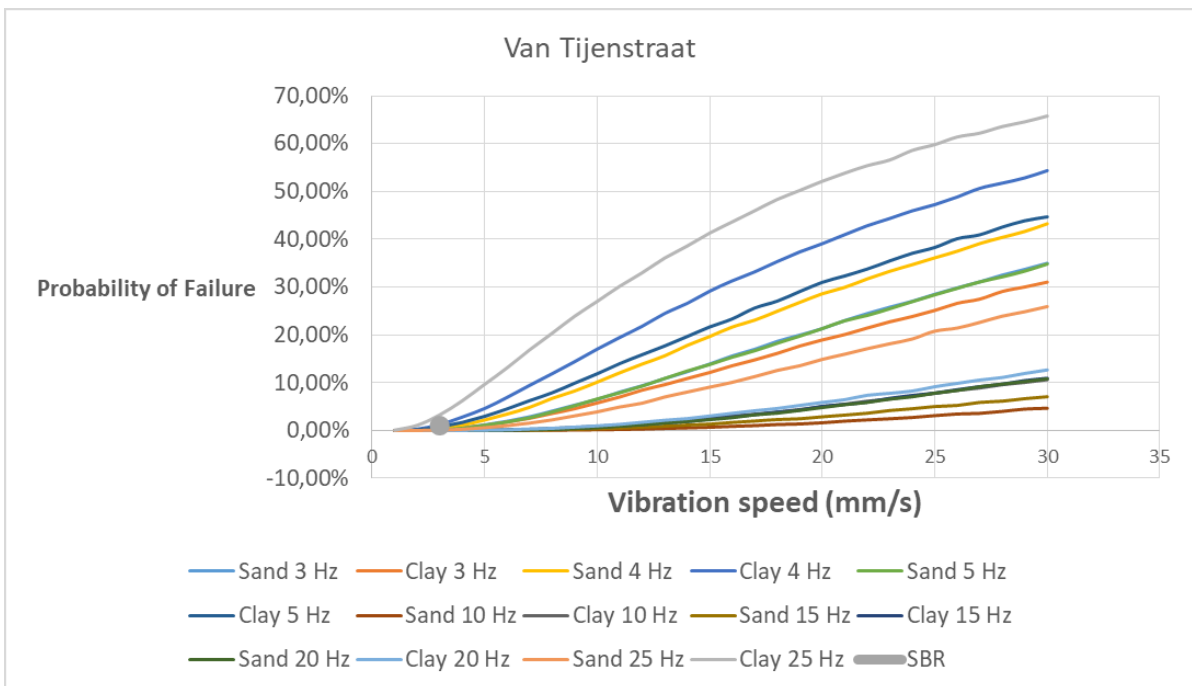


FIGURE 152

RESULTS BIESLANDSEKADE

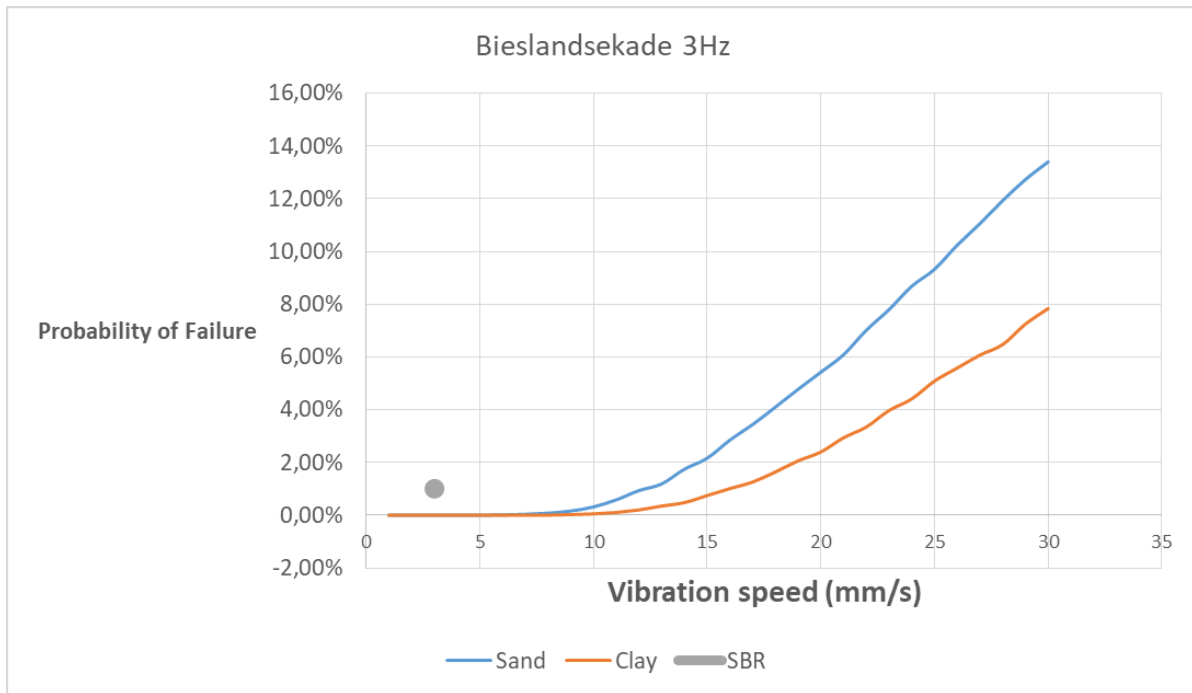


FIGURE 153

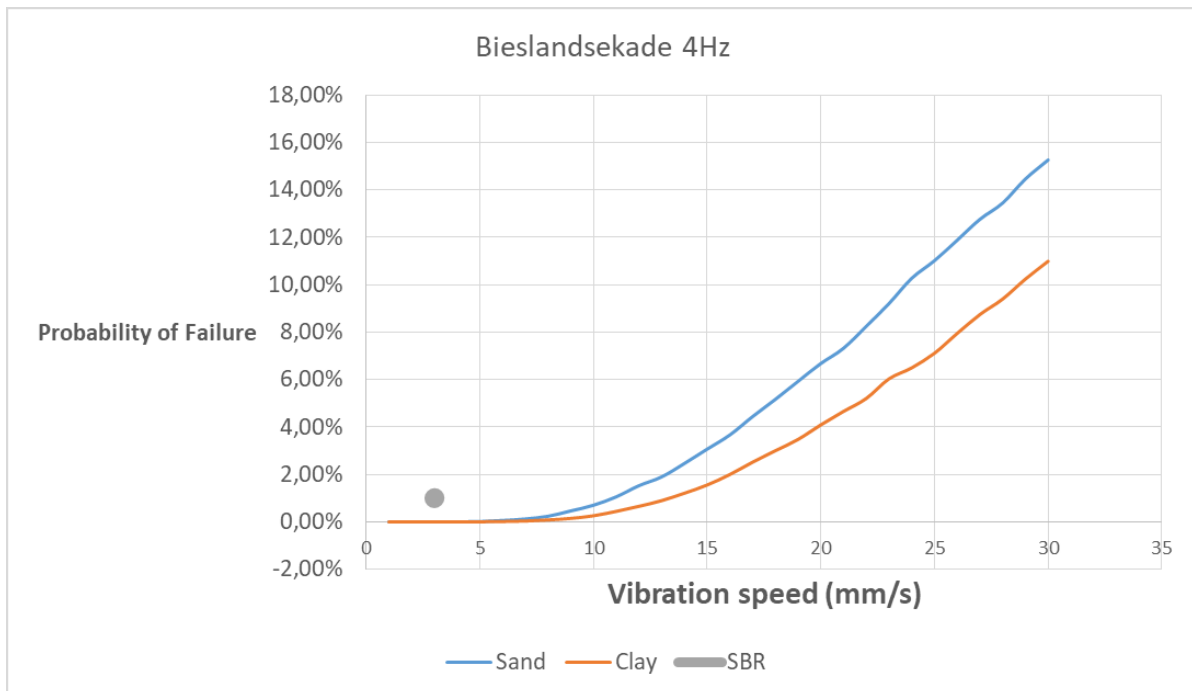


FIGURE 154

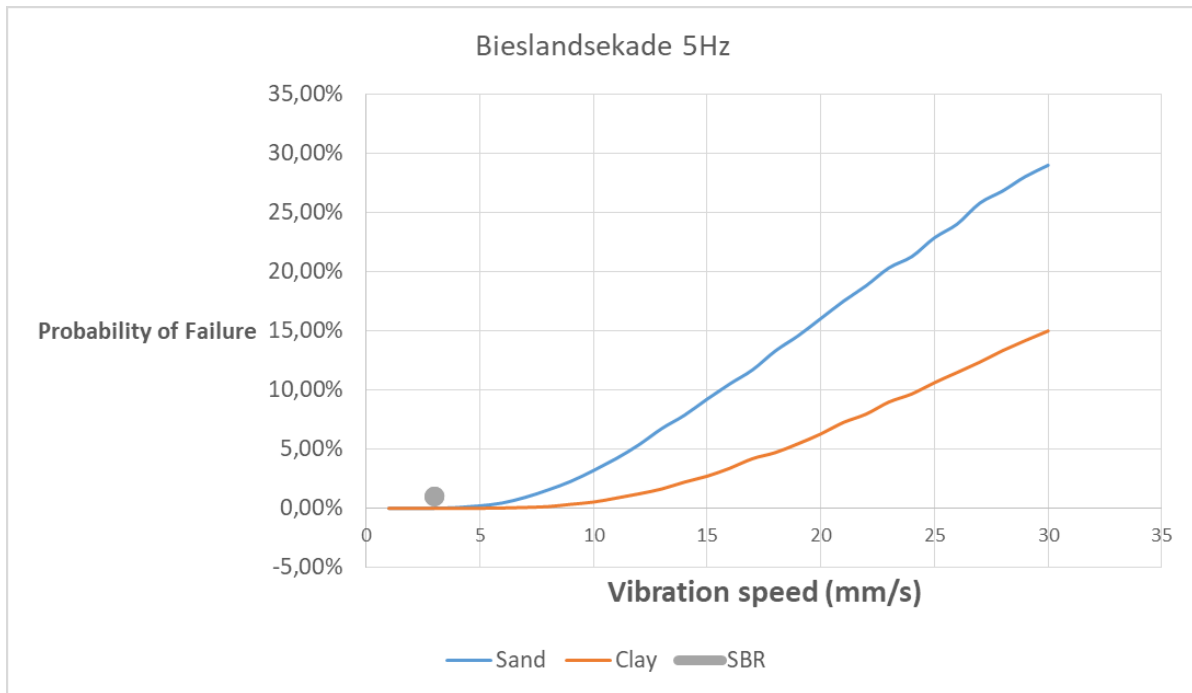


FIGURE 155

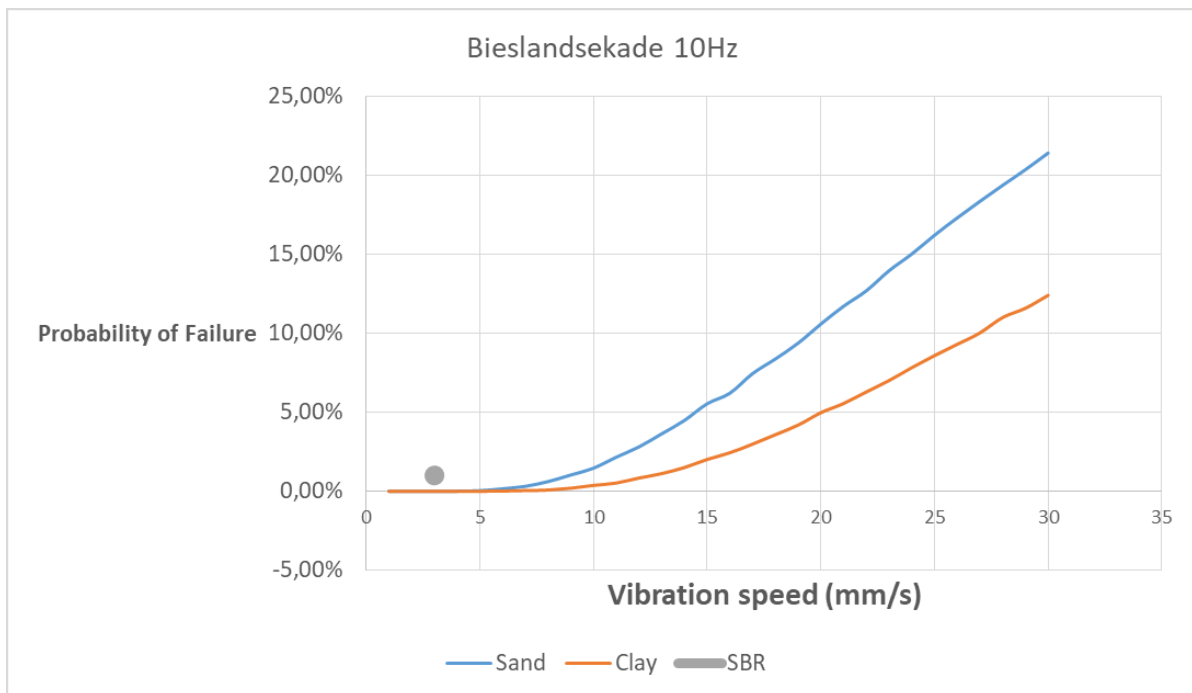


FIGURE 156

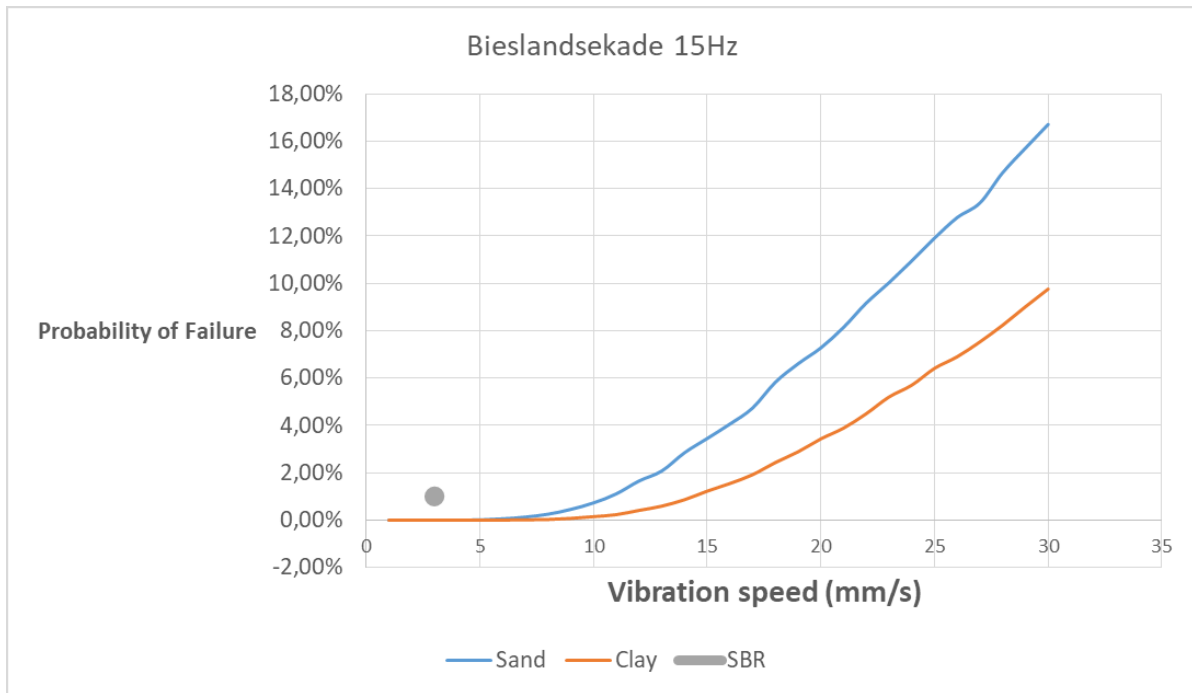


FIGURE 157

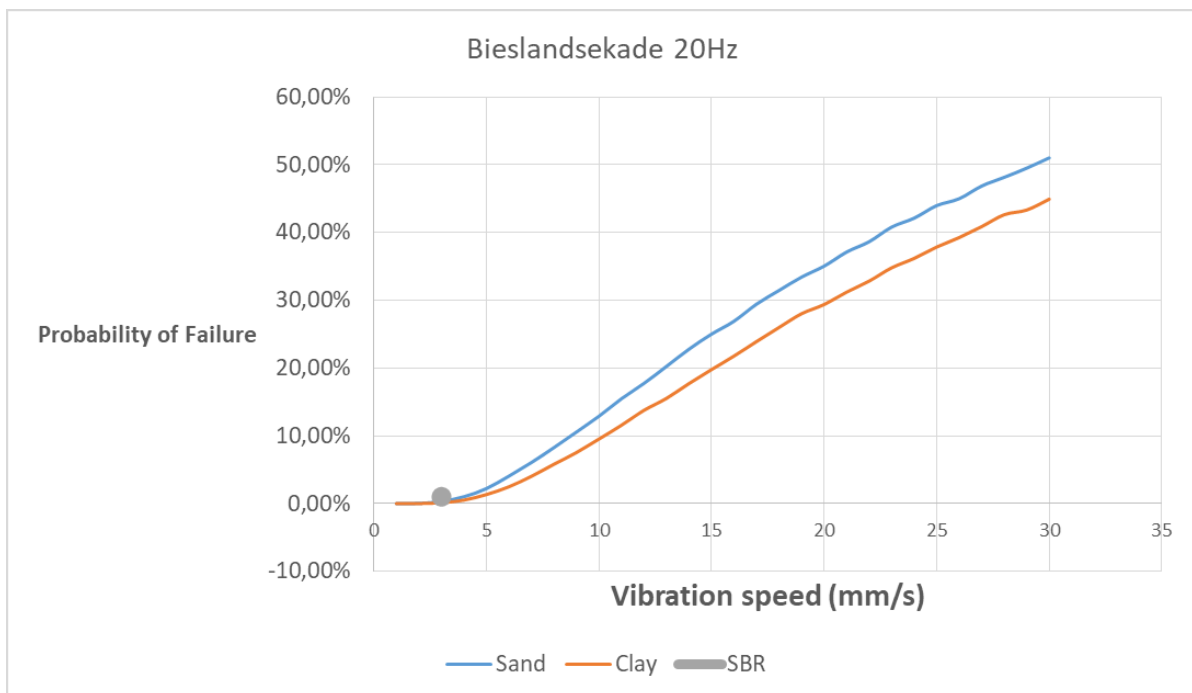


FIGURE 158

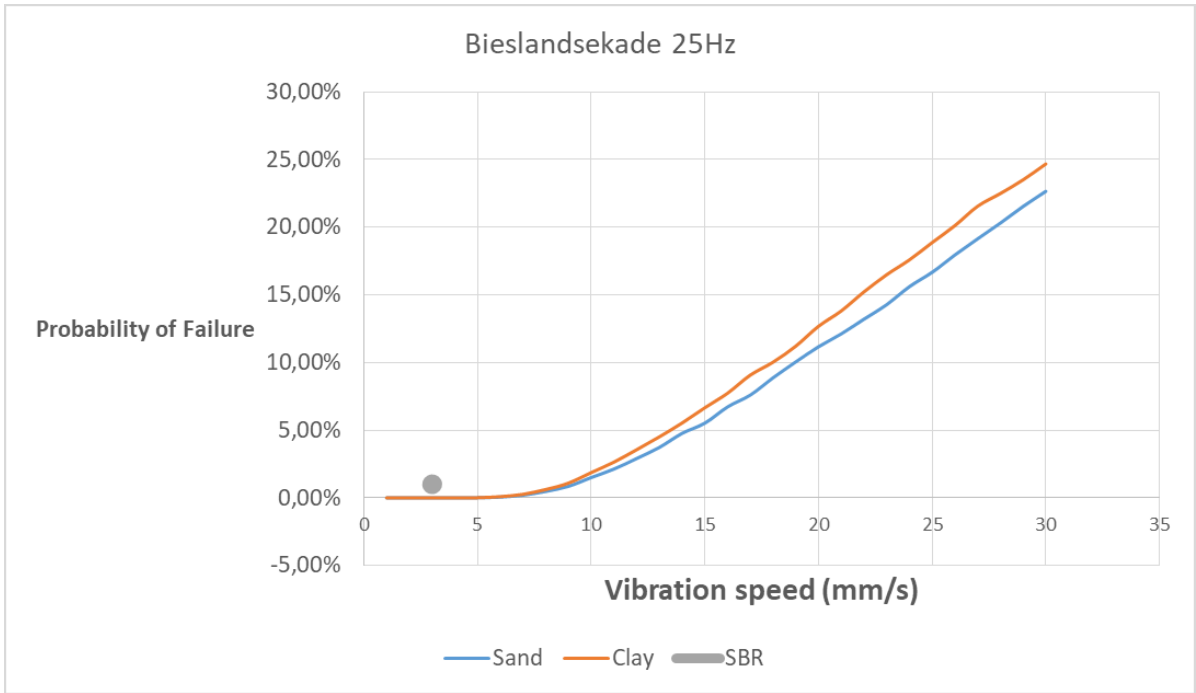


FIGURE 159

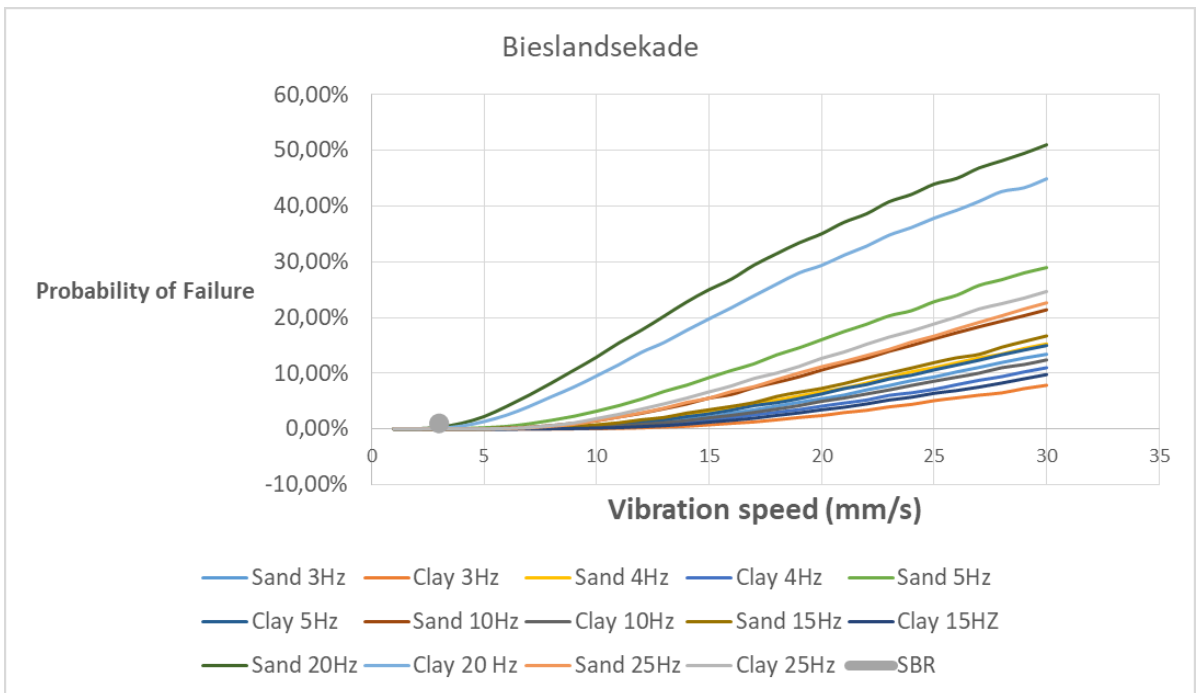


FIGURE 160

REFERENCES

- Boscardin, & Cording. (1989). *Building response to excavation-induced settlement*. Retrieved from
- Braile, L., (2007). *Seismic Waves*.
- Ceroni, (2004). *Evaluation of the natural vibration frequencies of a historical masonry building accounting for SSI*. *Soil Dynamics and Earthquake Engineering*, 64.
- Deckner, F. (2013). *Ground vibrations due to pile and sheet pile driving - influencing factors, predictions and measurements*. (Licentiate thesis), Stockholm.
- DUWO. (2016). *Oude Delft 81*. Retrieved from <https://www.duwo.nl/nc/over-duwo/onze-gebouwen/overzicht-gebouwen/complexinformatie/item/41/>
- EERI. (1988). *Diagonal cracks in brick wall of Notre-Dame Pavilion, Saint-Francois-d'Assise Hospital, Quebec City (Quebec)*. Retrieved from <https://www.eeri.org/1988/11/saquenay-quebec/02-6/>
- Gerrits. (2008). *Draagconstructies basis*.
- Head, & Jardine, (1992). *Ground-borne vibrations arising from piling*. CIRIA Technical Note, 142.
- Hendriks, & Rots, (2015). *Computational modeling of structures*.
- Hendry, Sinha, & Davies. (1997). *Design of Masonry Structures*.
- Hong, Y.-S. (2010). *Compressive Strength Study of Brick Masonry*. Kuala Lumpur.
- Kramer, S. L. (1996). *Geotechnical Earthquake Engineering*.
- Massarsch, & Fellenius. (2008). *Ground Vibrations Induced by Impact Pile Driving*. Paper presented at the International Conference on Case Histories in Geotechnical Engineering.
- Eurocode 1990, (2002a).
- Eurocode 1991-1-1, (2002b).
- Netzel. (2009). *Building Response due to Ground Movements*.
- Obrzud, & Truty. (2012). *Soil Elastic Young's Modulus*. Retrieved from <http://www.geotechdata.info/parameter/soil-young's-modulus.html>
- Oosterhoff. (2008). *Kracht + Vorm*.
- Proficient. (2012). *SBRCURNet*. Retrieved from <http://www.proficient-project.eu/Main.aspx?uri=4,122,129>

- Qi, (2006). *Finite Element Analysis*.
- Richart. (1970). *Vibrations of Soils and Foundations*.
- SBR Trillingsrichtlijn A: Schade aan bouwwerken, (2017).
- Schipper, (2017). Introduction to Seismic Essentials in Groningen.
- SCIA. (2018). *SCIA Academic Software*. Retrieved from <https://www.scia.net/nl/education/scia-engineer-academische-software>
- Silfhout. (2016). *Schoemaker Plantage*. Retrieved from <https://www.schoemakerplantage.nl/klinkerbuurt/>
- Soede. (2009). *Impact van trillingen door bouwactiviteiten op woningen en haar bewoners*. Retrieved from
- Steenbergen, R. D. J. M. (2016). *Probabilistic Design: Risk and Reliability Analysis in Civil Engineering*.
- Terwel, (2017). Building structures 1.
- Vrouwenvelder, Random Vibrations.
- Vrouwenvelder, Spijkers, & Klaver, (2006). Dynamics of Structures Part 1 Vibration of structures.
- Waarts. (1997). *Kans op schade aan bouwwerken door trillingen*. Retrieved from
- Wells. (2009). *The Finite Element Method: an Introduction*.
- Whenham. (2011). *Power Transfer and Vibrator-Pile-Soil Interactions within the framework of vibratory pile driving*.
- Willam, & Carol. (1996). *Discrete versus smeared crack analysis*. Retrieved from
- Woods, (1997). *Dynamic Effects of Pile Installations on Adjacent Structures*. NCHRP Synthesis 253.